WIND TUNNEL TESTS ON AN AIRCRAFT MODEL FITTED WITH A LIFTING FAN UNIT INSTALLED IN THE BODY

James Ernest Hackett B.Sc.(Eng.)

March 1964

A thesis for the Degree of Doctor of Philosophy in the Faculty of Engineering of the University of London.

SUMMARY

This thesis describes an investigation into several aerodynamic features of a wind tunnel model containing a lifting fan in its body. Most tests were performed in the Imperial College 5'x4' wind tunnel.

Many conflicting requirements defined model dimensions and the leading particulars of its 6.4" diameter, 23,200 RPM fan unit. Aerodynamic and Engineering design is discussed.

Lift, Drag and Pitching Moment were measured with and without wings at forward speeds between 15% and 65% of the 200 ft/sec jet velocity at incidences between ±20°. The addition of underfins removed the initial decrease in lift increments, which amounted to about 10%, as forward speed was raised. Forces measured in the $11\frac{1}{2}'$ x $8\frac{1}{2}'$ tunnel at R.A.E. were within 2 or 3% of the 5' x 4' tunnel results except at high incidence and at the higher forward speeds with wings fitted.

The development of the jet plume into a trailing vortex pair was demonstrated using smoke and tuft methods and a flow structure is suggested. With the exception of extreme incidences, surface flow patterns near the jet changed little with forward speed or incidence.

Flow measurements behind the fan were analysed using a specially designed integrating device, which is described. The results showed that as forward speed increased the fan progressed down its characteristic total head rise curve, mainly because of increasing inlet total head. This caused a reduction in fan lift and an increase in momentum drag.

The initial reduction in incremental lift as forward speed is increased is shown to be partly due to a loss of lift on the fan unit, an effect not greatly dependent upon incidence. Further loss of lift

is examined using a crude vortex. representation of the jet plume and some incidence effects are explained. It is tentatively proposed that, because of a decrease in the strength of the trailing vortex pair, the reduction of lift increment at the higher forward speeds is less than might be implied from the closer approach of the plume to the body.

Further experiments are required to achieve a better understanding of the jet plume. In particular the determination of trailing vortex strength over a speed range appears to be most desirable.

ACKNOWLEDGEMENTS

The author is indebted to the late Professor H.B. Squire, who suggested the project, for his advice and encouragement during the early stages of the work. Grateful thanks are due to Dr.J. Williams and Dr. L.A. Wyatt of the RAE and to Mr. N. Gregory of the NPL with whom the author had valuable discussions, and to Mr. W.J.G. Trebble of the RAE for his help during tests there.

The fact that the fan unit worked properly straight away is a tribute to the workshop staff of the Aeronautics Department, in particular to Mr.R.A. Lee who made the model. The hard work put into the electronics of the film reader by Mr. B.J. Belcher and the staff of the electronics workshop is greatly appreciated. Most of the photography is due to Mr.J.P. O'Leary who also gave considerable assistance during the third test series.

The author wishes to thank Mr. W.J.G. Trebble, Mr. N. Gregory and Mr. G. Jackson for valuable criticism during the draft stage of this thesis, and the Ministry of Aviation who supported the project financially.

LIST OF CONTENTS

LIST OF CONTENTS (CONTINUED)

LIST OF NOTATION

a, m	Lift curve slope
a_o	Sea level speed of sound under standard conditions.
a_2, a_3 ; A_1, A_2, A_3	See Appendix IV
A	Interference coefficient for lift. See Figure 7.7.
A_C	Area of motor cowling intake.
A_E	Flow area at duct exit.
A_F ; A_J	Fan annular area.
B	(In Chapter 2) fan boss : tip diameter ratio.
B	(In Chapter 8) Interference coefficient for drag.
c	Local fan blade chord.
C'	See Appendix IV
C_L	Lift coefficient
C_D	Drag coefficient
C_M	Nose up Pitching Moment coefficient measured about the axis of suspension of the model.
ΔC_p	Defined in Figure 5.15.
D	Drag
ΔD	Drag increment due to fan operation (datum with duct ends sealed.)
d_E	Equivalent diameter of duct.
d, d_t	Fan tip diameter
d_M	Diameter of fan motor stator.
$\bar{H}$	Mean total head at central plane, measured above ambient static pressure.
ΔH	Total head rise through fan.
H_o	(In Chapter 2 and Appendix I) Total head of flow approaching fan.
H_o	(In Chapter 8) Free stream total head.
H_c, H_1	Mean total head of the flow leaving the fan.
H_I	Mean total head of the flow approaching the fan.

L	Lift.
L_J	Theoretical lift of fan unit (see equation 2.1).
ΔL	Lift increment due to fan operation (datum with duct ends sealed).
δL	Lift increment due to the addition of underfins (datum with fan on).
m	(In Appendix IV.) Lift curve slope.
m	Mass flow through fan.
M	Nose up Pitching Moment measured about the axis of Suspension of the model.
ΔM	Pitching Moment increment due to fan operation (datum with duct ends sealed).
M_T	Fan tip peripheral Mach Number.
N	(In 2.5) R.P.M. of fan and motor.
N	(In 2.6) Number of fan blades.
N	(In 7.2) Body normal force given by Equation 7.11.
P P_J	Air power of jet.
P_I	Electrical power input to motor.
P_{I_T}	Electrical power input to motor during static lift test.
p_o	Free stream static pressure.
p_I	Mean static pressure ahead of fan.
p_2, p'_2, p_3, Δp_2, $\Delta p'_2$	Appendix IV.
R	Fan tip radius.
r	Radius of fan blade element.
$r_{b_{min}}$	Minimum permissible fan boss radius.
$r_{t_{max}}$	Maximum permissible fan tip radius.
T	Measured static lift.
V	Free stream velocity.
V_E	Duct exit velocity.
V_F	Axial velocity through fan
V_J	Jet velocity (in parallel duct).
V_{J_T}	Nominal efflux velocity defined by $T = \rho A_J V_{J_T}^2$
$V_{J_{MIN}}$	Minimum possible design jet velocity.
$V_{TIP_{MAX}}$	Maximum fan tip peripheral velocity.

$V_{J_{RMS}}$	Root mean square jet velocity.
V_S	Swirl velocity imparted by straighteners.
V_2, V'_2, V_3, V'_3, v_1, v_2, v_3	See Appendix IV.
α, α_B	Body incidence.
α_o	(In Chapter 7) Wing setting angle. Positive for wing leading edge above the body axis.
α_o, α_1, α_2, α_3	(In Chapter 2) As defined by Figure 2.3.
α_{12}	Defined by Equation 2.6.7.
α_w	Wing incidence.
β	Fan blade angle from plane of rotation to section datum.
η	Fan stage efficiency.
ρ	Air density.
σ	(Appendix IV) Fan blade solidity.
ξ	Bendeman figure of merit (See Section 6.3)
ω	Angular velocity of outflow from fan.
Ω	Angular velocity of fan.

1. INTRODUCTION

For many years heavier-than-air vehicles have flown which are capable of leaving the ground vertically, performing a mission, and then landing vertically. Until recently the presence in the mainstream of large rotating lifting blades has kept cruise speeds low and in combination with mechanical complexity has made such transport more expensive than that using conventional take-off techniques.

Recent aircraft contain powered lift installations which are enclosed by the structure and which are operated only when the aircraft wings will not sustain flight. One advantage of such a system is that the vertical lift capability compromises the cruise case less, though 'dead' engines must be carried throughout the flight.

Another possibility, the combined engine with tilting nozzles, avoids carrying some of this extra weight, but engine design must involve compromises between cruise and vertical lift requirements. It seems probable that some future aircraft will use more fully integrated lift/thrust systems which are in continuous use.

Current interest in the VTOL field focusses upon jet and fan lift. There is no sharp dividing line between these categories. The jet unit uses higher gas velocities and somewhat smaller areas than those needed by the fan unit with its lower outlet speeds. Dry weight considerations favour a jet-lift bias, but the higher Froude efficiency of the fan unit tends to restore the balance since less fuel is used. The overall choice depends on the length of hover time as well as on many design considerations. These may include the volume of the units, noise, response to control, availability of emergency power, recirculation effects, starting in the air, interaction between the unit and external flows, and the amount of aerodynamic interference present due to the intake and due to the sink effect around the periphery of the jet. These last aspects are of interest in the present work.

Chapters 2 and 3 will describe the aerodynamic and engineering design of a wind tunnel model intended to investigate several aspects of the aerodynamic interferences and interactions which may occur in VTOL installations.

In the autumn of 1961 three component force tests were carried out on the model in the Imperial College 5' x 4' wind tunnel over a range of forward speeds and incidences. Surface flow visualisation was also carried out. In June 1962 the force measurements were repeated in the R.A.E. $11\frac{1}{2}$' x $8\frac{1}{2}$' wind tunnel using doubled incidence increments. These results are reported per se by Trebble and Hackett (1963) who also make appropriate comparisons with another model (see also Trebble and Williams (1961)). Such comparisons are therefore omitted from this thesis and the $11\frac{1}{2}$' x $8\frac{1}{2}$' tunnel results are presented only in an investigation of the effect of tunnel constraint on measured forces. (See Section 7.6)

Throughout both the preparatory and the experimental work a need was felt for a knowledge of mean duct quantities, in order that forces associated with changing conditions at the fan could be investigated over the whole field of experiments. The labour involved in reducing by hand the necessary duct traverses was prohibitive and no solution was apparent initially. However early in 1962 the film reader described in Chapter 4 was devised which enabled the required data to be obtained. The results of this final series of tests are reported and discussed in Chapter 7.

2. AERODYNAMIC DESIGN OF MODEL

2.1 Introduction

This chapter deals with the overall design of the wind tunnel model and the ducted fan unit. Engineering design is dealt with in the next chapter. Because testing was to take place in the 5' x 4' wind tunnel the fan unit required was only half the diameter of those then in use at the government research establishments. It was therefore necessary to develop a unit of new design. The jet diameter to tunnel proportions are very similar to those of several RAE and NPL experiments.

The design sequence which is outlined in this chapter somewhat idealises that used originally. In practice several project studies and many design cycles took place during the six months in which the model was designed.

The aim throughout the design was to avoid expensive "one off" proprietary items and to use conventional techniques wherever possible. Any other course would have resulted in the production of the fan unit becoming an experiment in itself, rather than the means of performing a series of experiments in aerodynamics.

2.2 Fuselage design (See Figure 2.1)

Gregory and Raymer (1958-9), Wyatt (1959) and Melbourne (1960) have performed experiments which demonstrate that it is inadvisable to mount jet lifting units across the thickness of wings because suction ahead of the intake and on the undersurface near the jet can lead to considerable nett loss of lift and large nose-up pitching moments as forward speed increases. Because of this emphasis tended towards body-mounted lifting units (Trebble and Williams (1961), Gregory (1961) and Wyatt (1961)). The work described here was carried out in parallel with these experiments. The object has been to reduce further the horizontal area around the exit of the lifting unit, and to investigate the nature of flows which are associated with lifting fans.

The smallest envelope around a ducted fan unit is the cylindrical duct itself. Further reduction leaves an open rotor which is not of interest at present. An American and a German aeroplane employ lifting units mounted at the wing tips which are rotated for propulsion in forward flight. (See Yaggy and Mont (1961)). As this system restricts the basic design of the aeroplane because of the need to rotate the duct, a more useful pod-type of unit has been tested.

In an attempt to achieve a low drag coefficient with fan-off the shape of the body was derived from the airship R101. The fan axis is at right angles to the body centreline. The duct cylinder has flat ends in order to reduce lateral velocity components which may affect the fan and which complicate traverses across the duct for the determination of mass flow. By building up the sides of the body to meet the end planes of the duct it is possible to make the body diameter only about 30% greater than that of the duct and to have only a small horizontal area around the outlet of the duct. In order to promote attached flow over the intake lip this was given a generous radius (one fifth of fan diameter) on the upstream side of the inlet, reducing to 6% at the sides and rear of the duct (see Figure 2.2). Table I gives a summary of model dimensions.

If the duct aerodynamics is to be fully represented it is desirable to employ some form of fan system rather than separate suction and blowing. This allows any inlet-outlet interference to make itself felt and in particular it allows the effects of high velocity air on the upstream side of the inlet to be felt by the fan and at exit. (See Gregory et al (1962))

2.3 The Fan and Centrebody

Basic Design

Originally contra-rotating fans were considered because these made possible higher disc loadings than were attainable with a single fan. However as the design progressed it became apparent that high rotational speeds were required by any fan system having the required output. It was decided that the combination of contra-rotation with high speed was unacceptable for engineering reasons. These included difficulties in providing adequate bearing support in the centrebody, in designing a small enough gearbox and in the length of time needed to manufacture the system. Therefore a single fan design was used.

As the presence of the gearbox precludes central positions and the ends of the duct are unsuitable, the choice of axial position of the fan is limited to either one quarter or three quarters of a diameter from the inlet. The tests of Taylor (1958) show that the static thrust is approximately the same for the two positions. When combined with the requirements of gearbox geometry and lubrication the two possible fan positions give a choice between an inverted model with the fan downstream, and a model 'right way up' with an upstream fan. The latter was somewhat arbitrarly chosen as three factors appeared to favour it.

Firstly the effects of possible separations from the forward lip of the inlet are probably smaller for the upstream fan since the area of disturbed flow is less here. Gregory (1962) has shown that the separation region probably contains vortices whose axes run down the duct. It appears reasonable to arrange that these shall not have developed to significant size before the fan is encountered.

Secondly detailed design showed that with the fan in the upstream position the stator was best placed in the downstream position, and vice-versa. Had the fan been placed downstream then a pre-swirl stator would have been needed. Because pre-swirl vanes increase the power required for a given lift these were not used. A relatively small number of large chord straightener blades were used in order to reduce the number of wakes encountered during traverses of the exit plane.

Thirdly in the full-scale aircraft space will be limited and the fan may have to be placed high in the duct regardless of aerodynamic difficulties. In this respect the model may be more representative than some having long settling lengths before the fan.

By keeping fan blade angles moderate adverse effects due to non-axial flow near the inlet can be reduced. In order to avoid stall effects it was decided to limit the swirl angle at the fan boss to about 30 degrees. This condition determines several features of the fan. For example a relationship is defined between jet velocity and fan R.P.M. The diameter of the fan boss and centrebody is affected by the need to keep blade root tangential speeds high enough to give sufficient jet velocity and lift for accurate measurements to be made readily.

A factor of considerable importance is the need for the centrebody to house either a motor or a gearbox. For the present design a gearbox was needed and at one stage it appeared that the size of the whole model might be determined by the size of the gears themselves.

Various natural frequencies of vibration need to be checked (See 3,4). In particular the fan blade bending frequency may be near to that imposed by the wakes of centrebody supports unless care is taken. The natural frequency may be raised either by raising the centrebody diameter to shorten the blades, or by tapering the blades, or by reducing the number of blades and increasing their chord to achieve the same solidity. Natural frequencies near to those imposed by the gear teeth also need to be carefully avoided.

Centrebody Shape

The upstream end of the centrebody must be of streamlined shape but the shape of the downstream end is open to discussion. Contemporary models have blunt ends downstream which probably offer more resistance to the flow than necessary. An ellipsoidal rear end, similar to the intake end was therefore used. It was thought that this could only give less drag than a blunt-ended centrebody. The centrebody finally chosen was equivalent to a 2:1 ellipsoid with a length of circular cylinder inserted between the two ends to house the gearbox. (See Figure 2.2)

While the model was being manufactured some short qualitative tests were performed to investigate the properties of swirled flows round a 2:1 ellipsoid. Flow visualisation was carried out using smoke in the $3\frac{1}{2}$ inch swirl tunnel at Imperial College.

It was thought that some benefit might accrue from allowing the flow behind the fan to expand before the swirl was removed as the vortex-type pressure distribution might aid the boundary layer on the centrebody. Although the body diameter was only one third that of the swirl tube, the separation point did move downstream as swirl was increased, eventually becoming completely attached for swirl angles between 50 and 60 degrees. (See Figure 2.4) A vortex burst can be seen in one picture.

Although the expected effect was certainly present the swirl angles needed for significant movement of the separation point were higher than those likely to occur behind the ducted fan. It was decided to straighten the flow at full centrebody diameter.

2.4 Model size and jet velocity.

2.4.1 Introduction

In 2.2 and 2.3 the shape of the model has been fairly closely defined but no consideration has been given to model size, centrebody proportions, jet velocity, or matching a driving motor to the model dimensions. Before this can be done it is necessary to examine several aerodynamic and experimental factors which directly affect the size of the model. The way in which these restrict the design of the model is summarised by Figure 2.6

2.4.2 Limitations imposed by tunnel size

As no reliable corrections are known for the effect of tunnel constraint on round jet models it is desirable to keep the model smaller relative to the tunnel dimensions than is usual for aircraft models. Correction tables have been published by Heyson but the mathematical model used is not very representitive of real flows.

Other work, which has become available since the model was designed, gives recommended model sizes for tolerable interference forces (Butler and Williams (1959)). In the present work the experiments of Jordinson (1958) were used to predict free air jet penetration. An arbitrary criterion was adopted that the distance from the jet outlet to the tunnel wall opposite to it should be no smaller than the free-air jet penetration, at the lowest velocity ratio (i.e. V/V_J) of interest. For tests in the Imperial College 5' x 4' wind tunnel the requirements of motor size and static lift overrode this criterion which was achieved only at and above velocity ratios of 0.50. Later tests in the R.A.E. No.1 $11\frac{1}{2}'$ x $8\frac{1}{2}'$ tunnel brought this value down to about 0.25.

Recent work suggests that as the interference effect of the wind tunnel is substantially the same as that of the ground, one is representing real conditions by testing in a wind tunnel. While this might be used as an argument towards increasing the size of a model it should be remembered that ground clearance ought to be increased with forward speed to represent a practical flight path.

In order that clearance between the rear end of the model and the tunnel floor and roof is adequate at high incidence it is necessary to restrict the model length aft of the pivot to about 20" and to place the model centrally in the tunnel. Both this and the previous requirement make small model size desirable.

2.4.3 <u>Power, lift and jet velocity requirements</u>

Before deciding on duct and model size it is necessary to determine the air power required by various combinations of duct size and through velocity, and to examine the corresponding theoretical values of static lift.

If lift L_J lbs is produced by accelerating air from rest to V_J ft/sec in a duct having an equivalent diameter d_E ft then:

$$L_J = \rho\frac{\pi}{4}{d_E}^2{V_J}^2 \qquad \ldots \quad 2.1$$

and the corresponding air power is

$$P_J = \tfrac{1}{2}L_JV_J \qquad \ldots \quad 2.2$$

Figure 2.5 is the result of putting likely values of V_J and d_E into the above equations and gives values of air power and static lift.

As the model motor ran at constant R.P.M. it was necessary to vary V/V_J by altering the speed of the wind tunnel. As the range of V/V_J

from 0.2 to 0.6 had to be produced in a wind tunnel having speeds available from 40 ft/sec to 150 ft/sec it was clear that V_J should lie between 200 and 250 ft/sec. When combined with root blade angle requirements these values imply rotational speeds between about 20,000 and 30,000 R.P.M.

In order that fan lift forces should be large compared with model alone forces it was decided that the static lift of the fan unit should be at least 10 lbs. This is consistent with the need to measure accurately interference forces of about 10% of this with a balance which reads to 0.01 lb.

2.4.4 Limitation of tip Mach number of the fan

Because high rotational speeds were necessary the avoidance of compressibility effects at the fan blade tips became of importance. MacDougall (1951) gives performance figures obtained from propellors having Clark Y aerofoil section which was also employed for the model fan. These show that it is desirable to keep down the value of peripheral tip Mach number to 0.70 in order to avoid the compressibility drag rise. The 'Handbook of Aeronautics' Volume III was also consulted.

2.4.5 Centrebody diameter as a proportion of the fan tip diameter

The final value chosen for boss-tip diameter ratio is determined during final fan design in Section 2.6. In order to determine the power required by a fan of a given tip diameter it is necessary to estimate the range of centrebody diameters which are likely to occur. For a given tip diameter and through velocity maximum power is needed when the boss diameter is a minimum. As blade requirements place a minimum value on boss radius and tip Mach number limitation creates a maximum permissible tip radius, it is possible to determine a minimum value for r_b/r_T as follows:-

$$V_{TIP_{MAX}} = r_{T_{MAX}}\,\Omega = a_o M_{T_{MAX}} \qquad \dots\ 2.3$$

From Appendix I and 2.6.1

$$r_{b_{MIN}}\,\Omega = \frac{2/3 V_{J_{MIN}}}{\left(\frac{\omega r}{V_J}\right)_b} \quad \text{for pre-swirled conditions} \qquad \dots\ 2.4$$

$$\therefore\ \frac{r_{b_{MIN}}}{r_{t_{MAX}}} = \frac{2/3 V_{J_{MIN}}}{\left(\frac{\omega r}{V_J}\right)_b d_o M_{T_{MAX}}} \qquad \dots\ 2.5$$

Putting $V_J = 200$ ft/sec (see 2.4.3)

$\left(\frac{\omega r}{V_J}\right)_b = 1/3$ (see 2.6.2)

and $M_{T_{MAX}} = 0.70$ (see 2.4.4)

yields $\frac{r_{b_{MIN}}}{r_{t_{MAX}}} = 0.514$

We shall use this figure rounded off to 0.50. Results will also be quoted for 0.58 for comparison. It is unlikely that values greater than this will be of interest since the jet then has too annular a nature. The range of r_b/r_t values of interest includes that for maximum power required for the case with no pre-swirl. This is discussed in Appendix II.

2.5 Power Unit

2.5.1. Suitable types of power unit

The more likely possibilities included an air turbine or an electric motor within the model or a flexible drive from a motor outside the wind tunnel. Since high rotational speeds were required the latter was soon discarded. The air turbine appeared to be a possibility but ~~at the~~ at the time of initial design no suitable motor existed and published work concerning attempts to make small efficient air turbines was not promising (Llewelyn-Davies et al (1952)) R.A.E. have since had developed successful units of this kind. Recently (McWherter (1962)) details have been published of a very powerful hydraulic motor using high pressure fluid.

The only available possibility which existed at the time of design in a proved form was the electric motor, which allowed conventional techniques to be used throughout.

It was decided that the best type of electric motor for the present purpose was an induction motor powered by a high frequency supply unit. For the model motor a range of stator and rotor units usually used in machine tools appeared promising. The frequency changer used gave constant output frequency, variable speed capability would have doubled the cost. The Stator-Rotor units combined the advantages of rugged construction, cheapness and the possibility of building the motor into the model, which allowed a more compact design than the installation of a motor with its own casing and bearings.

The total cost of the Stator-Rotor unit and the associated frequency changer was approximately the same as had been quoted for a specially manufactured D.C. Motor. One advantage of the chosen system was that 95% of the cost was the frequency changer, which was well protected by a thermal overload cut out. The model motor could therefore be over run if necessary and regarded as expendable.

However in the present case the motor was run below its quoted power rating.

2.5.2 Sizes of likely electric motors

Even using the high speed motors made necessary by the fan blade and lift requirements it was very soon apparent that it was not possible to house a sufficiently powerful motor in the centrebody of the fan. The motor was therefore mounted in the forebody. The detailed design is described in Chapter 3.

A range of motors suitable for the forebody installation was selected. Using data from the makers catalogue the following relationship, valid only over a limited range of sizes for this particular type, has been derived relating motor diameter to power and speed.

$$d_M = 3.84 + \frac{3070\ H.P.}{N}$$

where d_M = Motor Stator diameter (Inches)

N = R.P.M. of motor.

The proportions of the model were such that the motor stator diameter could be no more than 70% of the fan tip diameter. Using this with the above formula it was possible to draw Figure 2.7 relating to rotational speed the maximum power that could be associated with a given fan tip diameter for 50% and 58% bosses. A 1:1 gear ratio has been assumed throughout in the calculations. (See Chapter 3) The power required by the fan has been calculated assuming 100% efficiencies throughout and zero pre-swirl.

2.5.3 Final choice of motor

From Figure 2.7 it is possible to determine further boundaries which modify Figure 2.6 by removing areas where motor size becomes excessive. Figure 2.8 shows the areas which remain if overall efficiencies of 100%, 70% and 50% are assumed in combination with 50% and 58% bosses. 70% represents a possible figure for combined stage and gearbox efficiencies. 50% allows the same stage and gearbox efficiencies leaving adequate power for the addition of pre-swirl if required. It can be seen that the design possibilities which remain are very restricted.

In practice only two fan synchronous speeds, 24,000 R.P.M. and 27,000 R.P.M. within the design range were available using standard electrical equipment. The lower speed was selected for the following reasons:-

(i) Power to be transmitted through the gearbox is little more than half of that for the 27,000 R.P.M. case. (See Figure 2.5) The amount of heat to be dissipated will be less and cooling problems will be eased.

(ii) The motor will have substantial reserve power, allowing the possibility of 'stretch' either by installing pre-swirl vanes or by small increases in R.P.M. For the 27,000 R.P.M. case the whole system would be running at full capacity and little flexibility would be possible.

(iii) Tip Mach number for the 24,000 R.P.M. configuration is well clear of the drag rise.

(iv) 24,000 R.P.M. was the highest speed obtainable using frequency changer equipment. Higher speeds require a more complicated inductor-alternator set.

(v) Noise levels will be lower at lower speeds. Even at 24,000 R.P.M. it was found advisable to wear ear protectors during tests.

It follows that the design point lies on the 24,000 R.P.M. line between tip diameters of about 5.9" and 7.4".

2.6 Fan blade and stator design

2.6.1. Theory

The design uses free vortex theory in the form given by the late Professor H.B. Squire in an unpublished note. The note is reproduced in full as Appendix I of this thesis.

In order to determine the advantages to be gained from introducing swirl to the flow before the fan the method of Appendix I was extended to include a pre-swirl term. The relevant velocity diagrams are given in Figure 2.3.

The following development summarises the procedure:-

From I.3 $$\left(\frac{H_1 - H_0}{\frac{1}{2}\rho V_J^2}\right) = \frac{P_J}{A_J V_J \frac{1}{2}\rho V_J^2} = 2\left(\frac{\Omega r}{V_J}\right)\left(\frac{\omega r}{V_J}\right) \qquad \ldots \quad 2.6.1$$

$\left(\frac{\omega r}{V_J}\right)_b$ will be chosen between 1/3 and 1/2 as recommended.

If Ω is known then $$r_b = \frac{P_J}{2\left(\frac{\omega r}{V_J}\right)_b \frac{1}{2}\rho V_J^2 A_J \Omega} \qquad \ldots \quad 2.6.2$$

In addition r_t may be determined from $r_t^2 = \frac{A_J}{\pi} - r_b^2$

Hence $B = {}^{r_b}/_{r_t}$ may be determined.

Stator vanes

We shall investigate the arrangement in which the total swirl due to the fan is counteracted equally by pre-swirl vanes and straighteners. The vanes will be untwisted and the angle of the straighteners will be such that they reduce to zero the total angular momentum.

Initial swirl velocity due
to the pre-swirl vanes $= -\frac{1}{2}\left(\frac{\omega r}{V}\right)_b V_J$ ft/sec

Swirl velocity imparted
by fan at radius r $= \left(\frac{\omega r}{V_J}\right)_b V_J B\left(\frac{R}{r}\right)$ (Free vortex dist.)

Swirl velocity imparted
by straighteners $= V_S$ ft/sec

$$\text{Total swirl momentum} = 2\pi R^2 \rho V_J^2 \int_B^1 \left\{\left(\frac{\omega r}{V_J}\right)_b B - \frac{1}{2}\left(\frac{\omega r}{V_J}\right)_b + \left(\frac{V_S}{V_J}\right)\left(\frac{r}{R}\right)\right\} d\left(\frac{r}{R}\right) = 0$$

This yields $\frac{V_S}{V_J} = \tan\alpha_3 = \left(\frac{\omega r}{V_J}\right)_b \frac{1-3B}{2(1+B)}$ with pre-swirl ...2.6.3

and $\frac{V_S}{V_J} = \tan\alpha_3 = \left(\frac{\omega r}{V_J}\right)_b \frac{-2B}{(1+B)}$ without pre-swirl ...2.6.4

Hence α_3 with or without pre-swirl.

Fan Blades

(i) flow angles (See Figure 2.3)

$$\tan \alpha_1 = \left(\frac{\Omega r}{V_J}\right) + \tfrac{1}{2}\left(\frac{\omega r}{V_J}\right)_b \qquad \ldots\ 2.6.5$$

Blade Rotation — Pre-Swirl — Fan Term

$$\tan \alpha_2 = \left(\frac{\Omega r}{V_J}\right) + \tfrac{1}{2}\left(\frac{\omega r}{V_J}\right)_b - \left(\frac{\omega r}{V_J}\right)_b . B. \left(\frac{R}{r}\right) \qquad \ldots\ 2.6.6$$

$$\tan \alpha_{12} = \tfrac{1}{2}\left(\tan \alpha_1 + \tan \alpha_2\right) = \left(\frac{\Omega r}{V_J}\right) + \tfrac{1}{2}\left(\frac{\omega r}{V_J}\right)_b - \tfrac{1}{2}\left(\frac{\omega r}{V_J}\right)_b . B. \left(\frac{R}{r}\right) \qquad \ldots\ 2.6.7$$

Hence α_1 , α_2 and α_{12} with or without pre-swirl.

(ii) C_L values and solidities

From Equation 6 of Appendix I

$$C_L = \frac{2}{S}\frac{\omega r}{V_J} \cos \alpha_{12} \quad \text{where } S = \text{solidity}$$

$$= \frac{2}{S}\left(\frac{\omega r}{V_J}\right)_b . B. \left(\frac{R}{r}\right) \cos \alpha_{12} \qquad \ldots\ 2.6.8$$

Limiting tip C_L to 0.50 (See Appendix I) and substituting in the appropriate value of α_{12} obtained from above allows the tip solidity to be calculated. The use of parallel or slightly tapered blades then produces a design which is aerodynamically acceptable.

2.6.2 Determination of fan boss and tip diameters

In 2.5.3 the design point was shown to be between tip diameters of 5.9" and 7.4" at a through velocity of 200 ft/sec. Neither the overall efficiency nor boss diameter has yet been specified. In order to complete the design some trial drawings had to be made in order to determine the most suitable combination of the remaining variables. In what follows a 4.6" diameter motor giving 6 H.P. at 24,000 R.P.M. has been assumed at the outset and it will be seen later that its size is consistent with the design conditions. Iteration between tip diameter and area was necessary to achieve this.

First determine P_J knowing $P_M = 6$ H.P.

Assume gear efficiency of 85% and seals-plus-windage loss of ½ H.P.

Then input to fan $P = 4.5$ H.P.

Assume stage efficiency of 85%

Then $P_J = \eta P = 3.8$ H.P.

Choose $A_J = 0.15\ ft^2$ $V_J = 210$ ft/sec $\Omega = 24{,}000$ R.P.M. $= 800\pi$ rads/sec

(Note that V_J has been raised slightly to allow for R.P.M. quotation at synchronous rather than true speed.)

Following the method of Appendix I (Pre-swirl conditions)

$$(H_1 - H_0) \times \cdot 15 \times 210 = 3.8 \times 550$$

giving $$\frac{H_1 - H_0}{\frac{1}{2}\rho V_J^2} = 1.29 = 2\left(\frac{\Omega r}{V_J}\right)\left(\frac{\omega r}{V_J}\right)$$

Take $\left(\frac{\omega r}{V_J}\right)_b = 1/3$ (boss condition) in order to reduce the straightening needed. Hence at the boss $\left(\frac{\Omega r}{V_J}\right)_b = \frac{3}{2} \times 1.29 = 1.935 = \tan \alpha_{12}$

if pre-swirl = $\frac{1}{2}\omega$. This figure gives reasonable blade angles at the boss. $\therefore$ $r_b = 1.935 \times \frac{210}{800\pi} = 0.154$ ft.

Boss diameter = 3.8"

For $A_J = 0.15$ ft^2 corresponding tip diameter = 6.4" } B = 0.578

Corresponding motor diameter = 0.70 d_t = 4.5"

2.6.3. Calculation of fan blade angles

Using equation 2.6.7 with and without the pre-swirl term included gave the upper graph of Figure 2.9 which shows the distribution of swirl angle along the length of the blade.

Solidity was determined by limiting C_L to 0.50 at the tip and applying equation 2.6.8 giving:-

$$0.50 = \frac{2}{S}\left(\frac{1}{3}\right) 0.58.1. \cos \alpha_{12}$$

This yields S = 0.252 for pre-swirl and Nc = 4.72"

and S = 0.266 without pre-swirl, Nc = 4.98"

Nc = 5.00" covers both cases.

Three or five blades were likely possibilities. As the chord of the former would have been greater than the blade length that possibility was rejected. Later it was found necessary to taper the five blades slightly in order to relieve root bending stresses and to raise the natural frequency. (See Chapter 3) This raised the design value of C_L at the tip of the blade to 0.525.

The centre diagram of Figure 2.9 was obtained by substituting into 2.6.8 the values of solidity and swirl angle appropriate to the 1.0" parallel blade with and without pre-swirl, and the tapered blade without pre-swirl.

10% Clark Y aerofoil section was chosen. The addition to the swirl angle of the incidence required for the appropriate value of C_L gave the blade angle distributions of the lower graph of Figure 2.9.

It can be seen that, for a given total head rise, the addition of pre-swirl lowers the blade angles by only about 2 degrees although power is increased considerably and the manufacture is made more complicated. The idea of employing a stator at entry was therefore rejected. This allows the possibility of reducing the total head rise coefficient from 1.29 to little more than unity, which in turn permits either increased velocity or a larger diameter jet. The possibility was not used and the extra available total head rise was regarded as a safety margin. Under most conditions the fan should operate below its design point and should use less than the maximum power available. The safety margin allows inlet maldistributions or adverse pressure differences to be overcome with a reduced risk of stalling the fan blades.

2.6.4 Straightener design

The design follows the recommendations given in Appendix I. Twelve circular arc blades of 1.30" chord were employed. This gave unit solidity about half way along the blade and demanded lift coefficients no greater than 0.55. The blade entry angle was determined using equation 2.6.4 which reduced to zero the total angular momentum. The blades were untwisted. Figure 3.2 shows the straightener ring before assembly.

2.7 The design of wings and Underfins. (sometimes called fences)

Wings

Since both body-mounted ducted fans and wings are likely to be positioned near to the aircraft centre of gravity, interferences between the two are of interest. In order to separate wing incidence effects from body effects wings were designed so that the angle relative to the body could be altered. Wing area was determined by considering conditions before and after transition between jet- and wing-supported flight.

High intake momentum drag will probably preclude transition speeds greater than one third of the jet speed corresponding to static thrust. If the maximum safe wing lift coefficient and the available jet lift are known then a minimum wing can be found.

For the present model transition from 14 lbs of powered lift to 14 lbs if wing lift at $C_L = 1.2$ needs wings 2 square feet in area for transition at a velocity ratio of one third. ($C_L = 1.2$ represents the probable full scale value. This has been used to obtain a wing of representative size, even though this lift coefficient will not be achieved at model scale). A wing of this area was designed for approximately elliptical load distribution. It has 2:1 taper and an aspect ratio of 6. The straight quarter chord line passes through the fan axis. The duct annular area is 7½% of the wing area. It is unlikely that full scale aircraft will have ducts any larger than this.

<u>Underfins</u> (abbreviated to 'fins' in some later chapters)

Following the recommendations of Gregory (1961) a pair of ventral fins was designed in order to investigate reported favourable interference effects. The fins were flat plates, one duct diameter deep and two long. They were situated one diameter apart and extended forwards to points one diameter ahead of the front of the duct exit. They were joined to the body along their upper edges.

'Perspex' was used to aid flow visualisation on the inside surfaces.

3 ENGINEERING DESIGN OF MODEL

3.1 General layout (See AER 6020, at end of thesis, and Figures 3.1 & 3.2)

In 2.3 we saw that a single fan design was preferable and in 2.6 it was shown that sufficient power could be obtained from a single motor. This is mainly a consequence of the high rotational speed which enables a motor of fairly high power density to be used.

The motor chosen was rated at 4 H.P. fully enclosed or 6 H.P. if ventilated. It was decided to air cool the motor using free stream air fed from air intake at the front of the model and exhausting at the sides as shown in Figure 2.1. This system produced little disturbance to the flow and made unnecessary the avoidance of balance constraints likely to be associated with an external cooling system. The obvious place to mount the motor was therefore ahead of the fan duct.

It was found that the motor shape best suited to the general outline had the highest length : diameter ratio of the range under consideration. The motor length was consistent with positioning the duct at the maximum thickness point 40% back from the nose.

Design studies showed that the best way of providing accurately positioned rigid mountings for the motor and bearings was to make the forebody and duct section from aluminium alloy castings. AER 6020, the general assembly drawing included with this thesis, shows the two main castings and the machined centrebody which is supported between two cast spiders located at the ends of the duct. Photographs of the model and some of its components are given in Figures 3.1 and 3.2.

3.2. Gearbox design

The right-angled spiral bevel gears needed for high speed had pitch-circle diameters of $1\frac{1}{2}$". The size of the cylinder needed to house the gearbox was determined by the plan view of the gears. The possibility of using a motor rotating more quickly than the fan had some attractions due to the greater power density obtainable. However it was found that the centrebody diameter became large compared with the size of the model if the gear ratio was changed from 1:1. This ratio gave the smallest gearbox volume and resulted in a centrebody diameter which gave an acceptable solution to the problem of fan blade resonance. The gearbox diameter of 3.70" is 58% of fan tip diameter.

At zero incidence with the motor off the oil level in the gearbox was just above the driven gear, leaving the majority of the driving gear exposed. For high positive incidences extra oil was added. This method gave adequate lubrication and heat transfer without undue churning losses. Molybdenised oil of S.A.E.20 grade was used. Both shafts could be adjusted axially to correct the backlash of the gears.

Cooling calculations proved difficult owing to the three dimensional nature of the problem and the awkward shapes involved. The makers quoted 96% efficiency for their spiral level gears but this was thought to be optimistic and 90% was used in calculations. Calculation of the heat transferred through the idealised outer cylinder of the gearbox to the duct flow gave an estimated temperature rise within the gearbox of 170°C for equilibrium. In practice 130°C was measured using a thermocouple. The difference probably combines the effects of axial heat flow, possible higher gear efficiency and the fact that power consumed was less than the total rating. The gearbox temperature fell as the gears became run-in. As a general safety measure the oil level in the gearbox was checked frequently and running times were kept down to 20 minutes where possible. However little oil replenishment was found to be necessary and runs of 40 minutes were made without difficulty.

3.3 Vibrations and Resonances. (See table 2)

Because imposed frequencies as high as 7 kc/s were present in the rig it was necessary to conduct a careful survey of the natural frequencies of the major moving parts. In addition shaft whirling speeds had to be estimated.

Design philosophy was based on keeping most of the fundamental frequencies above the rotational frequency of 400 c/s. Care was taken that no third harmonics coincided with the higher imposed frequencies. A resonance was noticed between 5,000 and 6,000 R.P.M during commissioning at R.A.E. Bedford when the fan blade fundamental bending mode was excited. During tests at Imperial College no troubles of this description were encountered because speed was not variable and start up and shut down were very rapid. The motor speed reached 23,200 R.P.M in about a second.

An aspect of particular importance is the whirling speed of the motor shaft. Because of the motor length and the cantilevered gear this tended to be low. The diameter of the shaft had to be increased above that of the original design in order to raise the whirling speed above the rotational speed. This fact accounts for the presence of the rather thick drive shaft in the duct. Because of the small difference between the rotational and whirling speeds and the unknown amounts of constraint and damping, the calculation was checked independently.

As mentioned in the previous chapter the fan blades were tapered slightly in order to raise their natural frequency in bending.

Calculations for five parallel blades gave a fundamental of about 1600 c/s which is the frequency at which one fan blade passes the wakes of the four centrebody supports. Taper in thickness and planform raised the bending fundamental to 2100 c/s.

The rotating parts were dynamically balanced to a standard similar to that applied to aircraft cold air units which rotate at 36,000 R.P.M. The need for careful assembly was emphasised by a trial calculation which showed that the omission of one gear key (on a 5/8" dia. shaft) could produce a rotating force of about 25 lbs. Parts were therefore carefully marked before final assembly.

3.4. Detail Design

The forebody and duct section are castings in aluminium alloy, the afterbody being a simple fibreglass shell. The stator is mounted between webs in the forebody with the rotor between angular contact ball races fitted into housings which are part of the model. This type of bearing requires a spring preload to hold the balls against their seats. The general assembly drawing shows the sets of coil springs which tension the fan- and motor-shafts in order to preload both sets of bearings. The front motor bearing and the lower fan shaft bearing are permitted to float axially in order to achieve this effect. Thermocouples were fitted to all bearings and in the gear-box while commissioning the model.

It was arranged that the motor shaft and the centrebody assembly could be removed from the model independently of each other. This involved fitting a removable seal plate which passes through the stator when the motor shaft is withdrawn. The seals are of the rubbing type made from 'Gaco' flexible plastic. They run near to their maximum allowable rubbing speed and have proved effective and reliable.

Due to its high circulation the 7/8" diameter drive shaft would have produced more than 1 lb side force if left exposed to the duct stream. A shroud was therefore fitted round the shaft which prevented the associated flow distortions which otherwise would have resulted.

The fan was made from an aluminium alloy casting, the blades being profiled on a copying and reducing machine. Stressing for fatigue was necessary since $1\frac{1}{2}$ million revolutions occur per hour of running. Pessimistic loading assumptions for the tapered blade gave an upper surface peak compressive stress of about 8,000 lbs/in^2 and a lower surface peak tensile stress of about 3,300 lbs/in^2, chiefly due to bending. As the quoted limit for long life in LM6 is about 7,000 lbs/in^2 it can be seen that the thinner root of the parallel blade design would have been inadmissible due to fatigue limitation, as well as on a natural frequency basis. Metal-to-metal tip clearance was approximately .008". This was further reduced by applying coats of paint to the duct wall.

3.5 <u>The design of the test rig</u>.

The model was suspended from the three component balance in the 5' x 4' wind tunnel at Imperial College, using the standard tunnel struts. These engaged either wing cleats or the cylindrical support struts shown in Figure 3.1. This figure shows slender lower struts which were later replaced by a stiffer version. Bracing wires were also added which decreased the amplitude of sideways oscillations due to buffeting which occured with the fan and tunnel running.

Because undesirable interference effects have been reported between strut guards and wings, no guards were used. The resulting high strut drag values were less significant than usual since force increments were required from the present tests. Strut drag tests were performed with a cylinder, similar to the body support cylinders, spanning the struts. At 100 ft/sec with the body on struts at zero incidence 15 lbs of drag measured with fan on included 5.75 lbs of strut drag. The cylinder was removed for the determination of the strut correction appropriate to the body-on-wing case. For fan-off tests covers could be fitted flush at boths ends of the duct which were sealed with 'Selotape'.

Static thrust tests were conducted with the jet pointing through an 18" diameter hole in the tunnel floor. All possible doors and windows were left open in order to reduce further the adverse effect on lift of flow recirculation. (See Figure 3.3)

Three high purity aluminium wires arranged as in Figure 3.1 served both as tail wires and power supply wires. Power was fed to their outer ends by long free-hanging cables which gave negligible balance constraint. Because currents could be as high as 60 amps for the on-line start, wires of 0.10" diameter were needed. Running currents were between 15 and 20 amps at 160 line volts and 400 c/s (nominal).

3.6 Probes for duct flow investigation

Pitot-static investigation of the duct were carried out half-way between inlet and outlet using three radial rakes of tubes. These were attached to the straightener ring which could be rotated during a traverse. A small reversible electric motor drove a worm which engaged the ends of the straightener blades and thus rotated the rakes. (See Figure 3.4) The worm shaft was also geared to a ten turn helical potentiometer which gave remote indication of the angular position of the traverse gear. Twenty three plastic tubes left the model through a 1" diameter cylinder suspended below the duct. (See Figure 3.3)

As the fan drive shaft was in the plane of the traverse the three rakes were given unequal angular spacing, so that the drive shaft occupies at 140° interval between rakes, the other two spaces being 110°. In this way uniform coverage can be obtained without duplicating readings at the ends of the traverse.

Five total head tubes were spaced so as to represent equal annular areas. Static tubes were mounted between each of the inner and outer pairs of total head tubes. Four static pressure holes in the duct wall enabled the readings of the outer static probes to be checked.

Because of the swirl present between the fan and the straighteners all tubes were inclined at 15° to the axial direction. Errors in alignment which resulted are discussed in Section 4.2.

4. THE SCOPE, MEASUREMENT AND REDUCTION OF DATA

4.1 Test procedure and scope

Table 3 summarises the tests which were performed at Imperial College and at R.A.E. Farnborough during 1961 and 1962. The former tests were made at constant incidence, which avoided changes of balance zeroes during a run. At Farnborough the tunnel speed took too long to settle for this to be convenient. The absence of data at 100 ft/sec in the R.A.E. tests is due to a tunnel resonance at this speed. The model fan ran at approximately 23,000 RPM in all tests.

For the first test series it was possible to work single handed. The model fan was switched on as the tunnel speed approached its test value. Tests were made at even hundreds of tunnel fan RPM. It was found that measurement of lift, drag and pitching moment at six forward speeds took 10 to 15 minutes. Zeroes were checked after each run. For some tests it was found necessary to run the tunnel and model fans before taking an initial zero in order to achieve repeatability of pitching moment zeroes.

Although power measurement and speed control were added for the R.A.E. tests the time per run was similar since three people took part.

In the third group of tests measurements were made of forces, model power and speed, tunnel speed and duct flow at one speed and incidence in 6 to 10 minutes, care being taken to ensure that the manometer readings had settled. One operator took photographs of the manometer for various rake positions, and controlled the traverse gear, while the author made the remaining measurements. As the films of manometer photographs were to be read automatically special care was taken with the photography. (See the following sections)

4.2 Methods of measurement (Imperial College results)

Force measurements were made using the overhead three-component balance. Zeroes were recorded before and after every run. The pitching moment balance was less reliable than the force balances. In the third series of tests forces were measured with the traversing rakes in the same position every time.

Tunnel speed was determined from the pressure drop across the tunnel contraction indicated by a Betz manometer. A vertical rake of pitot and static tubes showed no change in centreline distributions upstream of the model when the model fan was run. However tunnel RPM for a given working section speed changed considerably if model incidence was changed with fan on.

Fan R.P.M. Since fan thrust depends on the square of model fan R.P.M. this must be held constant and measured accurately. For the first series of tests the supply frequency was fixed and the variation of speed with load was assumed small. Subsequent checks justified this assumption, the speed variation over the range of test parameters being less than $\frac{1}{4}$%.

Variable input frequency on the Farnborough rig made close speed control necessary. Most speed measurements were made by measuring the frequency of the fan noise, which produced a substantial signal from a microphone placed in the tunnel roof above the model. Since the 2 kc/s fan blade frequency was combined with a strong 4 kc/s component, the signal from the microphone was fed to an oscilloscope where the output from an oscillator was arranged to form a Lissajous figure. The oscillator frequency was then measured using a counter. The results obtained agreed with those given by a stroboscope. When fine speed control was available at R.A.E. it was found possible to adjust the fan speed to give a noise frequency within 1 or 2 c/s of the 1950 c/s standard.

Power Input to Fans. The "two wattmeter" method was employed at Imperial College, though in fact a single wattmeter with a change-over switch sufficed. In a few tests voltage and current were also measured in order to estimate the power factor of the motor.

Duct Flow Investigation. (See Figure 4.3)

With the traverse gear described in Chapter 3 it was possible to make 165 total head and 66 static head measurements between the fan and straighteners at a plane half way down the duct. By this choice of traverse plane difficulties due to the presence of wakes were reduced. This was important because automatic data reduction was to be employed. (See 4.3)

Because of the swirl in the flow behind the fan it was necessary to incline the pitot and static tubes at 15° to the axial direction.

Calculated misalignment was $\pm 3^{\circ}$ for the end tubes, giving acceptable accuracy. The effect of changes of forward speed and incidence on flow direction is not known but the measurements by Gregory (1962) indicate that errors of significant sizes are likely to be confined to relatively small areas.

Pressure tubes from the model were lead to a vertical multi-tube manometer containing Carbon Tetrachloride. Special scales were attached which were used during data reduction. After considerable experiment the photographic and alignment details of Table 4 were developed. Calibration marks which reduced to 0.002" on the 35 mm negative were sharply defined. Further details are given in 4.3.3.

Photographs of 15 total and 8 static pressure manometer readings were taken at 10° intervals (See Figure 4.3), giving 11 frames of film for each of 35 test conditions. This was repeated for two configurations.

4.3 Methods of data reduction

With the exception of strut-drag corrections to fan-off data no wind tunnel corrections of any kind were applied (see 2.4, 5.2 and Chapter 7)

4.3.1. Reduction of forces and moments

Measurement of Lift, Drag and Pitching Moment were made at the incidences of Table 3 both with the duct ends sealed and with the fan running, wind tunnel R.P.M and reference pressure being noted throughout.

Required quantities are increments of measured forces and moment due to fan operation under various conditions. The formation of dimensionless groups will be discussed in the section which follows. In order to find the increments the

Fan-off forces are needed which correspond to the forward speed in the appropriate Fan-on condition.

Reduction may be based either on tunnel R.P.M readings or on reference pressure, both of which were calibrated against the centreline velocity upstream of the model. The former gives Fan-off forces at the Reynolds number corresponding to the Fan-on case. In the absence of large Reynolds No effects a comparison of forces ~~on an E.A.S basis~~ at the same dynamic head is sufficient, as in the present case. It is necessary to bear in mind the possibility of a change in tunnel calibration factor if reference pressures are used. However for the present tests the errors due to assuming constant calibration factor turned out to be less than 1% of fan static thrust. This implies that fan-off forces may be plotted against reference pressure and the forces corresponding to the fan-on case determined from the fan-on reference pressure directly.

The calculations for the body-on-struts case (first test series) were performed using both this and the true airspeed method and the agreement was satisfactory.

4.3.2 Calculation of Jet Velocity Ratio

A dominant parameter in the present work is the ratio of mainstream velocity to jet velocity. (See equations 4.3 and 4.4) This is also important because it is the main parameter by which the development of the jet plume may be described.

For the tests of Chapters 7 and 8 mean jet velocity was measured and a genuine velocity ratio could be formed. For tests in which no jet velocity was available, the nominal duct efflux velocity is frequently used as in Equation 4.4. In this case either the static thrust must be measured for each test or the true tunnel velocity must be determined. This is necessary because the fan runs at constant RPM and the equivalent airspeed of the jet, and the static lift, alter with ambient conditions.

As before either tunnel fan RPM or reference pressure may be used in reduction, since tunnel velocity calibrations were made in terms of both of these quantities. The reference pressure was used in preference to tunnel RPM firstly because it was a 'speed squared' measurement and secondly because it was not easy to obtain exact tunnel R.P.M settings because of an insensitive control. Checks showed fair agreement between the two methods.

4.3.3 Reduction of duct flow measurements using the Film Reader (See Figures 4.1 and 4.2)

In the previous section the need for measurements of both mass and momentum flux is made apparent. As the distribution of velocity changes with forward speed and incidence it is not possible to calibrate the duct in any simple manner. Because of this a data processing device was made which could read and integrate the data contained on manometer photographs. The principle of operation will now be described.

Consider a rake of pitot and static tubes which is connected to a multitube manometer traversed so that each point investigated represents the same area normal to the flow. The ~~sum is~~ summations are required of local static and total heads, local velocities and functions of local velocity required in boundary layer or statistical calculations.

Special scales are attached to the manometer which have alternate black and white divisions spaced according to the required functions. One scale is needed for each function. A series of photographs is taken with the rake at equally spaced positions, the tubes and scales being parallel to the length of the film.

After development the whole negative film is placed in the reader in which an image is projected onto a screen. (See Figure 4.1) The image moves continuously in a horizontal direction, the top of the manometer appearing first. A photosensitive cell placed in line with the image of a tube reading static pressure gives an increase in output when the lighter image of the manometer liquid is reached. For linear measurements this signal is used to start a counter fed by pulses from a photocell which reads the linear scale. The count is stopped by a signal from a photocell placed opposite to the image of the appropriate total head tube and is displayed on a counter.

For non-linear scales it is necessary to allow for the variation of zero point, due to the presence of differing static pressures on one photograph. A 'transfer counter' is used in the manner illustrated by Figure 4.2. This figure gives the sequence of operations used to read one pair of tubes on one frame.

Integration is carried out by allowing the output counter to sum the signals from every frame. The process is repeated for each pair of manometer tubes and is made easier by using a continuous loop of film. The integration of each scale quantity is carried out separately. The results of checks on the accuracy and repeatability of the reader are given in Appendix 3.

<u>Application of the reader to the results of Chapters 7 & 8 (See Figure 4.3)</u>

For the determination of the sums of local velocities and their powers the readings of the outer three total head tubes were subtracted from that of the outer static tube. The readings of the two inner total tubes were combined with those of the inner static tube. The use of only two static tubes in the rake assumed small variation of static pressure along any radius. Experiment showed that the assumption was justified.

Unfortunately the static tubes of rake 2 were damaged early in the test series. Wall static pressures have been used in this region. The following quantities were summed over the duct

(i) to (iv) local velocity, its square, cube and fourth powers,

(v) total head, measured above atmospheric pressure.

The sums were determined for the 35 speed/incidence combinations and two configurations given in Table 3.

No rake calibration corrections were applied since these were within approximately 1% of each other, which is comparable with the probable errors due to flow misalignment.

4.4 Reduction Parameters

The presence of the fan-mainstream interaction and induced circulation over the forebody, as well as the sink effects around the emerging jet, makes the choice of reduction parameters difficult.

The ratio of forward speed to fan tip or jet velocity is a fairly obvious speed parameter. Because of the differing natures of the effects which combine to give the nett incremental forces, a compromise is likely to result when this reduction parameter is chosen. Consideration must also be given to possible experimental difficulties in the determination of certain parameters, particularly those associated with the duct flow.

Table 5 gives three alternative systems which will now be discussed in turn.

(a) Reduction using duct flow quantities

For non-uniform duct flow, in the absence of external interference:-

$$\Delta L = \rho A_J \overline{V_J^2} \cos \alpha \qquad \ldots 4.1$$

$$\Delta D = \rho A_J \overline{V}_J V + \rho A_J \overline{V_J^2} \sin \alpha \qquad \ldots 4.2$$

giving the dimensionless groups-:

$$\frac{\Delta L}{\rho A_J \overline{V_J^2}} = \cos \alpha \quad \text{and} \quad \frac{\Delta D}{\rho A_J \overline{V_J^2}} = \frac{V}{\overline{V}_J} + \frac{\overline{V_J^2}}{\overline{V}_J^2} \sin \alpha \qquad \ldots 4.3$$

The mean velocity parameter has been used for the drag increment because at low incidence the inlet momentum term dominates the equation. Since incremental moments are strongly dependent on the moment of intake momentum, the mean velocity parameter is appropriate here too.

The duct flow measurements described in Chapter 7 were originally intended for use on the above basis. However it was found that large interference forces were present which obscured the effects caused by changes in duct conditions.

(b) Reduction on the basis of installed static lift T and nominal efflux velocity V_{J_T}

This approach was used both in the author's preliminary report and by Trebble and Hackett (1963). The nominal efflux velocity is defined by the equation $T = \rho A_J V_{J_T}^2$, where A_J is the fan annulus area, the equations corresponding to 4.3 are:-

$$\frac{\Delta L}{T} = \cos \alpha \quad \text{and} \quad \frac{\Delta D}{T} = \frac{V}{V_{J_T}} + \sin \alpha \qquad \ldots 4.4$$

It can be seen that experimental momentum drag will be greater than that of 4.4 since the increase in jet velocity has not been taken into account. Although the method is convenient and readily applied, difficulties can arise if tunnel interference affects the measured static lift. (See 6.3) Because of this comparison of forces measured in the 5' x 4' and 11½' x 8½' tunnels has been made on the basis of fan tip speed parameters. (See 7.6)

(c) Reduction using fan tip speed parameters

As rotational speed can be measured accurately and since the model dimensions are known, these groups are least susceptable to experimental error. As before no allowance is made for interaction or interference. However the system is compatible with that usually employed in fan performance calculations and automatically compensates for experimental variations in fan R.P.M.

5. INVESTIGATION OF FLOW PAST THE MODEL

5.1 Surface flows with the duct sealed

Surface flow patterns were produced using 'Dayglo' pigment and paraffin and illuminating the model with ultra-violet light after the stream had dried off most of the paraffin. (See Maltby and Keating (1960)) Tests were made with the main duct sealed at both ends and included an investigation of the effect of a transition wire and of the flow pattern changes due to the motor cooling system.

As the model had a good surface finish laminar flow was maintained at zero incidence as far back as the plane of the motor cooling outlet for all forward speeds. Here the emerging cooling air and the raised shoulders ahead of the main duct caused transition to turbulent flow. (The highest test speed was 140 ft/sec, giving $Re_l = 3 \times 10^6$. Transition caused by model geometry at $Re_x = 0.9 \times 10^6$). At high incidences a small separation bubble appeared on the top lip of the cooling intake, giving rise to a turbulent boundary layer over the top of the body. This improved the flow pattern just ahead of the main duct inlet.

Figure 5.1 shows side views of the model on struts at zero incidence with and without the transition wire. It was found difficult to promote transition at positions ahead of the wire shown. Since the transition wire affected the flow pattern only as far back as the cooling outlet, its use was discontinued.

By taping up one cooling outlet interference effects could be demonstrated. The smooth flow over the side of the body was then interrupted only by the wake of the support struts. Figure 5.2 shows that for the winged configuration some alleviation of the root stall occurred at the side with the cooling outlet left open. The effect was similar with both outlets uncovered. It seems probable that the cooling air delayed the root stall by acting as a fillet. No attempt was made to optimise the small plasticene fillets employed.

It can be seen from Figure 5.3(a) that the surface flow pattern with the body on struts at high incidence resemble those of similar axisymmetric bodies. (See Thwaites (1960) and Werlé (1960)) The use of a tuft wand at positive incidences showed additional vortices springing from the edges of the flat areas round the main inlet. (Which was sealed)

At zero incidence the flow over the wings was nearly all laminar and spanwise flow associated with root effects was present. During natural transition ahead of the trailing edge surface streamlines kinked back towards the mainstream direction. Figure 5.3(b) shows a region of reversed flow associated with the wing stall.

5.2. Flow observations with the fan operating

5.2.1 Flow into the duct

As explained in 2.2 a 20% radius on the forward side of the intake decreased steadily to 6% of jet diameter, at the sides and rear of the duct. The Dayglo and paraffin technique gave indistinct patterns on the lips and inside the duct entry. However the discernable features were consistent with a record of unsteady manometer tubes kept during the pitot-static traverses of Chapter 7.

Figure 5.4 summarises the observations of oscillating manometer readings. The shaded areas should not be interpreted as regions of separated flow. The total head tubes, approximately 0.10" from the outer wall, 4" down the duct, showed only small oscillations about a mean little lower than the readings of adjacent tubes. It maybe inferred that, half way down the duct, reversed flow regions could have occupied a maximum of 2% of the duct cross-sectional area. Tuft observations showed no separations on the radiused lip. Paraffin techniques indicated small separated regions just beyond the end of the radius at the positions indicated in Figure 5.4.

The very small separations present would probably have been avoided if lip radii had been larger in the regions 45° each side of the forward centreline. The upstream lip radius was adequate.

5.2.2 The development of the jet plume

This sub-section deals with medium and high forward speeds. The low-speed cases, in which tunnel floor effects were large, are discussed in Section 5.3. In order to avoid confusion with the wing vortex system, observations were limited to the case with the body on struts.

Jordinson (1958) shows that as a round jet emerges normally from a flat plate into a stream it is bent over, its cross section being distorted into a kidney-- and then into a horseshoe-shape. Figure 5.5(a) shows the downstream cross-section of the jet produced by the present model. The picture was taken using a "smoke screen" technique with the light slit approximately 6.2 diameters downstream of the jet exit. A small canister, suspended inside the wind tunnel ahead of the model supplied the smoke, which all passed through the duct, almost filling it. The "smoke screen" technique and the canisters are described by Maltby and Keating (1960). The image of the model was produced by switching on the tunnel lights for a brief period during the 10 seconds exposure required to photograph the smoke. Even with the tunnel speed almost half that of the jet, the plume approaches floor level at this section.

The tuft photographs of Figure 5.6, taken from the downstream side of the grid, indicate flow directions at a cross-section 4.2 diameters downstream of the jet exit. (See also Figures 5.7 and 5.8). At the lower tunnel speeds of Figures 5.6(a) and (b) patterns indicating a vortex pair can be seen. Vortex motion was also observed while taking the smoke photographs. The vortex on the left-hand side of the tuft pictures is less clearly defined. Figure 5.11 (b) indicates that this vortex may have been weaker, probably due to assymetry caused by the drive-shaft wake. (See Figure 7.2) The fact that the camera was mounted off-centre may also have made the left hand vortex less obvious. Figure 5.6 (d) indicates the tuft positions with the model fan switched off.

Figures 5.7 and 5.8 are sketches which combine information obtained from earlier photographs. The edge of the region of disturbed flow in Figure 5.7 is adequately clear of the floor only in the high forward speed case. It appears likely that the path and shape of the plume in the other cases is distorted by floor constraint. Unfortunately no similar observations were made in the R.A.E. $11\frac{1}{2}'$ x $8\frac{1}{2}'$ tunnel to confirm this.

A possible plume structure, deduced from the limited flow observations above, will now be described. The edges of a viscous jet directed downwards in still air may be represented by a series of co-axial vortex rings. As the speed of a horizontal mainstream is increased the downstream sides of the vortex rings are carried away, leaving a trailing vortex system. The process is analogous to vortex shedding by an accelerating wing. Figure 5.8 shows the resulting flow structure in which the vortex sheet towards the back of the jet rolls up as it is stretched and convected downstream to form the vortex pair of Figures 5.5 to 5.7.

As the presence of downstream vortices was demonstrated for most test conditions, it is useful to consider further their possible upstream origins. In the development above it is implied that the upstream elementary vortices remain wrapped around the front of the jet cylinder. A further possibility is that some vortices may end at a model surface, rather than loop within the fluid. The surface flow patterns, described in the section which follows, showed the extent of vortex rooting on the model.

5.2.3. Surface flows due to the jet

In the previous section the development of the vortex pair was described. In addition to the associated downwash field over the rear of the body, local effects existed near the jet which combined the flow around the jet cylinder with suctions due to mixing. The flow characteristics around the front of the jet in Figure 5.9(c) are similar to those to be expected on the equivalent cylinder-body junction. However the flow to the rear was strongly affected by jet suction since it was shielded from the mainstream. This was particularly marked with underfins added which delayed closure of the mainstream behind the jet. (Note the reversed flow on the inside of the fins in Figure 5.14(c))

The Forward Speed Effects

The flow patterns produced at zero incidence (Figure 5.9) show a general resemblance to the corresponding patterns around a jet issuing normally from a flat plate. (See Wood (1963)) Comparison in Figures 5.9, 5.12 and 5.13 between the medium and high forward speed cases shows that the local influence of jet suction was only slightly less marked at the higher mainstream speed. In regions of the afterbody less subject to local jet-suction effects the surface flow angles varied little with forward speed. Since clearance between the jet and the body decreased with forward speed it may therefore be inferred that there was a simultaneous reduction in the strengths of the vortices. It can be seen from Figure 5.6 that the vortex helix angles decreased as forward speed increased.

The Incidence Effects

(a) body on struts

Figure 5.10 illustrates that at negative incidences the flow patterns become more complicated, particularly at the lower forward speeds. Because of difficulties in obtaining good photographs of the flow patterns for speeds below 80 ft/sec*, a careful sketch was drawn for a typical condition. (Figure 5.10(c)). Five singular points could be seen in the vicinity of the jet at 75 ft/sec tunnel speed and -20° incidence. When the paraffin was still wet the small vortices near the jet were seen to be rotating in the directions which correspond to positive lift on the model. Oil seeping from the gearbox over the centrebody showed small vortex roots there too. However these may have been associated with a separation bubble on the centrebody. It is thought that small vortices may also extend a short way up inside the duct. The saddle points denoted in Figure 5.10(c) are also apparent in Figures 5.10 (a) and (b) and 5.9 (c). Slight indications of vortex rooting are also present in the latter.

At high positive incidences there was extensive vortex rooting behind the jet at all forward speeds at which patterns could be

---

* At negative incidences paraffin tended to accumulate in the region of interest behind the jet, where surface velocities tended to be low anyway. This made the drying time unacceptably long.

Because larger gravity effects were present extra care was required in the interpretation of these flow patterns.

produced. (See Figure 5.11) However force measurements showed that the patterns were accompanied by tunnel constraint forces. (See Section 6.5) Unfortunately no visualisation was carried out at RAE which might have indicated whether tunnel effect was solely responsible or not. The asymmetry of Figure 5.11 is probably associated with the fact that, due to distortion between the fan and the straighteners, the drive shaft wake was off-centre. (See Figure 6.5) Tests with one cooling outlet sealed showed little change in the vortex pattern behind the jet.

(b) <u>body on wings</u>

As in the case above flow patterns were affected more by changes in incidence than in forward speed. (Compare the difference between Figure 5.13(a) and 5.12(b) with the differences between the other photographs of Figure 5.12) It can be seen that the flow close to the sides of the jet is similar to that with the body on struts.

At zero incidence patterns with and without wings were very similar. At positive incidences flow behind the jet closed more readily, probably due to positive pressures below the wing. Simple flow patterns resulted right up to +20° incidence. (Compare Figure 5.12(e) with 5.11(b)) The reversed flow region above the wing of Figure 5.12(e) resembles that with the fan off in Figure 5.3(b).

When the wing stalled negatively parts of the body in its wake became strongly affected by jet suction. Figure 5.12(a) shows that there was extensive reversed flow behind the jet at -20° incidence. (c.f. Figure 5.10(a))

(c) <u>Surface flows on underfins (Figure 5.14)</u>

In view of their beneficial effect on lift under forward speed conditions (see Chapter 7.) flow over the perspex underfins was investigated.

It was found that with the fan off and the duct sealed at zero incidence the flow over the fins was uniform on both sides with no bubbles or edge separations.

With the fan on surface flow patterns showed that the sides of the jet became attached to the inside of the fins. This caused mainstream air to be deflected downwards between the fins, (See Figure 5.14(b)) leaving a region of slow moving air on the undersurface of the body just ahead of the jet.

Figure 5.14(c) was obtained by allowing the pigment in paraffin applied to the outside of the fins to be carried to the cleaned inner surface. The outside pattern was then rubbed off. The reversed flow region on the fins behind the jet is demonstrated. There was a corresponding reversed flow region on the body, with saddle points but no vortex roots.

An edge vortex outside the lower edge of the fin can be seen in Figure 5.14(a) which was not obvious at zero and negative incidences. Although no evidence is available to support the view, it seems likely that this became an alternative starting point for the vortex system found earlier. (See 5.2.2) If this was so the displacement of the trailing vortices away from body surfaces could have reduced adverse downwash effects.

5.3 <u>Interaction between the jet and the 5' x 4' wind tunnel</u>

As mentioned in 2.4.2 corrections applicable to lifting wings cannot be used in the present case. No suitable mathematical model yet exists which represents the jet plume as described in 5.2.2.

Upstream static pressure measurements and floor wool tuft observations were made over the range of test parameters. These gave indications of conditions under which the flow near the model might be noticably different from that in free air. Later tests in the RAE $11\frac{1}{2}'$ x $8\frac{1}{2}'$ tunnel allowed the corresponding changes in forces and moment to be estimated. (See section 7.6)

The overall picture of conditions in the smaller tunnel will now be described. At low forward speeds stagnation occurred when the jet hit the tunnel floor and a region of separated flow there increased in extent as the model incidence was raised. This accompanied a rise in static pressure at the standard tunnel static holes at the beginning of the working section. The effect was superimposed on an existing pressure gradient present due to lack of area compensation for tunnel boundary layers. Except in the floor stagnation cases the size of this gradient was reduced by fan operation. As the pressure rise was only a few millimeters of water the resulting horizontal buoyancy forces on the model were small. However Figure 5.15 shows that the static pressure rise due to fan operation was a large proportion of tunnel dynamic pressure and was strongly related to the extent of separation on the tunnel floor.

As forward speed increased floor stagnation disappeared but the static pressure rise ahead of the model continued to increase. However the forces on the model due to changes in pressure gradient were still less than 1% of fan static lift. It is apparent that local effects caused by floor stagnation at low forward speeds are more significant than the longitudinal pressure gradient . A rise in static pressure below the forebody may be expected to increase all the measured increments at positive incidences. The extent of the floor separation (Figure 5.15) corresponds closely to differences between increments measured in the 5' x 4' and $11\frac{1}{2}$' x $8\frac{1}{2}$' tunnels.

Although at the lowest tunnel speed only 6% of the working section flow passed through the model, the rate of flux of kinetic energy was $2\frac{1}{2}$ times that through the tunnel working section. The drag caused by removing horizontal momentum from the stream was equivalent to a model having $C_D A = 0.3\ {}^{V_J}/_{V}$, giving an increase in tunnel power factor of 0.07 at ${}^{V}/_{V_J} = 0.20$. It is unlikely that this would cause serious trouble at the tunnel fan or in the return circuit. With the tunnel fan set at 400 RPM the working section velocity was 40 ft/sec. Switching on the model fan reduced this to 30 ft/sec approximately. The corresponding effects at 1400 RPM are illustrated in Figure 5.16.

The solid blockage effect of the model alone gave calculated local velocity increases of about $\frac{1}{2}$% which rose to almost 1% when a jet cylinder extending to the floor was assumed. Because the volume and shape of the jet plume were variable and unknown in general, no attempt could be made to estimate wake blockage.

Fortunately the tunnel calibration factor was little changed by fan operation (see Figure 5.16) and pitot-static rake measurements on a vertical centreline ahead of the model showed the same uniformity of flow fan-on as fan-off.

6. FAN-OFF TEST RESULTS AND STATIC PROPERTIES OF THE FAN

6.1 Introduction

Before examining the interaction between fan- and model aerodynamics and the effects of the jet plume, it is desirable to establish the respective base conditions upon which these interactions are superimposed. This chapter therefore deals with characteristics of the model fan and the free-stream acting separately. For the fan-off tests both ends of the duct were sealed with flush covers.

6.2 Tests with fan off

The main purpose of these tests was to determine the base condition above which force increments due to fan operation could be measured.

Figures 6.1 to 6.3 show the fan-off force characteristics of the model for all test configurations except those in which wing datum angle was varied. No tunnel corrections have been applied, though strut drags have been subtracted.

The effect of a transition wire

Since Reynolds Numbers between 10^5 and 10^6, at which transition is likely to occur naturally, imply a movement of the transition line over the forward part of the body of the model within the range of test speeds, a transition wire was considered. Later flow visualisation showed that the transition point was fixed by model geometry (see Chapter 5). The use of the wire was therefore discontinued.

The lift and pitching moment coefficients were hardly affected by the wire. The drag coefficient was increased on average by about 10%.

The drag of the motor cooling system

Cooling air which enters the nose of the model through area A_c and which has free-stream total head, is ultimately ejected with only transverse momentum. The theoretical incremental drag coefficient is therefore $2A_c/A_{REF}$. In practice this is modified by interference effect both at inlet and at exit.

In order to determine the cooling penalty with the body on struts and fan duct sealed, drag measurements were made with a nose-cap fitted and with the cooling exit taped over. It was found that at zero incidence there was negligible change in drag when the cooling duct was opened. At 20° incidence there was additional drag of about two third of the value predicted above. (See comments concerning flow pattern in Chapter 5).

These findings imply favourable interference between the cooling system and the body on struts.

Drag with the fan duct open, fan off

The following incremental drag coefficients, based on body area, were found to vary little between 40 and 160 ft/sec.

	Increases in C_D		Open side facing
	$\alpha=0°$	$\|\alpha\|=20°$	
First cover removed	0.04	0.06	rearwards
		0.02	forwards
Second cover removed	0.05	no measurements due to buffet.	

6.3 Some properties of the fan at zero forward speed

The results of static lift measurements (See Table 6)

Early static lift readings with the body on struts were more than 1lb lower than the design value, even though all the doors and windows of the 5' x 4' tunnel had been opened. (The tunnel floor was 3.2 diameters below the jet exit.) Inclining the model to ±20° incidence did little to reduce the recirculation and ground effect which probably caused the deficit. An 18" diameter hole was therefore cut in the tunnel floor to allow the jet to escape. The static lift with the body on struts was then close to the predicted value.

Table 6 shows that, according to measurements made at Imperial College, the presence of wings reduced the static lift by nearly 2%, probably due to ground effect. This agrees with similar measurements by Wyatt (1961). The addition of underfins caused a further reduction of about 4%.

The static lift results of the third series of tests show the effects of successively adding the traverse rakes and pressure tubes to the plain body configuration tested earlier. The apparently large reduction in static lift caused by adding the plastic pressure tubes is probably mainly caused by the impingement of the jet on the tubes which were carried laterally to the manometer. (See Figure 3.3). The effect could not occur with the floor closed in the forward speed cases.

Table 6 includes values of the thrust coefficient $T/\rho(\Omega R)^2 A_j$ obtained from measurements in the 5' x 4' and $11\frac{1}{2}$' x $8\frac{1}{2}$' tunnels with closed and with vented working sections for the body on struts.

Bearing in mind the greater distance to the floor and the longer recirculation path, one would expect the thrust coefficient in the closed working section of the larger tunnel to be close to the vented value in either tunnel. While the observed agreement between the vented tunnel results is to be expected, it is difficult to explain the change due to closing the larger tunnel. Possibly the complete absence of wall venting was in some way responsible.

It is clear that when measuring static lift great care is necessary to vent the working section adequately. Because of the above unexplained features, fan tip-speed parameters have been used to reduce force increments for comparisons between the two tunnels in Chapter 7.

Measurements in the duct

With the single exception of the exit traverse at zero forward speed (Figure 6.5), all flow measurements were made at the central plane. Here two factors complicate the reduction and interpretation of data:-

(i) Measurements were in a flow with distributed swirl. Although tube readings were probably little affected (see 3.5) the additional assumption when reducing data, that swirl was constant at 15° probably resulted in an underestimate of boss velocities and an overestimate of velocities near the duct wall. The overall error which resulted was probably small since the errors at the extremes are likely to be only 1%.

(ii) The smoothing effect of the fan, described in Appendix IV, caused disturbance velocities due to forward speed effects to become small compared with those caused by the fan drive shaft shroud, which was in the traverse plane. Had the traverse been made any further upstream then tube readings would have been suspect because of the proximity of the fan. Wallis (1961) Page 294, shows that unless the traverse plane is carefully chosen, false high values of total head rise coefficient will be indicated by the probes. This is due to mixing losses within the blade wakes and to intermittency effects. Figure 6.6 shows that this difficulty has probably been avoided.

Figures 6.4 and 6.5 show the distribution of axial velocity at the central and exit planes respectively. The uniformity of the flow in the central plane is good away from the drive shaft, which also creates a large wake at the exit plane. The rotation and twisting of this wake between the central plane and the straighteners is close to that predicted using design figures.

At the exit plane static pressure decreased from atmospheric at the edge of the jet to about 1" water suction near the centrebody ($C_p \simeq -0.10$). No residual swirl could be seen using a tuft grid though, on the basis of calculations made after completion of testing up to 5° underturning might be expected.

The static pressure indicated by both wall holes and the static probes at the central plane was atmospheric, showing that the diffuser and straightener pressure rises were nullified by losses.

<u>The calculated Total Pressure rise characteristic</u>

The method given by Wallis (1961) has been used to determine the theoretical mean total head rise coefficients for the experimental range of jet velocities. Calculations were performed for five radii using design blade angles and included allowances for profile and secondary losses not taken into account in the original design. Tip losses were considered negligible (see 3.4). The calculated radial distribution of lift coefficient and total head rise coefficient are given in Figure 6.6.

Experimental points added to Figure 6.6 show that the measured total head rise coefficients were slightly low. This may be because fan blade angles were below the design values. Measurements showed a probability of $\frac{1}{2}^{\circ}$ difference from design values but were not sufficiently reliable for use in calculations because of a slight bow on the undersurface which caused uncertainty.

Figure 6.6 shows the change in mean radial total head distribution between the central and exit planes. The drop in total head beneath the blade tip is thought to be due to an accumulation of blade and duct boundary layer air, rather than tip loss, since tip clearance is small. A tip Mach number of 0.6 should give no drag rise penalty and a lift coefficient expected to be 0.6 should not cause stalling.

<u>The calculation of static lift from flow measurements</u>

Integration of flow quantities over the central and exit planes yielded the following results:-

Gross Thrust computed from total head and mass flow measurements at the central plane corrected to 23,200 RPM	15.70lbs
Nett Thrust computed from flow at the exit plane	13.45lbs
Corresponding measured thrust	13.65lbs

Of the 15.70 lbs gross lift measured at the central plane 0.58 lbs has still to be recovered by the straighteners. Because of the low straightener blade Reynolds number and underturning, it is estimated that half of this is lost.

The agreement between the force on the air at the exit plane and the measured thrust is probably fortuitous, since total head measurements here are suspect due both to turbulence and to flow inclinations. (See Wood and Higginbottam (1954)).

Probable breakdown of losses

Straightener penalty (see above)	0.27 lbs
Calculated drag of drive shaft shroud ($C_D \simeq 1.0$, confirmed by exit traverse)	0.60 lbs
Estimated drag on centrebody due to interference with the drive shaft wake (estimate from exit traverse)	0.30 lbs
Calculated drag of centrebody supports	0.35 lbs
Calculated turbulent skin friction of duct walls and centrebody. (Not included in traverse results)	0.30 lbs
Suction on rear of centrebody (from exit ~~value~~ plane measurements)	0.40 lbs
Total	2.22 lbs
Gross Thrust	15.70 lbs

∴ Expected nett thrust from combined flow traverses and drag calculations 13.48 lbs

This is 99% of the measured thrust.

The measured static thrust is 87% of the gross value calculated from the central plane measurements using the formula

$$T_{GROSS} = \rho A_J V_J \sqrt{2C_p T\left(1 - \left(1 + \frac{H}{p_o}\right)^{\frac{1-\gamma}{\gamma}}\right)}$$

Figure of merit

The Bendeman coefficient, $\xi = \dfrac{T}{\left(\frac{\pi}{2}\rho\right)^{\frac{1}{3}} d^{\frac{1}{3}} P^{\frac{2}{3}}}$ has been calculated from the static lift and electrical power measurements of the third test series. The fan tip diameter was used in the calculation. An experimental ξ value of 0.90 should be compared with $\xi = 2^{\frac{1}{3}}(A_E/A_j)^{\frac{1}{3}} = 1.44$, the theoretical value for expansion to full area.

The measured figure of merit is 62% of the theoretical one. An estimated breakdown of this figure is given below:-

Estimated electrical efficiency	90%	
Estimated efficiency of gearbox etc.	90%	
Measured thrust efficiency of duct and straighteners	87%	63%
Calculated fan rotor efficiency	90%	

Note that if the diffuser had worked perfectly the fan would have worked further down its total head rise characteristic curve, using less power. At the same time, however, because of the steepness of the characteristic curve, the static lift decreases with increase in diffusion. For example if the fan total head rise characteristic was vertical the mass flow through the unit would be unchanged by changes in pressure rise and would thus be independent of the diffuser ratio. The lift is then proportional to the duct exit velocity, which decreases with increase in diffusion. It follows that although diffusion improves the figure of merit, the static lift produced by a fan of given diameter can be decreased.

7. The lifting-fan nacelle model at forward speed

7.1 Introduction

In this Chapter an attempt will be made to give a qualitative and where possible a quantitative picture of the interactions and interferences between the model and the free stream.

In section 7.2 the interaction between the fan unit and the mainstream will be investigated. The results of duct flow measurements will be substituted into a theoretically derived expression for lift on the fan and shroud. These values will be compared with measured lift increments in 7.3 in order to demonstrate the remaining unexplained losses in lift.

Section 7.4 will extend the observations of 5.2.2 to provide a vortex model of the jet plume. This model will be used to explain the variation of jet interference forces with incidence, though the model is not yet sufficiently detailed to allow the accurate calculation of these forces.

The forces and moments not discussed in the earlier sections will then be summarised in section 7.5, while section 7.6 will deal with wind tunnel interference. That section will compare the results of tests performed in the R.A.E. No. 1 $11\frac{1}{2}'$ x $8\frac{1}{2}'$ wind tunnel with those of the $5'$ x $4'$ tunnel.

7.2 Internal interactions. The fan unit.

7.2.1. General discussion. The total head-rise characteristic curve.

The progression of the fan down its total-head rise characteristic curve will now be explained and illustrated by experimental results from the third test series.

Some reservations should first be noted. Since intake turning is achieved in the present model without the aid of turning vanes, the flow entering the fan will not be ideal. There will be a high velocity region below the upstream lip of the intake and cross flow. (See Gregory et al (1962)). Either can reduce the efficiency of the fan. In Appendix IV it is shown that the band of velocities which may arrive at the fan is quite narrow if fan blade or duct wall separation is to be avoided. Turner (1962) has demonstrated that a reduction in efficiency can be caused by cross flow, though with the high tip speed of the present fan the penalty may not be severe. The above considerations should be borne in mind during any simplified analysis based on the means of quantities across the duct, such as the treatment which follows.

Two assumptions are necessary in order to proceed. Firstly inlet losses are assumed to be negligible. This is acceptable provided that there is no lip separation, such as may occur at high forward speeds. As a first approximation the exit static pressure will be assumed to be atmospheric. Later it will be seen that the arguments which follow remain valid when exit conditions are affected by the interaction between the jet plume and the mainstream.

Consider two extreme shapes of fan characteristic total head rise curve based on tip speed parameters. For a characteristic which is horizontal the pressure difference across the fan is constant. At a given fan RPM the throughput adjusts itself so that the jet dynamic pressure is increased above the value without forward velocity, by an amount equal to the free stream dynamic pressure. Although the fan thrust is constant, the lift force on the shroud will increase. (See 7.2.3.).

At the other extreme, when the fan characteristic is vertical, there is no change in jet flow rate as forward speed is increased and the increased inlet total head is felt as an increase in static pressure ahead of the fan. The fan thrust is reduced as forward speed rises, while the shroud force remains constant.

It has been shown that the change in lift on the fan system as forward speed increases can be either positive or negative, depending on the slope of the fan characteristic. A fan system whose total head rise falls only slowly with increasing mass flow might be capable of producing additional lift force at constant R.P.M. to compensate for exit interference as forward speed increases.

7.2.2 Duct Flow Measurements

The most striking aspect of the results of flow measurements was that the mean velocity and total head downstream of the fan only varied by about 10% throughout the range of test conditions. (See Figure 7.2) Generally this small spread of results made trends difficult to identify when scatter was present.

Although all the tests concerning duct flow were analysed (using the film reader) test results will be quoted mainly for one incidence, since duct conditions varied little with this parameter, particularly with underfins added to the model. As the results for zero incidence are incomplete, $\alpha = -6^\circ$ will be used as an example.

The variation with forward speed of mean static pressures in the duct will be considered first. (See Figure 7.1) Curves (1) show that the static pressure at inlet rises with forward speed as would be expected from previous arguments.* This rise is less than the dynamic head of the forward stream because of the slight increase in jet velocity. (4) is the inlet static pressure which would result if the jet velocity was unchanged by changes in the pressure difference across the fan, i.e. if the total head rise characteristic was vertical.

(2) is the measured static pressure in the swirled flow at the traverse plane. There was some correlation between these static pressures and measured lift increments. In calculating the pressure rise through the straighteners to obtain curve (3) allowance has been made for the decrease in swirl as the fan moves down its characteristic curve.

---

*Although trends are correctly illustrated the static pressures at inlet calculated from central plane measurements should not be expected to yield a gross pressure rise which agrees with the total head rise, which can be determined with more certainty. This is because the dynamic head maldistribution at inlet cannot be determined from measurements below the fan. The use of mean jet velocity in the expression $p = H_o - \frac{1}{2}\rho V_J^2$ would lead to a static pressure which is too high. Because of this $V_{J_{RMS}}$ has been used for lines (1) in Figure 7.1, though there is no justification for the implied assumption that the distortion index is the same at both planes.

The decrease in static pressure at exit as forward speed increases is caused by interaction between the mainstream and the emerging jet, and will be discussed in 7.3. The result is a lower pressure difference across the fan, which progresses even faster down its characteristic total head rise curve than was assumed in 7.2.1, where the fan exhausted to ambient static pressure. The progression of the fan down its sloping characteristic is also reflected by the difference between curve (4) and curves (1), which is caused by the increasing jet velocity.

Figure 7.1 shows that the addition of underfins each side of the duct exit very much reduces the suction at exit under forward speed conditions. The fan experiences a greater pressure difference at a given forward speed and therefore has progressed down its characteristic more slowly than without fins.

The predicted operating points in Figure 7.3 are based on the assumption that $\Delta H/\frac{1}{2}\rho V_J^2 = 1 - V^2/V_J^2$, which assumes ambient exit static pressure. The total head rise given by the intersection of this expression with the characteristic curve is generally between 10% and 15% above the experimental measurements.

The fan-mainstream interaction also affects the power supplied to the fan. Figure 7.2 shows the decrease in power as the fan moves down its characteristic. The increased pressure difference across the fan with fins added is reflected by an increase in power required.

7.2.3 Theoretical forces on the lifting unit

As mentioned in 7.2.1. the force on the lifting unit is divided between the fan itself and the shroud. The force on the fan is readily obtained as

$$L_{FAN} = A_J \Delta H \quad \dots 7.1$$

However the calculation of the lift force on the shroud is less straightforward. It will be seen in the analysis which follows that the momentum arguments used at zero forward speed may not be extended to the case with a free-stream. Necessary assumptions concern fore-aft symmetry of the model about the duct axis and the superposition of fan alone and free-stream alone flow fields without mutual interference.

Theoretical Shroud Force, (a) Zero Forward Speed

For this case the flow field is symmetrical about the duct axis. Consider the three-dimensional circular intake shown below:-

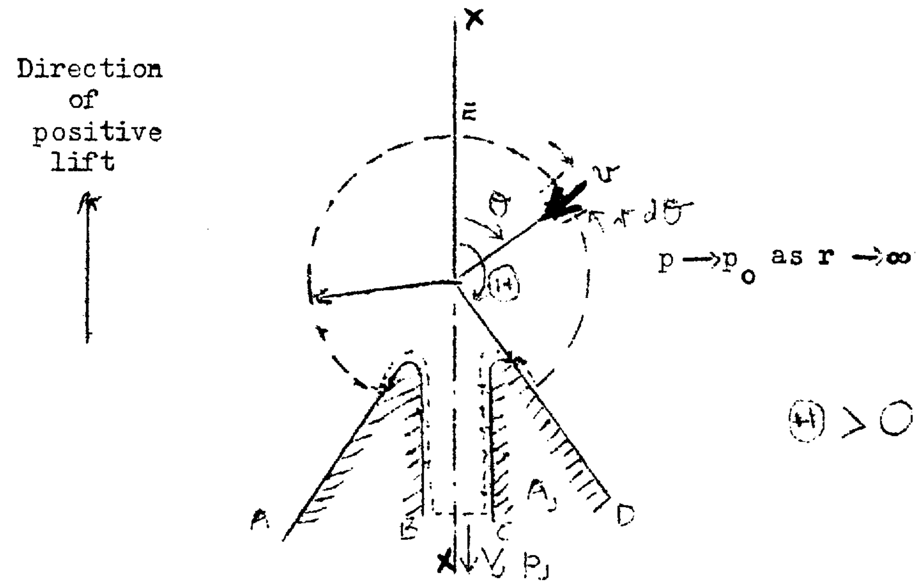

Area of spherical surface AED = $2\pi r^2(1 - \cos \Theta)$

$$\therefore v = \frac{A_J V_J}{2\pi r^2(1 - \cos \Theta)} \quad \text{, by continuity.}$$

Vertical momentum flux through an elementary ring of fluid

$$= (2\pi r . \, r d\Theta . \rho v) . \, v \sin \Theta$$

Total Vertical Momentum, — Flux entering through AED

$$= \lim_{r\to\infty} \int_0^{\Theta} 2\pi r^2 \rho v^2 \sin\theta \, d\theta$$

$$= \lim_{r\to\infty} \frac{2\pi r^2 \rho (A_J V_J)^2}{4\pi^2 r^4 (1-\cos\Theta)^2} \left[-\cos\theta \right]^{\Theta}$$

$$= \lim_{r\to\infty} \frac{\rho (A_J V_J)^2}{2\pi r^2 (1-\cos\Theta)}$$

$$= 0 \qquad \ldots 7.2$$

Notice that the above result is independent of Θ and is thus true for an intake in a flat surface and for a shroud ring, provided that this has sufficient frontal area to sustain the lift given by Equation 7.5, below. The fore-aft cross section of the model is similar to the flat plate case, while the transverse section is more like a shroud ring (and has adequate thickness). It therefore appears reasonable to assume that the above result is true for the intake of the nacelle model. A small loss of lift might occur because the surfaces do not extend to infinity.

In view of (7.2), the total momentum flux through the control volume EABCDE $= -\rho A_J V_J^2$ ... 7.3

From Bernoullis equation $(p_o - p_J) = -\frac{1}{2}\rho V_J^2$

∴ pressure force on fluid along BC $= -\frac{1}{2}\rho V_J^2 A_J$ ... 7.4

∴ force on air along AB and CD $= (7.3)-(7.4) = -\frac{1}{2}\rho V_J^2 A_J$

Hence the reaction on the shroud $= \underline{\underline{+\frac{1}{2}\rho V_J^2 A_J}}$ ... 7.5

(b) Shroud Lift at Forward Speed V

Because the axial symmetry of the zero forward speed case can no longer be invoked, it is dangerous to use a momentum argument similar to that above. Momentum integrals over the part of the bounding surface at infinity are often different from zero in these cases.

In what follows the static pressure acting on an element of surface at a point A will be determined without and with the fan operating, the free stream being present throughout. In order to allow for the case without radial symmetry the velocity induced by the fan operating alone has been assumed to be at an angle to a radius to the point.

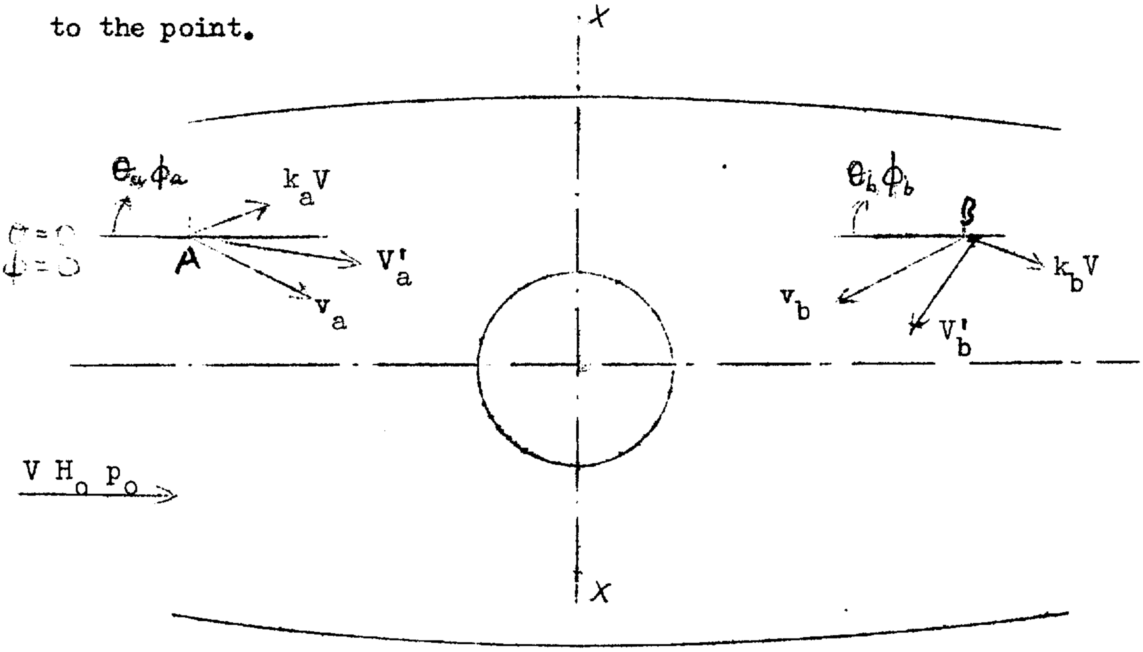

v = local surface velocity for $V = 0$ $(v \propto V_J)$

p = corresponding static pressure

θ = angle between free stream direction and v

kV = local surface velocity for free-stream only, assuming that the duct is blanked off.

P = static pressure corresponding to kV.

ϕ = angle between the free stream direction and kV

V' = vector resultant of kV and v

P' = corresponding static pressure.

We are interested in the change of static pressure caused by operating the fan with the free-stream on, i.e. $(P'-P)$

Now $P_a = H_o - \frac{1}{2}\rho k_a^2 V^2$

$P'_a = H_o - \frac{1}{2}\rho V'^2_a$

and $V'^2_o = k_a^2 V^2 + v_a^2 + 2k_a V v_a \cos(\theta_a - \phi_a)$

$$\therefore P'_a - P_a = -\frac{1}{2}\rho V'^2_a + \frac{1}{2}\rho k_a^2 V^2$$

$$= -\frac{1}{2}\rho v_a^2 - \rho k_a V v_a \cos(\theta_a - \phi_a) \qquad \text{... 7.6}$$

The first term is the depression caused when the fan is operated without the free-stream, while the second concerns the interaction between the flow fields. It is implied in the above argument that v and kV may be added vectorially without mutual interference.

Consider now a model which has fore-aft symmetry about XX. Apart from the enlarged radius on the upstream side of the intake, the model approximates closely to this. Compare the values of static pressure at points A and B which are mirror images in XX. If the flow fields also have the expected symmetry then:-

$$v_a = v_b$$

$$k_a = k_b$$

$$\pi - \phi_a = \phi_b - \pi$$

$$\theta_a - \pi = 2\pi - \theta_b$$

adding, $\theta_a - \phi_a = \pi - (\theta_b - \phi_b)$

$$\therefore P'_b - P_b = -\tfrac{1}{2}\rho v_b^{\,2} - \rho k_b V v_b \cos(\theta_b - \phi_b)$$

$$= -\tfrac{1}{2}\rho v_a^{\,2} - \rho k_a V v_a \cos(\pi - (\theta_a - \phi_a))$$

$$= -\tfrac{1}{2}\rho v_a^{\,2} + \rho k_a V v_a \cos(\theta_a - \phi_a) \qquad \ldots 7.7$$

As before the first term is the depression due to the fan alone, and is equal to the first term in Equation 7.6 because of the assumed symmetry. However although equal in magnitude the interaction term has the opposite sign to that in Equation 7.6. It follows that the nett lifting force on symmetrically disposed elements will be equal to that of the fan acting alone.

Therefore, at forward speed V, Shroud Force $= \tfrac{1}{2}\rho V_J^{\,2} A_J$ ... 7.8

The induced terms in Equations 7.6 and 7.7 will also result in a nose up pitching moment due to fan operation which is proportional to forward speed and jet velocity and which depends on model geometry. This is part of the moment which turns the air into the duct. The remainder is supplied by the vertical part of the duct walls.

7.2.4 Forces on the lifting unit derived from flow measurement, using the above results.

$$\left.\begin{array}{ll} \text{From (7.8) Shroud lift} & = \tfrac{1}{2}\rho V_J^{\,2} A_J \\ \text{From (7.1) Fan lift} & = A_J \Delta H \\ \text{Force on duct items,} & \\ \text{including diffuser} & = k\tfrac{1}{2}\rho V_J^{\,2} A_J \end{array}\right] \qquad \ldots 7.9$$

k will be determined from static lift tests.

In practice the mean axial velocity V_M at the traverse plane will be available. Writing Equation 7.9 in terms of V_M -:

Shroud lift $= \frac{1}{2}\rho\bar{V}_M^2\left(\frac{A_M}{A_J}\right)^2 A_J = 0.86 \times 0.15 \times \frac{1}{2}\rho\bar{V}_M^2$

Fan lift $= A_J\ \Delta H = 0.15\ \Delta H$

Force on duct items $= k\frac{1}{2}\rho\bar{V}_M^2\left(\frac{A_M}{A_J}\right)^2 A_J = k \times 0.86 \times 0.15 \times \frac{1}{2}\rho\bar{V}_M^2$

Nett lift on unit $= N = 0.15\Delta H + 0.129\ \frac{1}{2}\rho\bar{V}_M^2(1 + k)$ ... 7.10

The substitution of static lift results into (Equation 7.10) yields

$k = -.341$ with rakes installed, no underfins

$k = -.230$ no rakes, no underfins.

In both cases the drag loss is dominant, as was seen in Chapter 6. The first k value is appropriate to the tests under consideration.

Finally $N = 0.15\Delta H + 0.129\ \frac{1}{2}\rho\bar{V}_M^2 \times .659$

$= 0.15\Delta H + 0.085\ \frac{1}{2}\rho\bar{V}_M^2$ ... 7.11

Figure 7.4 shows the components and the nett force (Equation 7.11) on the lifting unit for $\alpha = -6°$, plotted against forward speed parameter. The rising shroud- and falling fan lift can be seen clearly. The gross lift fell slightly with forward speed. The fall was increased when the drag of duct items was subtracted to obtain the nett lift.

In Figure 7.5 the forces are shown which would be experienced by the two idealised lifting units mentioned earlier. In calculating the nett thrust the losses of Equation 7.11 have been assumed. As forward speed rises gross and nett thrust both rise for the unit with the horizontal characteristic, but fall for the unit with the vertical one. It is important to note that the horizontal characteristic refers to constant $\Delta H/\frac{1}{2}\rho(\Omega R)^2$ and not to $\Delta H/\frac{1}{2}\rho V_J^2$. It is not possible to match the variation of observed pressure difference across the fan to a constant value of the latter.

As well as the variations with forward speed noted above it can be seen from Figure 7.5 that a decrease in exit static pressure from the ambient to the measured value gives an increase in total lift for the horizontal characteristic but a decrease for the vertical one. For the former the increase in nett thrust with forward speed could offset loss of lift due to jet interference. If the shroud areas were large and the areas around the jet exit were small a desirable increase in lift with forward speed might result. The essential feature of the unit with the horizontal characteristic is that, because the pressure difference across the fan is constant, any decrease in exit static pressure is reflected at the inlet, and the fan force is unchanged. As can be seen from Figure 7.5(a) this is accompanied by an increase in shroud force.

The lifting characteristics of the model fan unit can be regarded in terms of the two extreme cases. The fact that nett thrust decreased with forward speed is unsatisfactory, especially in view of the additional loss due to jet plume interference. However it is difficult to see how the slope of the total head rise characteristic can be decreased without alteration to fan geometry or blade angle as mass flow increases. Variable pitch could be used to give a characteristic which effectively has a positive slope, which is unstable for fixed geometry devices. In the interests of simplicity fixed geometry is clearly desirable. Although the slope of the characteristic is reduced as the fan approaches the stall, any solution using this effect would be artificial since static lift would be capable of improvement. A fan or blower is needed whose elements are insensitive to incidence.

7.3 Measured Force Increments and Calculated Forces on the Fan Unit.

In Figures 7.6 and 7.7 measured force increments and forces on the fan unit, calculated using Equation 7.11, are compared for tests at various incidences.

The first observation is that the decrease in measured lift increment with forward speed was only of order 10%. This is some measure of the success of paring away the area around the jet exit to reduce the downward force due to suction. For a jet issuing from a flat surface, such as a wing, the corresponding figure might reach 50%. Trebble and Hackett (1963) demonstrate how this loss is reduced further for bodies which are truncated behind the jet. However these would suffer from high cruise drag if their use was contemplated for lifting engine nacelles.

Secondly the initial loss of lift is not due entirely to under-surface effects. To these are added a loss of lift due to the progression of the fan down its total head rise characteristic, which would occur solely due to intake effects with rising forward speed, but which is accentuated by exit suction. Duct losses, the drag of straighteners etc., also increase with forward speed and are probably subject to scale effect.

However it can also be seen that the loss of lift, beyond that due to fan effects, increases with incidence. This is to be expected since the tail of the model then approaches the vortices in the jet plume. (See Chapter 5 and Section 7.4). Also included in the difference between the broken and full lines of Figure 7.6 are the forces due to intake assymetry in the fore-aft sense not allowed for in deducing Equation 7.8, lift forces on the duct walls with the model at incidence and the effects of maldistribution of the duct flow.

The recovery of measured lift increment above $V/\Omega R$ of about 0.10 is not associated with the fan interaction. With underfins added the additional loss is eliminated completely. It is suggested that some of this benefit arises from an increase in static pressure on the underside of the model between the underfins. Surface flow visualisation indicated that air here was slow moving. These increased surface pressures ahead of the jet would also be consistent with observed increases in nose up pitching moment which the fins cause. Further lift benefit probably results because the underfins move the vortices in the jet plume away from the body surfaces.

Figure 7.7 is a comparison between the measured drag increments and values calculated from duct flow measurements. The latter comprise the drag due to the removal of free-stream momentum from the measured mass flow plus the streamwise component of the normal force N, calculated from Equation 7.11.

It can be seen that the differences between the measured and the calculated incremental drag values are of the same order as those for incremental lift. The suctions on the sloping surfaces behind the jet probably contribute both to lift and drag interference effects. However it seems likely that the variations of static pressure on the duct walls has a more significant effect on drag- than on lift-increments.

Figure 7.7 also shows that estimated drag increments based on the nominal efflux velocity V_{J_T} can be considerably in error. A better estimate is given by measured values of mass flow. Failing this estimates based on the operating points predicted as in Figure 7.3 are to be preferred to those based on V_{J_T}. Note should also be taken of the increase in drag due to tunnel constraint, illustrated for $\alpha = +12°$ in Figure 7.7. Corresponding high values of incremental lift were also measured in the smaller tunnel. (See Section 7.6 and Table 7).

To conclude this section we turn to Figure 7.8, based on the same data as Figure 7.6, which shows the difference between the measured lift increments and the calculated forces on the fan unit. Points at positive incidences should be considered with care, since tunnel interference effects were present. It was not considered legitimate to combine lift increments from the $11\frac{1}{2}'$ x $8\frac{1}{2}'$ tunnel tests with the fan unit forces obtained in the smaller tunnel since the fan operating point was probably also affected.

There remains for negative incidences a clear downward trend in the interference force 'A'. This force varies less with forward speed than might be expected considering that the vortices in the jet plume approach the body more closely at the higher forward speeds. Possible reasons for this, and further explanations of the interference effects due to the jet plume will be investigated in the following section.

7.4 External Interference. The jet plume.

7.4.1 The Vortex Model

In this section and in Figures 7.9 and 7.10 a vortex model is proposed which is consistent with the observations of Section 5.2.2 and Figure 5.8. However further detailed measurements are required to verify the detailed structure of the proposed model. This model should be regarded as a basis for further research and is used here mainly to demonstrate the nature, rather than the magnitude, of lift interference. With the body on struts the observed interference forces were never more than about 10% of static lift.

The formation of vortex rings

In the vortex model shown in Figure 7.9 vortex rings leave the jet exit at half the speed of the jet and are stretched and distorted while being convected downstream. Two such rings are shown. The parts of the rings which originated at the downstream side of the jet have progressed further than those from the upstream side. In order to understand this it is necessary to consider the nature of three-dimensional shear layers.

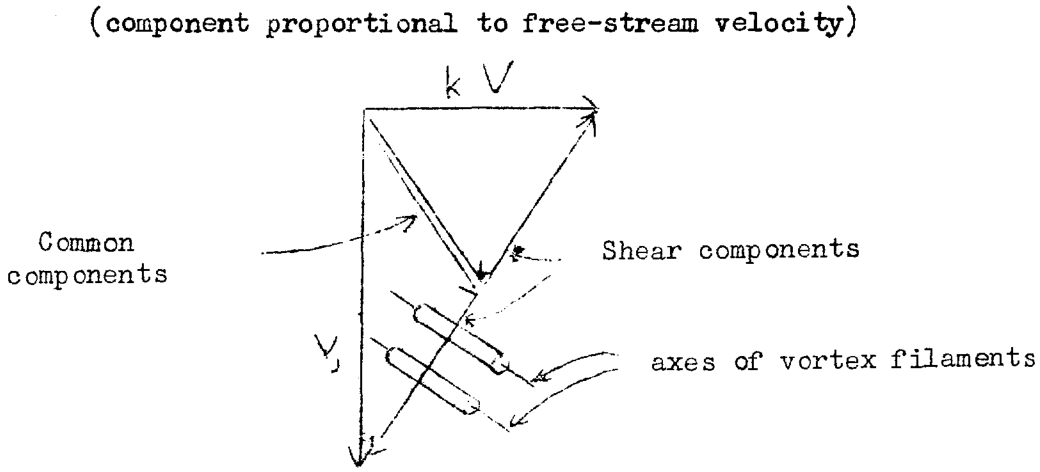

The axes of the vortex filaments are normal to the direction of relative shear between the two streams. In the case of the jet in free air the shear is streamwise and plane vortex rings are produced. However as soon as a mainstream is added the axes of the vortex filaments at the sides of the jet become inclined as shown by the above diagram. Only those at the front and rear of the jet remain horizontal.

Consider now the necessity for vortex element to be continuous. The vortex element which has just emerged on the upstream side of the jet can only be linked to one on the downstream side which emerged earlier. The rings are therefore distorted from the outset.

The transverse components of the vortex rings

In Figure 7.9 it can be seen that the downstream sides of the vortex rings may be parallel to the upstream sides of rings which were shed earlier, forming vortex doublets. At positions of interest on the body the velocities induced by these doublets are likely to be very small. Although distinct rings have been postulated for the purpose of explanation, the overall process has a continuous nature.

Transverse vortices are shed during the starting process without pairing to form doublets, so that the forward acceleration of a lifting jet leaves starting vortices in the same way as does an accelerating wing.

Vortex stretching

In addition to the distortion mentioned above the vortex rings are probably stretched by convection. It is important to note that, although the strength K of any individual filament is unchanged by stretching, overlapping of filaments can increase the strength of a trailing vortex. Therefore vortex strength may vary along the path of the trailing vortices, without the need for further transverse vortex filaments.

7.4.2 The idealised model for the calculation of interference effects

The model proposed above has been simplified to the form shown in Figure 7.10(a) in which vortices are assumed to spring from the streamwise edges of the duct in a fully rolled-up condition. Their paths lie in planes which diverge at a total angle of 10°. A hyperbolic cosine form has been assumed for the shape in side view, the constants being determined from the flow observations of Chapter 5. The further assumption has been made that the paths shown are not affected by change of incidence. Some support for this is given by the fact that, away from the stall, the increase in lift increment caused by adding wings is almost independent of incidence.

Vortex strength

The assumptions concerning vortex strength are the weakest feature of the present analysis and further experimental evidence is needed before accurate predictions of interference force can reasonably be expected. However since, in the present case, these forces are only about 10% of static lift, some insight may be obtained from the following approach.

Firstly the effect at the body of the transverse vorticity in the trailing sheet has been assumed negligible. In spite of the formation of transverse vortex doublets this is probably unjustified for the real flow. However when used to predict forces due to cross-flow over the afterbody, the consequences may not be serious. Any nett lift due to vortices spanning the jet will be a function of the rate of change of area along the body, rather than body area per se. However downwash at the wing quarter chord may be incorrectly predicted.

Secondly assumptions must be made about the strength of the trailing vortices. One possible approach might be to determine the distribution of strength along one vortex needed to produce the observed slope or curveature of the other. This would involve the solution of a number of simultaneous equations equal to the number of control points selected. An attempt to use this approach failed at an early stage because of difficulties concerning the jet and free stream components of the velocity at the control points.

At the jet exit and far downstream velocity components probably have their full respective values. However at points in between viscous effects are probably important. Vertical velocity falls due to viscous mixing while the free stream component probably has a more wake-like character. As both effects are important in the region of interest it was not possible to make reasoned assumptions about typical velocities within the combined fields, upon which vortex-induced effects could be superposed.

The method finally used to determine trailing vortex strength returned to the observations of flow patterns. Control points were chosen on the near fuselage along the horizontal line of maximum diameter. Flow directions were measured on photographs taken at zero incidence and are presented in Figure 7.11. The induced downwash at the control points was taken as twice that calculated at the model centreline. The streamwise components comprised an induced component and a fan-off component calculated from the pressure distributions measured on a model of the R101, reported in R and M 1169.

In Figure 7.12 values of vortex strength are presented, based on the above assumptions. The values are strictly an apparent vortex strength because of the assumptions which have been made. In addition to velocities induced by the trailing vortices in the real flow the downwash includes components due to local mixing near the outlet, bound vorticity and upper surface intake effects, all of which have been ascribed to the trailing vortex pair. It is likely that at least part of the variation of apparent strength along the vortex is due to the above effects. (Since the contributions to downwash at a given control point arise very largely from a short length of vortex just below it, it may be inferred that the vortex strength has the value indicated by the control point having the same x coordinate.)

It can be seen that, subject to the above reservations, the vortex strength is approximately inversely proportional to forward speed. Since, in addition, $^{q}V/_{K}$ is found to be directly proportional to forward speed, there results a downwash velocity which varies little over the speed range considered.

7.4.3 The induced flows and associated interference forces.

Figures 7.13 to 7.15 show the downwash distributions produced by trailing vortices having constant strength. The calculation of induced velocities was carried numerically, using desk machine methods since integrals along the vortex proved intractable.

The load gradings were calculated on the assumption that the rear of the body lay in a cross flow equal to the induced velocity at the model centreline. A circular cylinder cross-flow drag coefficient if unity was assumed. All cross-flow Reynolds numbers were subcritical.

The lower part of Figure 7.15 shows the variation of interference force with incidence. The force has been plotted relative to that at zero incidence because the loads calculated in the duct region are unrealistic, and the zero incidence case encompasses most of this effect. The main interest attaches to the variation of interference force with incidence, which is seen to be of the same sort and size as that found in model tests and plotted in Figure 7.8. At $\alpha = 18°$ a change of flow structure probably reduced the lift interference. It is not clear to what extent this was due to tunnel constraint.

Figure 7.16 shows velocities induced at the wing quarter chord by the constant strength trailing vortices postulated above. Since the choice of vortex strength cannot be justified as previously and as bound vortices in the jet plume are ignored, the lift on the wing which results will not be quoted.

However it is instructive to consider the way in which the lift induced by the trailing vortices varies with forward speed. (Since the shape of the jet plume has been assumed to be unaffected by change of incidence, there will be no variation with this parameter).

It can be seen from the lower diagram of Figure 7.16 that, although allowance has been made for the diminution of trailing vortex strength as forward speed increases, the interference lift changes from negative to positive. The calculations allow for both horizontal and vertical velocities induced at the wing quarter chord.

Force tests show that the addition of the wings both deepens the "lift bucket" and steepens the subsequent recovery of lift increment as forward speed is raised. (See Figure 7.19) If it was legitimate to assume the same vortex strengths as were used in the calculation of downwash over the body, then the greater part of both effects could be explained. qualitatively

7.5 The results of force tests

7.5.1 Summary of Sections 7.2 to 7.4

After the derivation of the forces on the fan unit in Section 7.2 it was seen that the subtraction from the measured lift increments of the vertical component of the normal force on the fan unit, removed much of the initial variation of interference lift with forward speed. (See Figure 7.8) The vortex model of Figure 7.9 was then proposed and described in detail. The subsequent simplification and further investigation of this model involved several assumptions which are difficult to justify. However the simplified model gave several results which are consistent with measured variations of lift increment. For example the changes of downward force on the rear fuselage were of the right order, and if measured vortex strengths were available, it appears likely that the extra interference in the presence of wings could be explained.

The observation that downwash over the rear fuselage varies little with forward speed, arises directly from the flow observations, which have also been used to determine vortex strength. It must be noted that, because the model was designed for low interference forces, these amount to only 10% of static lift. The combined scatter of force and duct flow observations may amount to one quarter or one third of this. However, subject to the reservations above and to those expressed in the appropriate sections, the following conclusions may be drawn:-

1. With the body on struts at low forward speeds variations in lift interference with forward speed are due mainly to the fan-mainstream interaction, which is not greatly affected by change of incidence (see Figure 7.2). At higher forward speeds induced circulation effects probably account for the rise in incremental lift.

2. The observed loss of lift at positive incidences is a consequence of the closer approach of the rear fuselage to the trailing vortex pair within the jet plume. (See Figures 7.3 and 7.14) Flow observations indicate that the downwash which is responsible probably changes little in velocity between forward speeds of 35% and 65% of the jet velocity (See Section 7.4.2).

3. Force tests show that the addition of wings amplifies both the initial fall-off and the subsequent rise of incremental lift as forward speed is raised (see Figure 7.19). Calculations which assume a jet plume model with constant strength trailing vortices can predict both of these effects.

4. Although the experimental evidence is limited it appears that within the above speed range, the trailing vortex strength is inversely proportional to forward speed. Clearly the strength must return to zero forward speed, so this result must be kept strictly within the present context.

Further experiments are required to determine values of trailing vortex strength over the whole forward speed range.

7.5.2 Additional force data

The results of force tests given so far (Figures 7.6 and 7.7) have been quoted only as required to illustrate the discussions about the interaction processes. Tables 7A to 7D, Figures 7.17 to 7.22 and Appendix VII are intended to provide a fuller description of incremental forces and moments over the complete ranges of configuration, attitude and forward speed. Only major points of interest will be dealt with here. Hackett (1962) and Trebble and Hackett (1963) give comprehensive results of tests in the 5' x 4' and $11\frac{1}{2}$' x $8\frac{1}{2}$' wind tunnels respectively. The comparison between results measured in the two tunnels will be given in Section 7.6.

Figure 7.20 is derived from tests in the larger tunnel. The remainder of Figures 7.17 to 7.22 pertain to the 5' x 4' tunnel, in which the forces on the model were increased at high incidence by tunnel constraint. Similarly, because of the floor stagnation mentioned in Section 5.3, the low forward speed results are suspect.

With the body on struts the "lift bucket", which occurs as forward speed is raised, almost disappears at large negative incidences. The increments are generally more dependent upon incidence than upon forward speed. (See Figure 7.17). With the exception of cases where the wing was stalled, all drag increments were close to those in Figure 7.7.

The presence of wings introduces an additional component of lift increment which is almost wholly speed dependent (see Figure 7.19). At the ends of the incidence range stall effects are apparent on incremental plots. (See Figures 7.17 and 7.18). However the total lift on the model shows a less violent variation.

Tables 7C and 7D show that the chief virtue of underfins lies in the removal of the "lift bucket" with the body on struts and its reduction with wings added. The underfins probably both reduce entrainment near the jet and by moving the vortices away from the body, decrease the downwash over it. In combination with a crude "jet flap" effect between the fins, these can result in significant gains in lift as forward speed rises.

Figure 7.20 shows the lift increases which result from the addition of underfins. These include fan off gains, since the significant increment is that in total lift, the underfins being extended only during flight with directly powered lift. There is less benefit in the presence of wings. Although the drag increment is little affected the incremental pitching moments are increased at negative and decreased at positive incidences.

Figure 7.21 shows that curves of pitching moment increments collapse quite well when plotted against incremental drag minus the streamwise thrust component. This is partly because the removal of free stream momentum from a plane above the model gives rise to a force, proportional to forward speed, which lies above the intake. This appears in balance measurements as a combination of drag and nose-up pitching moment increments. There are further contributions to both from suctions behind the jet exit.

7.6 Wind Tunnel Interference (See Tables 7 and Appendix VII)

In this section the forces measured in the 5' x 4' wind tunnel are compared with those measured in the RAE No.1 $11\frac{1}{2}$' x $8\frac{1}{2}$' tunnel at Farnborough. In order to remove the uncertainties about the measurement of static lift, mentioned in 6.3, the results have been reduced using tip-speed parameters, as previously in this Chapter. Tip speed was determined from the fan noise frequency. All of the test results were plotted and the values given in

Tables 7A to 7D were read off at convenient intervals of forward speed ratio so that direct comparison could be made between tunnels. Results are quoted only from the immediate vicinity of experimental points.

Body on Struts

(a) Lift Increments

Table 7A gives the results of the second and third test series. Allowance has been made for the presence of the traverse rakes in the third series by applying a 3% correction to lift increments. The assumption of static lift dependence involved is justified for the small correction needed.

With the exception of the extreme incidences most discrepancies between the results obtained in the two tunnels were less than 2% with the body on struts. With underfins added the RAE lift increments were between 0% and 4% higher than those measured at Imperial College. (See Table 7C).

At high positive incidence the lift increment rose steadily as forward speed increased in the 5' x 4' tunnel but decreased slowly in the $11\frac{1}{2}$' x $8\frac{1}{2}$' tunnel. At the highest forward speed the difference was 15%. A rising characteristic was obtained at all incidences with fins added and the high incidence discrepancy did not appear.

(b) Drag and Pitching Moment Increments

Agreement between drag increments was good up to + 6° incidence where the increments in the smaller tunnel started to rise from the linear characteristic obtained in the $11\frac{1}{2}$' x $8\frac{1}{2}$' tunnel. It is though that floor stagnation is chiefly responsible at low speeds (see Chapter 5) and that deviations at higher speeds at high incidence are associated with the lift discrepancies mentioned above.

There was considerable scatter in pitching moment increments in both tunnels. However the increments measured at RAE were generally lower and varied less with incidence. The incidence effects occurred under the same conditions as did the lift and drag discrepancies, but the reason for a slight overall shift is not apparent.

Body on Wings

Table 7B compares the results of the first and second series without fins, since no tests were performed on wings in the third series. The configuration with fins and wings (see Table 7D) was not tested at Imperial College.

Consider first some effects which are likely to lead to differences between the results obtained in the two tunnels. As shown in 7.4.3 a proportion of each lift increment is associated with changes in wing incidence induced by the jet. Tunnel constraint in the 5' x 4' tunnel with fan off is sufficient to make conventional corrections desirable. With the fan on the tunnel constraint may influence the amount of induced incidence to a greater extent, in a manner which cannot be predicted using standard tunnel correction techniques. As with the body on struts, constraint which changes with jet inclination may also be encountered at high incidences.

A further effect which may influence the comparison is the variation of wing stalling angle with tunnel constraint, forward speed and turbulence level. Any of these may influence the extent of separation induced on the wing by a particular jet configuration. In incremental plots this might appear as differences between tunnels in the conditions needed to produce rapid changes in lift increment, due to the stall.

In view of these considerations worse agreement is to be expected between tunnels than for the body on struts case. Table 7B shows this to be so. Agreement is good only at low speeds and at low incidences. At most incidences lift recovery with forward speed starts sooner giving up to 15% more lift increment in the smaller tunnel. Agreement was within ±3% at moderate incidences for $\frac{V}{\Omega R}$ up to 0.10.

Summary of 7.6

ON STRUTS (NO FINS)

In a tunnel which was about 7 jet diameters high and of usual proportions, errors in lift increment were less than 2% at incidences below 15°, at all forward speeds between 20% and 65% of the jet velocity, the range in which tests were made.

ON WING

Errors were less than 3% at speeds below $\frac{V}{\Omega R} = 0.10$ (i.e. $V/V_J \simeq 0.30$). At higher speeds differences of up to 15% were mainly associated with the earlier recovery of lift increment in the smaller tunnel. These errors are important because small tunnel results tend to be optimistic.

8. CONCLUSIONS

A nacelle-shaped model containing a lifting ducted fan has been designed for use in the 5' x 4' wind tunnel at Imperial College. The driving motor and fan unit are an integral part of the model. Engineering and design problems have been discussed. Wings having an area about thirteen times that of the duct could be fitted with the quarter chord line intersecting the duct centre-line halfway between inlet and outlet. Their setting angle could be varied. Underfins, one duct diameter deep and two long, could be attached each side of the duct exit extending in a streamwise direction to points one diameter ahead of the front of the duct.

Measurements of Lift, Drag and Pitching Moment have been made for four model configurations at forward speeds between 15% and 65% of the jet velocity and incidences between -20^{o} and $+20^{o}$. In addition comparisons have been made with forces measured in the RAE No.1 $11\frac{1}{2}$' x $8\frac{1}{2}$' wind tunnel.

In order that the interaction between the fan unit and the mainstream should be better understood, static and total head traverses have been made immediately behind the fan. The results, recorded on film, were reduced using a specially designed film reader, which has been described. The forces on the fan and shroud have been estimated using the results of these duct flow measurements.

The structure of the jet plume has also been discussed and a crude vortex model has been suggested which is consistent with surface flow and smoke observations. This model has provided tentative explanations of some of the observed interference effects.

<u>The loss of lift at forward speed</u>

Many tests involving fan or jet systems, including the present ones, have shown that the total lift on the model may decrease as forward speed increases. For the extreme case of a small fan in a large wing this loss can exceed 50% of the static lift. There is sometimes a subsequent recovery which may start at forward speeds between 30% and 50% of the jet velocity, leading eventually to lift greater than the static value. For the present model the size of the maximum loss increased with incidence and was greater with wings fitted.

Much of the present work has been directed towards understanding the reasons for the loss of lift and towards a reduction in its magnitude. In order to reduce the adverse effects of jet plume interference, the normal area around the jet exit was made as small as was consistent with the desired streamlined shape of the nacelle. By this means the maximum loss of lift at zero incidence, including the loss caused by the fan - mainstream interaction, was kept down to 10%. Trebble and Hackett (1963) have shown that, by truncating the body behind the jet, further reduction of the loss is possible. However greater benefit resulted from the addition of the underfins described above. With underfins but without wings fitted the incremental lift on the body rose continuously with forward speed. Considerable reduction in the lift loss also occurred when wings were added. The lift gains due to underfins appear to be significantly greater than would be explained by a reduction of entrainment and induced downwash associated with the jet. It is thought that when constrained between underfins, the lifting jet acts as a crude jet flap.

<u>The reduction of lift on the plain body by Fan-Mainstream Interactions and by Jet Plume effects</u>

Because some success had been achieved in the reduction of the loss of lift, the study of the various contributions to the loss was not easy since the variations in the measurements concerned amounted only to about 10%. However, using the results of the duct flow experiments it has been possible to estimate the loss of lift due to the interaction between the fan and the mainstream. The calculations concerning the forces which result from flows induced by the jet plume were of a more qualitative nature since no measurements were made within the external flow field.

The nett change with forward speed or incidence in the lift sustained by an element of body surface is affected by distinct contributions from the fan and jet-plume systems which, however, cannot be separated mechanically. It is instructive nevertheless to consider separately the major contributions to lift interference.

Experiments have shown that the fan-mainstream interaction effects vary mainly with forward speed. The fan is caused to progress down its characteristic total head rise curve as forward speed increases and there results a decrease of total lift on the fan-shroud combination. The loss of lift could be overcome if the flow through the lifting unit increased sufficiently rapidly with decreasing pressure rise.

In contrast, the jet plume interference appears to be more dependent upon incidence than upon forward speed over the range considered. This is associated with the closer approach of the rear fuselage to the jet plume at higher incidence, resulting in loss of lift. It is thought that, within the limited speed range considered, the movement of the jet plume towards the body as forward speed is increased is accompanied by a complementary reduction in the strength of the trailing vortices within the plume.

Although it is difficult to justify the use of the crude vortex model for the prediction of induced flows over the wings, it has been found possible to predict the steepening of both the initial fall off and the subsequent rise in incremental lift which occurs when wings are added to the plain body.

Some alleviation of adverse lift interference can probably be obtained by reducing the surface area behind the jet and by changing the slope of the fan characteristic. However the increase in lift caused by the deployment of underfins probably has the greater practical significance.

Pitching Moment and Drag

It has been shown that about half of the difference between measured drag increments and estimates based on nominal efflux velocity, is the nett result of an increase in mass flow through the fan and the accompanying decrease in normal force on the unit. The difference which remains is probably associated with the same suctions aft of the jet which lead to loss of lift. With the exception of cases in which the wing became stalled, the drag increments were the same for all configurations.

It has been shown that pitching moment increments are strongly related to the removal of free stream momentum from above the model. Additional contributions result from increases in static pressures ahead of the jet and decreases behind it. The effect is probably increased considerably when underfins are added.

If the upper surface intake was considered for use in the body of an aircraft there would be a large variation of nose up pitching moment which would be approximately proportional to forward speed. At $\frac{V}{V_J} = 0.4$ a high transition speed, a control jet placed at the aircraft tail, say four diameters behind the jet, would require a thrust equal to 20% of the total lift. However if the plain nacelle was mounted on a pylon below the wing of a larger aircraft, the control moment required might be reduced by placing the inlet plane of the unit slightly below the vertical c.g. of the aircraft.

Tunnel Interference

Probably the most important result was that with the 5' x 4' tunnel closed, the static lift was 7% below that obtained after cutting a hole in the tunnel floor to allow the jet to escape and opening all the doors and windows. The tunnel floor was 3.2 diameters below the jet exit.

Floor stagnation occurred below the model in the 5' x 4' wind tunnel below velocity ratios V/V_J ranging from approximately 0.20 at an incidence of -20° to 0.40 at $+20^{\circ}$. When floor stagnation was absent the operation of the model fan did not noticeably alter the flow distribution ahead of the model on a vertical centre-line, but there was a marked decrease in tunnel speed for given tunnel fan R.P.M., particularly at low speeds.

A comparison of forces measured in the 5' x 4' and in the $11\frac{1}{2}$' x $8\frac{1}{2}$' tunnels yielded the following results-:

(i) With the body on struts at 18° incidence an apparent lift benefit in the smaller tunnel increased with forward speed to 10% of static lift at a velocity ratio of 0.60. Somewhat surprisingly this high incidence effect disappeared when underfins were added.

At lower incidences lift increments agreed to within ±2%

(ii) With wings added the lift increment recovered, after the initial fall, at a lower forward speed in the smaller tunnel. This gave an apparent lift benefit which rose from 3% at one third of the jet velocity to 15% at a velocity ratio of 0.60. The above differences are important because results tend to be optimistic if the tunnel is too small.

(iii) The above apparent lift benefits in the smaller tunnel were usually accompanied by correspondingly greater drag and pitching moment increments.

LIST OF REFERENCES

Author(s)	Date	Title etc.
Butler, S.F.J. Williams, J.	1959	Further comments on High-lift testing in Wind Tunnels, with particular reference to Jet Blowing Models. NATO AGARD Report 304
Collar, A.R.	1940	The Design of Wind Tunnel Fans A.R.C. R.&M. 1889
Goldsmith, R.H. Hickey, D.H.	1963	Characteristics of Aircraft with Lifting-Fan Propulsion systems for V/STOL.
Gregory, N. Raymer, W.G.	1958-9	Wind Tunnel Tests on the Boulton-Paul Rectangular Wing (Aspect Ratio 2) with a Lifting Fan. 1958 Series I A.R.C.20,356 1959 Series II A.R.C.21,127
Gregory, N.	1961	Personal communication.
Gregory, N. Love, Edna M.	1962	The Effect of Forward Speed on the Inlet Flow Distribution and Performance of a Lifting Fan installed in a Wing NPL Report Aer 1018 (ARC 23,839)
Hackett, J.E.	1962	Some Preliminary Results of Force Tests on a Fan-Lift Model. Imperial College Department of Aeronautics TN20.
Heyson, H.H.	1960	Jet Boundary corrections for Lifting Rotors centered in Rectangular Wind Tunnels. N.A.S.A. TR R-71
Heyson, H.H.	1962	Linearised theory of Wind Tunnel Jet-Boundary Corrections and Ground Effect for VTOL-STOL Aircraft.
Jordinson, R.	1958	Flow in a Jet Directed Normal to the Wind. A.R.C. R.& M.3074.
Llewelyn-Davies, D.I.T.P. Tye, W.D. MacPhail, D.C.	1952	The Design and Installation of Small Compressed Air Turbines for Testing Powered Dynamic Models in the Royal Aircraft Establishment Seaplane Tank. A.R.C. R.& M. 2620.

Author(s)	Date	Title etc.
Melbourne, W.H.	1960	Experiments on a Delta Wing with Jet-assisted Lift. Imperial College Ph.D. thesis (See also A.R.C. R.& M. 3288)
McCluney Gallagher Raktham, K.	1960	The Prediction of Lift and Pitching Moment characteristics on the S.C.1 during Transition Flight. Short Bros and Harland Ltd. AD/TN/52
MacDougall, A.R.C.	1951	Revised High-Speed Lift and Drag Data for Clark Y Sections for Propellor Performance Calculations. A.R.C. R.& M. 2474.
McWherter	1962	VTOL Wind Tunnel Techniques and Facilities B.P. Air No.24 page 25.
Preston, J.H.	1950	The Effect of a Wind Tunnel Fan on Irregularities in the Velocity Distribution A.R.C. R.& M. 2307
Taylor, R.T.	1958	Experimental Investigation of the Effects of some shroud Design Variables on the Static Thrust Characteristics of a Small-Scale Shrouded Propellor Submerged in a Wing. N.A.C.A. TN.4126
Thwaites, B.	1960	Incompressible Aerodynamics, Oxford University Press. Page 413
Trebble, W.J.G. Hackett, J.E.	1963	Low Speed Wing Tunnel Tests on a Streamlined Body Containing a Ducted Lifting Fan. R.A.E. TN Aero.2893
Turner & Sparkes	1962	Preliminary notes on some fan tests with inlet maldistribution
Vogler, R.D.	1963	Surface Pressure Distributions Induced on a Flat Plate by a Cold Air Jet Issuing Perpendicularly from the Plate Normal to a Low-Speed Free-Stream Flow N.A.S.A. TN D-1629

Author(s)	Date	Title etc.
Worle	1960	Separation on Axisymmetrical Bodies at Low Speed. La Recherche Aeronautique No.90 Sept-Oct 1960.
Wallis	1961	Axial Flow Fans Newnes
Wood, Charles C. Higginbotham, James T.	1954	Effects of Diffuser and Centrebod Length on Performance of Annual Diffusers with Constant Diameter Outer Walls and with Vortex Generator Flow Controls.
Wood, M.	1963	Personal communication
Wyatt, L.A.	1959	Preliminary note on wind tunnel tests of a wing fitted with Multiple Lifting Fans. R.A.E. Tech-Note Aero 2643 (A.R.C. 21,377)
Wyatt, L.A.	1961	Tests on tandam-mounted lifting fans in a nacelle (Not yet published)
Yaggy, P.F.	1961	A Wind Tunnel Investigation of a Four Foot Diameter Ducted Fan-mounted at the Tip of a Semi-span Wing. NASA TN D-776.

APPENDIX I

Wind Tunnel Fan Design by the late Professor H.B. Squire

Introduction

The object of this note is to draw attention to an existing method of fan design[1] for wind tunnels which, with some slight improvements, is sufficient for all requirements. This method is simple because it assumes that the flow ahead of the fan is axial and uniform and that the flow behind has an axial velocity which is uniform and swirl velocity inversely proportional to the distance from the axis. This flow corresponds to uniform circulation along the blades and a uniform increase in total head across the fan. Under ideal conditions the straightener vanes transform the swirl energy behind the fan into pressure energy.

Attempts to modify this simple procedure to allow for non-uniform velocity distribution ahead of the fan or to obtain a preferred total head distribution behind the fan have often been proposed. These are based on the assumption that 'strip theory' may be applied to the fan blade elements at any radius. It is extremely unlikely that a theory of this kind is even qualitatively correct. For example in an analogous situation of a wing spanning a closed-working-section wind tunnel which has a wall boundary layer, the use of strip theory to determine the variation of wing lift near the wall is completely erroneous. It is also well known that the application of strip theory to calculate the effect of wing twist is unreliable. For fans there is, presumably a tendency for the circulation distribution along the blades to become nearly uniform in the same way that the effect of wing twist is reduced by trailing vortices.

It follows from what is stated above that, for a single stage consisting of a fan and a set of straightener vanes, for ideal conditions, the losses of power are entirely due to the profile drag of the fan blades and vanes: for calculation of stage efficiency the profile drag power losses can be easily calculated and some estimate of the losses due to secondary flow should be made. But no elaborate calculation from thrust and torque distributions can be expected to give more reliable results.

Since the losses are profile drag losses these are reduced by reducing the fan tip speed, providing the blades remain unstalled and an increase in the number of stages is not required. This was pointed out by Glauert but has not been emphasised in some recent papers.

A further point in relation to the general design of subsonic wind tunnels is that the axial velocity at the fan should not be too small ~~a proportion of thsmall~~ a proportion of the working section speed. In other words the expansion between working section and fan section should preferably not be more than 3.

Some assumption must be made about lift curve slope and maximum lift of the fan blade sections. The work of Himmelscamp[2] and Weske[3] has shown that root maximum lift coefficients up to 3.0 are obtainable but that $C_{L_{MAX}}$ at the tip will not be more than 0.7. This is due to the centrifugal flow in the boundary layer of the fan blades. There are some corresponding variations in lift curve slope between root and tip. The tip $C_{L_{MAX}}$ is therefore likely to be the limiting condition of the design.

It often happens that a fan has to work under more severe conditions than expected in the original design. Some allowance should be made for this possibility.

Conditions determining the design

Consider the work done on a mass of fluid ρ of unit volume at radius r as it passes through the fan. The increase in energy is H_1-H_0. Work is done by the blades which, while moving with angular velocity Ω impart on angular momentum $\rho\omega r^2$ to this unit volume and hence the work done on unit volume is $\rho\Omega\omega r^2$ so that

$$H_1-H_0 = \rho\Omega\omega r^2 \qquad (1)$$

Part of this increase in total head is in the form of an increase of pressure and part is in the form of an increase of kinetic energy. The increase in pressure is found by applying Bernoullis equation to the flow relative to the fan blades; the relative angular velocity decreases from Ω to $(\Omega-\omega)$ on passage through the fan (Figure 2.3) and hence

$$p_1-p_0 = \tfrac{1}{2}\rho\left[\Omega^2-(\Omega-\omega)^2\right]r^2$$

$$= \rho(\Omega-\tfrac{1}{2}\omega)\omega r^2 \qquad (2)$$

The swirl kinetic energy is $\frac{1}{2}\rho\omega^2 r^2$ and the sum of this and the above increase in pressure gives the increase in total head (1)*.

---

*The function of the straightener blades is to transform this swirl into pressure energy so that downstream of them a uniform increase of pressure is obtained equal to the increase of total head (1).

Also downstream of the fan ωr^2 is constant and hence the flow corresponds to a free vortex flow with a tangential velocity ωr inversely proportional to radius r.

Equation (1) may be written

$$\frac{H_1 - H_0}{\frac{1}{2}\rho V^2} = 2\left(\frac{\Omega r}{V}\right)\left(\frac{\omega r}{V}\right) \tag{3}$$

The flow reaching the straighteners approaches them at an angle $\alpha_3 = \tan^{-1}\left(\frac{\omega r}{V}\right)$ to the axial direction and leaves at zero angle. (See Figure 2.3) Thus the angle of deflection imparted by the straighteners is $\tan^{-1}\left(\frac{\omega r}{V}\right)$ and a reasonable upper limit for this is $26\frac{1}{2}°$ corresponding to $\left(\frac{\omega r}{V}\right)=\frac{1}{2}$. We shall adopt this as a standard value for the blade root radius. If desired, however, a lower value, say $\left(\frac{\omega r}{V}\right)=\frac{1}{3}=\tan^{-1}18°$ may be taken but this would require a larger boss diameter. Putting $\left(\frac{\omega r}{V}\right)_b=\frac{1}{2}$ we obtain from (3)

$$\left(\frac{\Omega r}{V}\right)_b = \frac{H_1 - H_0}{\frac{1}{2}\rho V^2}$$ where suffix b refers to the boss.

This fixes the blade rotational speed at the root and hence determines the boss radius r_b if angular velocity Ω is known.

The lift coefficient C_L of the fan blade section based on the resultant mean velocity is given by[5]

$$C_L = 2\frac{s}{c}(\tan\alpha_1 - \tan\alpha_2)\cos\alpha_{12} \text{ where } s = \frac{2\pi r}{N} \text{ is the gap}$$

between the blade elements in the equivalent cascade. Now $\tan\alpha_1 = \frac{\Omega r}{V}$

and $\tan\alpha_2 = \dfrac{(\Omega-\omega)r}{V}$ we obtain

$$C_L = 2\left(\frac{s}{c}\right)\left(\frac{\omega r}{V}\right)\cos\alpha_{12}$$

If, for example, at the blade roots $\left(\frac{s}{c}\right)_b = 1.0$, $\left(\frac{\omega r}{V}\right)_b = \frac{1}{2}$ we obtain from (4) $\frac{\Omega r}{V}$ and hence $\alpha_1 = 45°$ $\alpha_2 = 26\frac{1}{2}°$ $\alpha_{12} = 37°$

At the tips if $\frac{\Omega r}{V} \gg 1$ we have $\alpha_1 \simeq \alpha_2 \simeq \alpha_{12}$, $\cos\alpha_{12} \simeq \frac{V}{\Omega r}$ and hence $C_{L_t} \simeq 2\left(\frac{s}{c}\right)\frac{\omega r}{V}\frac{\Omega r}{V} \simeq 2\left(\frac{s}{c}\right)\left(\frac{H_1-H_0}{\rho V^2}\right)\left(\frac{\Omega r}{V}\right)^2$ (7)

It seems desirable (see Section 1) to keep the design lift coefficient at the blade tips down to 0.5.

Example

Power input $\eta P = 100$ H.P.

(After allowance has been made for fan stage efficiency $\eta = 0.90$)

Fan disc area = 31 sq. ft.

Axial velocity at fan = 100 ft/sec.

Angular velocity $\Omega = 100$ radians/sec.

Thus (H_1-H_0) 31 x 100 = 100 x 550

$$\frac{H_1-H_0}{\frac{1}{2}\rho V^2} = \frac{550}{31\times 11.89} = 1.493$$

We take $\left(\frac{\omega r}{V}\right) = \frac{1}{2}$ and hence from (4) $\left(\frac{\Omega r}{V}\right)_b = 1.493$. Thus we get a boss radius of 1.493 ft. We round this off and take $r_b = 1.5$ ft. Also $\pi\left(r_t^2 - r_b^2\right) = 31$ so that $r_t = 3.38$ ft.

If we suppose the fan to have 6 blades of constant chord with gap chord ration 1.5 at the root, then the chord is

$$c = \frac{2\pi r_b}{6\times 1.5} = 1.048 \text{ ft}$$

The results of the calculations are given below.

FAN c=1 foot 6 blades

(1)	(2)	(3)	(4)	(5)	(6)	(7)	(8)	(9)	(10)	(11)
1.5	1.5	0.498	1.002	56.3°	45.1°	11.2°	51.4°	0.624	1.5	0.93
2.0	2.0	0.393	1.627	63.5°	58.4°	5.1°	61.1°	0.483	2.0	0.72
2.5	2.5	0.299	2.201	68.2°	65.6°	2.6°	67.0°	0.391	2.5	0.58
3.0	3.0	0.249	2.751	71.6°	70.0°	1.6°	70.8°	0.329	3.0	0.49
3.38	3.38	0.221	3.159	73.5°	72.4°	1.1°	73.0°	0.292	3.38	0.44

(1) rft (2) $\frac{\Omega r}{V}$ (3) $\frac{\omega r}{V}$ (4) $\frac{(\Omega-\omega)r}{V}$ (5) $\alpha_1 = \tan^{-1} \frac{\Omega r}{V}$

(6) $\alpha_2 = \tan^{-1} \frac{(\Omega-\omega)}{r} V$ (7) $\alpha_1 - \alpha_2$ (8) α_{12} (9) cos α_{12} (10) $\frac{s}{c}$

(11) C_L

The table shows the blade lift coefficient for the example chosen and the inflow and outflow angles α_1 and α_2 for the equivalent cascade. The selection of blade sections and angles has not yet been made.

Straightener design

The form of straightener proposed by Collar[5] consists of untwisted blades set along the wind. There is some risk that these will be stalled at the root if the swirl angle is $26\frac{1}{2}°$ as is proposed. It seems preferable to use cambered blades designed to remove the mean swirl or the swirl at the root. It is unlikely that untwisted blades of ~~unfirom~~ uniform chord set to remove the mean rotation will be satisfactory. Previous experience suggests that the removal of swirl at all radii is not easy and that adjustable trailing edges are a desirable feature.

Sheet metal trailing edges, which can be bent, should be satisfactory for this purpose. The complication of twisted vanes should not be accepted if it can be avoided. The best way of selecting vanes for the mean section is probably the cascade theory of Canter[4]. If there is a residual swirl in the outgoing stream but the angular momentum is zero, then mixing in the diffuser downstream will eventually eliminate this swirl.

Example (continued)

STRAIGHTENERS. Gap-chord ratio = 1.0 at root

r	$\frac{\omega r}{V}$	$\alpha_3=\tan^{-1}\frac{\omega r}{V}$	$\frac{s}{c}$	α_{34}	$\cos\alpha_{34}$	C_L
1.5	0.498	26.5°	1.00	14.0°	0.970	0.97
2.0	0.373	20.5°	1.33	10.0°	0.985	0.98
2.5	0.299	16.65°	1.67	8.5°	0.989	0.99
3.0	0.249	14.0°	2.20	7.1°	0.992	0.99
3.38	0.221	12.5°	2.25	6.3°	0.994	0.99

Note

Outflow angle α_4 for straighteners is zero

$$2\tan\alpha_{34} = \tan\alpha_3$$

References

1. Glauert Aerodynamic Theory Volt 4 pp.338-341
2. Himmelscamp
3. Weske
4. Carter
5. Collar R and M 1885

APPENDIX II

Centrebody diameter for maximum power

As mentioned in 2.3.1 the centrebody diameter is strongly affected by the limitation on α_{1_b}. If axial velocity is constant over the annulus* and a fan of given tip diameter and rotational speed is considered,$^{\phi}$ then for constant root swirl angle the axial velocity may be increased as centrebody diameter is increased, thus increasing the energy output per unit annular area. Since the annular area decreases with increasing centrebody diameter there is a stage at which the total power output starts to fall. This may be demonstrated as follows:-

$$V_T^2 = V_J^2 + \Omega^2 r_t^2 \quad \text{for zero pre-swirl}$$

$$\left(\frac{V_T}{V_J}\right)^2 = 1 + r\cot^2\alpha_{1_b} \quad \text{where} \quad R = \left(\frac{r_t}{r_b}\right)^2$$

$$P_J = \tfrac{1}{2}\rho A_J V_J^{\,3} = \tfrac{1}{2}\rho\pi r_b^{\,2}(R-1)\frac{V_T^{\,3}}{(1 + R^2\cot^2\alpha_{1_b})}$$

$$\frac{dP_J}{dR} = \text{const} \times \frac{(1 + R\cot^2\alpha_{1_b})^{\frac{1}{2}}\{1 + R\cot^2\alpha_{1_b} - 3/2(R-1)\cot^2\alpha_{1_b}\}}{(1 + R\cot^2\alpha_{1_b})^3} = 0$$

at turning points.

$$\therefore \left\{1 + 3/2\cot^2\alpha_{1_b} - R\left(3/2\cot^2\alpha_{1_b} - \cot^2\alpha_{1_b}\right)\right\} = 0$$

$$R = \frac{1 + 3/2\cot^2\alpha_{1_b}}{\frac{1}{2}\cot^2\alpha_{1_b}}$$

$$= 2\tan^2\alpha_{1_b} + 3$$

---

* This appears desirable for a fan of good static efficiency. It has been suggested that a lower velocity sleeve on the outside of the annulus may reduce interference effects under forward speed conditions.

ϕ This is necessary because of limitations on tip Mach Number.

Limiting α_{1b} to 30° yields a centrebody diameter of 53.4% of the fan tip diameter for zero pre-swirl. The diameter varies only slowly with α_{1b} . If the corresponding calculation is made for the case with pre-swirl then a centrebody diameter of 77.5% of fan tip diameter is obtained for maximum power.

APPENDIX III

Further details of the automatic data reduction process

The special scales

Scales of velocity, its square, cube and fourth powers, were made in addition to a velocity scale calibrated in ft/sec for a vertical alcohol manometer. (This scale is referred to in Figure 4.2 as the "conventional scale").

The scales were engraved on 'Trefolite' which is a plastic sheet having alternate black and white laminations. A minimum graduation size of .030" was imposed by film definition. It was arranged that the smallest graduation on each 26" scale was approximately 0.040".

The scale factors for V^3 and V^4 were chosen to be convenient whole numbers of ft^3/sec^3 and ft^4/sec^4 respectively when used with a vertical alcohol manometer. The choice was influenced by the 0.040" minimum graduation sizes which occurred at high velocities.

The linear V^2 scale is also the transfer scale. A constant graduation size of 0.040" was chosen. (i.e. 0.040" of black, then 0.040" of white, etc.)

Small graduations occur at low velocity on the V scale and a factor of almost 12 ft/sec per count would occur if a 0.040" step was placed here. To overcome the coarseness of scale which would have resulted a linear section was introduced at the low velocity end of the scale which blended into a non linear scale having a factor of 1 ft/sec per count on a vertical alcohol manometer. This made necessary the introduction of an added constant in the calibration. (See Table next page). Only the first $\frac{3}{4}$" of scale was affected.

SCALE FACTORS

C = Total count on decade counter   N = number of frames scanned.

V's in ft/sec units throughout

MANOMETER FLUID	$\overline{V}$ (= m_1)	$\overline{V^2}$ (= m_2)	$\overline{V^3}$ (= m_3)	$\overline{V^4}$ (= m_4)
ALCOHOL S.G.= 0.80	$29 + \frac{C}{N}$	$139.91 \frac{C_2}{N}$	$75{,}000 \frac{C_3}{N}$	$25 \times 10^6 \frac{C_4}{N}$
WATER S.G.= 1.00	$32.4 + 1.118 \frac{C}{N}$	$174.89 \frac{C_2}{N}$	$104{,}710 \frac{C_3}{N}$	$39.06 \times 10^6 \frac{C_4}{N}$
CARBON TETRA-CHLORIDE S.G.= 1.52 (WITH DYE)	$40.0 + 1.378 \frac{C}{N}$	$265.82 \frac{C_2}{N}$	$196{,}360 \frac{C_3}{N}$	$90.25 \times 10^6 \frac{C_4}{N}$

Should the reader output be used to operate a tape punch only a linear scale would be required since individual results could be recorded and the sums of powers of velocity could be obtained using an appropriate computer programme.

At present individual points are obtained by running the reader slowly and recording individual totals. Figure 7.1 was obtained in this way. At full speed the summing of five quantities over 15 tubes x 11 frames took 30 minutes.

Before taking photographs it is necessary to make a check on manometer and scale zeroes. This is needed because the electronic circuits accept signals in one sequence only. Starting from the top of the manometer, one should see:-

(i) Static Head
(ii) The zero of the non-linear scales
(iii) Total Head
(iv) A distance below the total head tubes greater than that between (i) and (ii).

It is possible to employ Simpson's rule for integration if end points either of the traverse or outside the rakes are known to have zero velocity. For the former it is necessary to take two similar photographs for the 'odd' traverse positions. For zeroes at the ends of the rake all that is necessary is to sum the "odd" tubes twice. Calculation is then as for the normal Simpson integration.

Some results of reader repeatability and accuracy tests

The results given in the following table give the film reader output counts obtained from a film having five frames. The measurements correspond to the difference between the readings of one pair of manometer tubes on this film. Each frame corresponds to a different rake position. For comparison hand measurements are given which were made using dividers to transfer the appropriate column lengths to the "conventional scale". Their accuracy is unlikely to be better than ±1%, consequently powers greater than V^2 will not have been obtained with adequate accuracy using hand methods.

Since the film reader 'sees' coarser scales for the higher powers of V it is unlikely that counting difficulties will occur. Over a range of tubes and frames the errors due to the relative coarseness of the graduations for higher powers should be smoothed out in a statistical manner. The size of graduations corresponding to the quartic scale at the speeds of the present example is 0.10" in 10" scale length.

The figures in the table are successive readings on the decade counter and are therefore cumulative totals (thus exclude the added constant in the case of the velocity scale)

	REPEATED READINGS OF SAME FILM										
Scale \ Run No	1	2	3	4	5	6	7	8	9	Corresp. "Hand Read" Figures	
V	151	152	150	151	150	150	151			151	Frame 1
	295	296	294	295	293	293	295			294	Frame 2
	432	433	429	432	428	427	432			432	Frame 3
	575	576	571	574	571	569	575			575	Frame 4
	718	718	714	717	713	713	717			718	Frame 5
V^2	233	232	230	231	230	229	233	234	233	233	Frame 1
	448	447	446	447	444	441	451	449	449	448	Frame 2
	644	644	645	644	637	637	647	647	646	651	Frame 3
	857	856	859	857	852	845	863	862	861	866	Frame 4
	1069	1068	1073	1070	1059	1059	1075	1076	1077	1081	Frame 5
V^3	82	84	83	83	84	83					Frame 1
	156	157	156	155	158	157					Frame 2
	221	222	221	222	223	222					Frame 3
	293	295	295	295	295	295					Frame 4
	366	368	369	368	368	368					Frame 5
V^4	53	53	53	53							Frame 1
	98	98	98	98							Frame 2
	136	136	136	136							Frame 3
	180	180	180	179							Frame 4
	224	224	223	224							Frame 5

The switching pulses were monitored on an oscilloscope. With experience it became obvious when the occasional spurious count came through as the decade counter did not then 'lock in' solidly. In case of doubt for either observation the count was repeated until a constant answer appeared and the switching pulses were sharp.

APPENDIX IV

The interaction between the fan and non-uniformities in the upstream flow

(a) Velocity deviations at constant static pressure

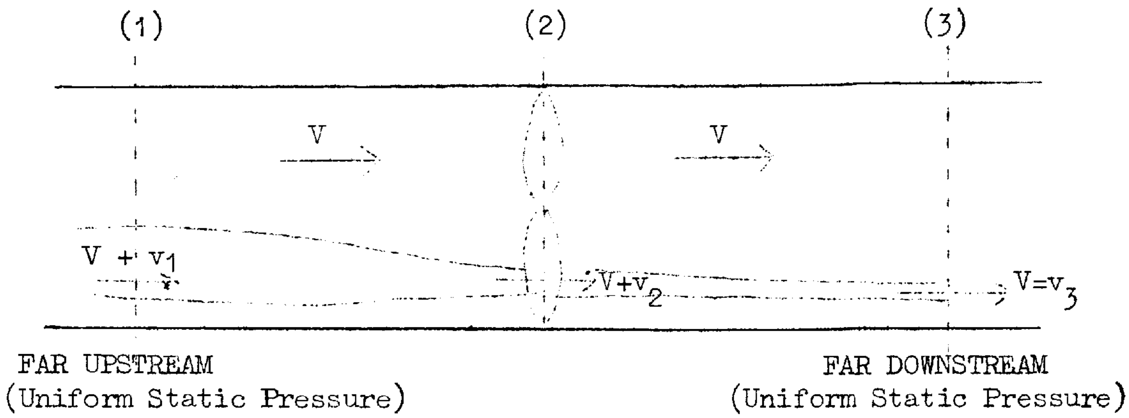

Preston (1950) derives the following result relating small local velocity deviations downstream of a fan to those upstream:-

$\frac{v_3}{v_1} = \frac{2 - C'}{2 + C'}$ where $C' = \frac{a}{2}\frac{\sigma}{\lambda}$, the symbols being those of Collar(1940)

At the centre of the annular area, under static lift conditions, $C' = 2.40$. At both the upstream and downstream stations of Preston's analysis the static pressure is constant and non-uniformities in total head exist.

It can be shown that $\frac{v_2}{v_1} = \frac{2}{2 + C'}$, and $\frac{v_3}{v_2} = \frac{2 - C'}{2}$ where v_2 is the velocity deviation at the fan plane. For the model fan in the static lift condition $\frac{v_2}{v_1} = 0.455$ and $\frac{v_3}{v_2} = -0.20$ giving $\frac{v_3}{v_1} = -0.091$. The inversion is characteristic for $C' > 2.00$. It is clearly desirable that C' should be close to 2.0 if large damping is required. Notice that Preston's solution needs sufficient settling length both upstream and downstream of the fan for the static pressure to become uniform across the duct.

(b) Complementary dynamic and static head deviations at constant total head

Flows upstream of VTOL fans with well shaped flush intakes which avoid separation on the upstream lip and which have no turning devices within the stream tend to have constant total head across the duct since air is taken directly from the mainstream with very small losses. Measurements made by Gregory and Love (1962) show a high velocity region just below the upstream intake lip, associated with the pressure gradient across the flow which turns it into the duct.

A characteristic of a disturbance at constant total head is that if allowed sufficient settling length, the flow will become uniform of its own accord. This is not so in the case above in which, in potential flow, the disturbance would persist.

An attempt has been made to estimate theoretically the effect of the fan on non-uniformities of the present type. This has not been successful for the upstream part of the flow. Although an upstream effect similar to that of 7.3.1 will probably be present, it is not clear whether the upstream influence of the fan will change the natural rate of settling.

The development of disturbances arriving at the fan plane is dealt with below. It is assumed that duct area is constant and that the outlet static pressure, p_3 and in inlet total head H_2 are constant across the duct, as in the static lift case. Velocity deviations of finite size and area have been assumed. Actuator disc theory has been employed.

In subtracting incremental pressures in the analysis which follows it is necessary to make the assumption that the effects are confined to one radius, or that the twist of the fan blades is small. The effect of the straighteners has not been considered.

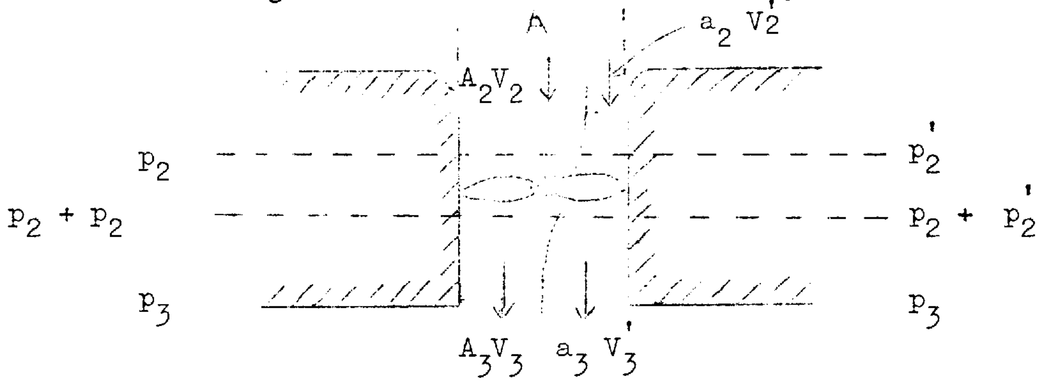

Equating axial momenta between (2) and (3)

$$A_2(p_2 + \Delta p_2) + \rho A_2 V_2^2 + a_3 (p_2' + \Delta p_2') = A p_3 + \rho A_3 V_3^2 + \rho a_3 V_3'^2$$

This may be written, after applying Bernoullis equation betwwen planes (2) and (3) and rearranging:-

$$\tfrac{1}{2}\rho V_2^2 A_2 + \tfrac{1}{2}\rho V_2'^2 d_2 - \tfrac{1}{2}\rho V_3^2 A = (2A_3 - A_2 - A)\Delta p_2 + (2a_3 - d_2)\Delta p_2'$$

using continuity and area relationships the RHS becomes

$$RHS = a_2\left(2\frac{V_2}{V_3} - 1\right)\left(\Delta p_2' - \Delta p_2\right)$$

Put $\Delta p = \dfrac{\rho N C r \Omega 2 CL}{4\pi}$ and $C_L = m\left(\beta - \tan^{-1}\dfrac{V}{\Omega r}\right)$

$$RHS = \tfrac{1}{2}\rho\left(\Omega r\right)^2 a_2\left(2\frac{V_2}{V_3} - 1\right)\left(\frac{N_C}{r}\right)\left(\frac{m}{2\pi}\right)\left(\tan^{-1}\frac{V_2}{\Omega r} - \tan^{-1}\frac{V_1}{\Omega r}\right)$$

Dividing by $\frac{1}{2}\rho(\Omega r)^2 A$ and writing $\frac{V}{\Omega r} = \tilde{V}$ and $\frac{a}{A} = \tilde{a}$ etc. we obtain

$$-\tilde{V}_3^{\,2} + \tilde{V}_2^{\,2}\tilde{A}_2 + \tilde{V}_2'^{\,2}\tilde{a}_2 = \tilde{a}_2\left(2\frac{\tilde{V}_2}{\tilde{V}_3} - 1\right)\left(\frac{NC}{r}\right)\left(\frac{m}{2\pi}\right)\left(\tan^{-1}\tilde{V}_2 - \tan^{-1}\tilde{V}_2'\right)$$

If quantities at (2) are stated then $\tilde{V}_3$ is the only dependent variable which remains and the equation may be rewritten in the form

$$\tilde{V}_3^{\,3} + D\tilde{V}_3 + E = 0$$

Inserting conditions at $R/R = 0.8$ for the static case ($\tilde{V}_2 = 0.40$) and assuming that $\tilde{a}_2 = 0.10$, gives the following results:-

$\tilde{V}_2'$	D	E	$\tilde{V}_3$	$\tilde{p}_3$	C_L'	$\tilde{H}_3'$	$\tilde{V}_3'$	$\tilde{a}_3$
0.32	-.1678	+.01086	.373	1.941	1.025	3.440	1.224	0.0262
0.36	-.1637	+.00526	.388	1.929	0.810	2.755	0.909	0.0397
0.44	-.1657	-.00526	.412	$>H_3$	-	-	-	-

(See below)

The last result is not valid because $p_3 > H_3$ is implied. This would cause separation which invalidates the area assumptions of the above analysis. Cross plotting showed that $\tilde{p}_3 = \tilde{H}_3$ at $\tilde{V}_2 = 0.41$. Note that for $\tilde{V}_2' = 0.32$, C_L' is approaching the maximum normally allowed in blade element calculations. It can be seen that, for the assumed conditions, disturbances which arrive at the fan are changed in sign and amplified. At the same time the disturbed area is reduced for $\tilde{V}_2' < \tilde{V}_2$. The band of velocities which may arrive at the fan without producing either duct or fan blade separation appears to lie between 8% below and 2% above the mainstream velocity.

As deviations upstream of the fan, produced by turning, are likely to be considerably more than this (see Gregory and Love (1962)) and since downstream measurements in the present tests indicate no velocity deviations of significant size below the fan under any test condition and no serious separations, it is apparent that further examination is needed.

The theoretical treatment has the following weaknesses:-

(i) A 'sharp edged' deviation has been assumed. In practice this would be 'smeared' by viscous effects and by the tendency for the edges of a step in the blade loading profile to be smoothed out as on a finite wing.

(ii) Super-velocities found at the exit plane in the theoretical solution would be dissipated by viscous forces. It seems unlikely that the disturbed area would contract very much.

(iii) Actuator disc theory assumes the fan to be negligibly thin. This is not a good assumption since the distances from the fan to which interest attaches are comparable with its thickness.

Doubts about the present experimental comparisons are as follows:-

(i) The contraction effect caused by the fan drive shaft may have suppressed velocity deviations and/or separations.

(ii) An upstream lip radius of 10% of fan diameter in Gregory's experiment produced local velocities of 150% of the static value when $V/V_{J_T} = 0.55$. The lip of the present model had 20% radius and would have produced less pronounced supervelocities.

It is an experimental fact that even the high velocities found by Gregory and Love (1962) were heavily damped and no regions of total head decrease through the fan were found.

Further experimental and theoretical effort is required to obtain an understanding of the mechanisms of the attenuation of disturbances which fans can cause.

APPENDIX V

Tables 1 to 7

TABLE 1 MODEL DIMENSIONS

BODY

Length	40.5"
Maximum width	9.0"
Maximum depth	8.0"
Maximum cross sectional area	0.46sq.ft.
Distance from nose to wing quarter chord	16.4" (=40% body length)
Distance from nose to duct axis (Which is at right-angles to the body centre line)	16.4"

DUCT + CENTREBODY

Duct length	8.0"
Duct diameter (=d)	6.4"
Distance from inlet to fan plane	2.25"
Annular area of duct (7½% of wing 1)	0.15sq.ft.
Distance from inlet to straighteners	6.0"
Inlet radius on upstream side of duct (=20%d)	1.3"
Inlet radius on downstream side of duct (=6%d)	0.38"
No radius on duct outlet	
Centre body length	9.0"
Maximum centrebody diameter	3.7"
Length of cylindrical portion of centrebody (ends are ellipsoidal)	3.0"

FAN and STRAIGHTENERS

Tip diameter (=d)	6.4"
Boss diameter (=58%d)	3.7"
FAN	
5 Blades 10% Clark Y section	
Root Blade Angle	$32\frac{1}{2}^{\circ}$
Tip Blade Angle	$17\frac{1}{2}^{\circ}$
Mean Chord	1.0"
STRAIGHTENERS	
12 Blades, Thin cambered plates	
Blade Chord	1.3"

WING 1

Span	34.0"
Area	2.0sq.ft.
Aspect Ratio	6.0
Taper Ratio	2.0
Unswept quarter chord	
Aerofoil Section	NACA0012
Wing-Body angle adjustment between	$\pm 30^{\circ}$

STRUTS

Diameter	1.0"
Distance between outer ends	29.0"
Distance from nose of body	16.4"

TYPE OF RESONANCE \ EXCITING FORCES		ROTATIONAL FREQUENCY = f	ONE FAN BLADE CROSSING FOUR SPIDER WAKES = 4 f	FAN BLADES PASSING A FIXED POINT = 5 f	GEAR TOOTH IMPOSED FORCES = 18 f	FIVE FAN BLADES CROSSING FOUR SPIDER WAKES = 20 f
OSCILLATION OF BEARINGS AGAINST SPRINGS	10 c/s	600 RPM (1800 RPM)	LITTLE COUPLING	LITTLE COUPLING	33 RPM (100 RPM)	30 RPM (90 RPM)
FAN BLADE BENDING	2,120 c/s	$M_T > 1$ ≠	31,800 RPM	25,400 RPM	7,100 RPM* (21,300 RPM)	6,350 RPM* (19,100 RPM)
FAN BLADE TORSION	9,600 c/s APPROX.	$M_T > 1$ ≠	$M_T > 1$ ≠	$M_T > 1$ ≠	31,900 RPM	28,800 RPM
MAINSHAFT WHIRL	490 c/s	29,400 RPMØ				
CANTILEVER WHIRL	615 c/s	36,950 RPM				
FANSHAFT WHIRL	615 c/s	36,950 RPM				

NORMAL ROTATIONAL SPEED IS 23,200 RPM (387 c/s)

THIRD HARMONICS EXCITED AT RPM SHOWN IN BRACKETS

* RESONANCES OBSERVED BETWEEN 5,000 AND 6,000 RPM

Ø 27,000 RPM PRODUCED NO WHIRL

≠ UNIT TIP MACH NUMBER OCCURS AT 36,500 RPM

TABLE 2 CALCULATED ROTATIONAL SPEEDS FOR RESONANCE

1

WIND TUNNEL AND TEST DATE	Imperial College 5' x 4'. Late 1961
CONFIGURATIONS	On Struts, On Wings, (without underfins)
VARIABLES	V, 30 ft/sec to 130 ft/sec. 20 ft/sec intervals α, = −20°, −18°, to +18°, +20°. 3° intervals α_o, −10° to +20°. 5° intervals consistent with $\lvert\alpha_W\rvert < 20°$
MEASUREMENTS AND TESTS	Lift, Drag and Pitching Moment. Surface Flow Visualisation. Determination of Floor Stagnation Regime. Pitot-static traverse of duct exit in the static-lift condition.

2

WIND TUNNEL AND TEST DATE	Royal Aircraft Establishment 11½' x 8½'. No 1 June 1962
CONFIGURATIONS	On Struts, On Wings, with and without underfins.
VARIABLES	V, 20 ft/sec to 80 ft/sec and 120 ft/sec. 20 ft/sec intervals α, −18° to +18°. 6° intervals α_o = 0°
MEASUREMENTS	Lift, Drag and Pitching Moment.

3

WIND TUNNEL AND TEST DATE	Imperial College 5' x 4'. October 1962.
CONFIGURATIONS	On Struts with and without underfins
VARIABLES	V, 30 ft/sec to 110 ft/sec, 20 ft/sec intervals α, −18° to +18°. 6° intervals
MEASUREMENTS AND TESTS	Lift, Drag and Pitching Moment } Electrical Power Input } Simultaneously Fan RPM } (Series 3a) Duct Flow Measurements } Flow Visualisation on Fins Check force tests with pressure tubes disconnected (Series 3b)

TABLE 3 Summary of Tests on Lifting Fan Model, with Fan Running

CAMERA	ALPHA Model 6 1:1.8/50 lens. (35mm single lens reflex, focal plane shutter)
FILM + EXPOSURE	PAN F (50 A.S.A) 1/5 sec at f.8 Developed in Contrast FF for $2\frac{1}{2}$ minutes at 70°F
LIGHTING	Two 100w household bulbs 18" above the top of the manometer. White reflector below manometer. White paper behind tubes Methyl Violet dye in $C.Cl_4$ fluid.
SETTING UP	Distance from film-plane to tubes = 43" Camera opposite mid height to within $\pm\frac{1}{4}$" Tilt in film plane less than $\pm$1/10 degree Scale zero to satisfy conditions of Appendix 3.

TABLE 4. PARTICULARS OF MANOMETER PICTURES

REDUCTION OF	DIVISORS		
	(a)	(b)	(c)
FORWARD SPEED	$\bar{V}_J$	V_{J_T}	ΩR
LIFT INCREMENT	$\rho A_J \bar{V}_J^2$	T	$\rho A_J \left(\Omega R\right)^2$
DRAG INCREMENT	$\rho A_J \bar{V}_J^2$	T	$\rho A_J \left(\Omega R\right)^2$
PITCHING MOMENT INCREMENT	$\rho A_J \bar{V}_J^2 d$	Td	$\rho A_J \left(\Omega R\right)^2 d$

TABLE 5. SOME POSSIBLE REDUCTION PARAMETERS

TABLE 6. MEASURED VALUES OF STATIC LIFT

SERIES (TUNNEL)	RPM	TUNNEL CONDITION	BODY ON STRUTS		BODY ON WING		REMARKS
			NO UNDERFINS	WITH UNDERFINS	NO UNDERFINS	WITH UNDERFINS	
1 (5' x 4')	23,200	CLOSED	12.70 lbs (C_T =0.170)	-	-	-	Underfins not used
		VENTED (floor & walls)	13.65 lbs (C_T =0.183)	-	13.45 lbs	-	
2 ($11\frac{1}{2}$' x $8\frac{1}{2}$')	23,600	CLOSED	13.05 lbs (C_T =0.169)	12.65 lbs	13.05 lbs	12.35 lbs	After bearing failure
		VENTED (floor only)	13.80 lbs (C_T =0.179)	-	-	-	
3 (5' x 4')	22,800	VENTED (floor & walls)	13.05 lbs (C_T =0.180)				Tested on return from RAE.
			12.65 lbs	12.25 lbs	-	-	Traverse takes installed in duct.
			11.75 lbs	11.15 lbs	-	-	Rakes plus pressure tubes*

*See text, Section 6.3

$\frac{V}{\Omega R}$	α°	TEST SERIES 3b (5'x4' TUNNEL) (1)*	(2)	(3)	TEST SERIES 2 ($11\frac{1}{2}$'x$8\frac{1}{2}$' TUNNEL) (1)	(2)	(3)
.030	−18				.0860	−.0180	.0084
	−12				.0880	−.0096	.0075
	−6				.0914	−.0010	.0098
	0				.0908	+.0100	.0084
	6				.0889	.0174	.0112
	12				.0872	.0280	.0055
	18				.0835	.0370	.0075
.060	−18	.0879	−.0058	.0252	.0872	−.0063	.0255
	−12	.0883	+.0038	.0260	.0895	+.0023	.0216
	−6	.0886	.0135	.0328	.0900	.0108	.0241
	0	.0880	.0226	.0296	.0900	.0220	.0255
	6	.0849	.0335	.0300	.0860	.0302	.0260
	12	.0814	.0430	.0372	.0840	.0386	.0220
	18	.0795	.0520	.0355	.0818	.0472	.0255
.090	−18	.0788	.0060	.0420	.0894	.0050	.0442
	−12	.0874	.0152	.0425	.0883	.0140	.0400
	−6	.0864	.0245	.0504	.0875	.0235	.0440
	0	.0851	.0342	.0504	.0849	.0350	.0478
	6	.0813	.0440	.0504	.0819	.0420	.0460
	12	.0795	.0522	.0600	.0793	.0500	.0422
	18	.0803	.0640	.0580	.0810	.0595	.0470
.120	−18	.0903	.0170	.0598	.0920	.0163	.0644
	−12	.0860	.0268	.0642	.0891	.0258	.0597
	−6	.0850	.0360	.0704	.0853	.0352	.0632
	0	.0835	.0462	.0720	.0798	.0448	.0698
	6	.0799	.0444	.0726	.0791	.0533	.0670
	12	.0788	.0632	.0830	.0786	.0615	.0630
	18	.0820	.0783	.0808	.0790	.0700	.0666
.150	−18	.0924	.0283	.0786			
	−12	.0860	.0383	.0844			
	−6	.0865	.0472	.0920			
	0	.0832	.0580	.0942			
	6	.0781	.0655	.0963			
	12	.780	.0754	.1052			
	18	.0860	.0945	.1038			
.180	−18	.0957	.0418	.1038	.0971	.0404	.1042
	−12	.0904	.0517	.1050	.0908	.0498	.0982
	−6	.0890	.0597		.0870	.0594	.1037
	0	.0840	.0709	.1160	.0830	.0688	.1143
	6	.0769	.0789	.1240	.0813	.0785	.1180
	12	.0779	.0912	.1320	.0789	.0820	.1203
	18	.0902	.1130	.1280	.0801	.0955	.1167

$$(1) = \frac{\Delta L}{\rho(\Omega R)^2 A_J}$$

$$(2) = \frac{\Delta D}{\rho(\Omega R)^2 A_J}$$

$$(3) = \frac{\Delta M}{\rho(\Omega R)^2 A_J d}$$

VALUES SHOWN OBTAINED AS CROSS PLOTS

*INCLUDING 3% CORRECTION FOR DRAG OF TRAVERSE RAKES.

TABLE 7 FORCE TESTS IN TWO WIND TUNNELS, (A) BODY ON STRUTS

		TEST SERIES 1 (5'x4' TUNNEL)			TEST SERIES 2 ($11\frac{1}{2}$'x$8\frac{1}{2}$' TUNNEL)		
$\frac{V}{\Omega R}$	α^o	(1)	(2)	(3)	(1)	(2)	(3)
.030	− 18				.0878	−.0183	−.001
	− 12				.0900	−.0083	+.0060
	− 6				.0930	+.0020	.0030
	0				.0930	.0094	.0102
	6				.0930	.0193	.0049
	12				.0918	.0293	.0160
	18				.0895	.0360	.0184
.060	− 18	.0792	−.0078	.0173	.0780	−.0085	.0180
	− 12	.0852	+.0080	.0270	.0832	+.0039	.0261
	− 6	.0840	+.0163	.0307	.0838	.0133	.0292
	0	.0830	.0263	.0342	.0826	.0215	.0315
	6	.0817	.0340	.0360	.0806	.0307	.0260
	12	.0830	.0440	.0360	.0812	.0392	.0214
	18	.0910	.0522	.0332	.0826	.0455	.0260
.090	− 18	.0680	0	.0320	.0640	−.0008	.0326
	− 12	.0838	.0178	.0470	.0796	+.0150	.0462
	− 6	.0800	.0270	.0525	.0790	.0244	.0539
	0	.0782	.0352	.0562	.0767	.0335	.0520
	6	.0790	.0432	.0568	.0750	.0412	.0490
	12	.0790	.0544	.0523	.0743	.0490	.0400
	18	.0918	.0619	.0493	.0795	.0548	.0433
.120	− 18	.0558	.0053	.0459	.0504	.0055	.0466
	− 12	.0850	.0287	.0686	.0792	.0255	.0602
	− 6	.0862	.0380	.0748	.0790	.0350	.0738
	0	.0790	.0458	.0780	.0750	.0434	.0740
	6	.0790	.0540	.0762	.0720	.0520	.0714
	12	.0744	.0669	.0710	.0728	.0620	.0640
	18	.0920	.0727	.0690	.0798	.0634	.0630
.150	− 18	.0460	.0090	.0546			
	− 12	.0980	.0388	.0850			
	− 6	.0986	.0489	.0925			
	0	.0948	.0567	.1029			
	6	.0862	.0660	.0993			
	12	.0718	.0813	.0905			
	18	.0920	.0840	.0890			
.180	− 18	.0368	.0090	.0620	.0304	.0140	.0366
	− 12	.1145	.0493	.1032	.1002	.0463	.0860
	− 6	.1107	.0603	.1172	.0963	.0573	.0991
	0	.1106	.0670	.1272	.0890	.0608	.1202
	6	.0932	.0770	.1260	.0840	.0698	.1210
	12	.0702	.1000	.1100	.0837	.0800	.1140
	18	.0912	.0943	.1100	.0800	.0793	.1098

$$(1) = \frac{\Delta L}{\rho(\Omega R)^2 A_J}$$

$$(2) = \frac{\Delta D}{\rho(\Omega R)^2 A_J}$$

$$(3) = \frac{\Delta M}{\rho(\Omega R)^2 A_J d}$$

VALUES SHOWN OBTAINED AS CROSS-PLOTS

TABLE 7(continued) FORCE TESTS IN TWO WIND TUNNELS
(B) BODY ON WING

$\frac{V}{\Omega R}$	α^{o}	TEST SERIES 3b (5'x4' TUNNEL) (1)*	(2)	(3)	TEST SERIES 2 ($11\frac{1}{2}$'x$8\frac{1}{2}$' TUNNEL) (1)	(2)	(3)
.030	−18						
	−12						
	−6						
	0	N O T E S T S P E R F O R M E D					
	6						
	12						
	18						
.060	−18	.0859	−.0070	.0290			
	−12	.0893	.0040	.0312			
	−6	.0895	.0140	.0322			
	0	.0903	.0237	.0370			
	6	.0883	.0320	.0355			
	12	.0878	.0416	.0380			
	18	.0834	.0495	.0360			
.090	−18	.0890	.0018	.0520	.0914	.0055	.0490
	−12	.0930	.0142	.0540	.0915	.0143	.0520
	−6	.0923	.0244	.0563	.0929	.0227	.0492
	0	.0947	.0339	.0585	.0914	.0340	.0470
	6	.0912	.0420	.0580	.0918	.0407	.0483
	12	.0893	.0550	.0564	.0899	.0468	.0482
	18	.0863	.0559	.0509	.0834	.0532	.0420
.120	−18	.0949	.0150	.0755	.0986	.0160	.0710
	−12	.0995	.0249	.0790	.0987	.0253	.0750
	−6	.0982	.0350	.0805	.0982	.0340	.0800
	0	.1034	.0440	.0810	.0985	.0440	.0820
	6	.0969	.0522	.0759	.0973	.0520	.0790
	12	.0932	.0600	.0738	.0946	.0593	.0740
	18	.0907	.0640	.0660	.0890	.0660	.0660
.150	−18	.1044	.0249	.1025			
	−12	.1117	.0350	.1058			
	−6	.1093	.0463	.1043			
	0	.1150	.0544	.1043			
	6	.1056	.0622	.0959			
	12	.1024	.0693	.0920			
	18	.0982	.0738	.0820			
.180	−18	.1128	.0320	.1308		.0367	.1153
	−12	.1262	.0453	.1373	.1209	.0470	.1208
	−6	.1236	.0558	.1300	.1182	.0574	.1251
	0	.1273	.0650	.1270	.1170	.0680	.1365
	6	.1150	.0725	.1190	.1150	.0770	.1280
	12	.1130	.0792	.1113	.1116	.0842	.1200
	18	.1100	.0836	.1000	.1042	.0890	.1100

$$(1) = \frac{\Delta L}{\rho(\Omega R)^2 A_J}$$

$$(2) = \frac{\Delta D}{\rho(\Omega R)^2 A_J}$$

$$(3) = \frac{\Delta M}{\rho(\Omega R)^2 A_J d}$$

VALUES SHOWN OBTAINED AS CROSS-PLOTS

Δ INCREMENTS ARE MEASURED ABOVE A DATUM WITH FINS.

* INCLUDING 3% CORRECTION FOR DRAG OF TRAVERSE RAKES

TABLE 7(continued) FORCE TESTS IN TWO WIND TUNNELS
(C) BODY ON STRUTS WITH FINS.

		(5'x4' TUNNEL)			TEST SERIES 2 ($11\frac{1}{2}$'x$8\frac{1}{2}$' TUNNEL)		
$\frac{V}{\Omega R}$	α^o	(1)	(2)	(3)	(1)	(2)	(3)
.030	− 18				.0842	−.0180	.0085
	− 12				.0876	−.0080	.0075
	− 6				.0892	+.0007	.0053
	0				.0890	.0117	.0130
	6				.0876	.0208	.0115
	12				.0876	.0290	.0095
	18				.0840	.0369	.0097
.060	− 18				.0754	−.0080	.0220
	− 12				.0822	.0047	.0260
	− 6				.0852	.0120	.0280
	0				.0840	.0215	.0317
	6				.0834	.0303	.0284
	12				.0830	.0370	.0317
	18				.0820	.0442	.0273
.090	− 18				.0672	−.0008	.0360
	− 12				.0878	.0140	.0475
	− 6				.0882	.0234	.0530
	0		NO TESTS PERFORMED		.0890	.0320	.0530
	6				.0870	.0409	.0530
	12				.0880	.0470	.0547
	18				.0850	.0520	.0467
.120	− 18				.0602	.0043	.0520
	− 12				.0940	.0250	.0740
	− 6				.0934	.0349	.0750
	0				.0904	.0434	.0762
	6				.0870	.0515	.0760
	12				.0950	.0584	.0730
	18				.0904	.0608	.0710
.150	− 18						
	− 12						
	− 66						
	0						
	6						
	12						
	18						
.180	− 18				.0480	.0124	.0940
	− 12				.1056	.0483	.1240
	− 6				.1060	.0580	.1320
	0				.1070	.0660	.1280
	6				.1040	.0760	.1238
	12				.1126	.0845	.1210
	18				.1112	.0808	.1078

$(1) = \frac{\Delta L}{\rho(\Omega R)^2 A_J}$

$(2) = \frac{\Delta D}{\rho(\Omega R)^2 A_J}$

$(3) = \frac{\Delta M}{\rho(\Omega R)^2 A_J d}$

VALUES SHOWN OBTAINED AS CROSS-PLOTS

INCREMENTS ARE MEASURED ABOVE A DATUM WITH FINS.

TABLE 7(continued) THE RESULTS OF FORCE TESTS
(D) BODY ON WING WITH FINS

APPENDIX VI

Illustrations

(A decimal numbering system is used.
The first figure is that of the
appropriate chapter)

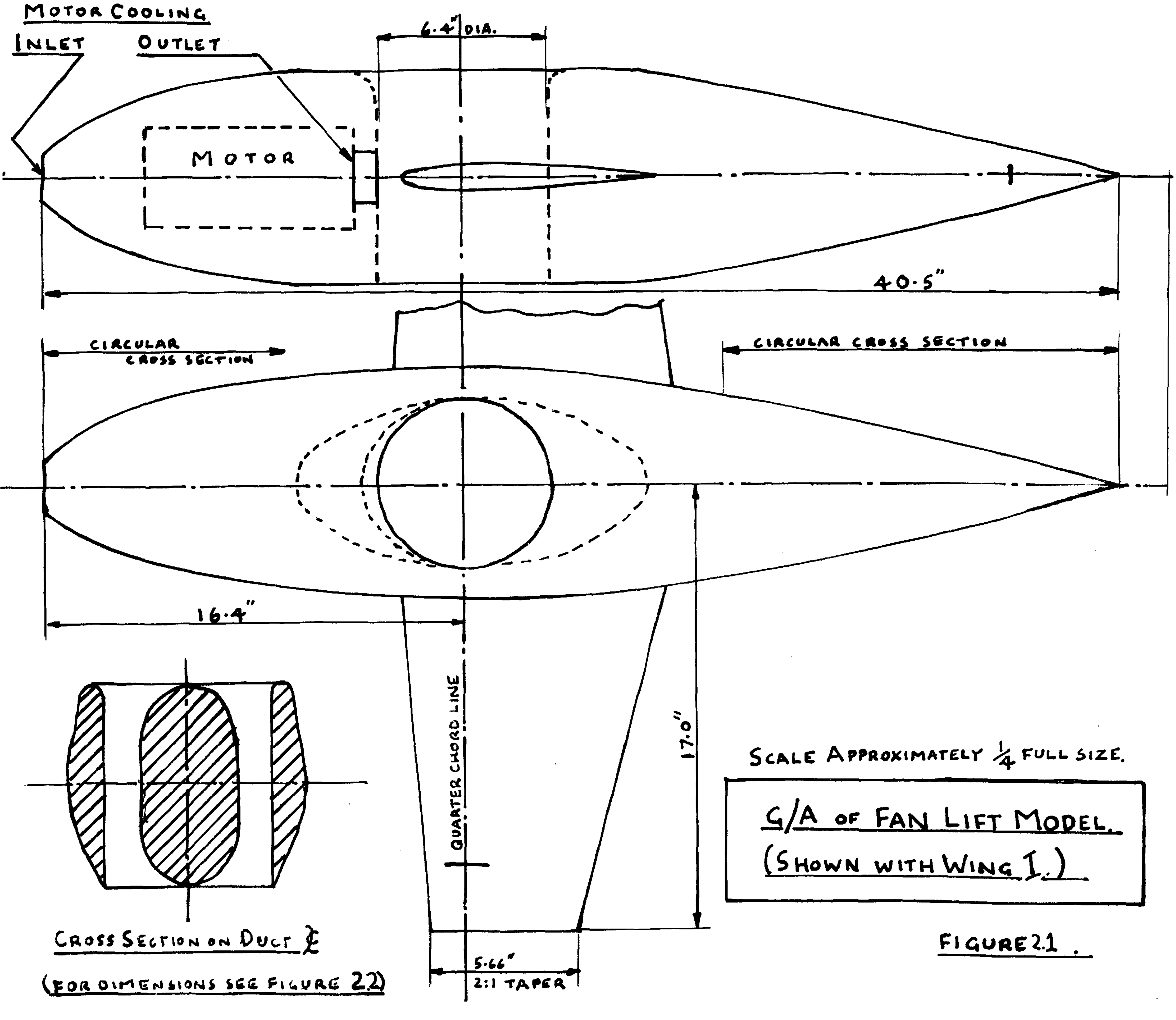
MOTOR COOLING
INLET
OUTLET
6.4" DIA.
MOTOR
40.5"
CIRCULAR CROSS SECTION
CIRCULAR CROSS SECTION
16.4"
QUARTER CHORD LINE
17.0"
5.66"
2:1 TAPER
SCALE APPROXIMATELY 1/4 FULL SIZE.
G/A OF FAN LIFT MODEL.
(SHOWN WITH WING I.)
CROSS SECTION ON DUCT ℄
(FOR DIMENSIONS SEE FIGURE 2.2)

FIGURE 2.1.

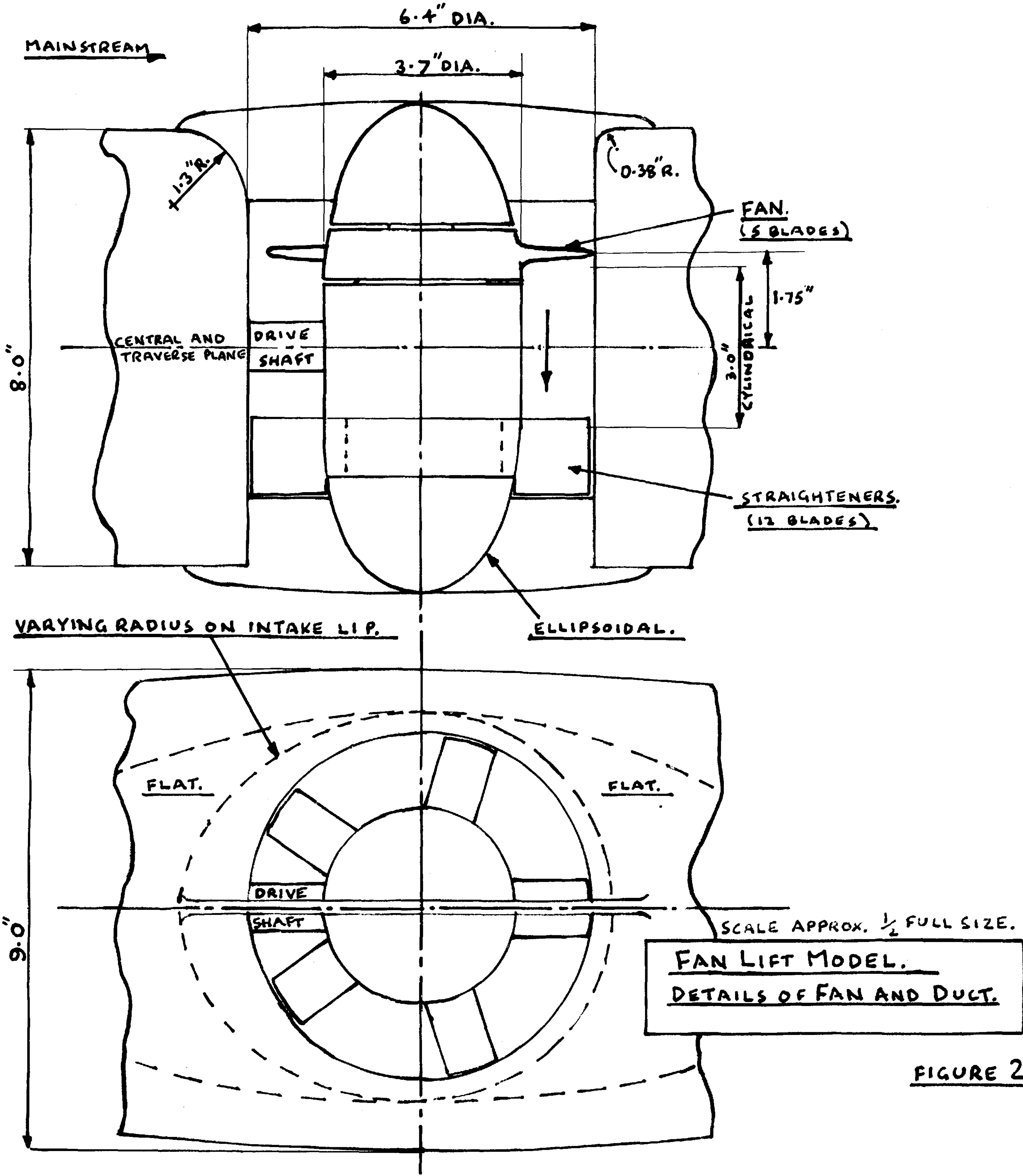
MAINSTREAM
6·4" DIA.
3·7" DIA.
1·3" R.
0·38" R.
FAN.
(5 BLADES)
1·75"
3·0" CYLINDRICAL
8·0"
CENTRAL AND TRAVERSE PLANE
DRIVE SHAFT
STRAIGHTENERS.
(12 BLADES)
VARYING RADIUS ON INTAKE LIP.
ELLIPSOIDAL.
FLAT.
FLAT.
DRIVE
SHAFT
9·0"
SCALE APPROX. 1/2 FULL SIZE.
FAN LIFT MODEL.
DETAILS OF FAN AND DUCT.

FIGURE 2.2

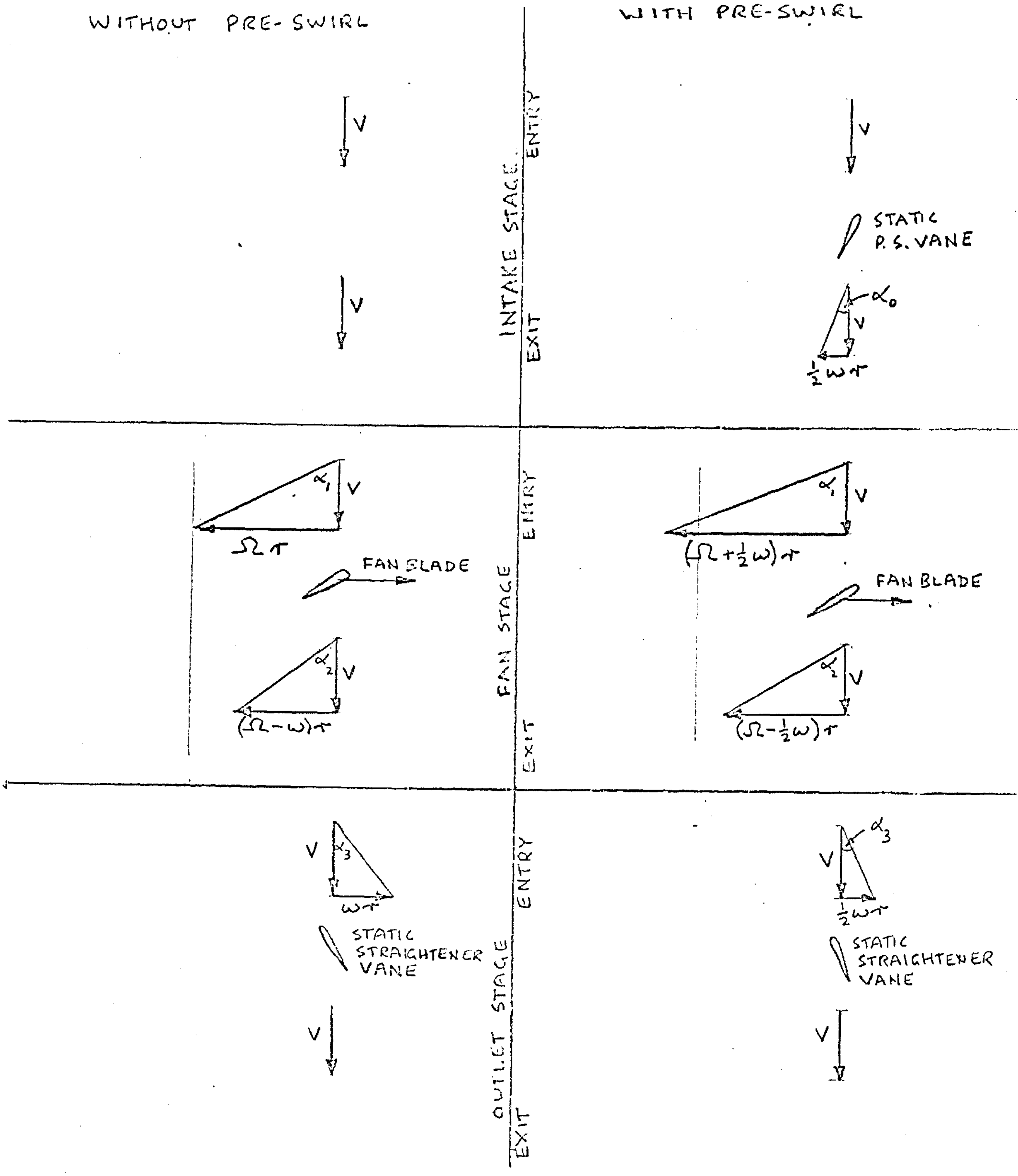

VELOCITY DIAGRAMS FOR FLOW THROUGH A FAN UNIT

FIGURE 23

(SEE SECTION 2.6 AND APPENDIX I)

(i) $\phi = 0°$

SEPARATION ALMOST AT FULL DIAMETER

(ii) $\phi_{max} \simeq 20°$

SLIGHTLY SMALLER SEPARATED REGION

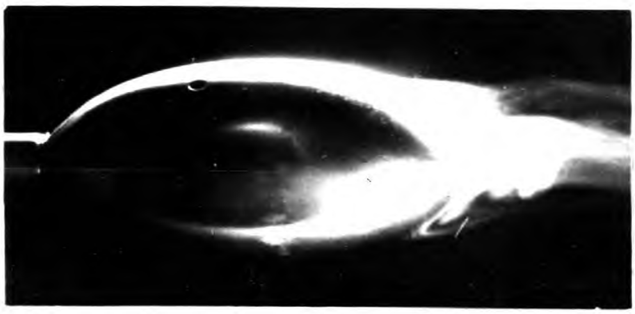

(iii) $\phi_{max} \simeq 40°$

SEPARATED REGION FURTHER DECREASED

(iv) $\phi_{max} \simeq 60°$

ATTACHED FLOW FOLLOWED BY VORTEX BURST

FLOW PHOTOGRAPHS USING TITANIC CHLORIDE SMOKE OF A 2:1 ELLIPSOID IN THE 3" SWIRL TUNNEL

EXPONENTIAL VORTEX SWIRL DISTRIBUTION
SCALE APPROXIMATELY FULL SIZE

FIG. 2.4

(SEE SECTION 2.3)

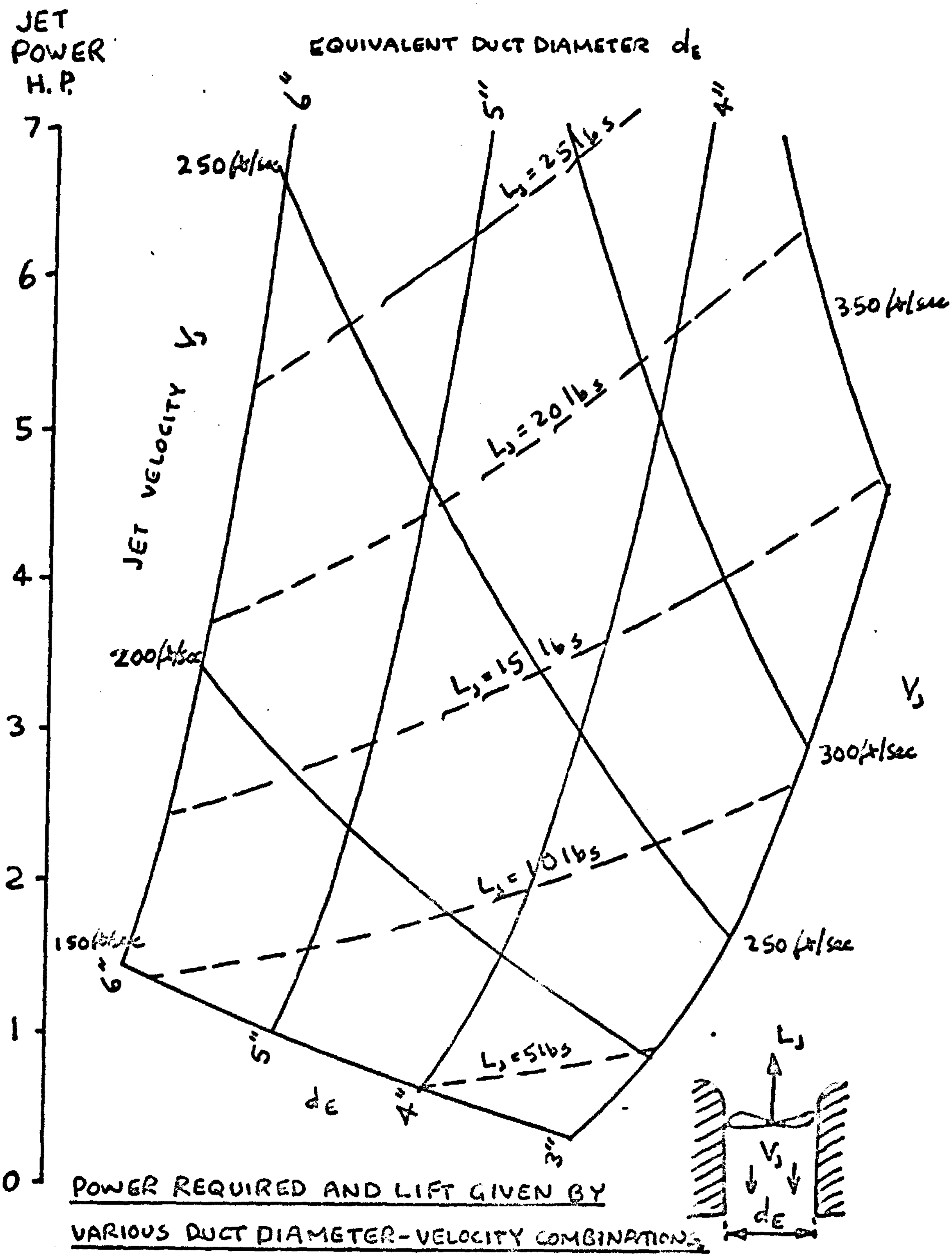

POWER REQUIRED AND LIFT GIVEN BY VARIOUS DUCT DIAMETER-VELOCITY COMBINATIONS

FIGURE 2.5
(SEE SECTIONS 2.4 AND 2.5)

FIGURE 2.6
(SEE SECTION 2.4)

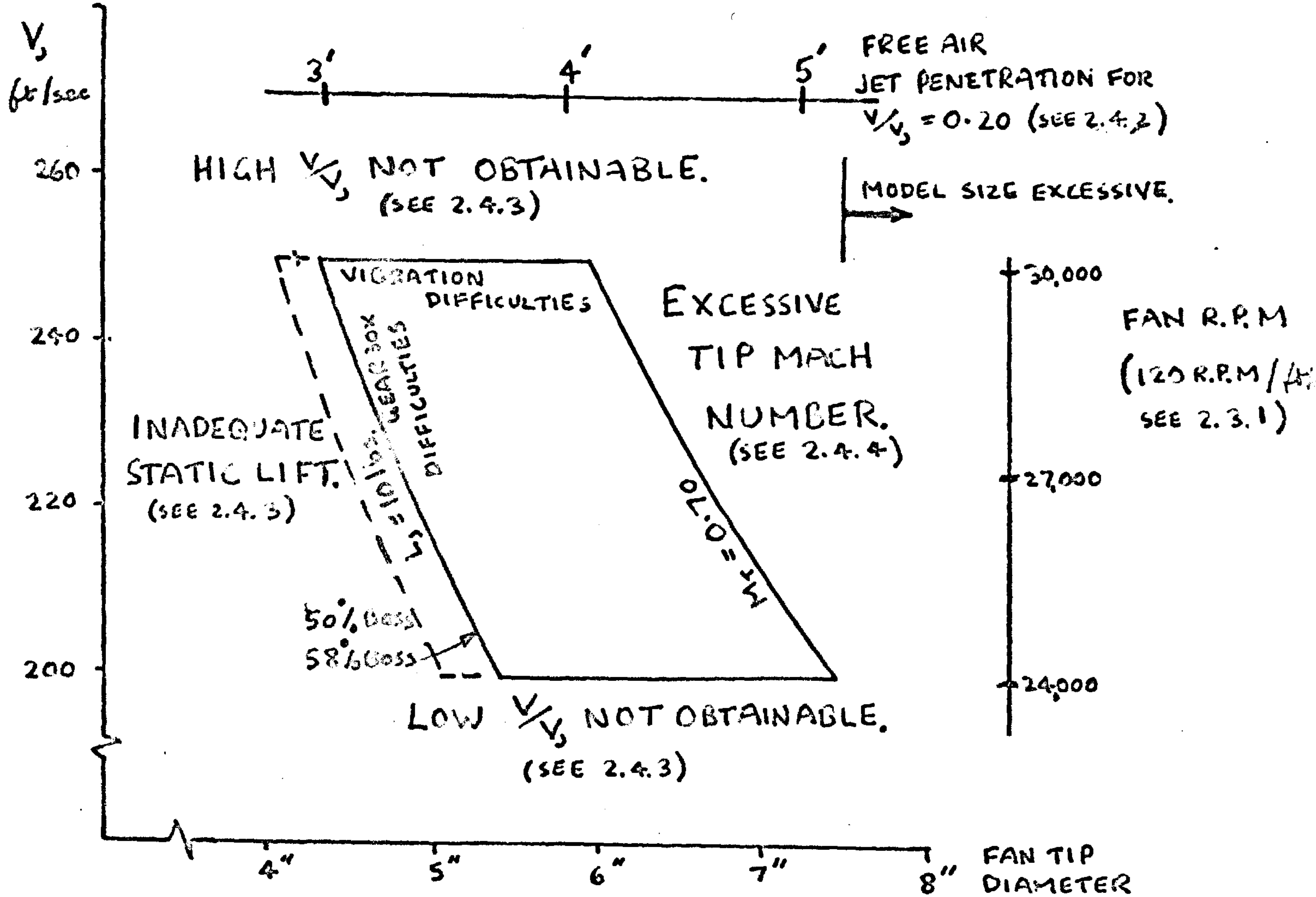

DESIGN BOUNDARIES ARISING FROM AERODYNAMIC CONSIDERATIONS. FIGURE 2.6

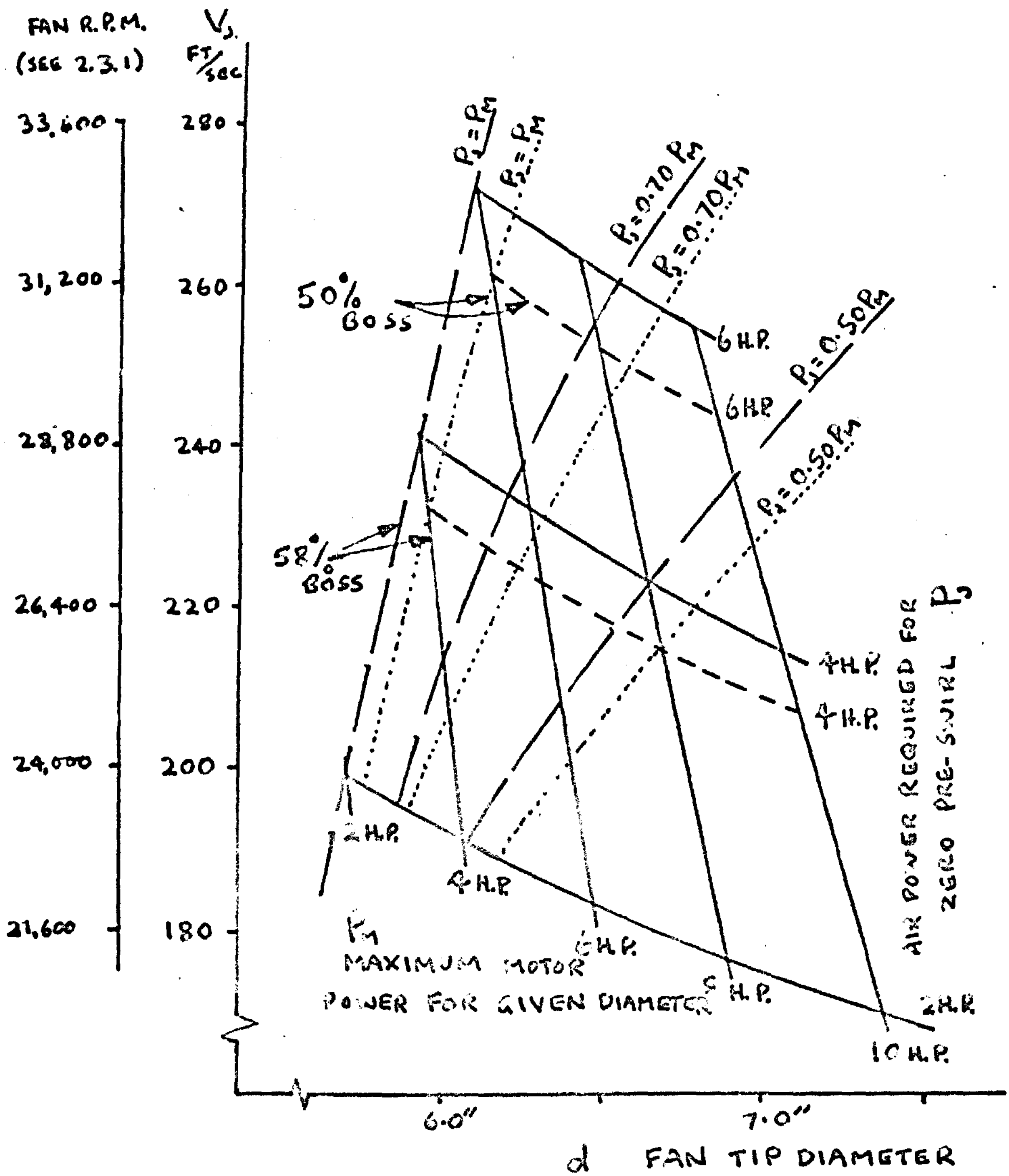

COMPARISON OF POWER REQUIRED WITH THE SPACE-LIMITED POWER AVAILABLE.

FIGURE 2.7

(SEE SECTION 2.2.3)

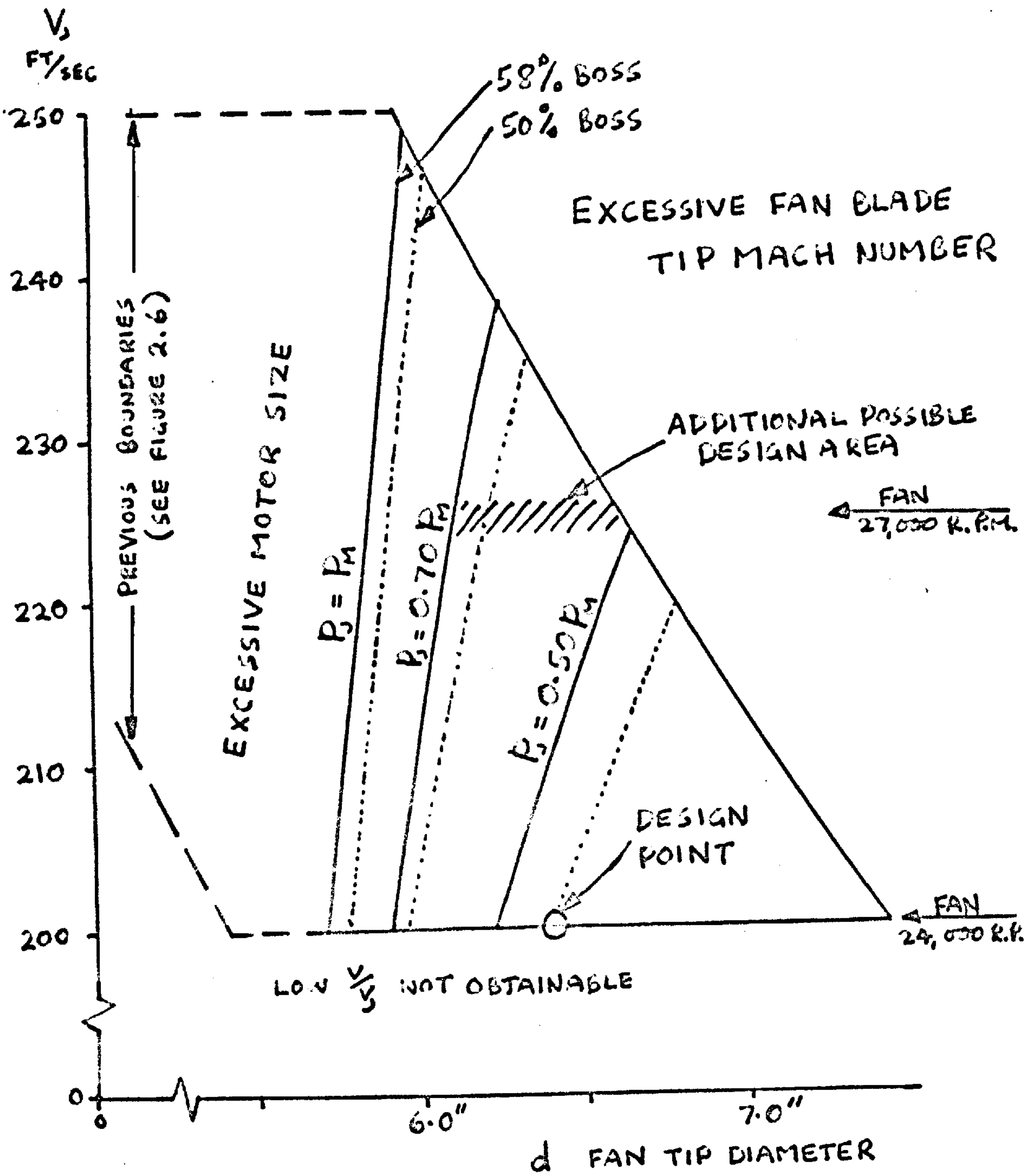

DESIGN BOUNDARIES INCLUDING CONSIDERATION OF MOTOR SIZE.

FIGURE 2.8

(SEE SECTIONS 2.5 AND 2.6)

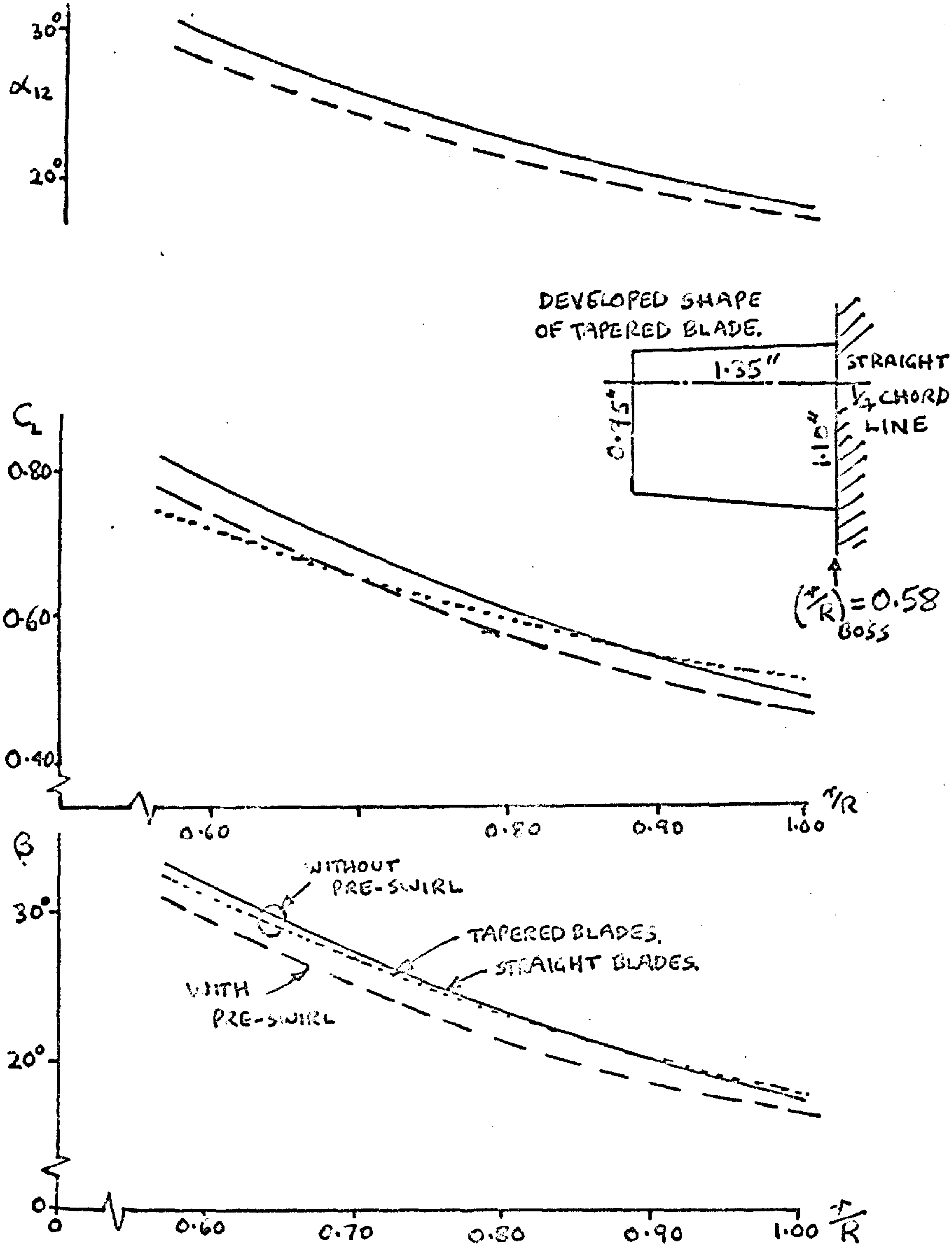

DESIGN FEATURES OF FAN BLADES.

FIGURE 2.9

(SEE SECTION 2.6.3)

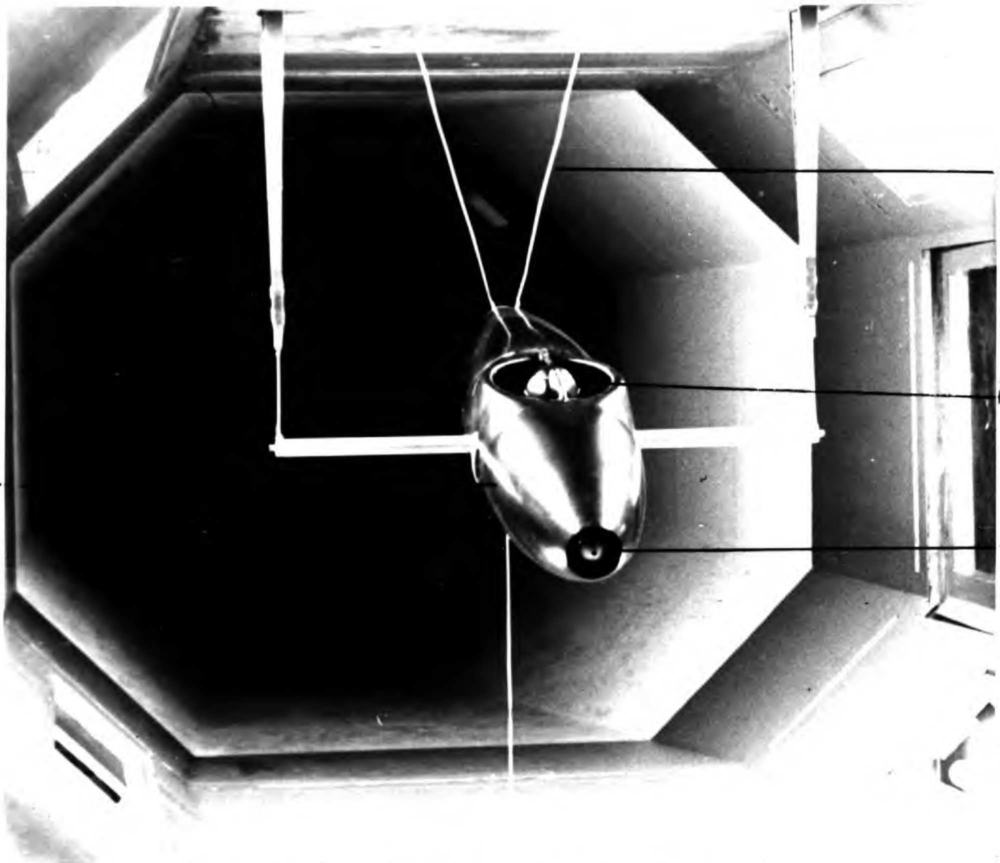

VIEW SHOWING INTAKE OF DUCT

VIEW SHOWING DUCT OUTLET

SIDE VIEW

GENERAL VIEWS OF FAN-LIFT MODEL

FIG. 3.1

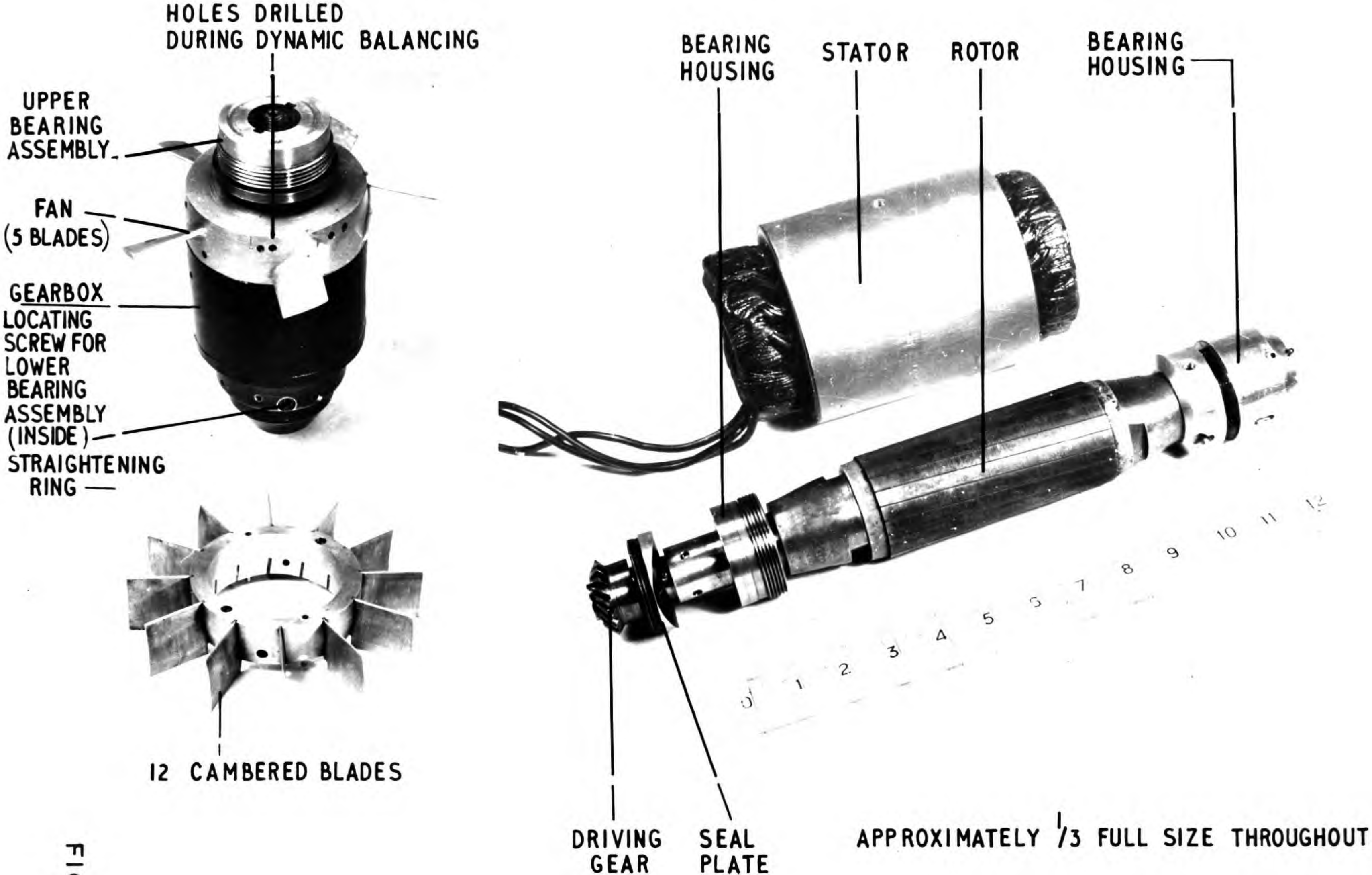

SOME COMPONENTS OF THE FAN-UNIT AND MOTOR

FIG. 3.2

FIG. 3.2

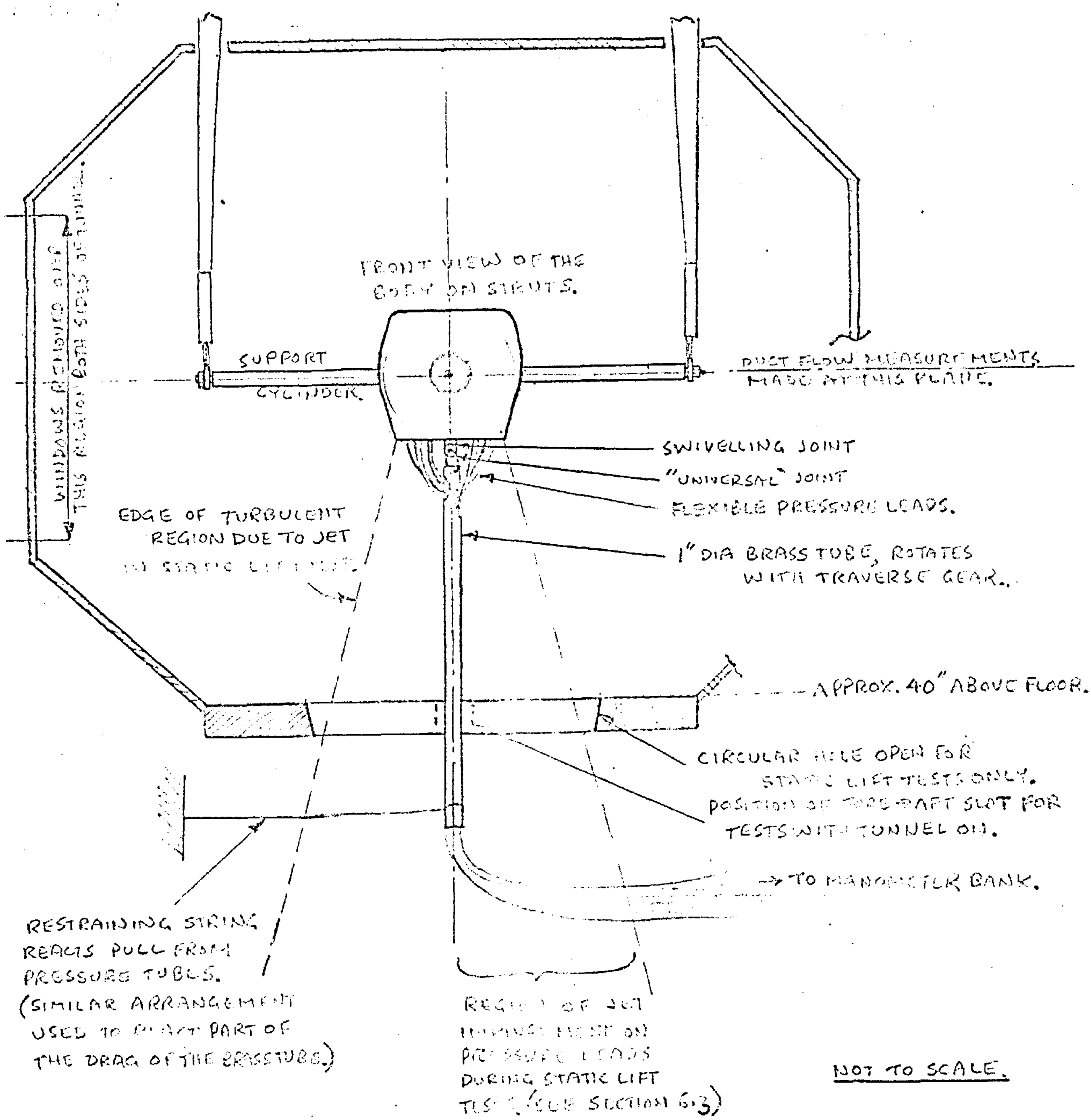

THE TEST RIG FOR TESTS INVOLVING FLOW MEASUREMENTS WITHIN THE DUCT

FIGURE 3.3

(SEE SECTIONS 3.5, 3.6, 6.2, 7.1)

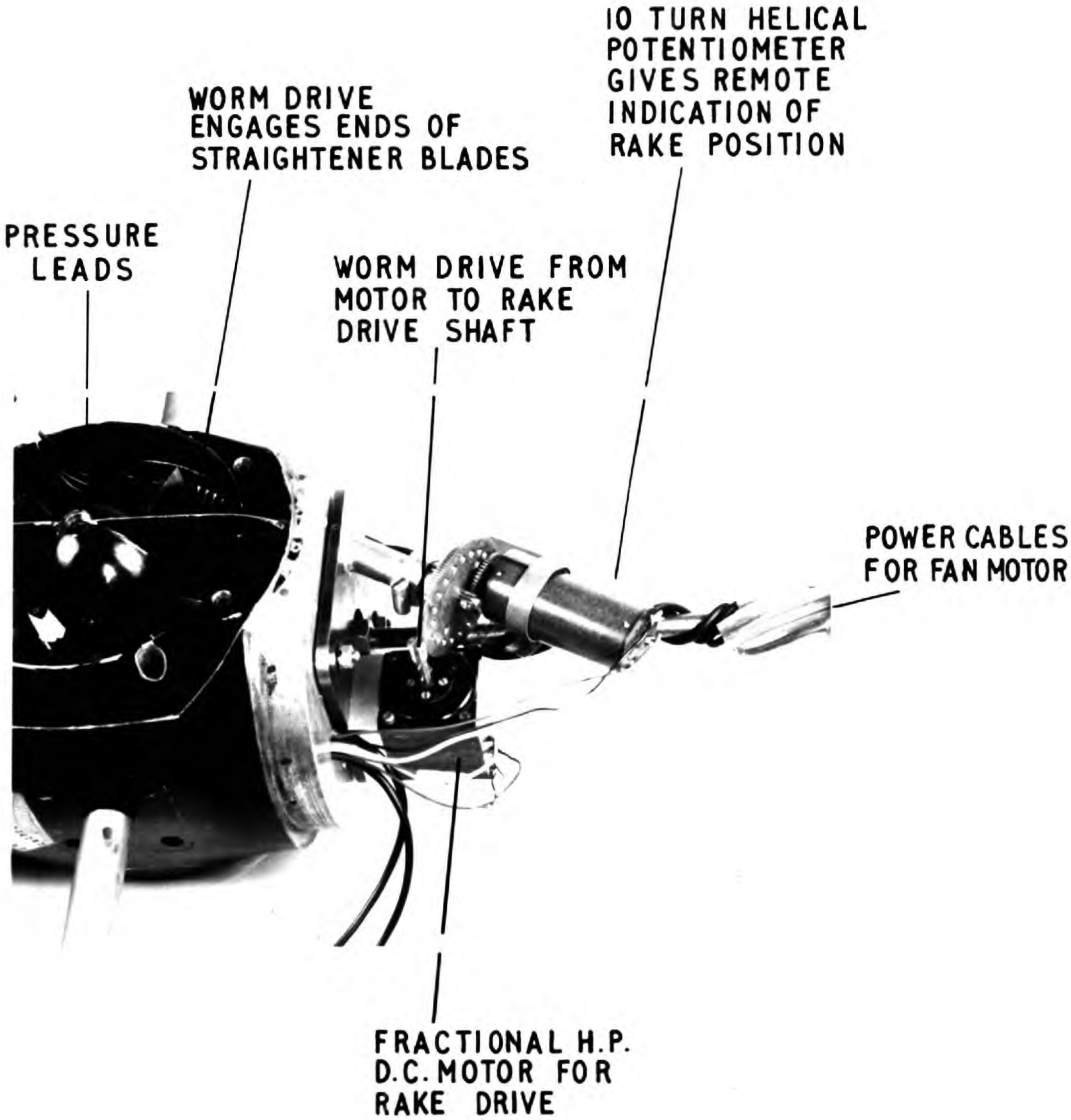

THIS IS A VIEW OF THE BOTTOM OF THE MODEL
WITH THE REAR SHELL REMOVED

THE TRAVERSE GEAR DRIVE + POSITION INDICATOR

FIG. 3.4

FIGURE 4.1

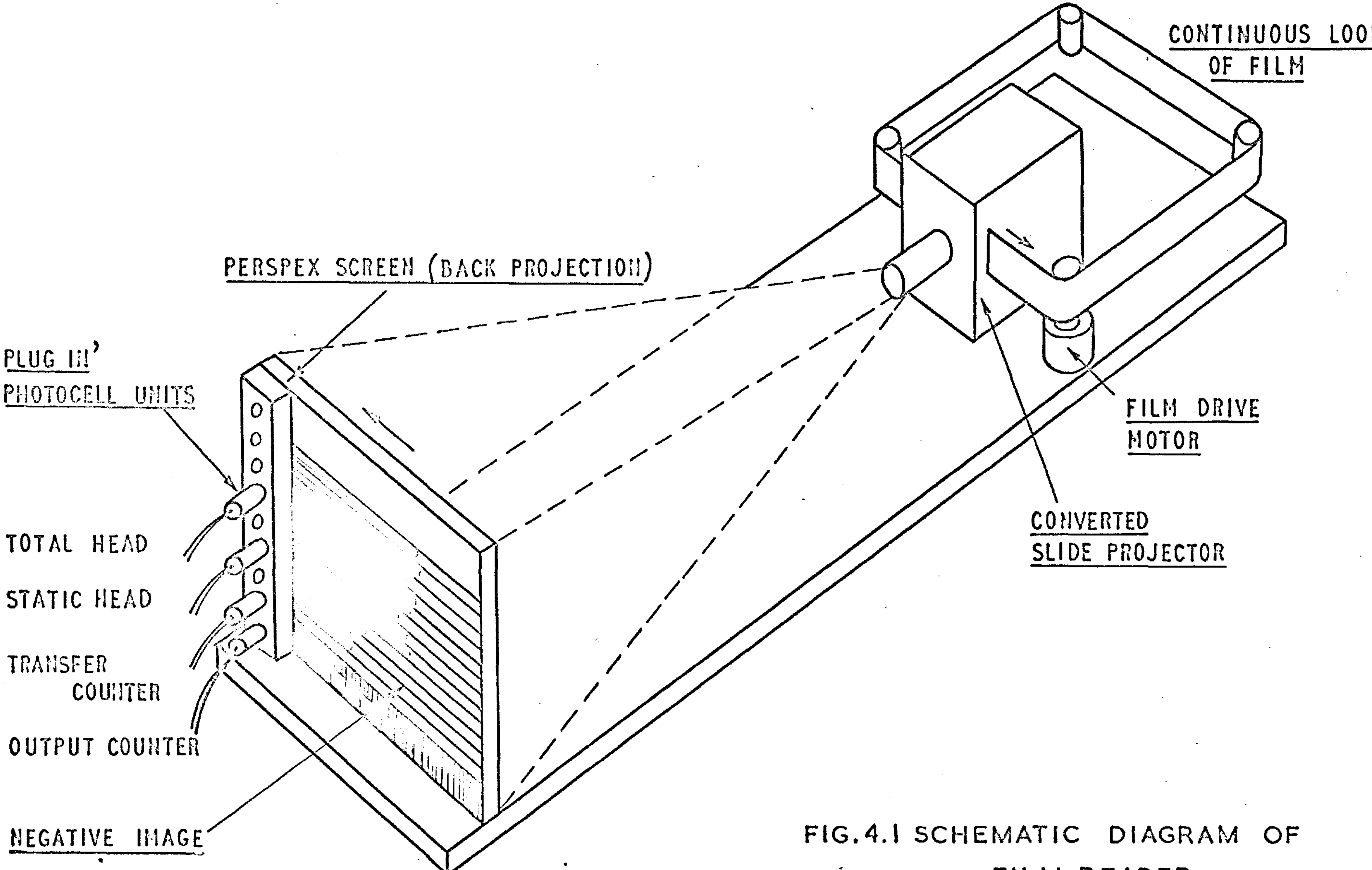

FIG. 4.1 SCHEMATIC DIAGRAM OF FILM READER

(SEE SECTION 4.3.3)

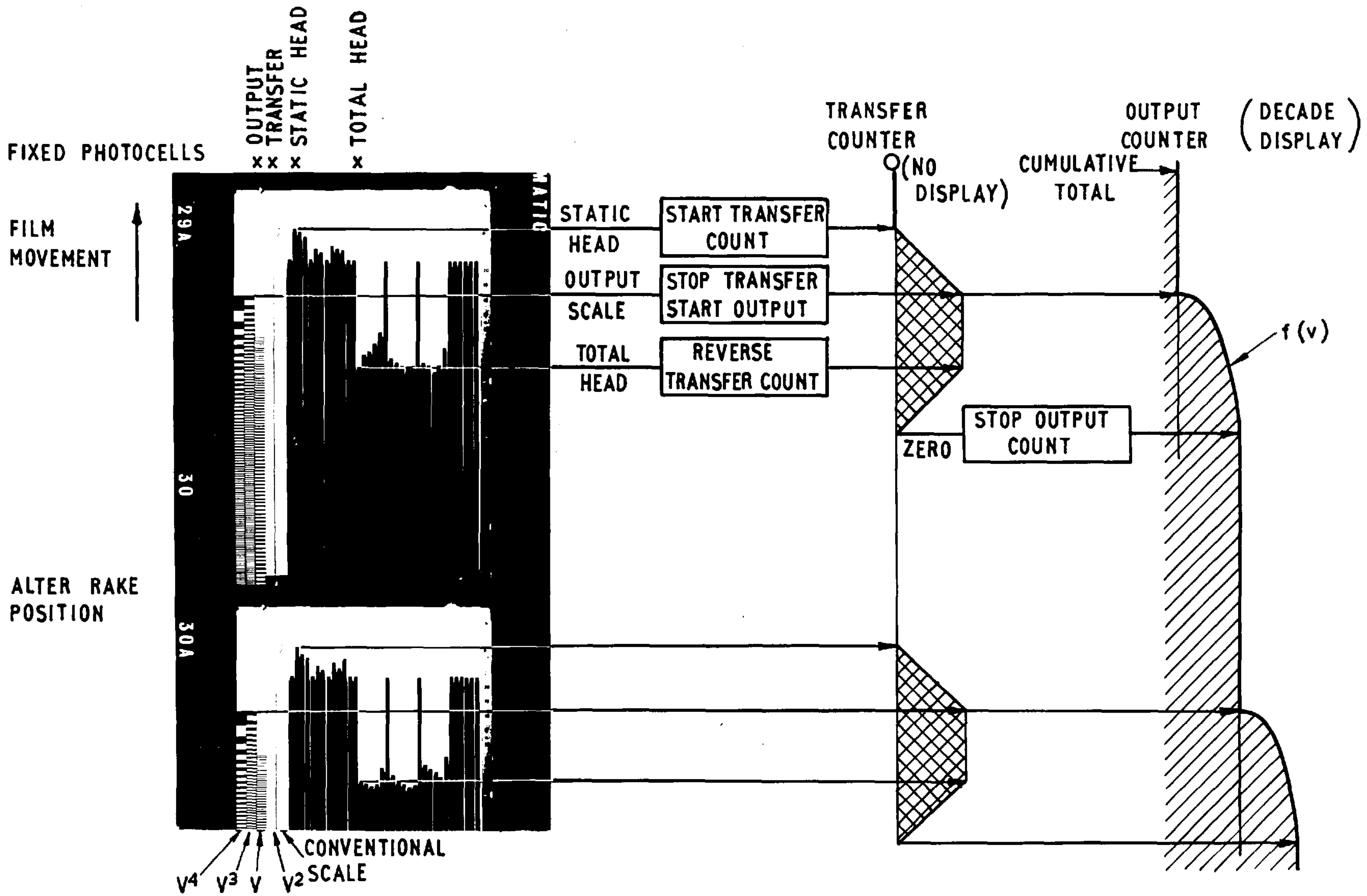

SEQUENCE OF OPERATIONS PERFORMED BY FILM READER (SEE SECTION 4.3)
(THIS IS A POSITIVE PICTURE, THE READER USES A NEGATIVE ONE)

FIG.4·2

FIG.4.2

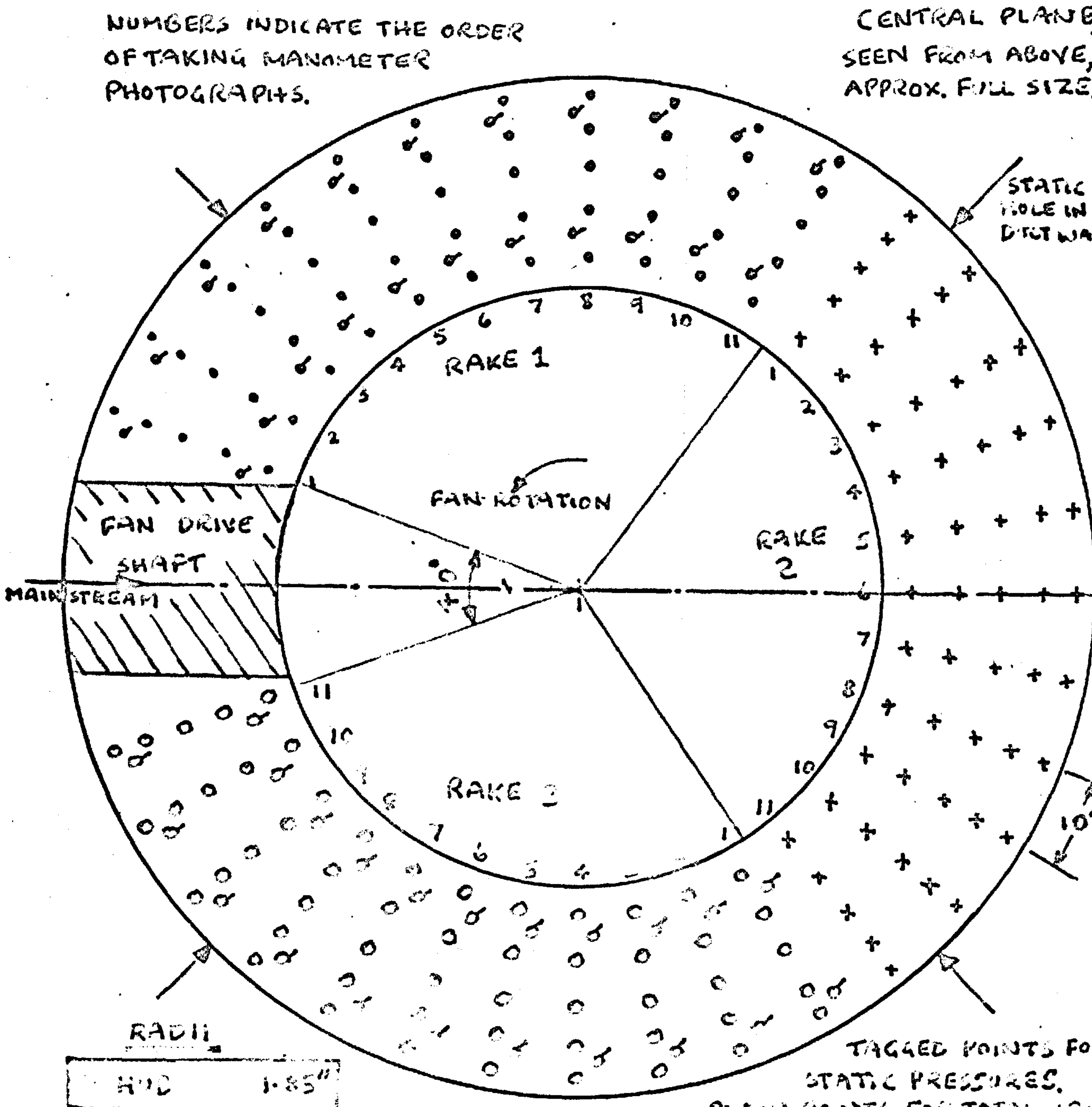

RADII

HUB	1.85"
TOTAL TUBE	2.05"
STATIC TUBE	2.21"
TOTAL TUBE	2.37"
TOTAL TUBE	2.64"
TOTAL TUBE	2.91"
STATIC TUBE	2.99"
TOTAL TUBE	3.09"
DUCT WALL	3.20"

DETAILS OF TRAVERSE POSITIONS.

FIGURE 4.3

(SEE SECTIONS 4.2 AND 4.3.3)

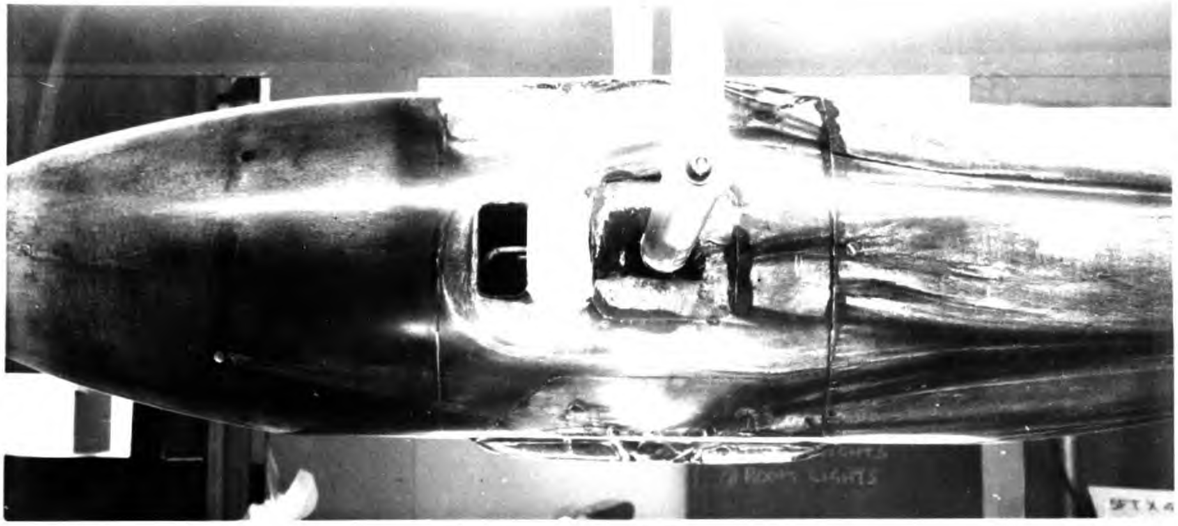

(a) $\alpha = 0^{\circ}$ 134 ft / sec

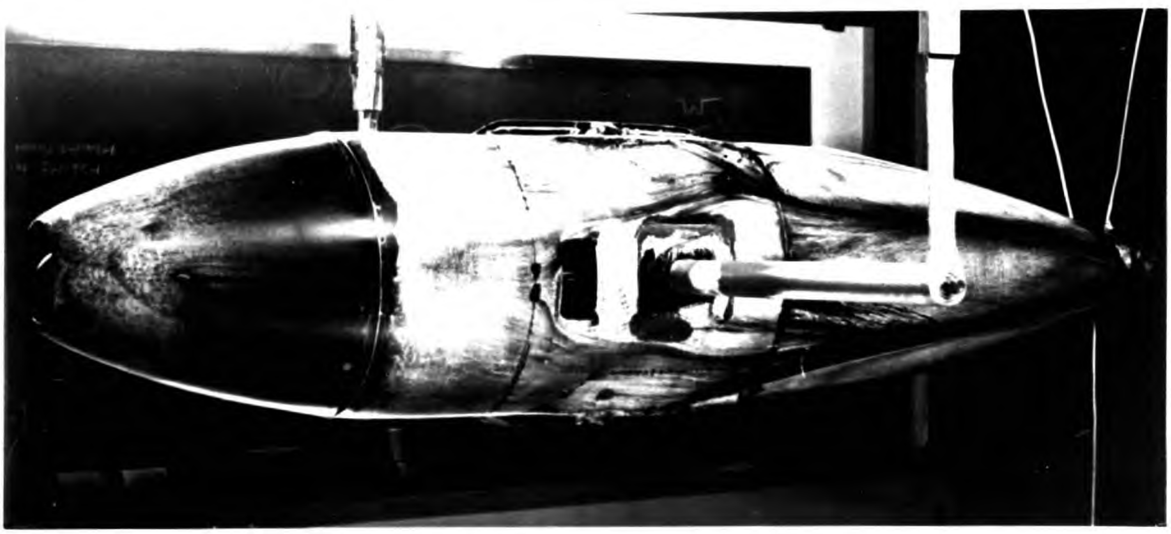

(b) $\alpha = 0^{\circ}$ 134 ft / sec WITH TRANSITION WIRE

SURFACE FLOWS WITH THE BODY MOUNTED ON STRUTS.
(FAN OFF)

FIG. 5·1.

(SEE SECTION 5.1)

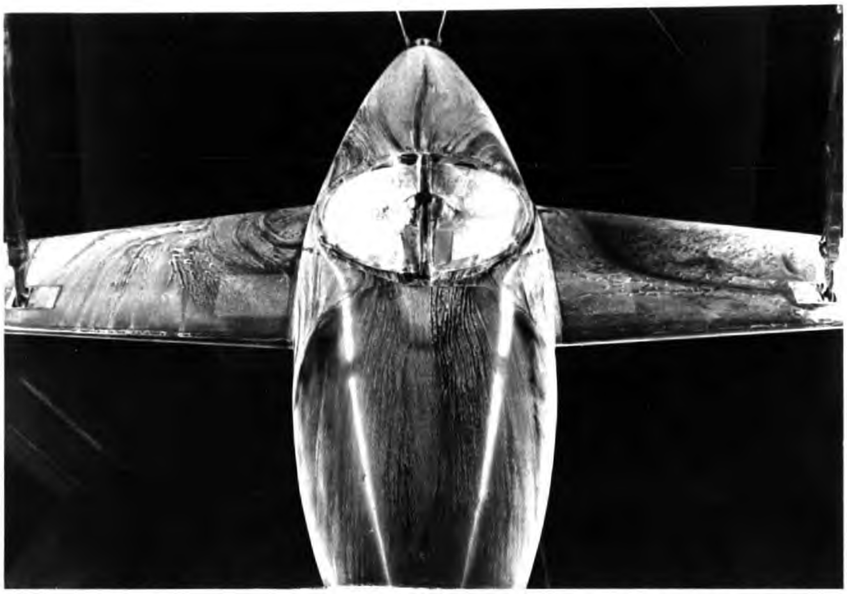

COOLING OUTLET OPEN $\alpha = +15^{\circ}$ 136 ft/sec COOLING OUTLET CLOSED

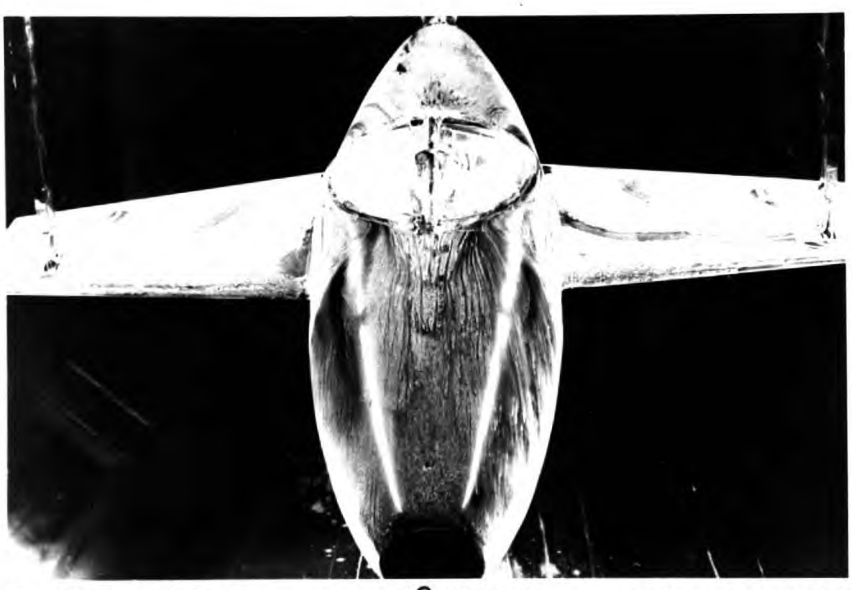

COOLING OUTLET OPEN $\alpha = +18^{\circ}$ 136 ft/sec COOLING OUTLET CLOSED

DELAY OF THE WING STALL BY OPENING THE MOTOR COOLING OUTLET (FAN OFF)

FIG. 5.2

(SEE SECTION 5.1)

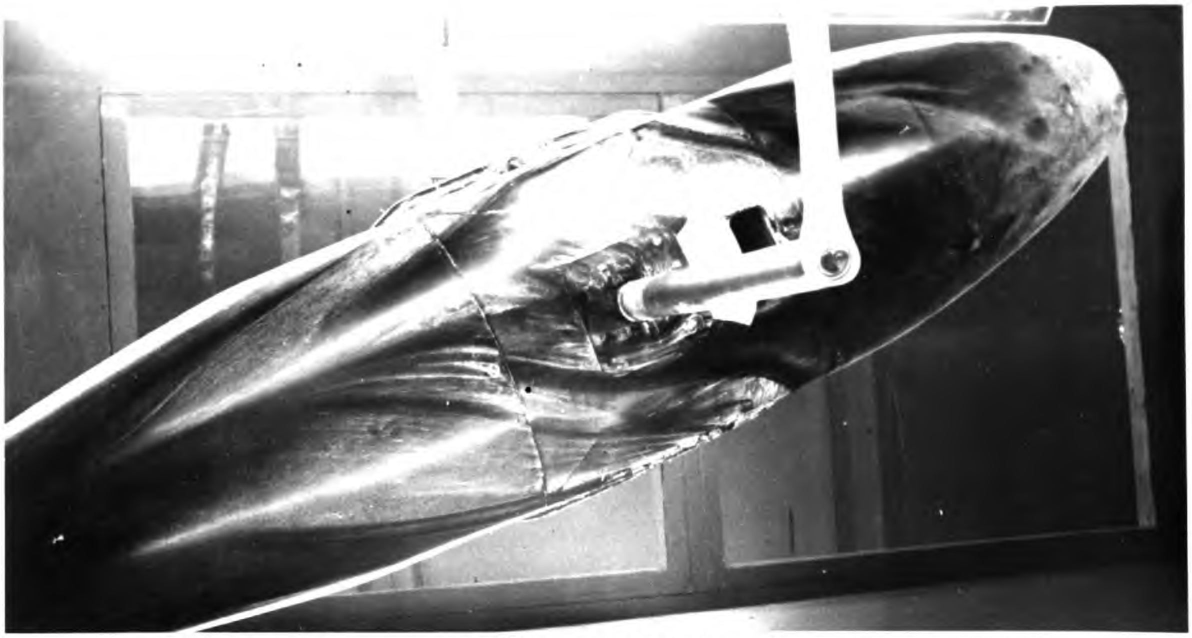

(a) ON STRUTS AT $\alpha = +20^{\circ}$ 136 ft/sec

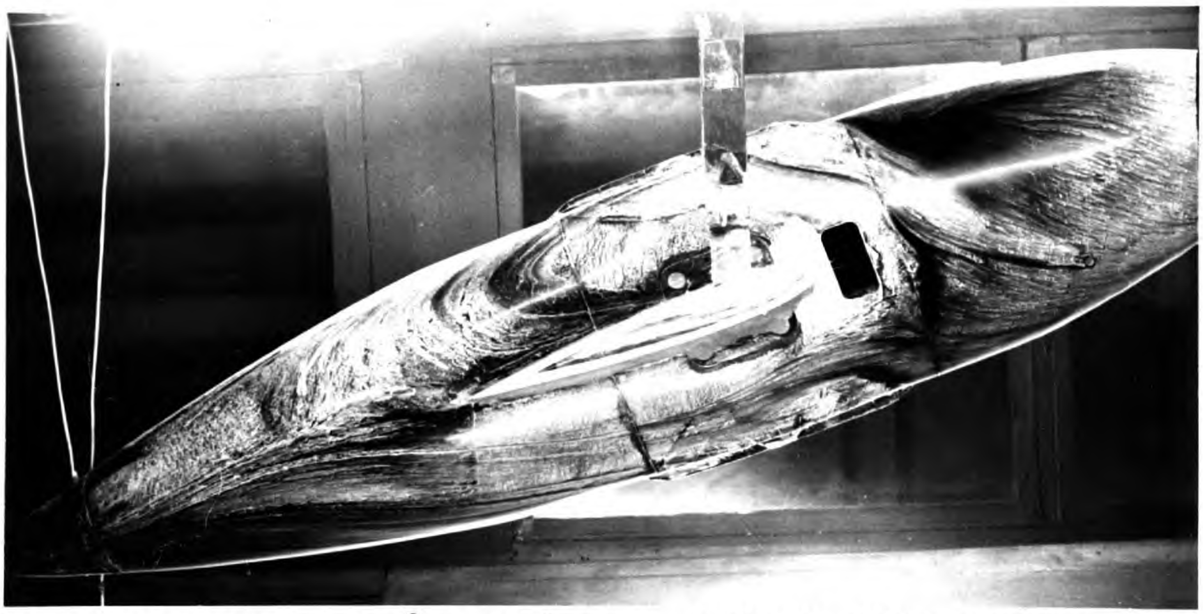

(b) ON WINGS AT $\alpha = +18^{\circ}$ 136 ft/sec SHOWING STALL EFFECTS

SURFACE FLOWS AT HIGH INCIDENCE. (FAN OFF)

FIG. 5.3

(SEE SECTION 5.1)

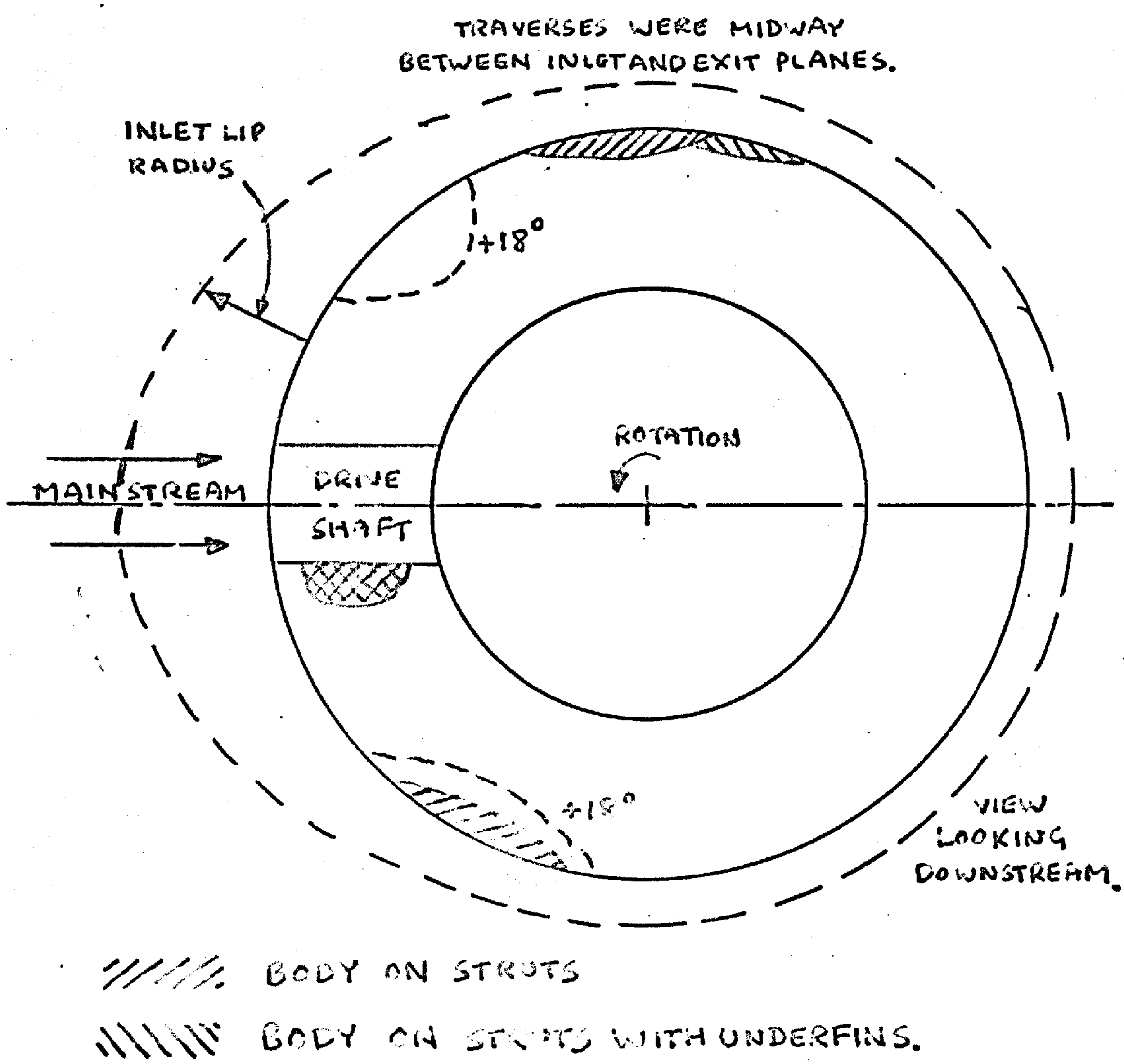

AT ZERO FORWARD SPEED ALL READINGS OSCILLATED.

WITHIN THE REMAINDER OF THE TEST RANGE THE SHADED AREAS INCREASED ONLY SLIGHTLY WITH FORWARD SPEED.

THIS PLANE IS $1\frac{1}{2}$" APPROX, DOWNSTREAM OF FAN.

AREAS IN WHICH MANOMETER READINGS OSCILLATED.

FIGURE 5.4

(SEE SECTION 5.2.1)

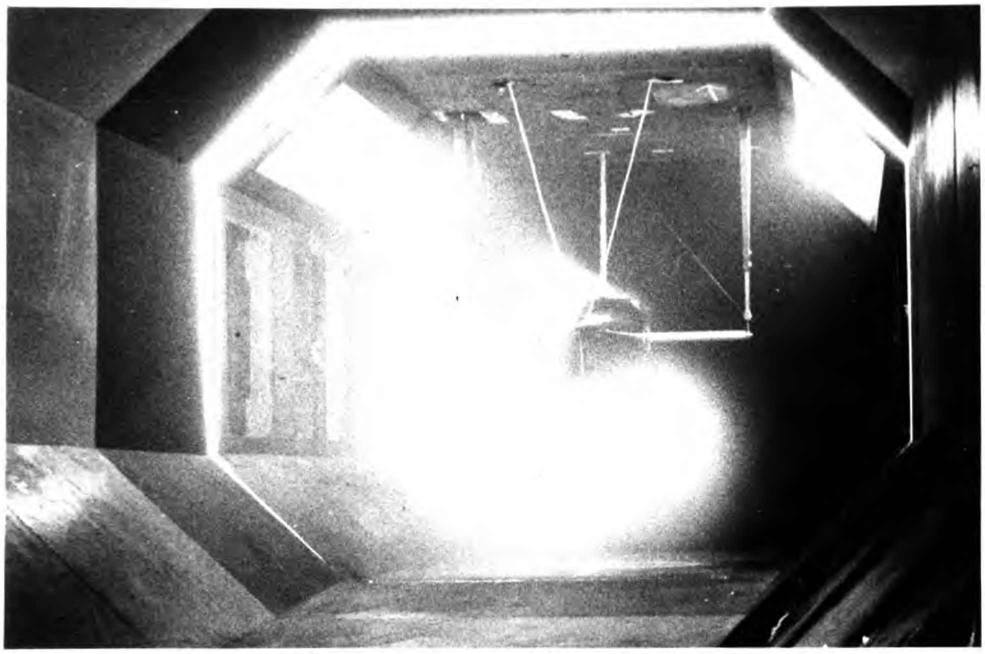

(a)

"SMOKE SCREEN" TECHNIQUE 40" BEHIND DUCT

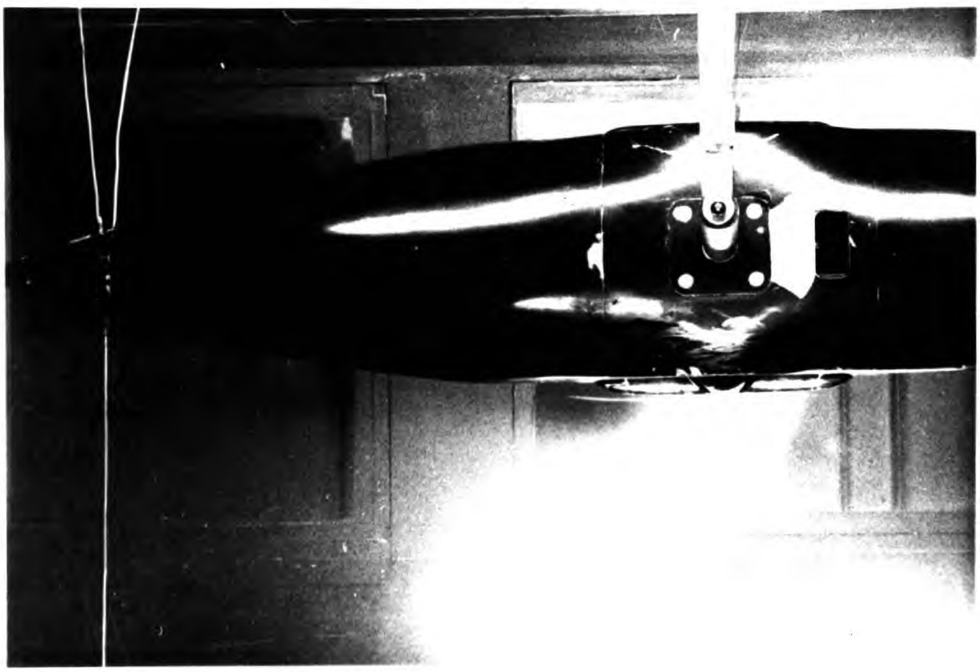

(b)

SIDE VIEW

SMOKE PHOTOGRAPHS AT $\alpha = 0^\circ$ $V = 92$ ft / sec

$\left(V/V_{J_T} = 0 \cdot 47 \right)$

FIG. 5.5

(SEE SECTION 5.2)

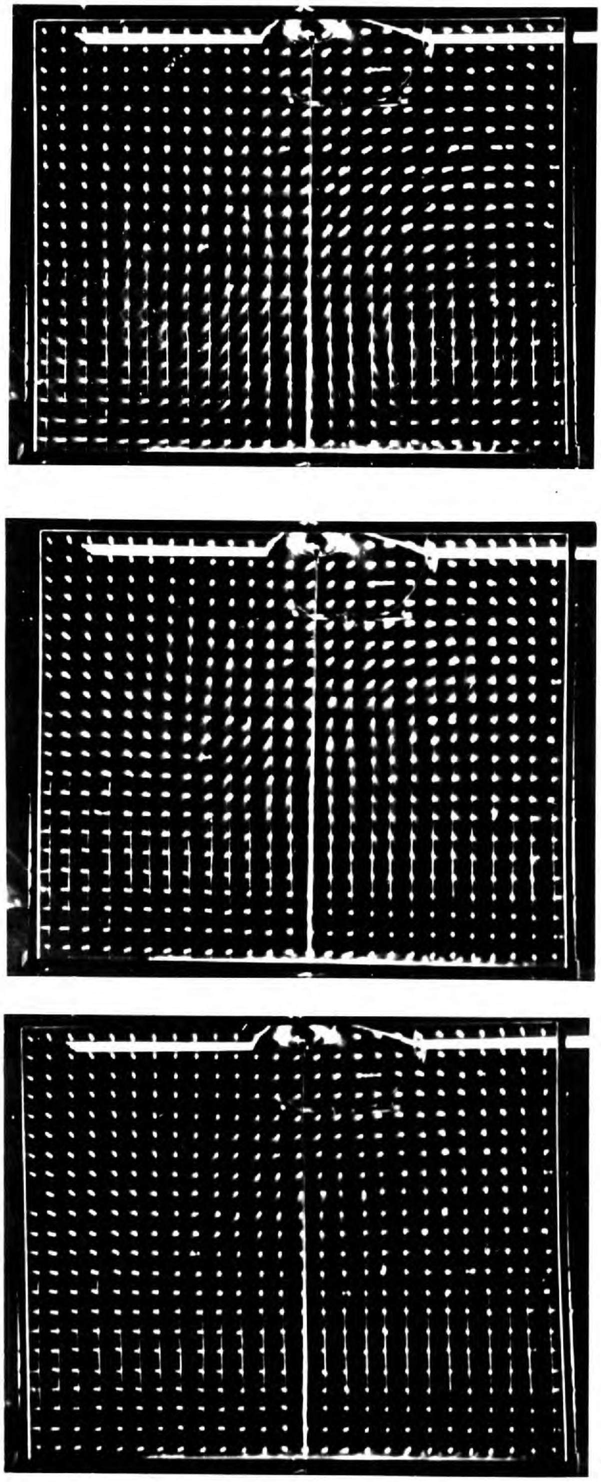

(a)

52 ft/sec

$V/V_{J_T} = 0{\cdot}266$

Approx. height of vortex centres

Floor level

(b)

92 ft/sec

$V/V_{J_T} = 0{\cdot}470$

Approx height of vortex centres

Floor level

(c)

130 ft/sec

$V/V_{J_T} = 0{\cdot}665$

Floor level

TUFT GRID 27" BEHIND DUCT ℄ $\alpha = 0°$
(TUFTS ON 1" MESH EACH 1" LONG
WHOLE GRID 25" WIDE 21" HIGH)

FIG. 5.6

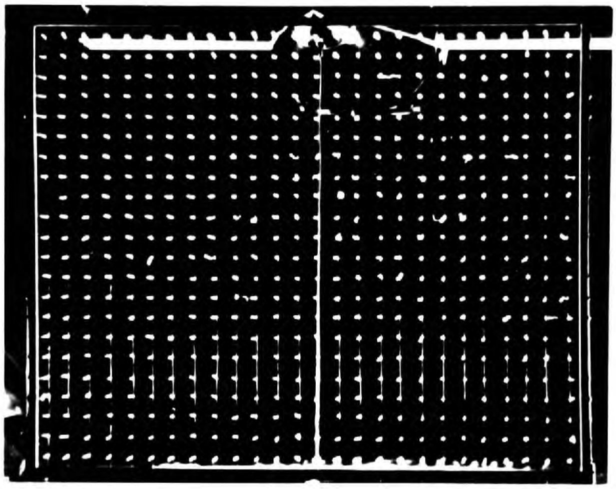

(d)

52 ft/sec

FAN OFF

TO BE COMPARED WITH FIG 5.6(a) (b) and (c)

FIG. 5.6
(cont.)

FIGURES ARE VALUES OF V/V_{J_T}

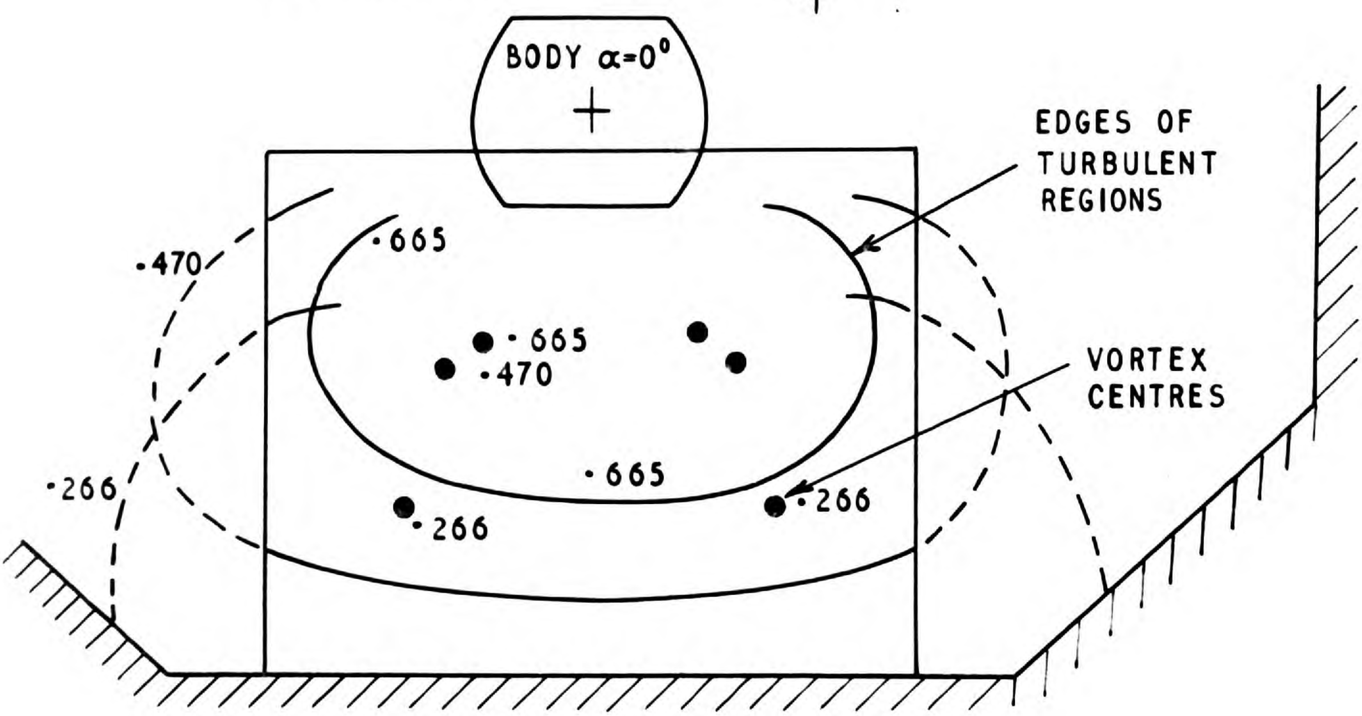

INFORMATION DERIVED FROM FIG. 5.6
(SEE SECTION 5.2)

FIG. 5.7

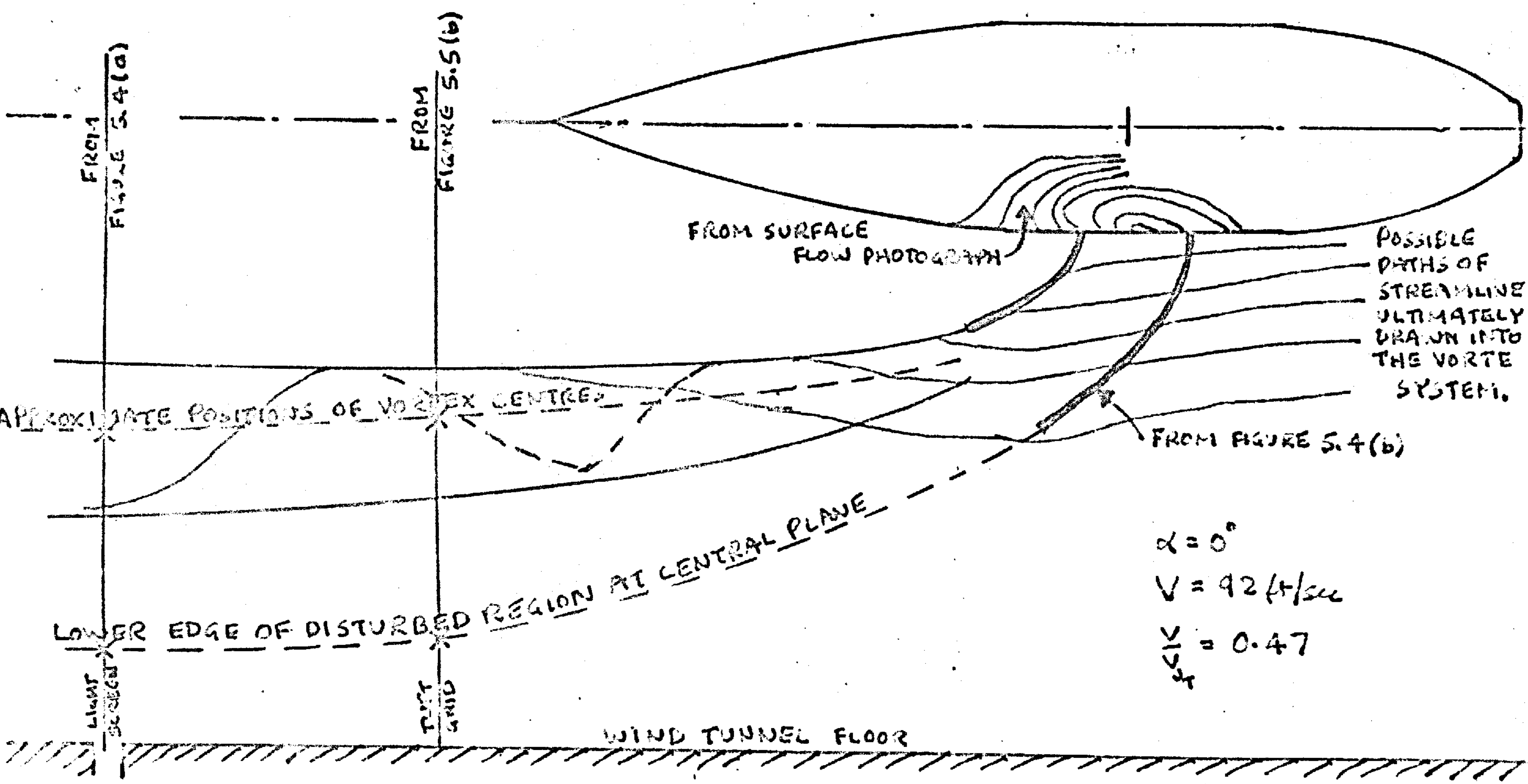

POSSIBLE STRUCTURE OF JET PLUME, DEDUCED FROM LIMITED SMOKE, TUFT, AND SURFACE FLOW OBSERVATIONS.

FIGURE 5.8
(SEE SECTION 5.2)

FIGURE 5.8

73 ft/sec →

$\frac{V}{V_{J_T}} = 0{\cdot}373$

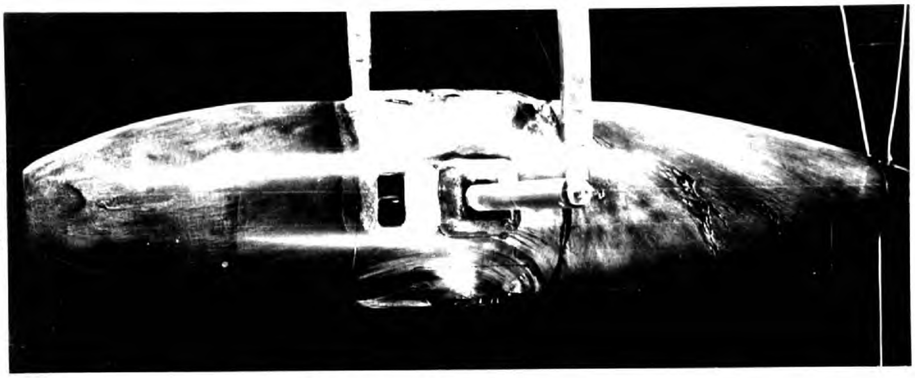

(a)

SIDE VIEW

130 ft/sec →

$\frac{V}{V_{J_T}} = 0{\cdot}664$

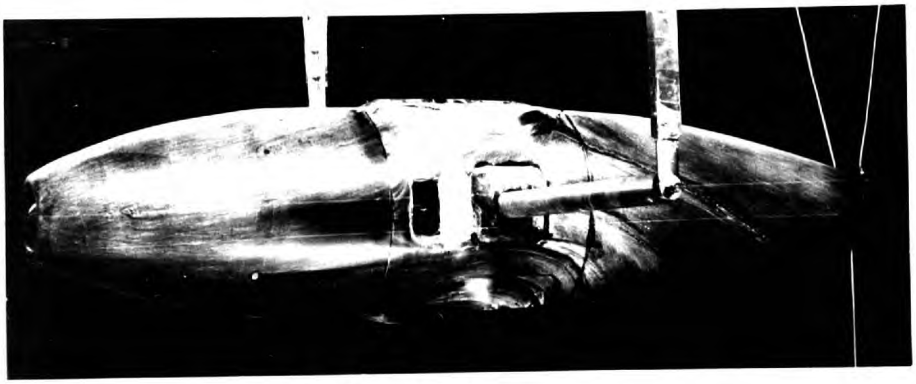

(b)

SIDE VIEW

92 ft/sec →

$\frac{V}{V_{J_T}} = 0{\cdot}470$

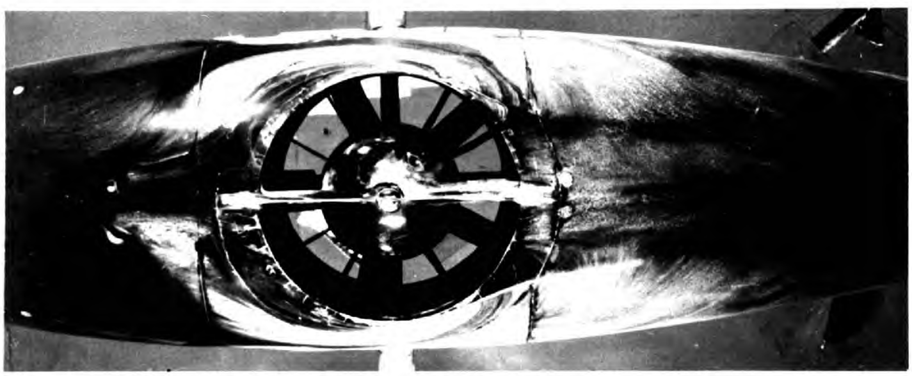

(c)

VIEW FROM BELOW

BODY ON STRUTS $\alpha = 0°$ (FAN ON)

FIG. 5·9

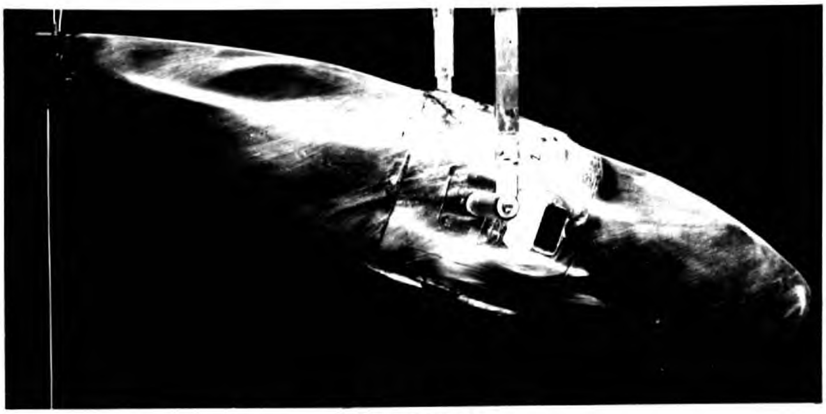

(a)

SIDE VIEW

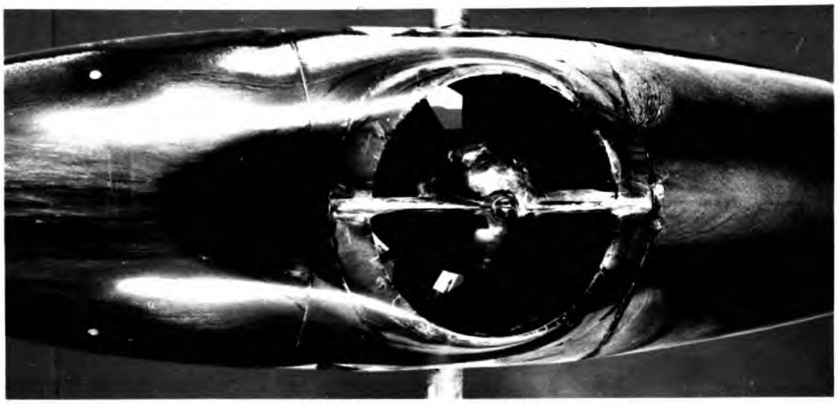

(b)

VIEW FROM BELOW

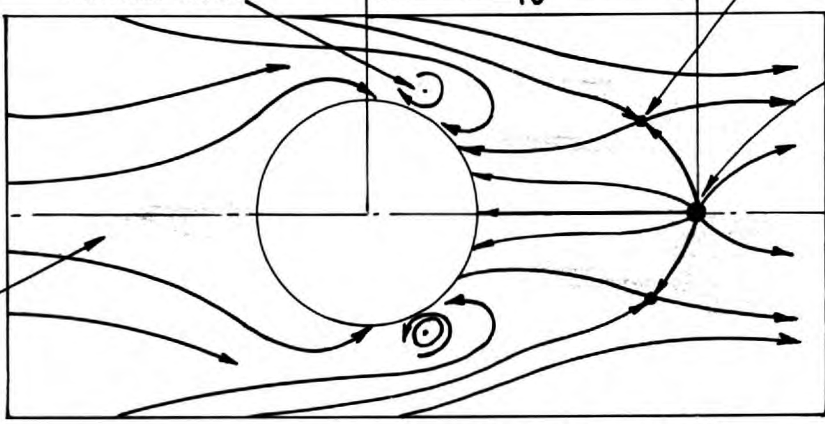

(c)

DEVELOPED VIEW OF REGION AROUND THE JET OUTLET.
(TAKEN FROM A SKETCH DRAWN FROM THE FLOW PATTERN)

BODY ON STRUTS $\alpha = -20^\circ$ (FAN ON)

FIG. 5.10

(SEE SECTION 5.2)

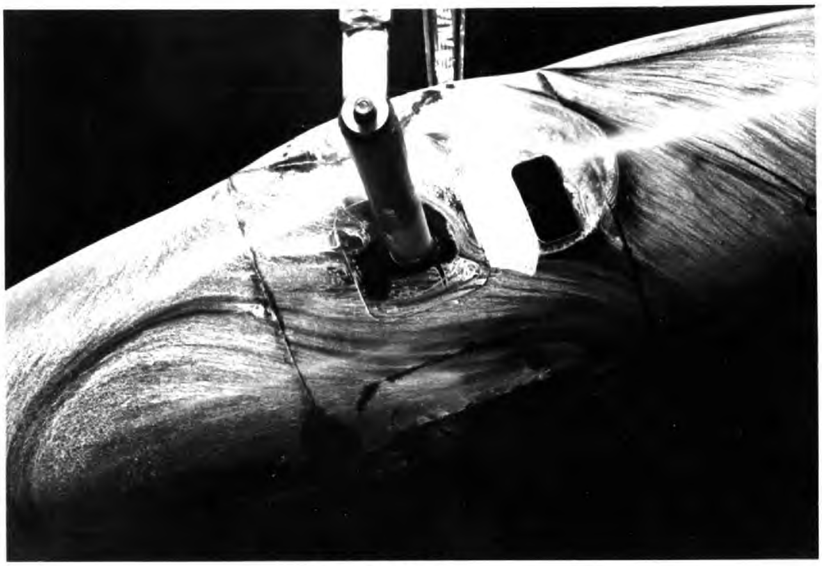

(a)

SIDE VIEW

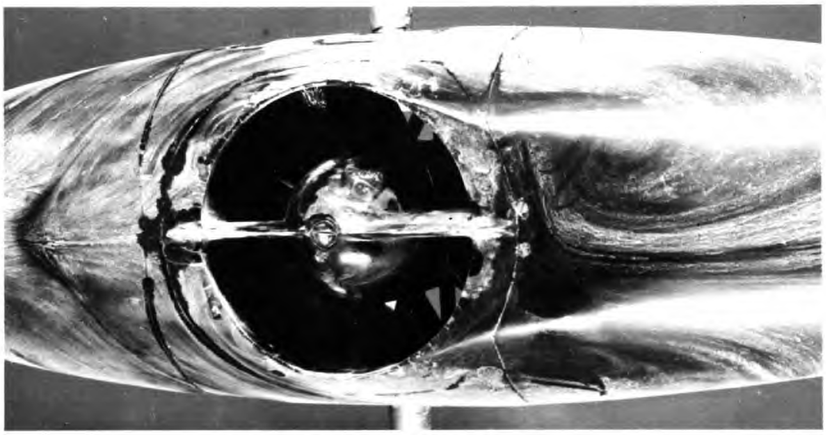

Wake of drive shaft is situated this side of centre at up-stream side of duct (see Fig. 6.5)

(b)

VIEW FROM BELOW

BODY ON STRUTS $\alpha = +20^\circ$ 90 ft/sec (FAN ON)

$V/V_{J_T} = 0 \cdot 46$

SHOWING ATTACHMENT OF TRAILING VORTICES AT HIGH INCIDENCE

N.B. TUNNEL CONSTRAINT FORCES WERE NOTICEABLE IN THIS CONDITION.
CLOSING THE COOLING OUTLET DID NOT NOTICEABLY AFFECT THE VORTEX PATTERN

FIG. 5.11

(SEE SECTION 5.2)

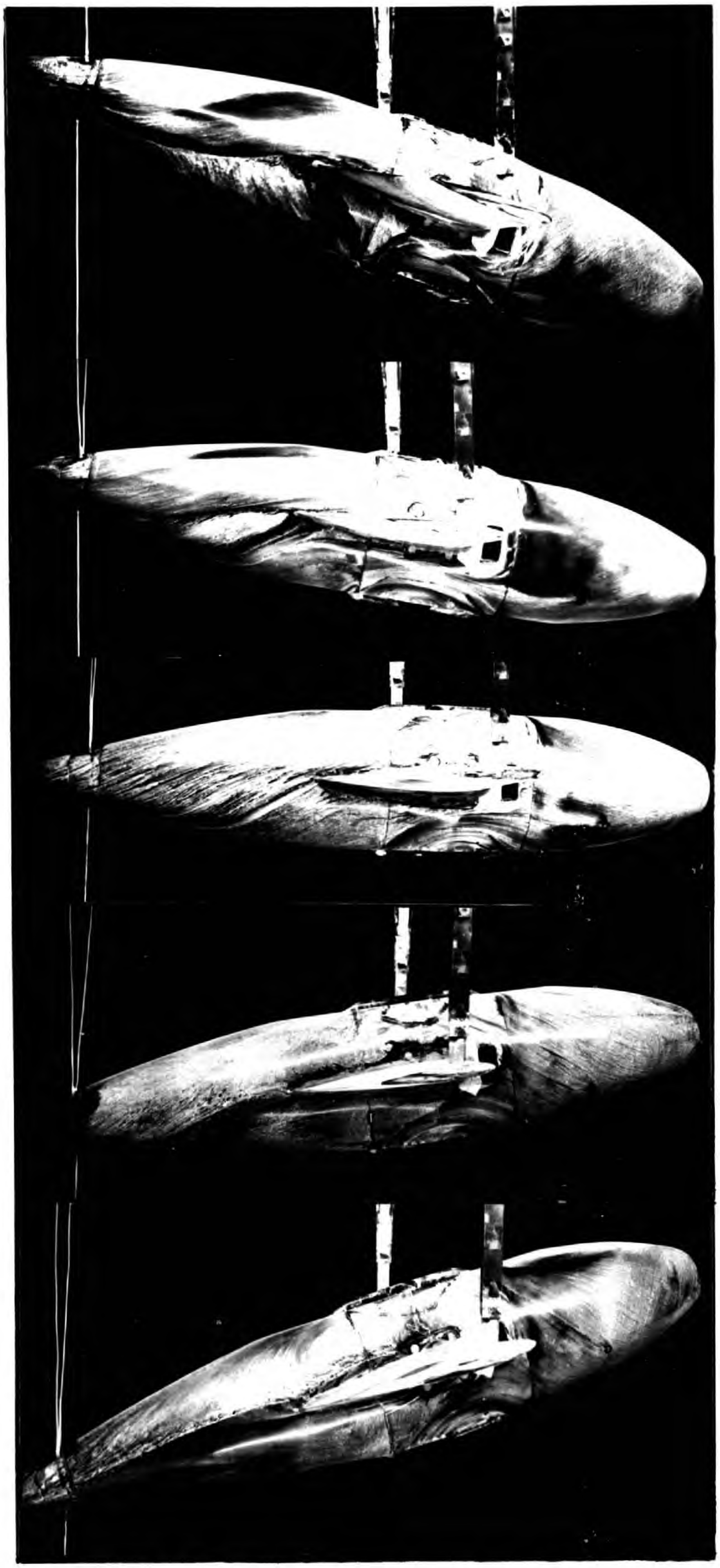

SIDE VIEWS

BODY ON WING. 136 ft/sec (FAN ON)

$V/V_{J_T} = 0{\cdot}70$

FIG. 5.12

(SEE SECTION 5.2)

(a)

$\alpha = -10^0$

SIDE VIEW

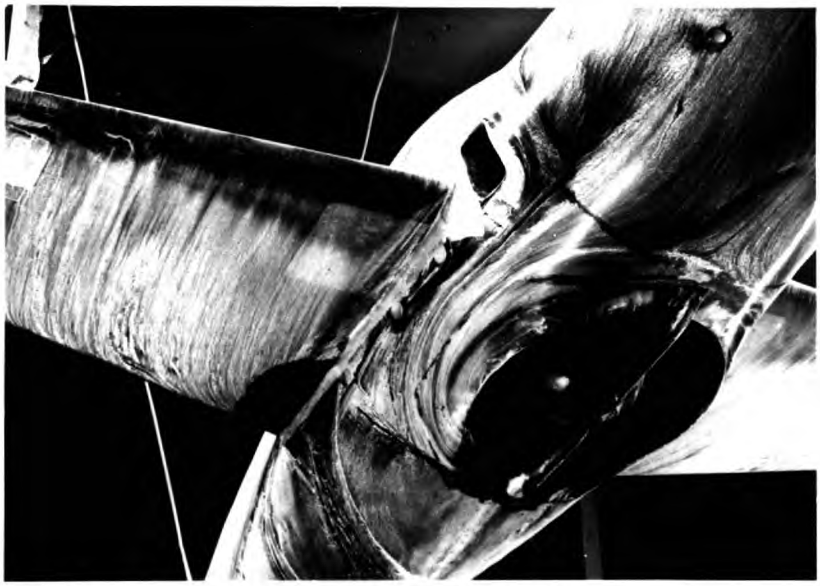

(b)

$\alpha = -10^0$

VIEW OF AREA AROUND JET EXIT

BODY ON WING 93 ft/sec (FAN ON)

$V/V_{J_T} = 0 \cdot 48$

FIG. 5.13
(SEE SECTION 5.2)

(a)

EXTERNAL FLOW

(b)

INTERNAL FLOW

(c)

SHOWING REVERSED FLOW REGION INSIDE FIN (SEE TEXT)

FLOWS OVER PERSPEX UNDERFINS (FAN ON)

93 ft/sec $\alpha = +10^{\circ}$

$V/V_{J_T} = 0{\cdot}49$

FIG. 5.14

(SEE SECTION 5.2)

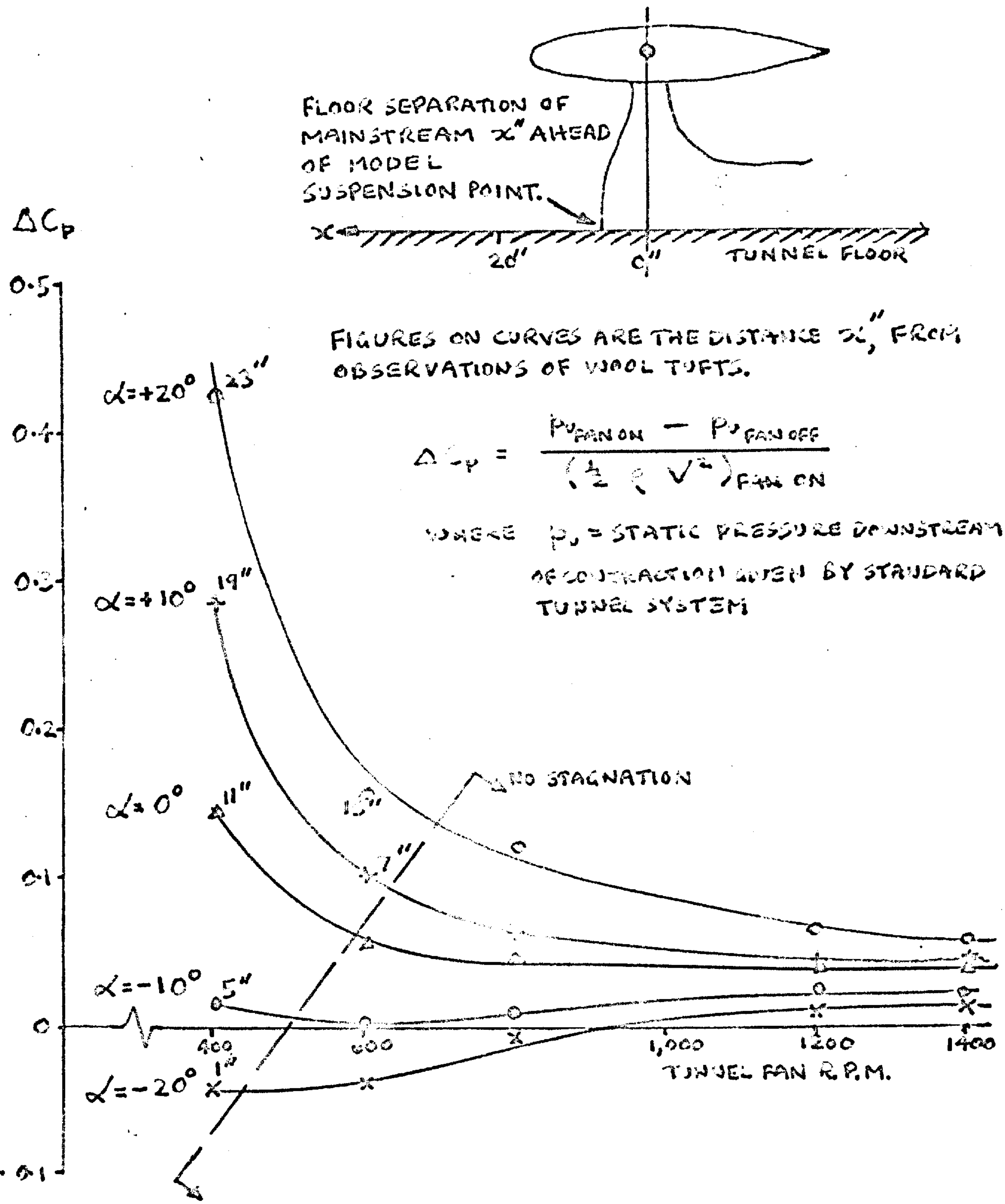

THE EFFECTS OF FAN OPERATION ON UPSTREAM STATIC PRESSURE

FIGURE 5.15

(SEE SECTION 5.3)

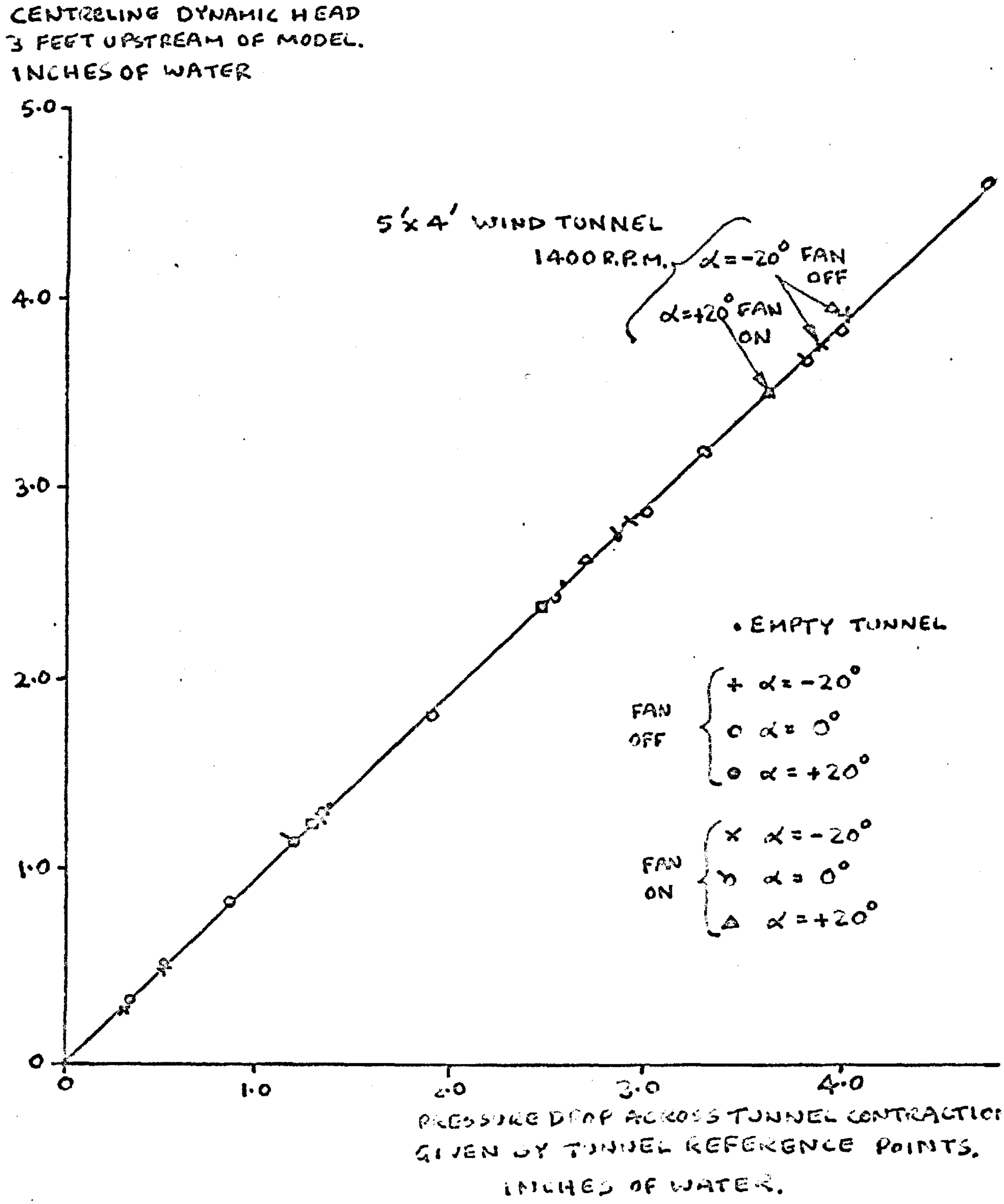

5'x4' TUNNEL CALIBRATION UNDER VARIOUS TEST CONDITIONS

FIGURE 5.16
(SEE SECTION 5.3)

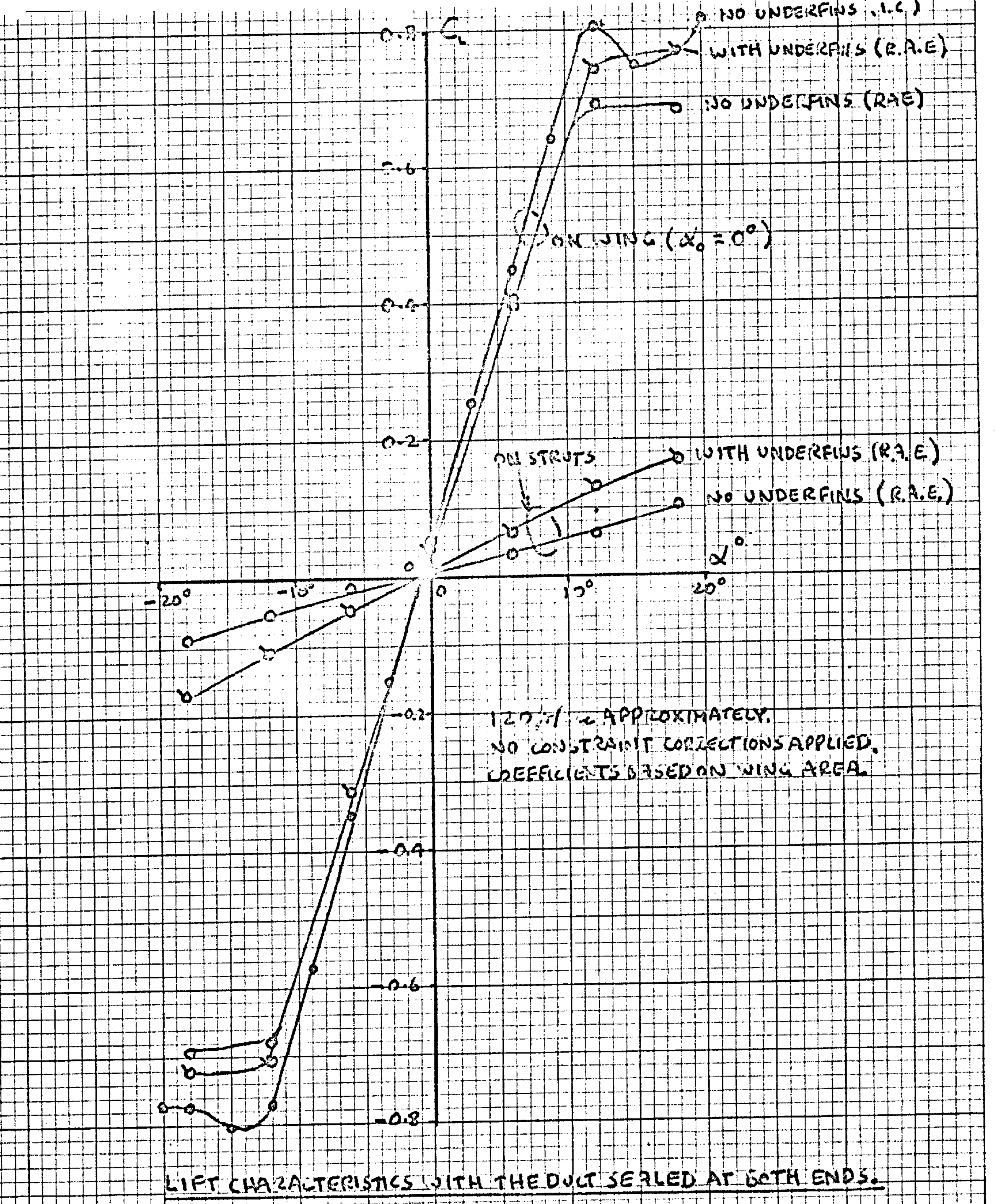

LIFT CHARACTERISTICS WITH THE DUCT SEALED AT BOTH ENDS.

FIGURE 6.1

(SEE SECTION 6.2.)

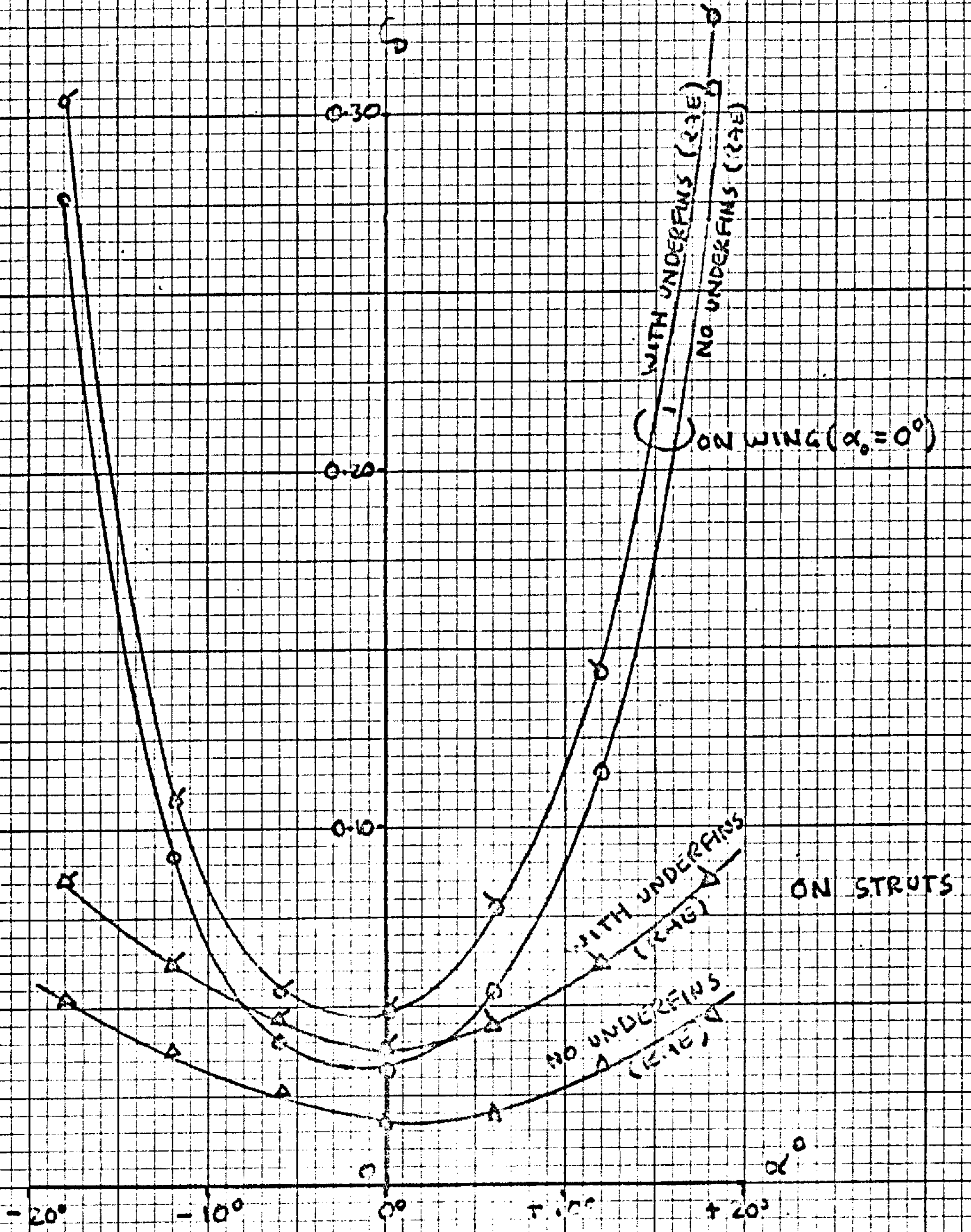

120 ft/sec APPROXIMATELY.
NO CONSTRAINT CORRECTIONS APPLIED.
COEFFICIENTS BASED ON WING AREA.
CALCULATED LAMINAR SKIN FRICTION COEFFICIENT FOR FINS, TO ABOVE SCALE, = 0·0017.

DRAG CHARACTERISTICS WITH THE DUCT SEALED AT BOTH ENDS.

FIGURE 6.2

(SEE SECTION 6.2)

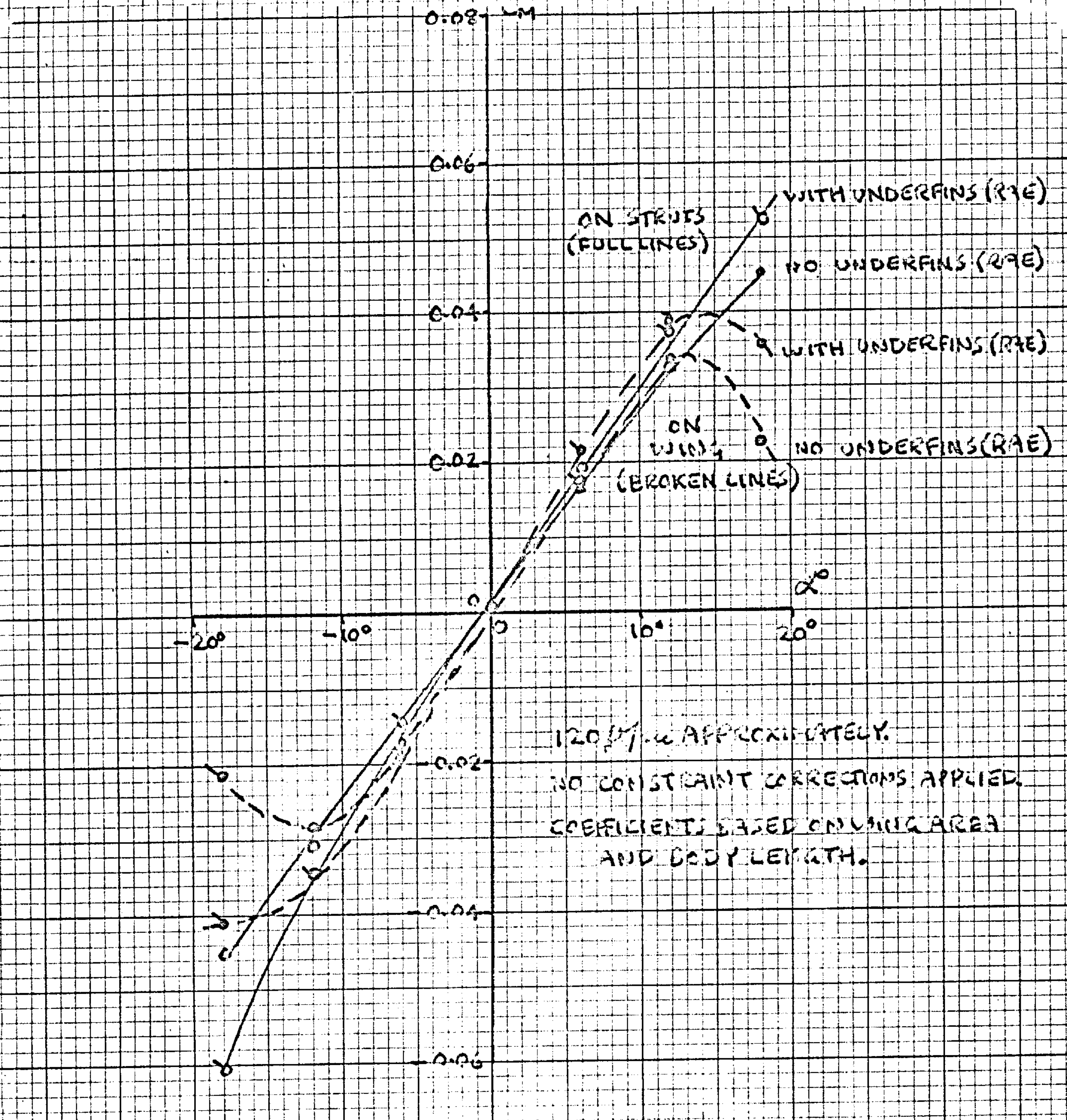

PITCHING MOMENT CHARACTERISTICS WITH DUCT SEALED AT BOTH ENDS

FIGURE 6.3

(SEE SECTION 6.2)

DISTRIBUTION OF AXIAL VELOCITY BETWEEN FAN AND STRAIGHTENERS (TUNNEL SPEED ZERO)

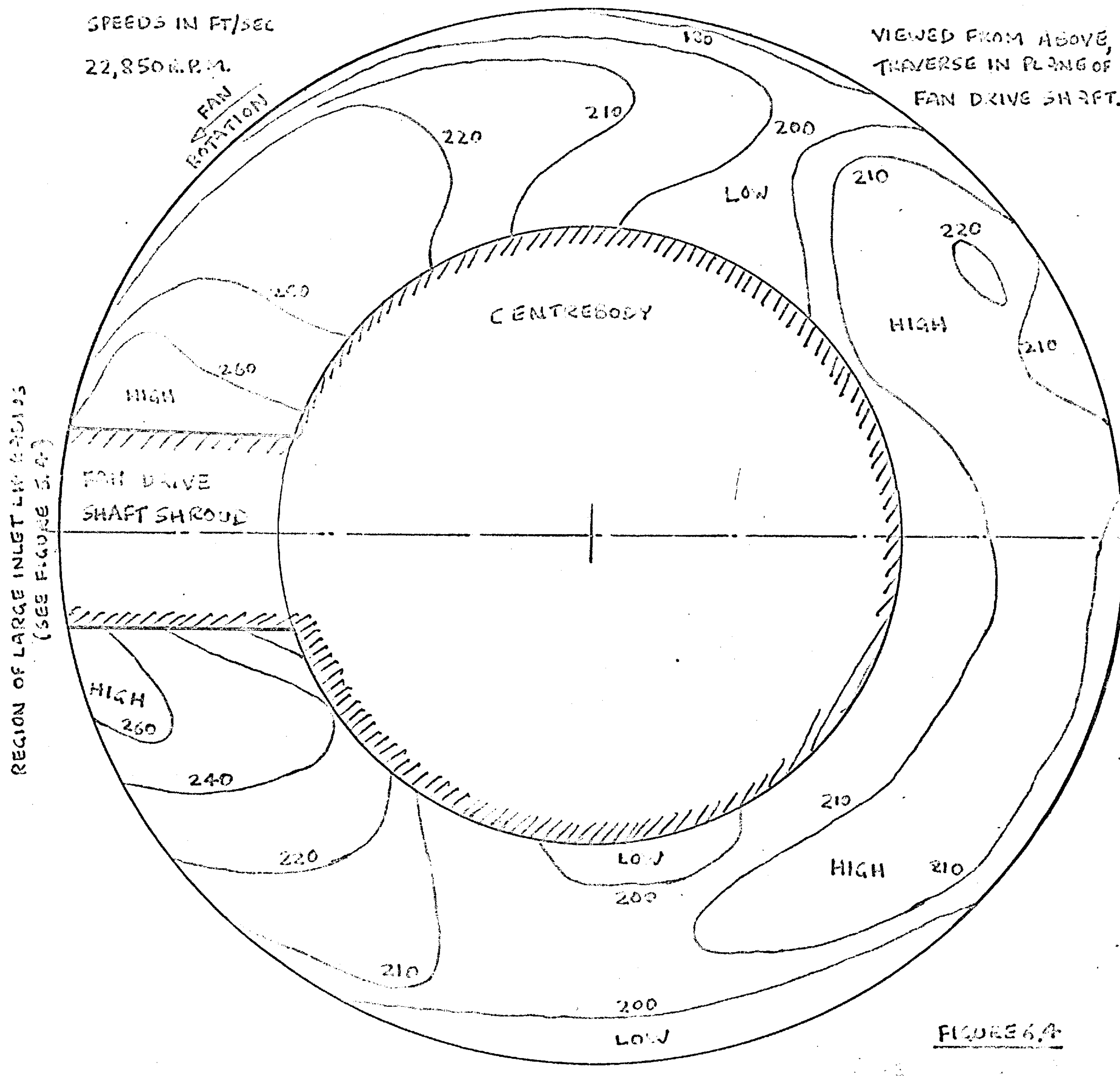

FIGURE 6.4

AXIAL VELOCITY DISTRIBUTION AT THE DUCT EXIT PLANE. (TUNNEL SPEED ZERO.)

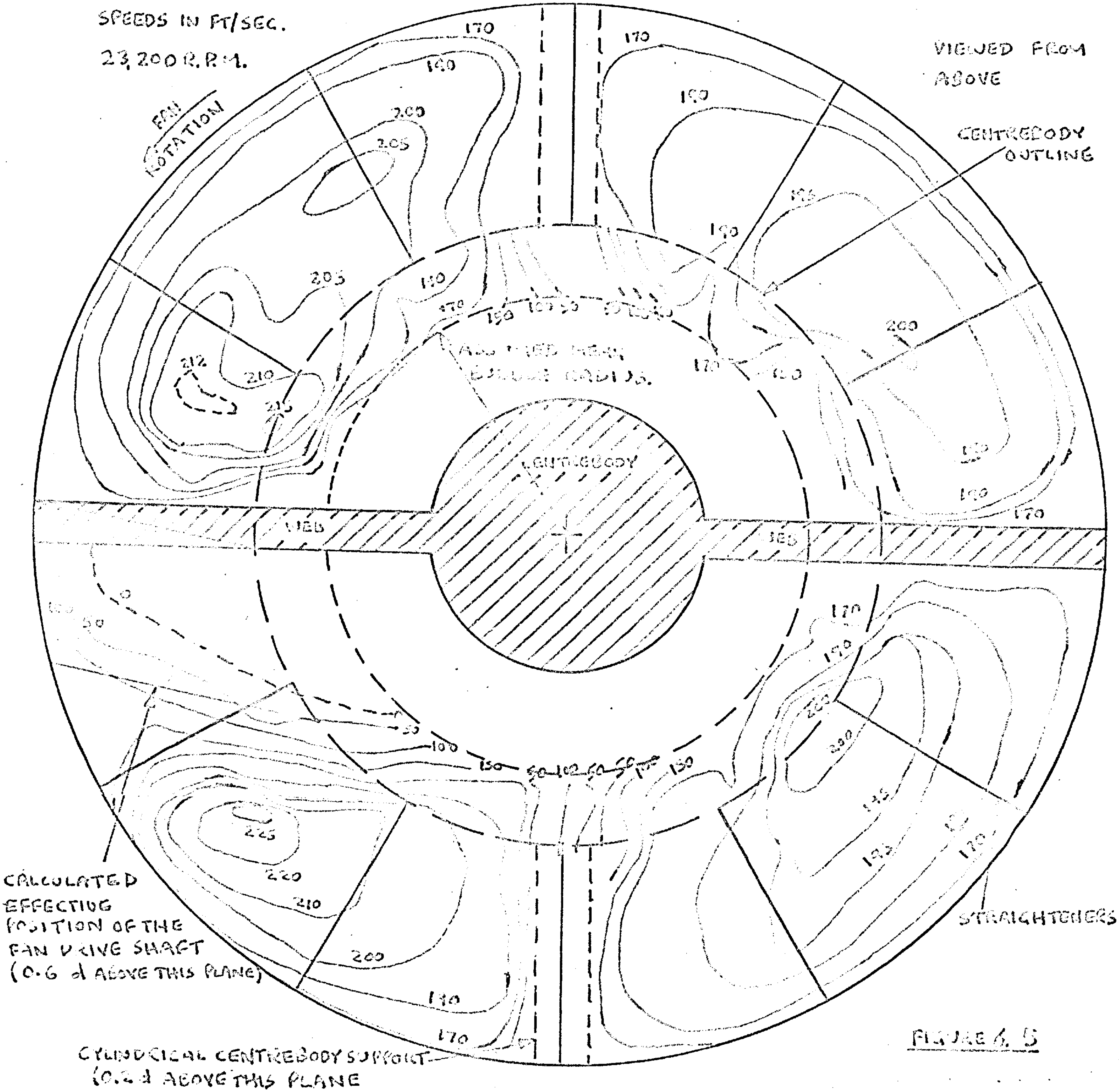

FIGURE 6.5

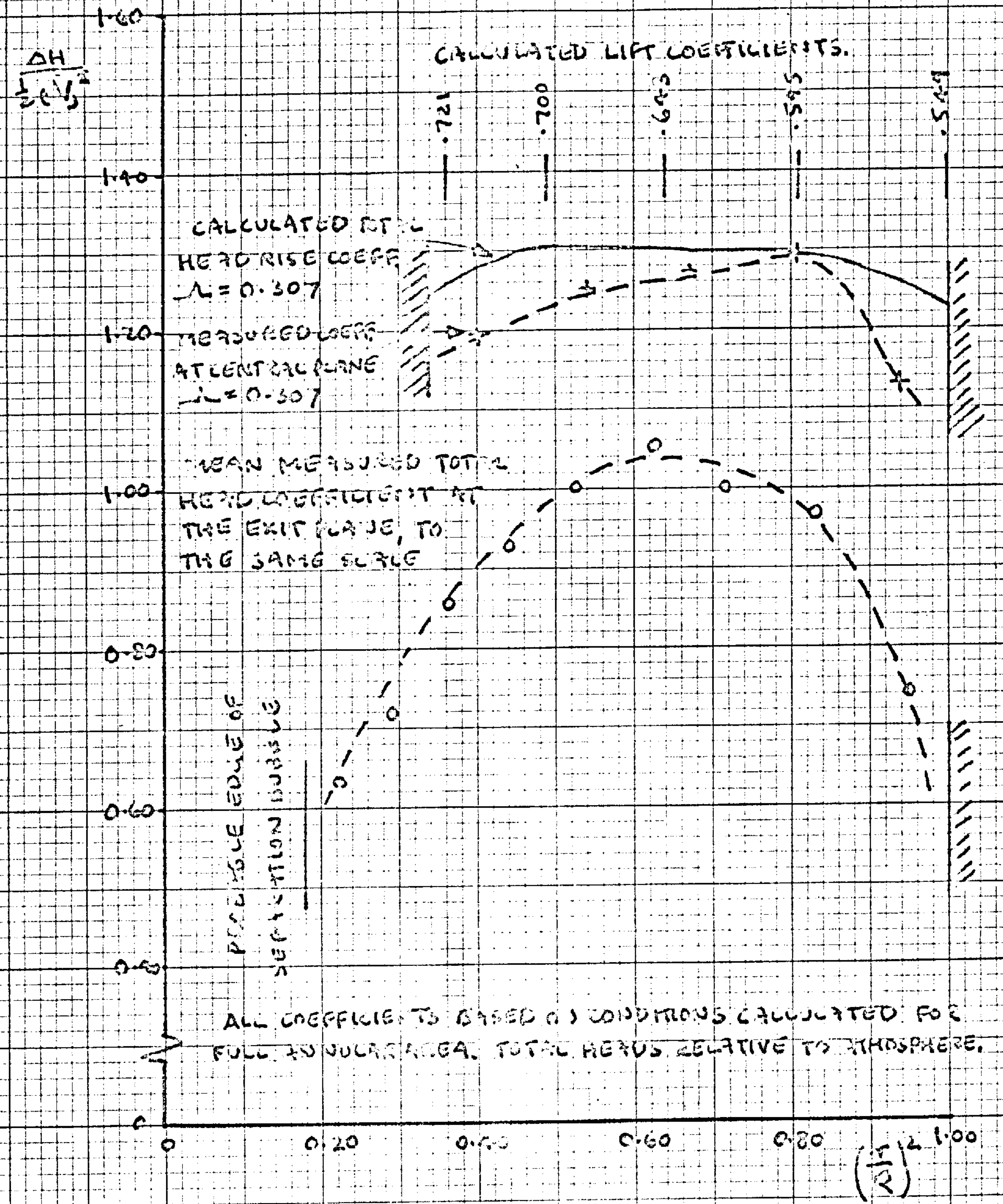

RADIAL TOTAL HEAD DISTRIBUTIONS IN STATIC LIFT CONDITION

FIGURE 6.6

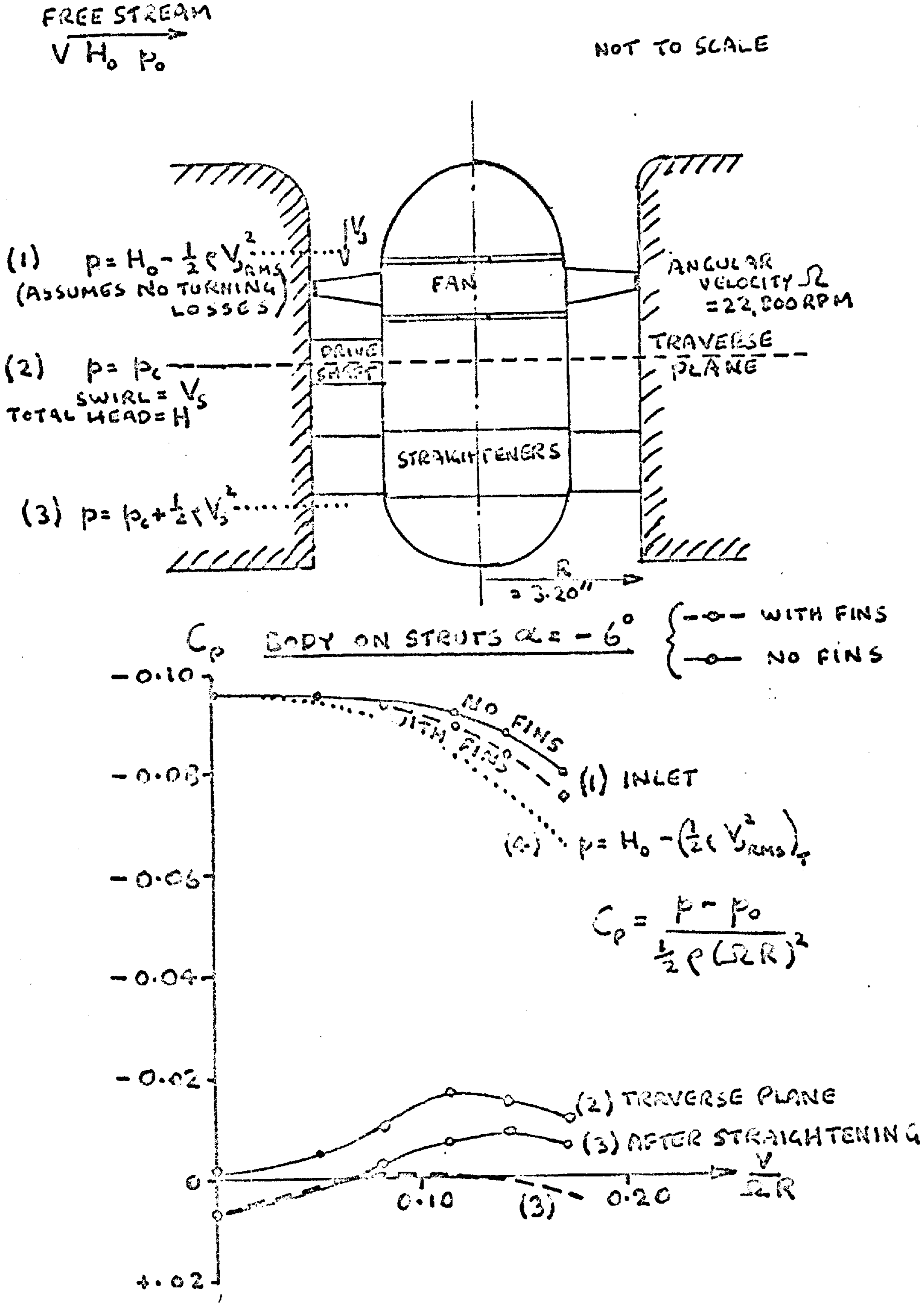

THE VARIATION OF DUCT STATIC PRESSURES WITH FORWARD SPEED

FIGURE 7.1

(SEE SECTION 7.2.2)

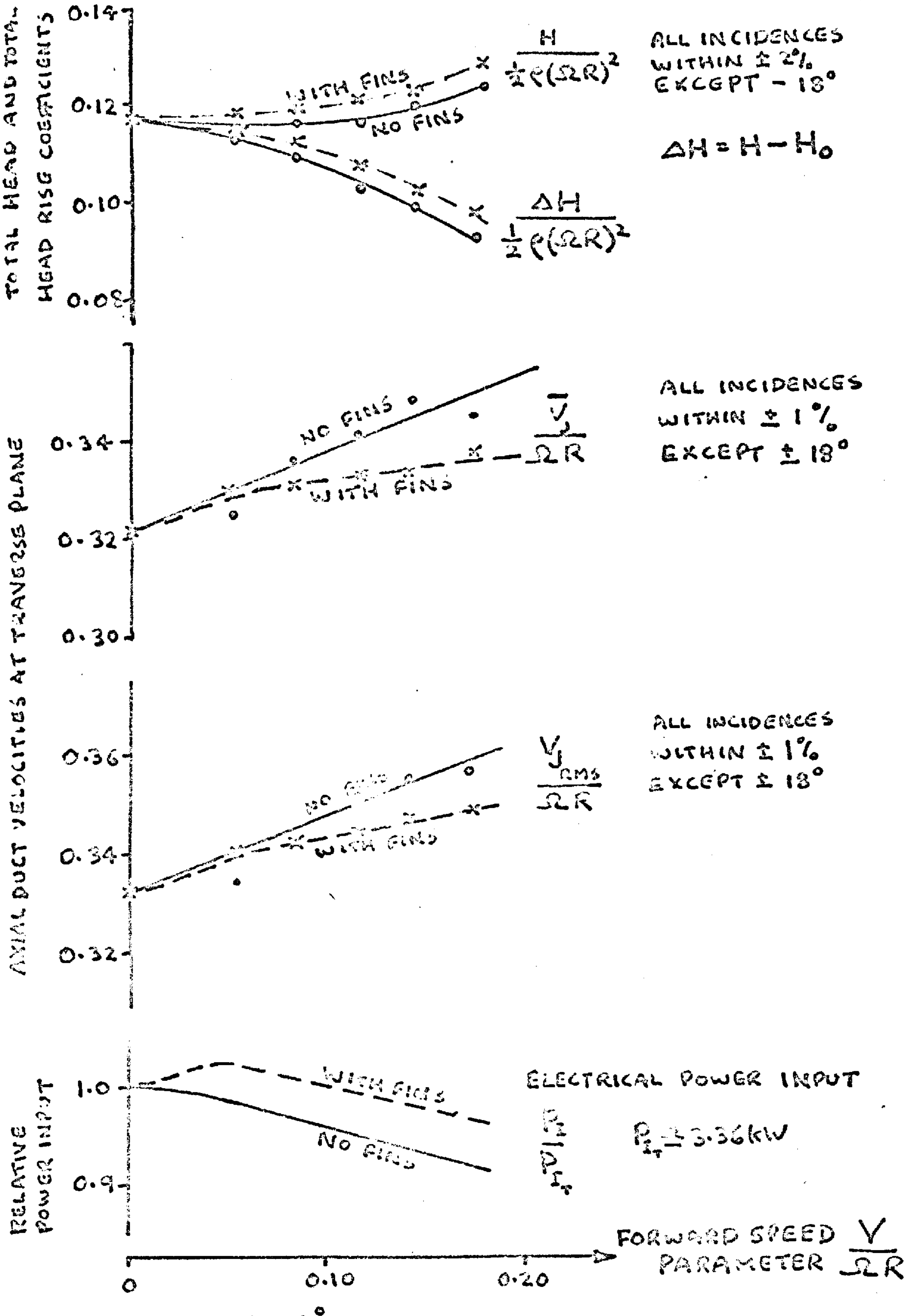

BODY ON STRUTS, $\alpha = -6°$

VARIATION OF MEAN DUCT CONDITIONS WITH FORWARD SPEED

FIGURE 7.2
(SEE SECTION 7.2.2)

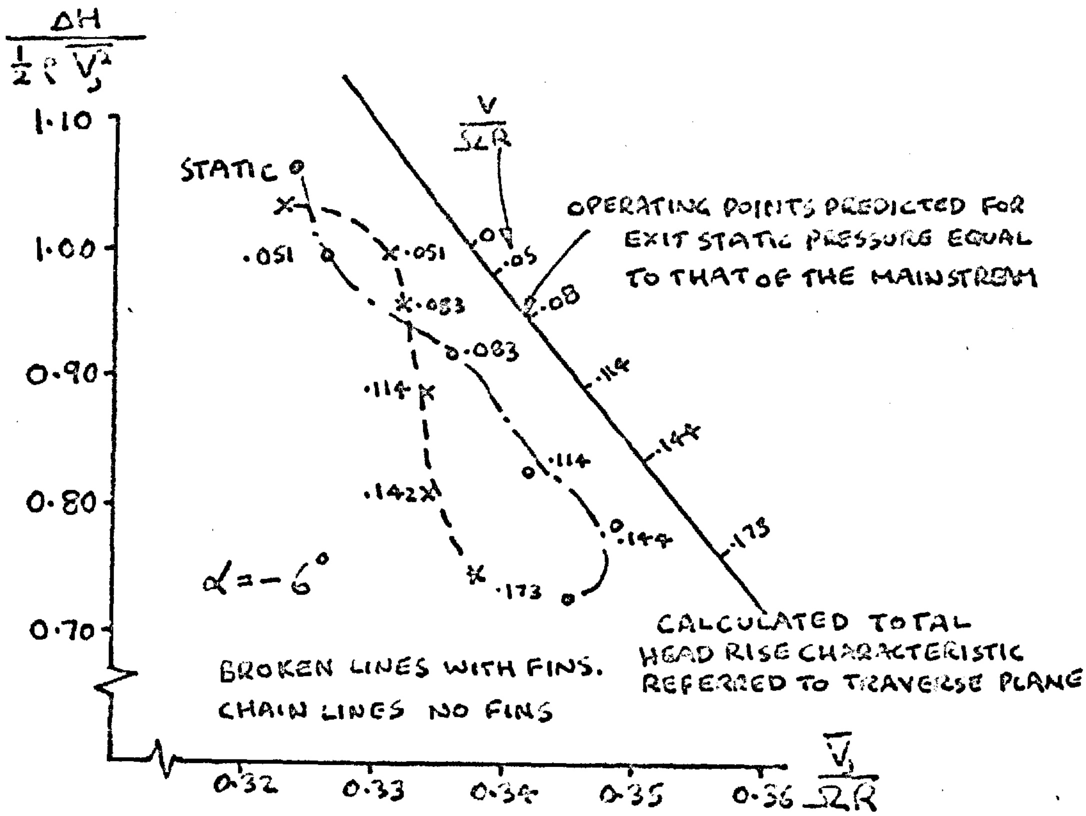

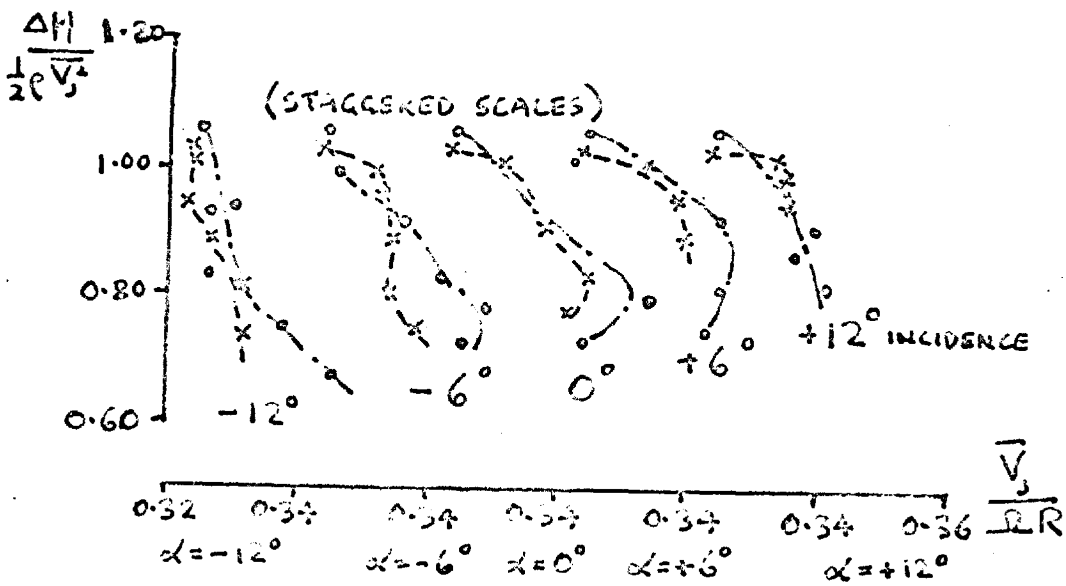

BODY ON STRUTS

TOTAL HEAD RISE CHARACTERISTICS

AT VARIOUS INCIDENCES.

FIGURE 7.3

(SEE SECTION 7.2.2)

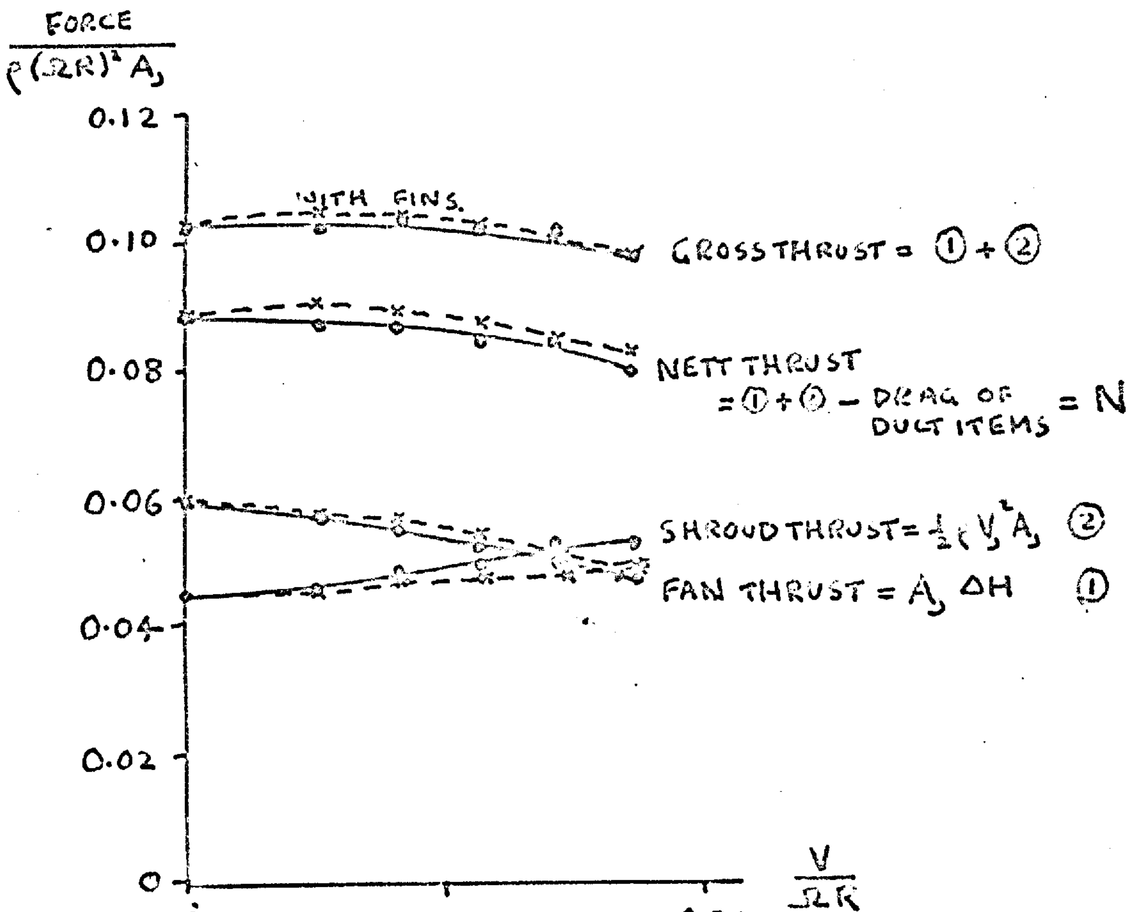

BODY ON STRUTS, $\alpha = -6^\circ$

BREAKDOWN OF FORCES ON THE LIFTING UNIT

FIGURE 7.4

(SEE SECTION 7.2.4)

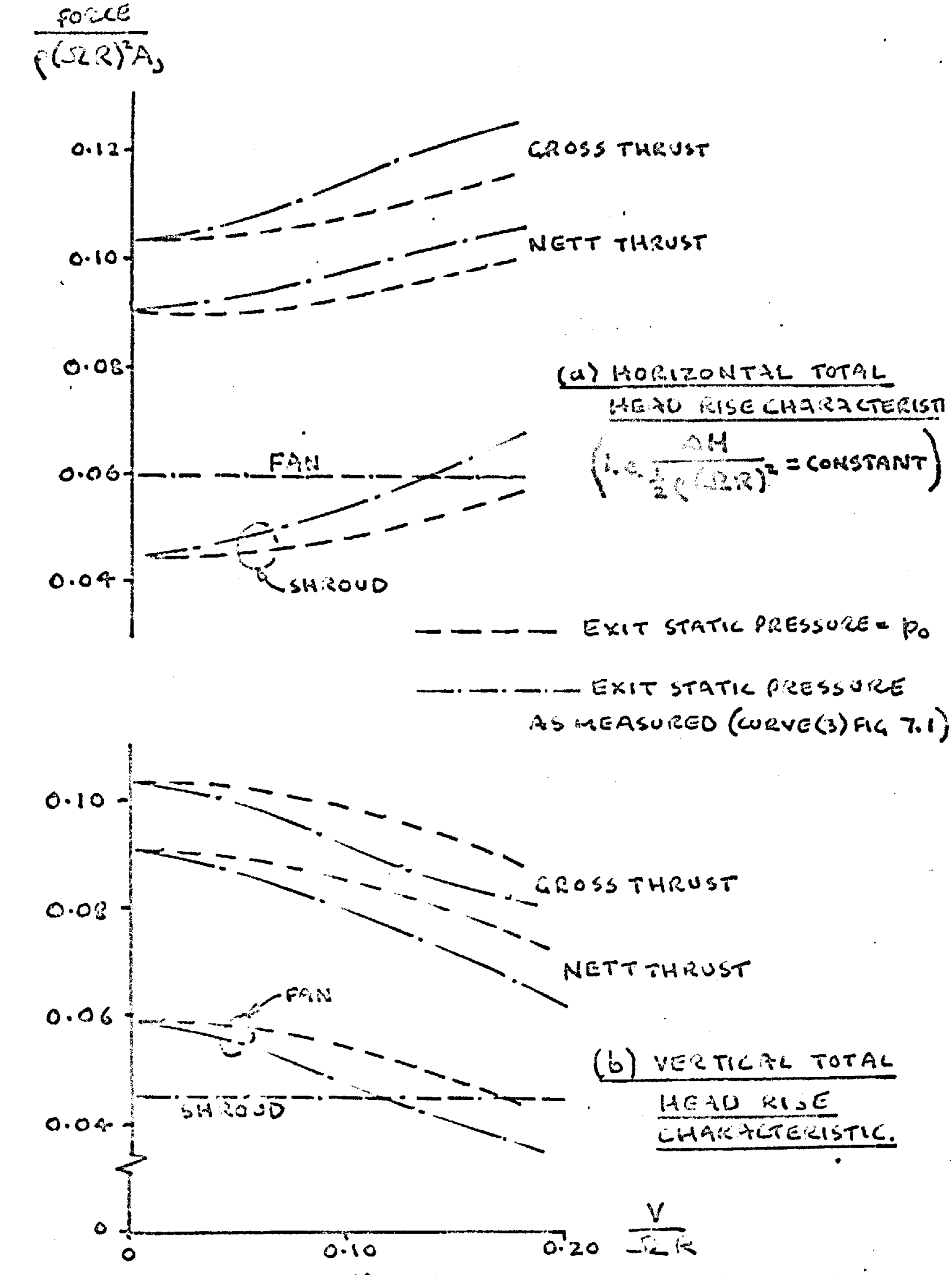

MEASURED CONDITIONS AT $\frac{V}{\Omega R} = 0$ USED AS DATUM THROUGHOUT.

BREAKDOWN OF FORCES ON TWO IDEALISED LIFTING UNITS.
(FORCES ACTING ON THE SURFACE AROUND THE EXIT ARC EXCLUDED.)

FIGURE 7.5
(SEE SECTION 7.2.4)

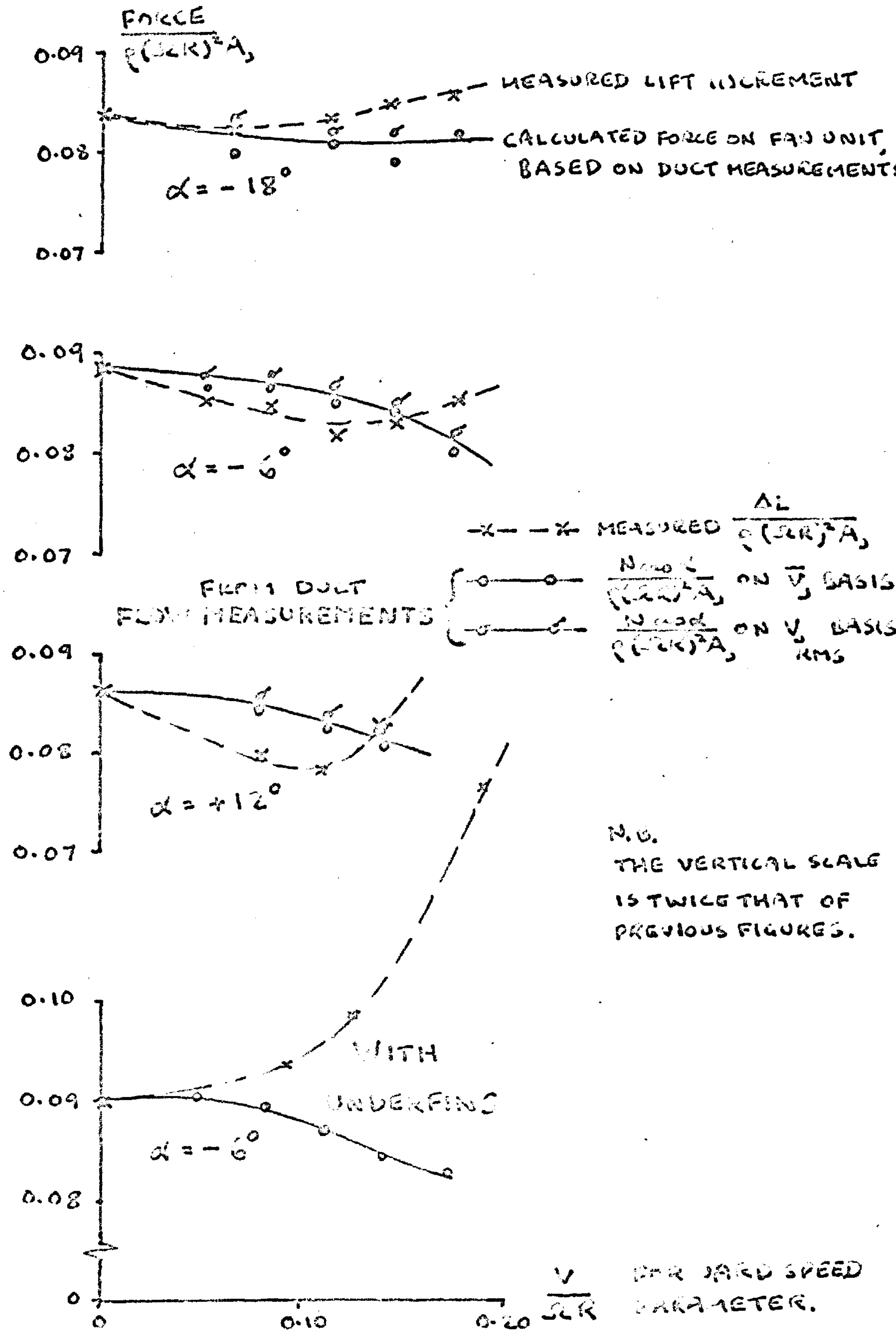

BODY ON STRUTS.

MEASURED LIFT INCREMENTS AND ESTIMATED FORCES ON THE LIFTING UNIT.

FIGURE 7.6
(SEE SECTION 7.3)

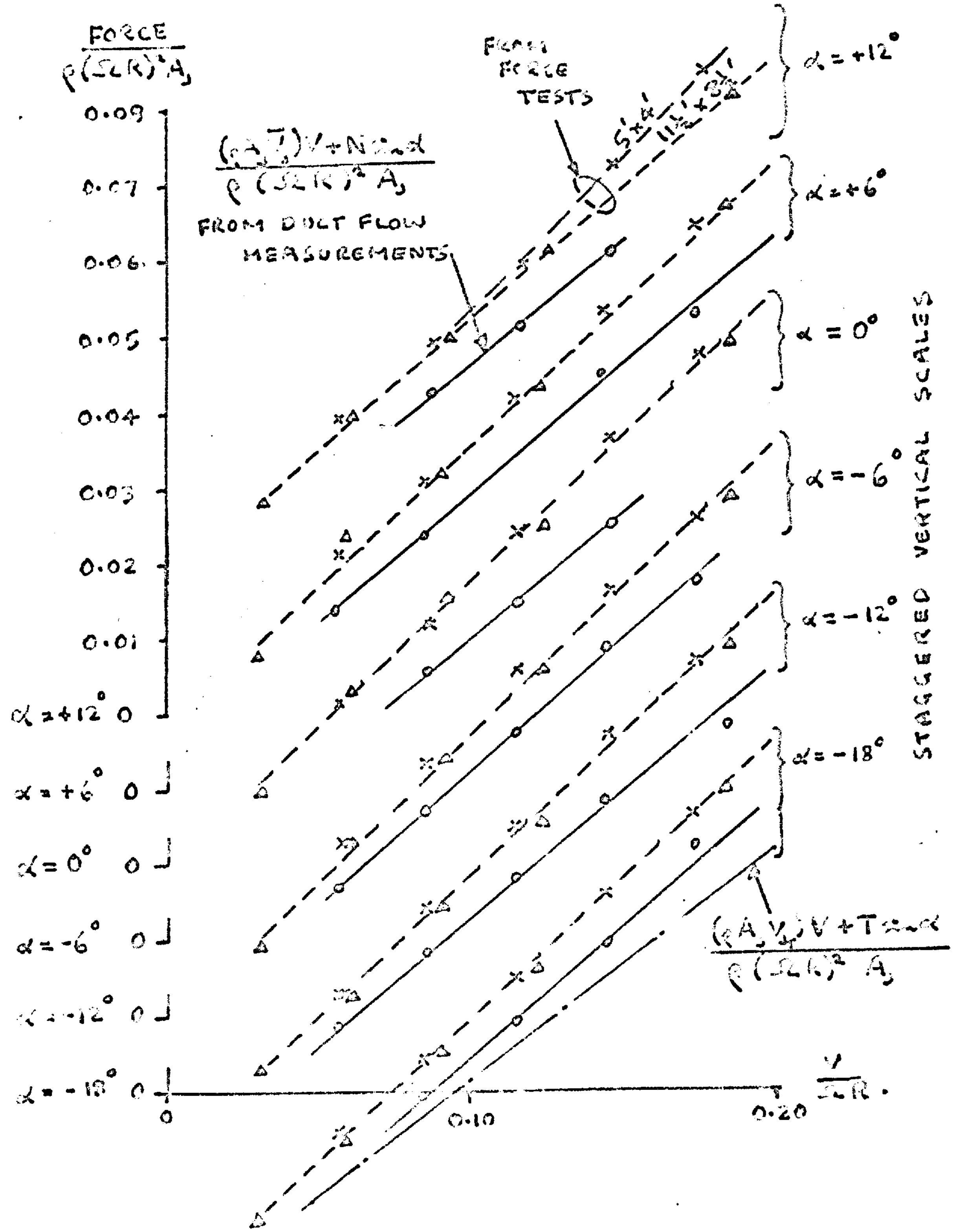

BODY AND STRUTS.

MEASURED DRAG INCREMENTS AND ESTIMATES FROM DUCT FLOW MEASUREMENTS.

FIGURE 7.7.
(SEE SECTION 7.3)

$$A = \frac{\Delta L - N\cos\alpha}{\rho\,(\Omega R)^2 A_J}$$

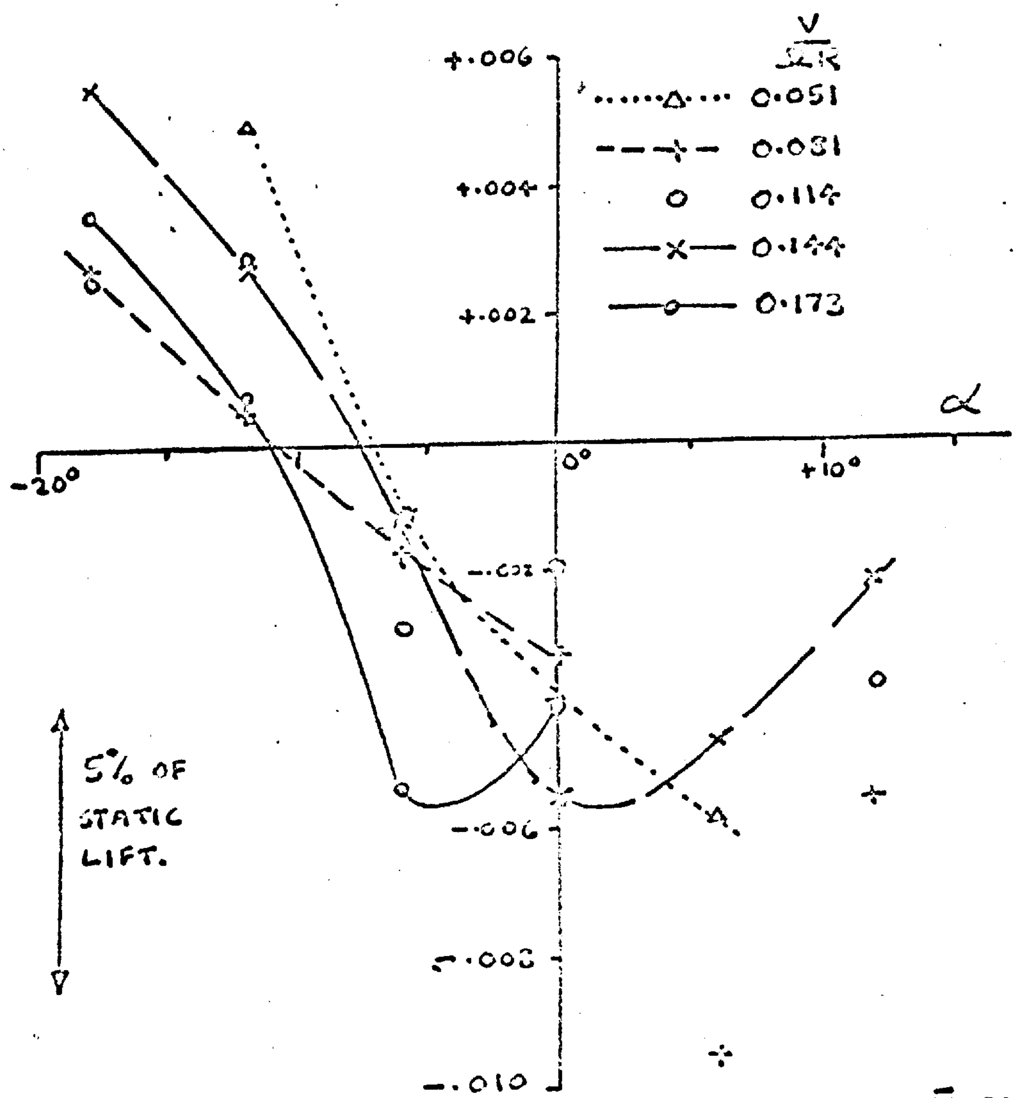

THE FORCE N ON THE LIFTING UNIT WAS CALCULATED ON A $\bar{V}_J$ BASIS.

BODY ON STRUTS

INTERFERENCE LIFT AFTER ALLOWANCE FOR THE INTERACTION BETWEEN THE SLIPSTREAM AND THE FAN UNIT.

FIGURE 7.8

(SEE SECTIONS 7.3 & 7.4.3)

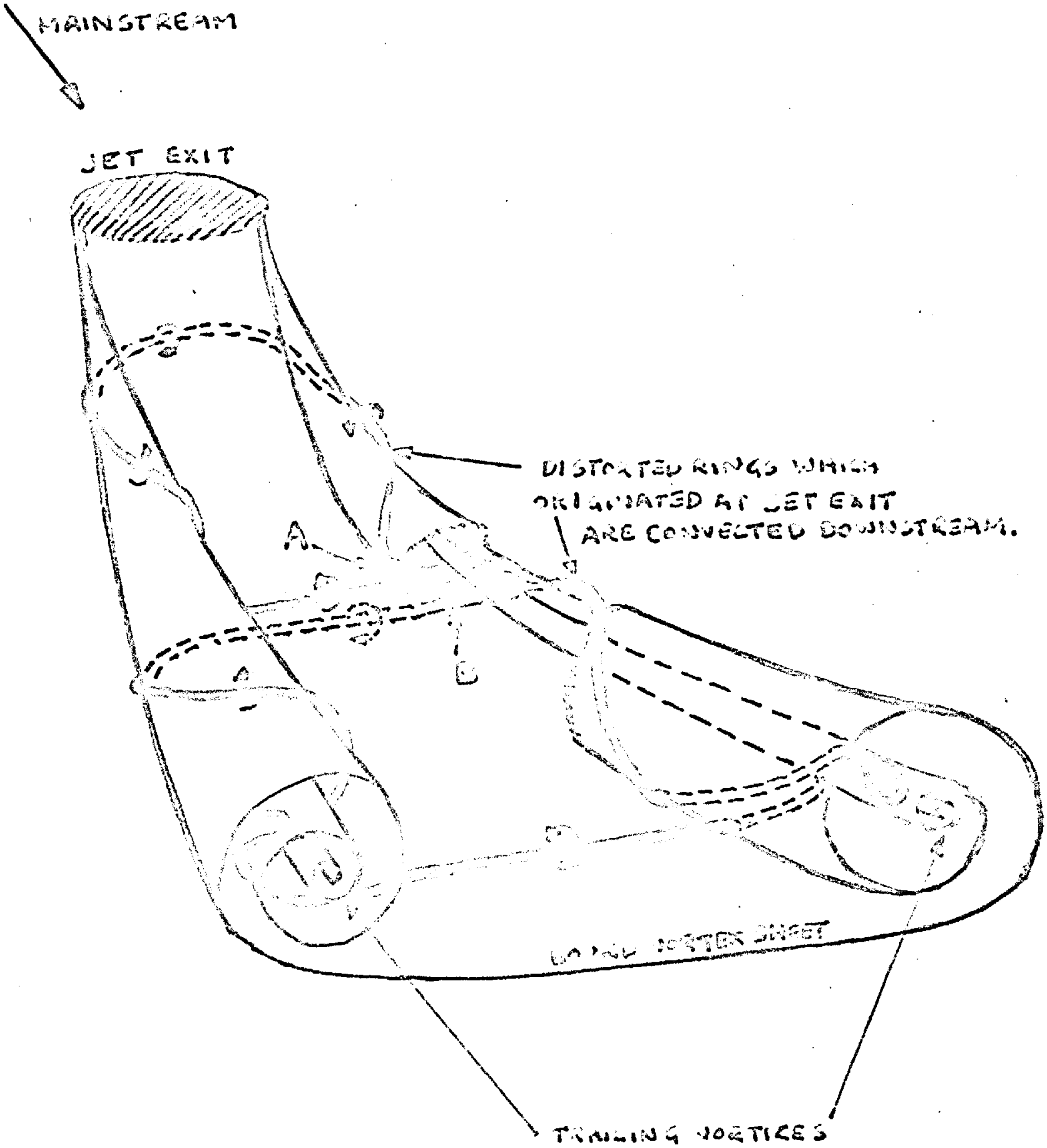

A POSSIBLE VORTEX REPRESENTATION OF THE JET PLUME.

FIGURE 7.9

(SEE SECTION 7.4.1)

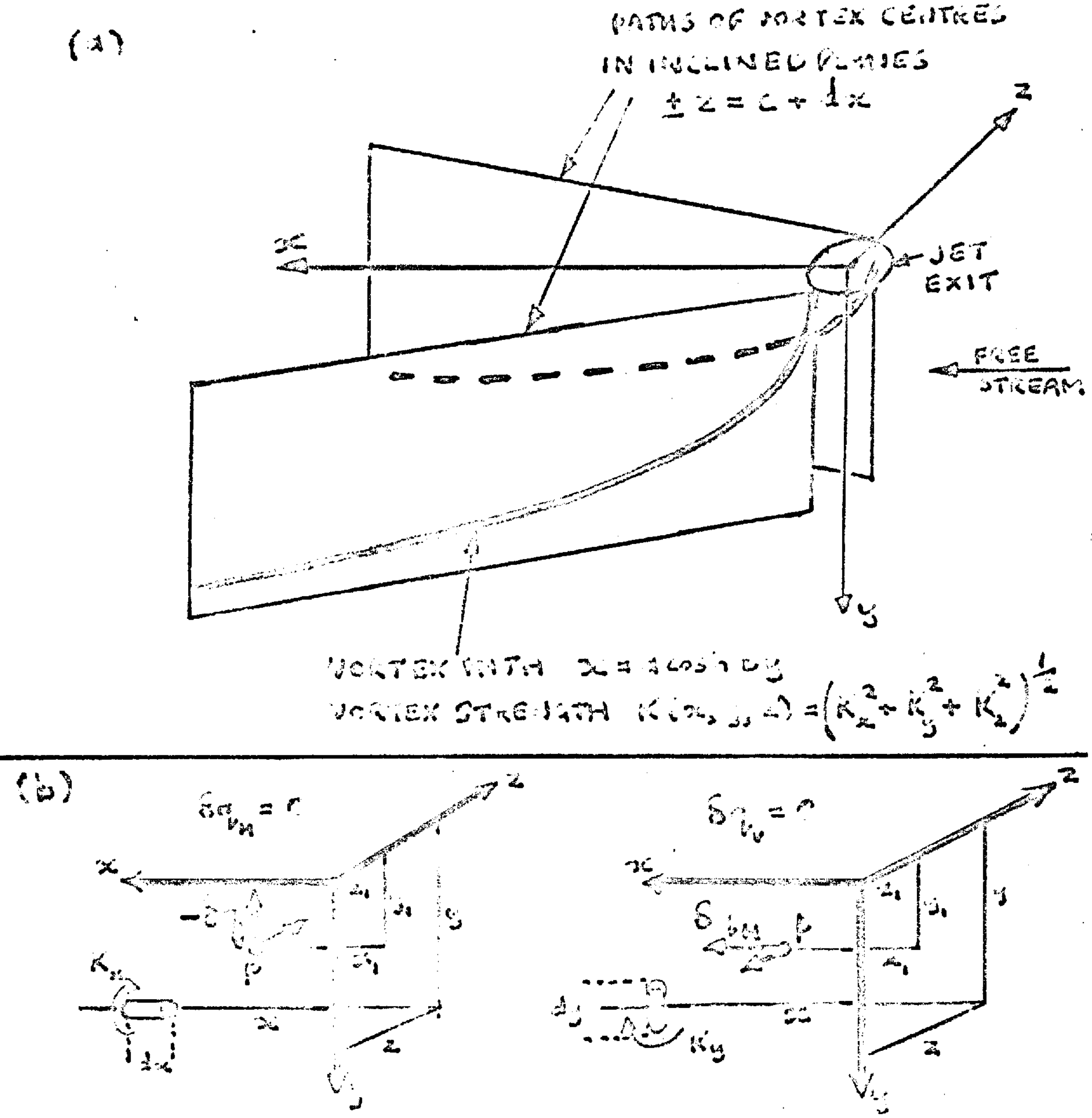

$$\delta q_{v_{K_x}} = -\frac{K_x(z-z_1)\,dx}{4\pi r^3} \qquad \delta q_{u_{K_y}} = \frac{K_y(z-z_1)\,dy}{4\pi r^3}$$

$$r^2 = (x-x_1)^2 + (y-y_1)^2 + (z-z_1)^2$$

(a) THE IDEALISED VORTEX MODEL OF THE JET PLUME

(b) INDUCED VELOCITIES DUE TO STREAMWISE + VERTICAL VORTEX ELEMENTS

FIGURE 7.10

(SEE SECTION 7.4.1)

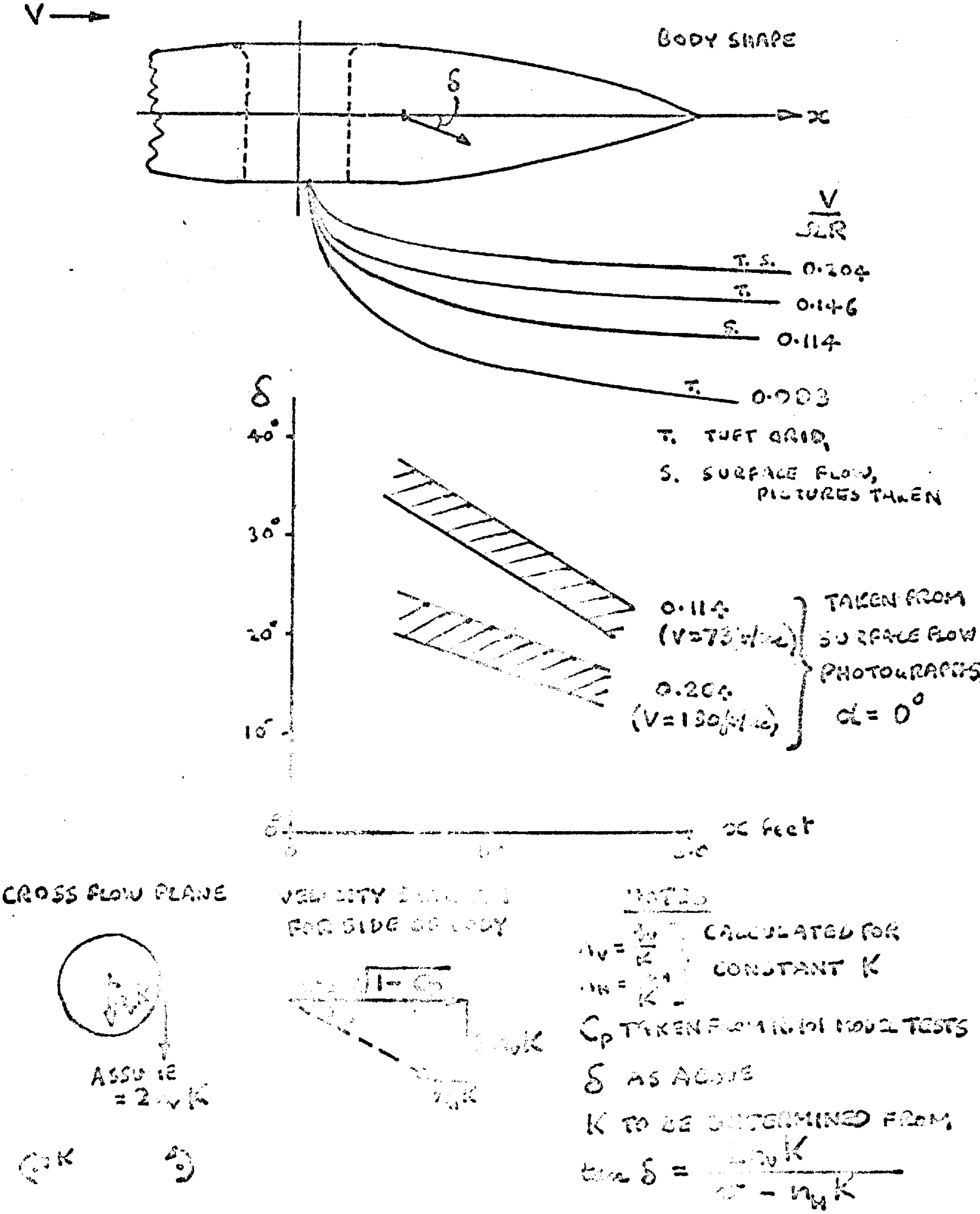

THE DETERMINATION OF VORTEX STRENGTH

FIGURE 7.11

(SEE SECTION 7.4.2)

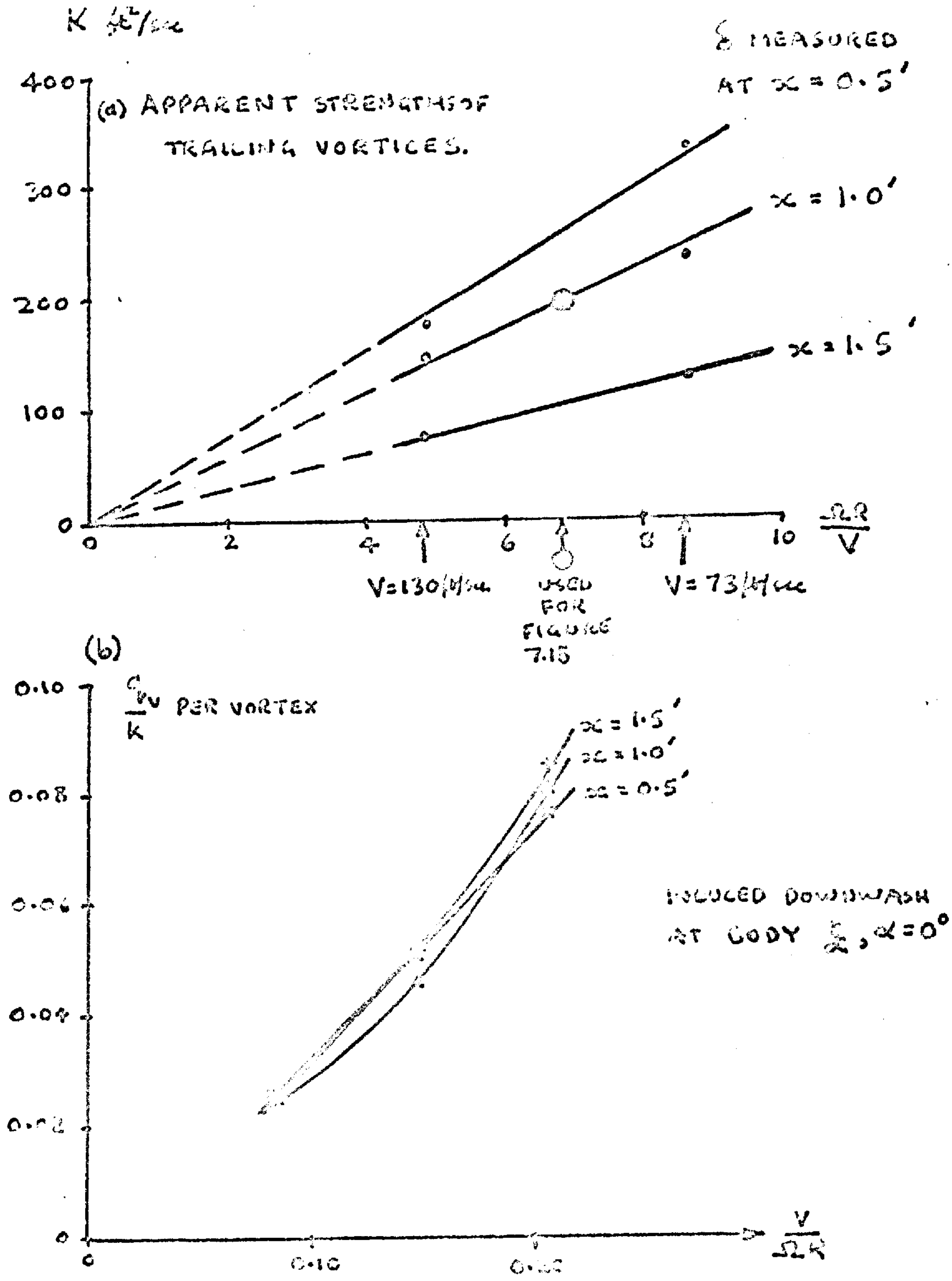

THE EFFECT OF CHANGES OF FORWARD SPEED ON APPARENT VORTEX STRENGTH AND INDUCED VELOCITIES ON BODY.

FIGURE 7.12
(SEE SECTION 7.4.2)

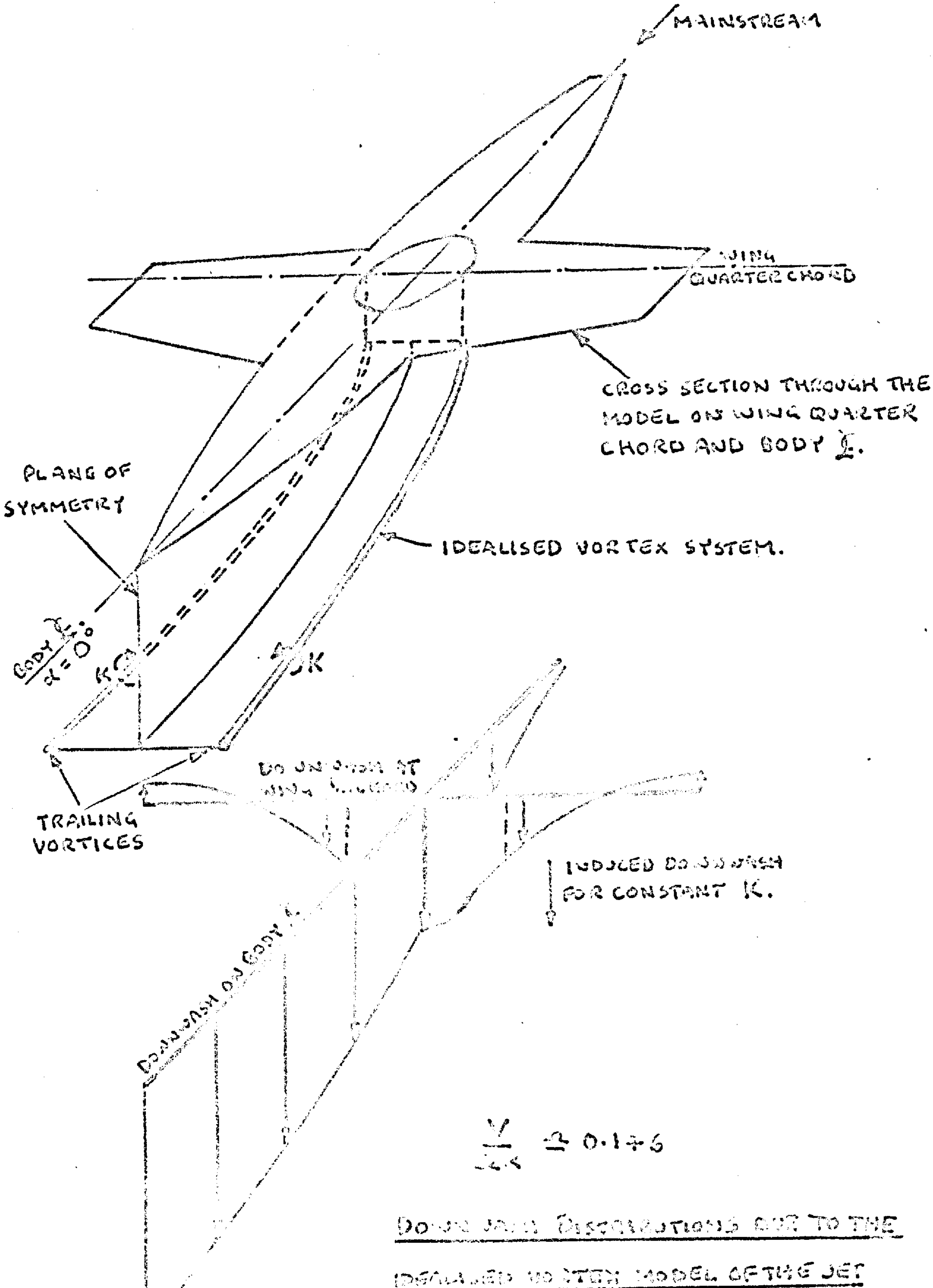

DOWNWASH DISTRIBUTIONS DUE TO THE IDEALISED VORTEX MODEL OF THE JET PLUME. (i) $\alpha = 0°$

FIGURE 7.13
(SEE SECTION 7.4.3)

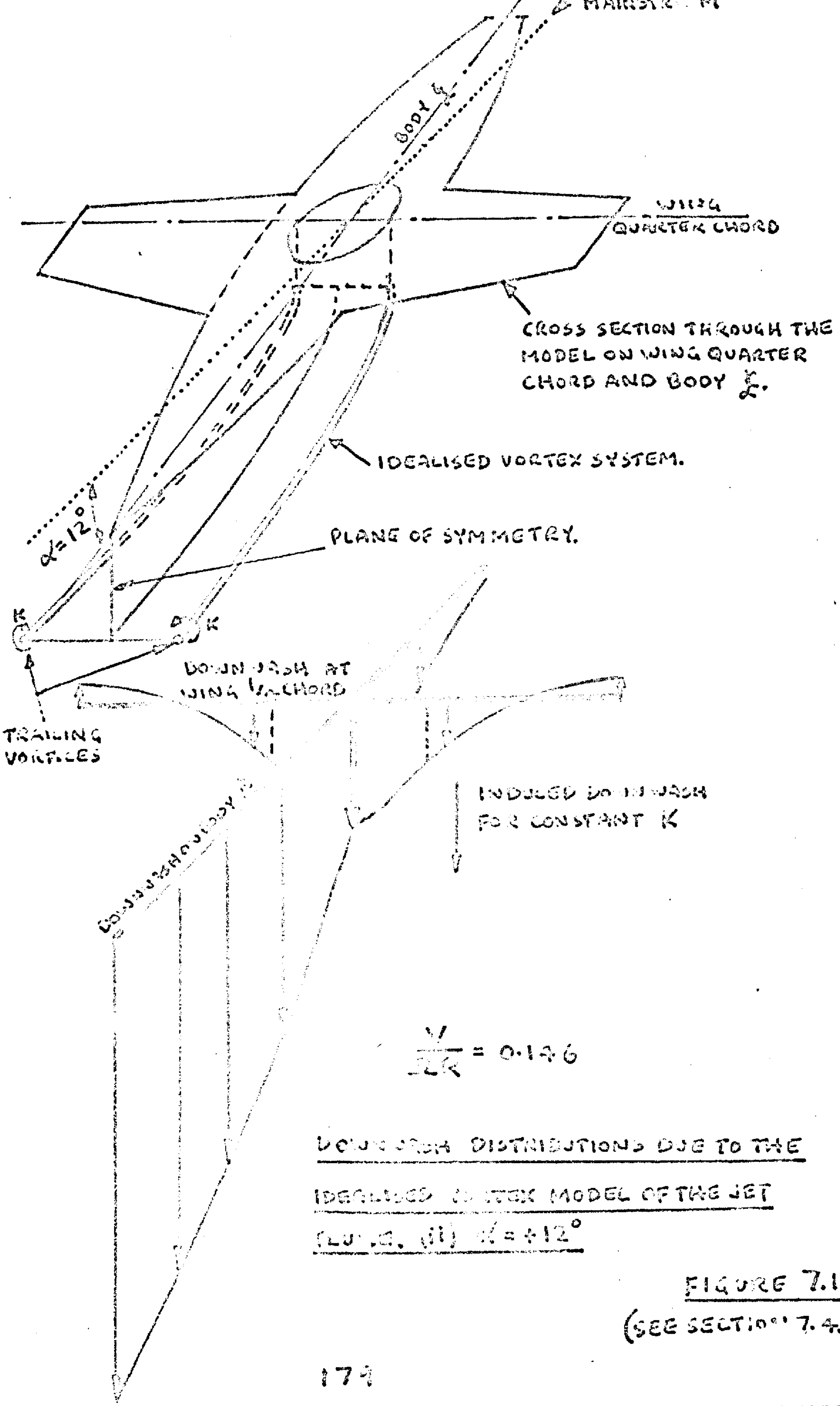

$$\frac{V}{\Omega R} = 0.146$$

DOWNWASH DISTRIBUTIONS DUE TO THE IDEALISED VORTEX MODEL OF THE JET (L.U.G. (II) $\alpha = +12°$

FIGURE 7.14
(SEE SECTION 7.4.3)

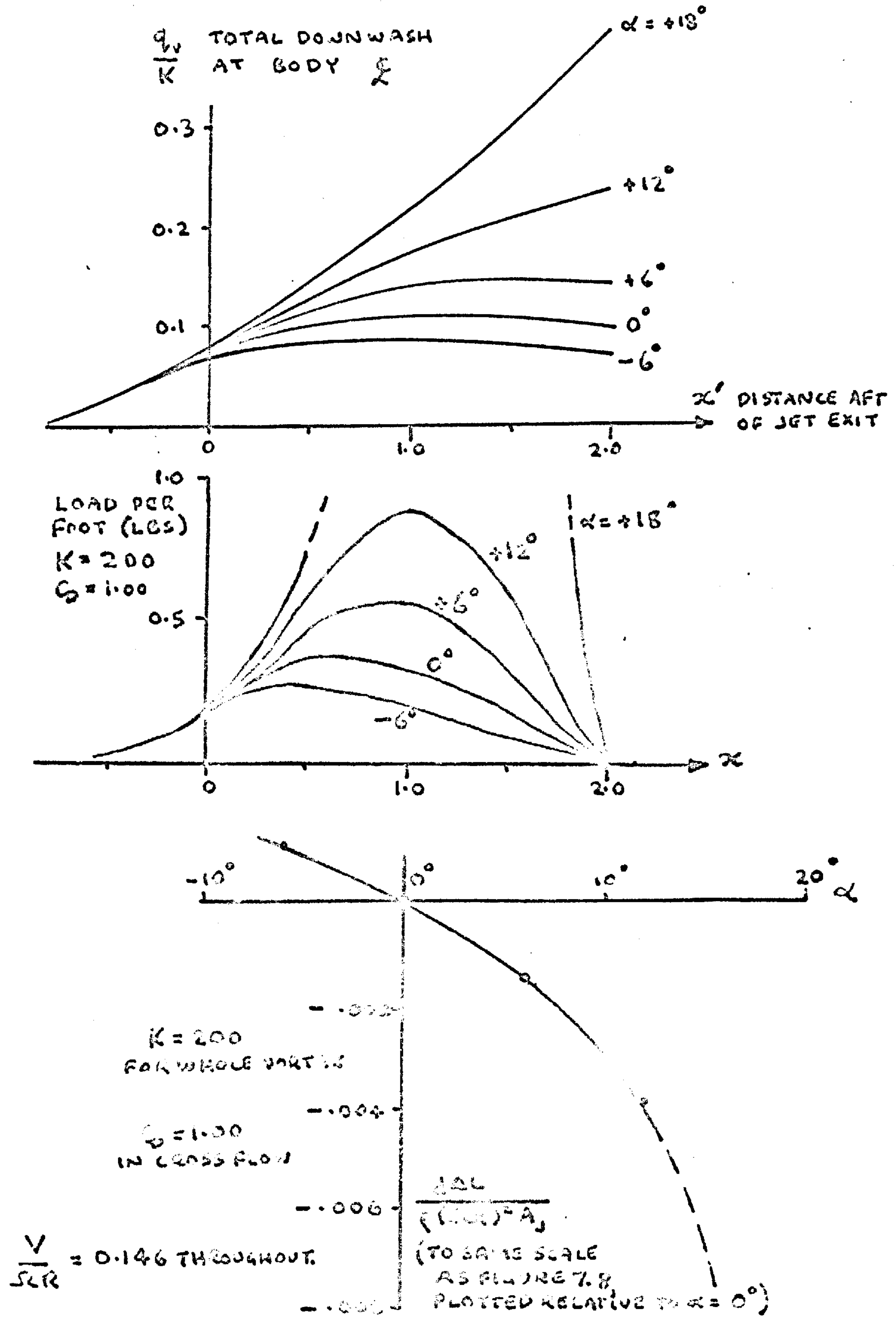

THE EFFECT OF INCIDENCE ON [illegible] LIFT FORCE ON BODY

FIGURE 7.15
(SEE SECTION 7.4.3)

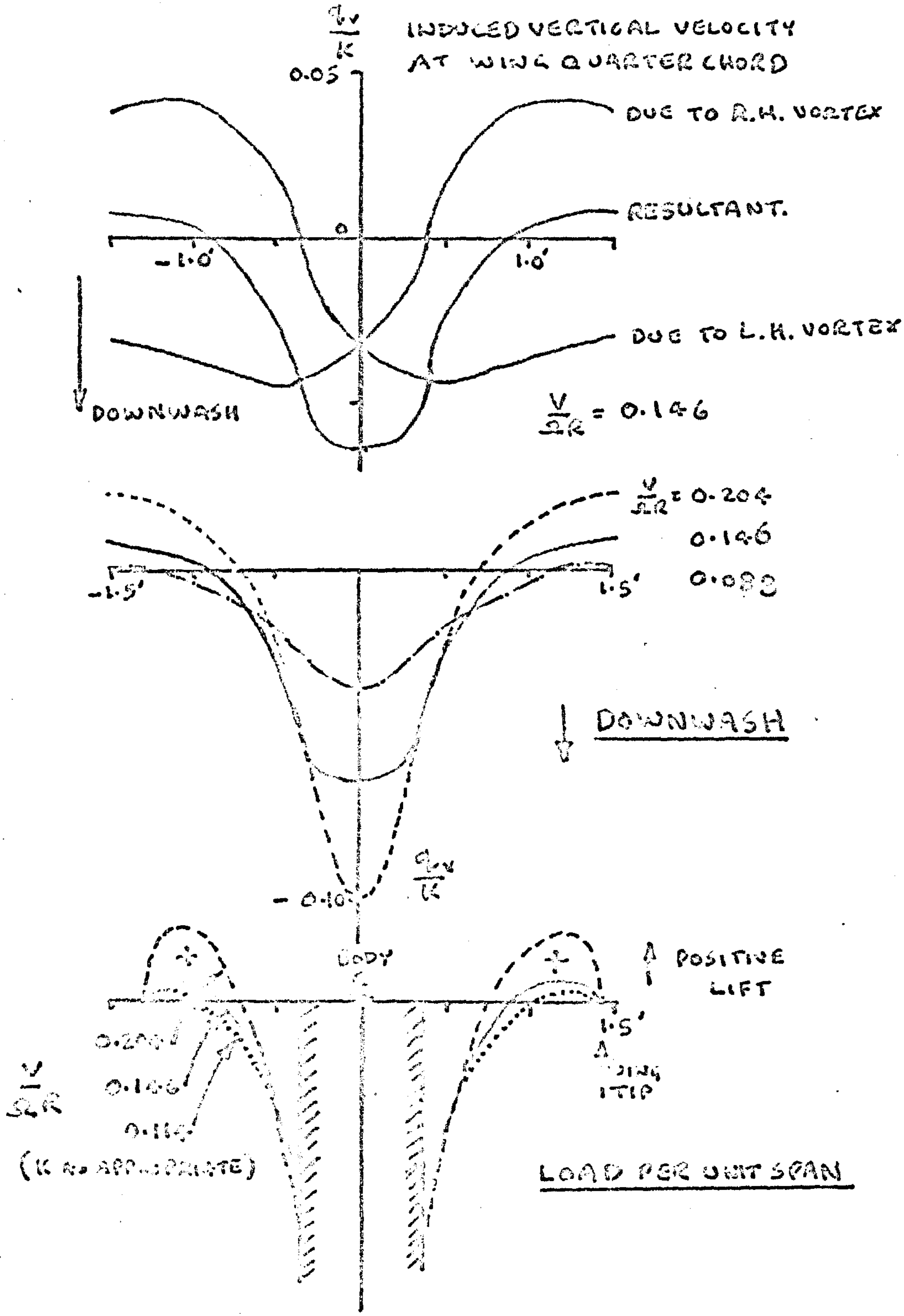

INDUCED DOWNWASH AND LOADS AT WING QUARTER CHORD.
(K, CONSTANT, AS DETERMINED IN FIGURE 7.12)

FIGURE 7.16.
(SEE SECTION 7.4.3)

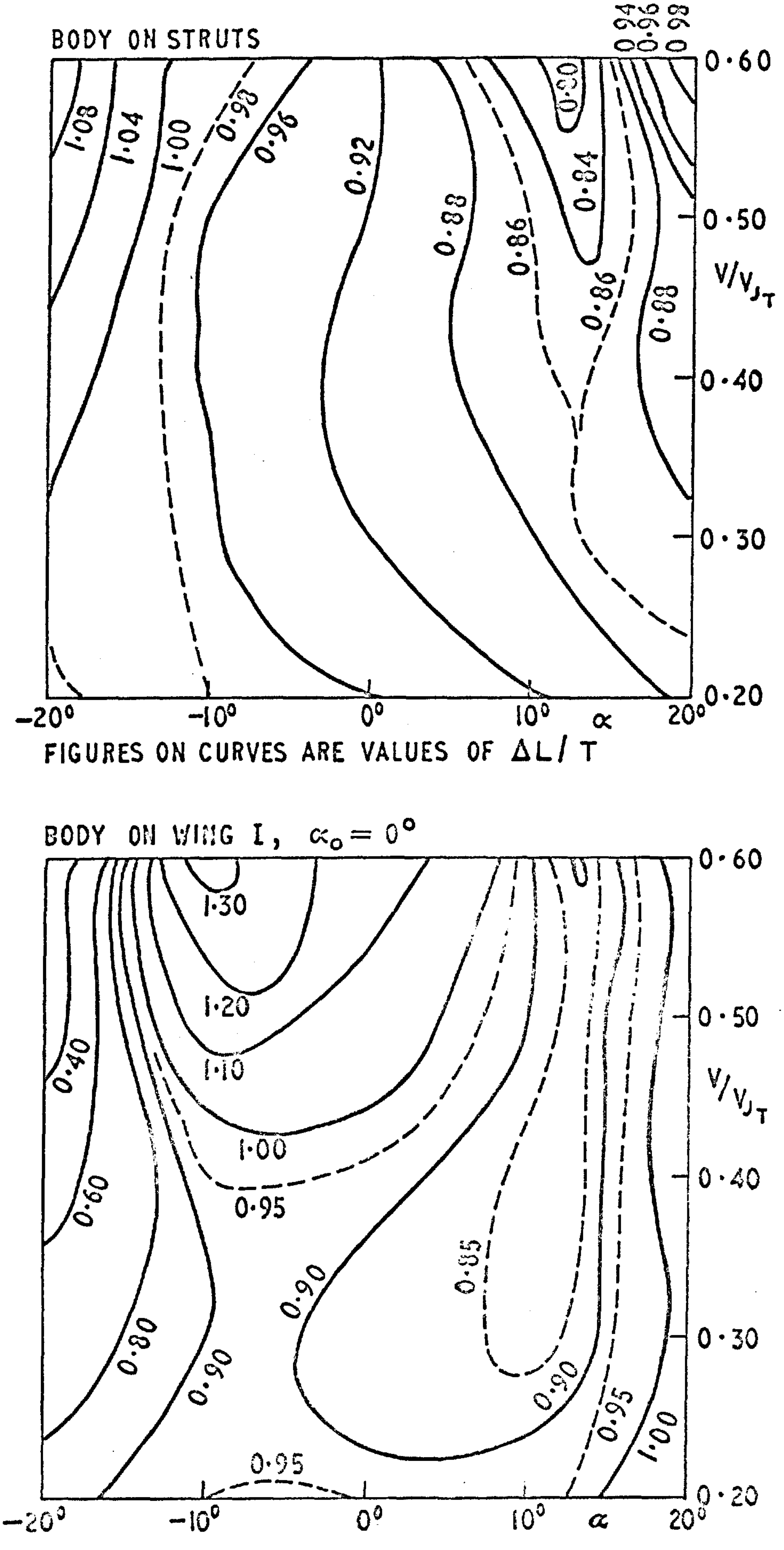

FIGURE 7.17

VARIATION OF LIFT INCREMENT WITH V/V_{J_T} AND INCIDENCE

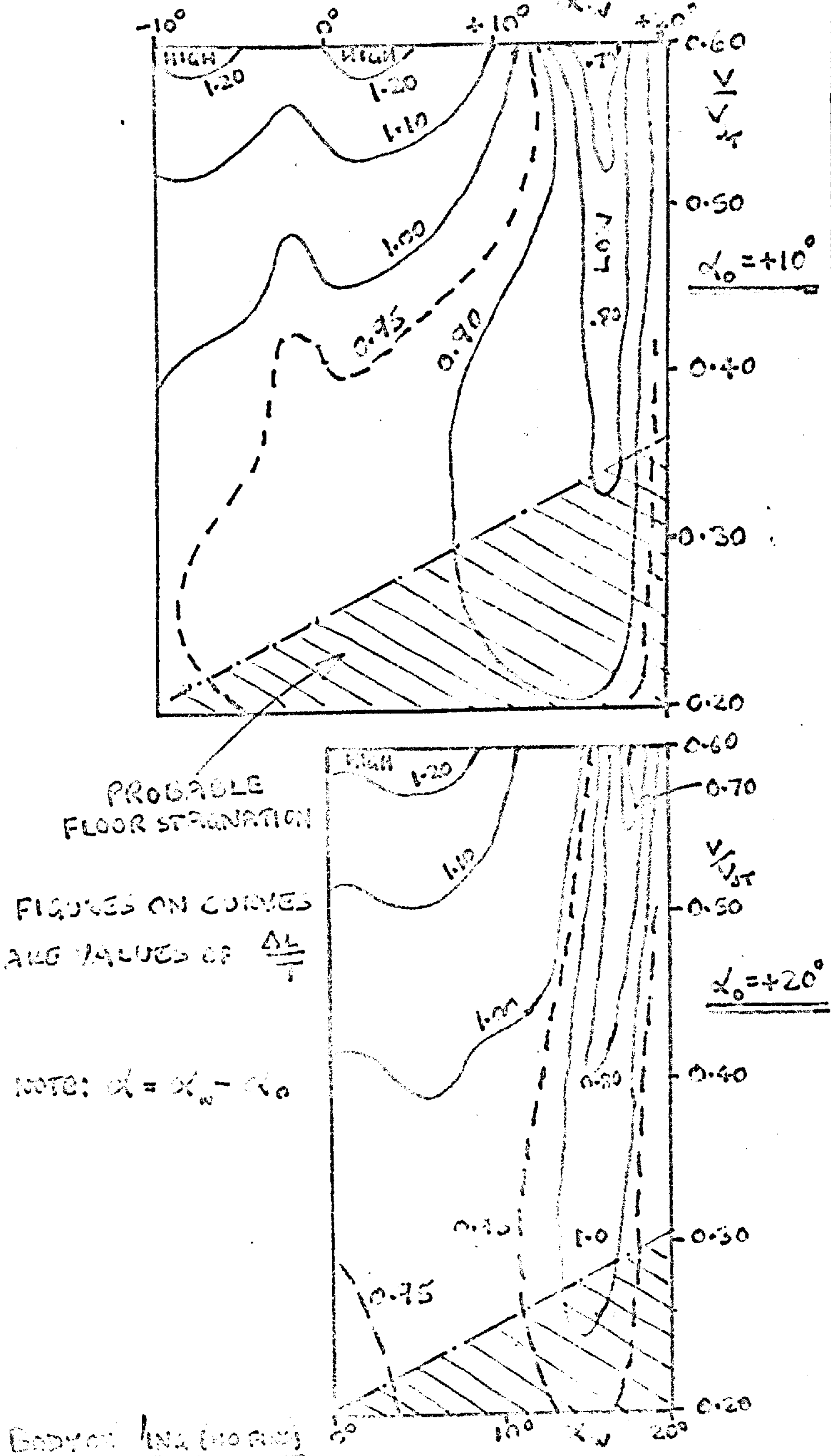

BODY ON WING (NO RIB)
CONTOURS OF CONSTANT LIFT INCREMENT FOR VARIOUS WING SETTING ANGLES α_0. (I.E. FIRST TEST SERIES)

FIGURE 7.18

(SEE SECTION 7.5.2)

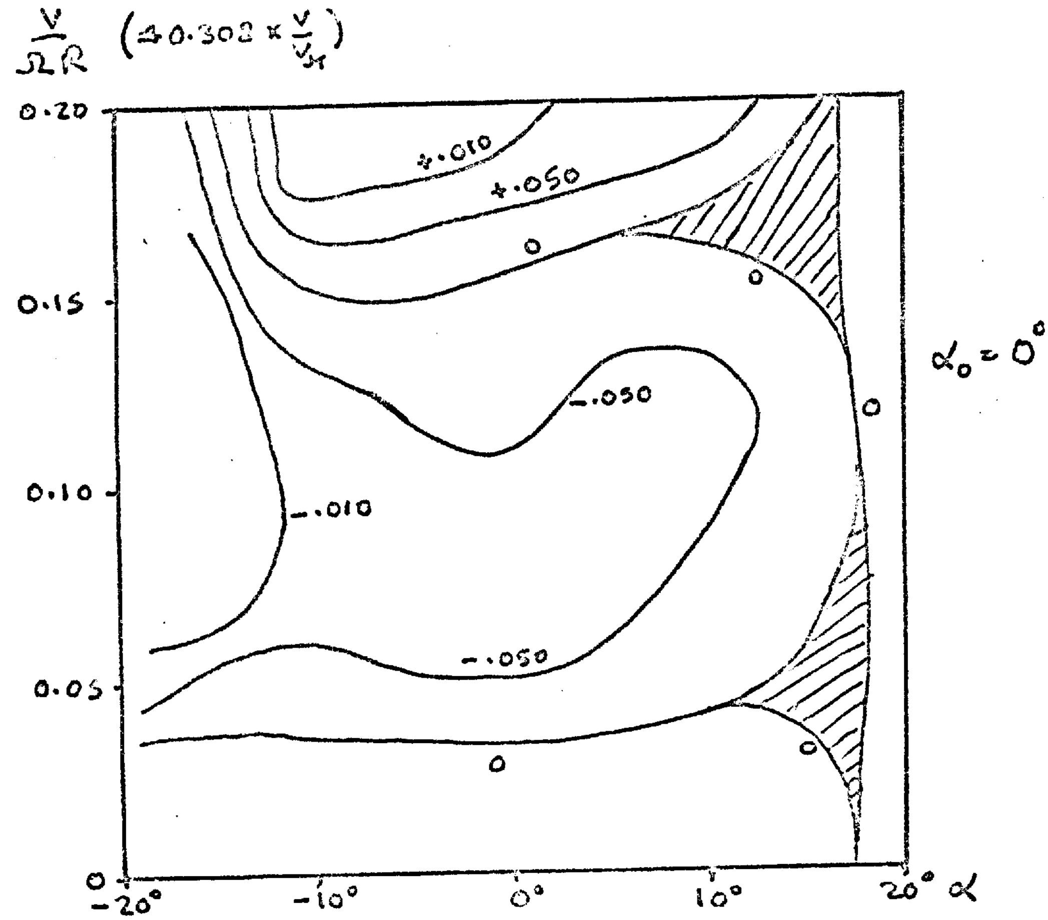

FIGURES ON CURVES ARE PROPORTIONAL GAINS IN $\Delta L / \rho(\Omega R)^2 A$,

GAINS IN INCREMENTAL LIFT DUE TO THE ADDITION OF WINGS TO THE PLAIN BODY.

FIGURE 7.19

(SEE SECTION 7.5.1)

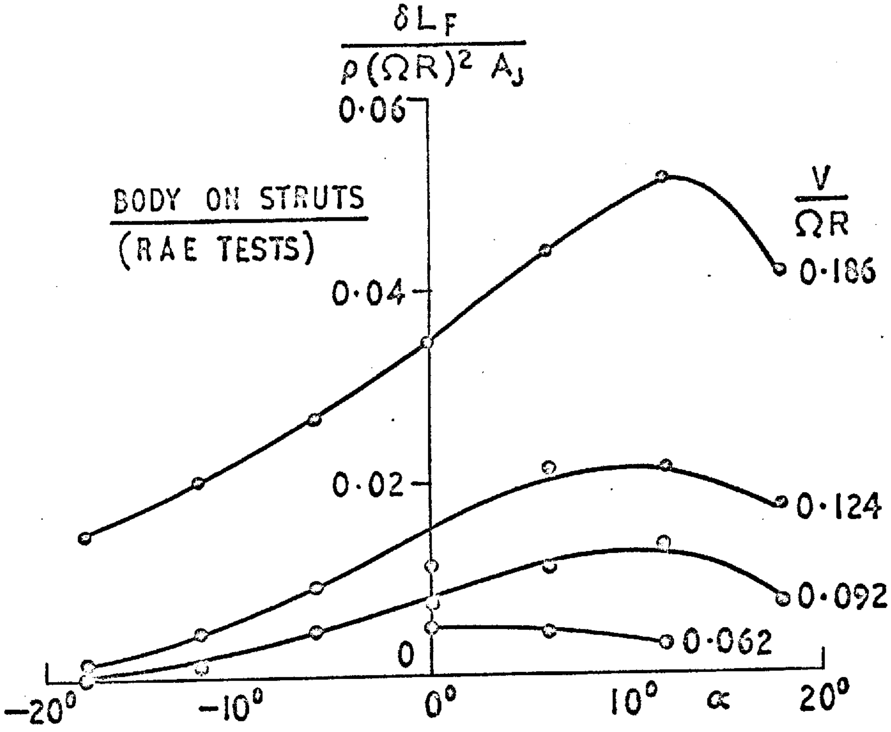

$$\delta L_F = \left(LIFT_{\substack{FAN\ ON \\ FINS\ ON}}\right) - \left(LIFT_{\substack{FAN\ ON \\ FINS\ OFF}}\right)$$

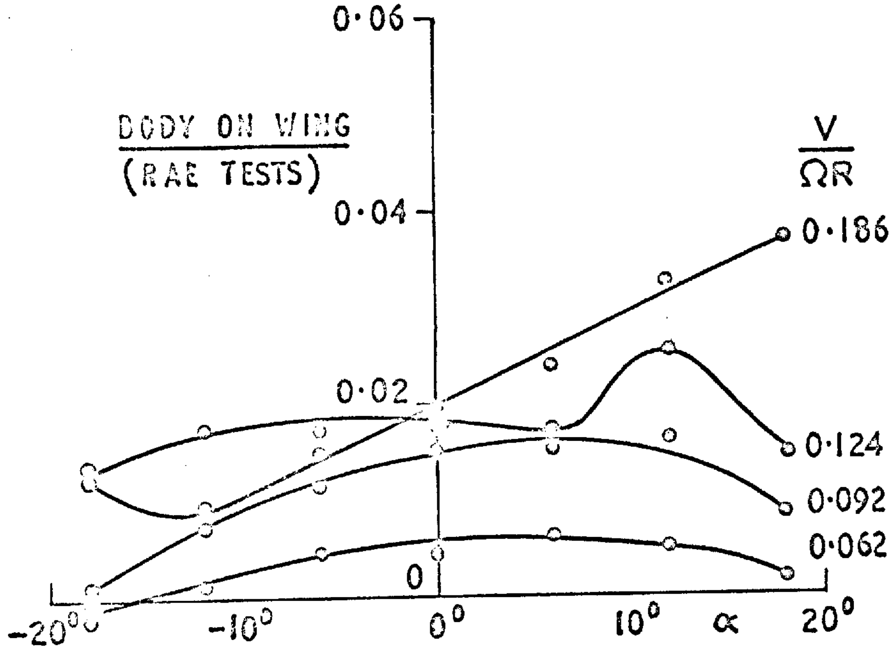

THE EFFECT OF UNDERFINS.

INCREASES IN TOTAL LIFT DUE TO THE ADDITION OF UNDERFINS WITH FAN ON

FIGURE 7.20

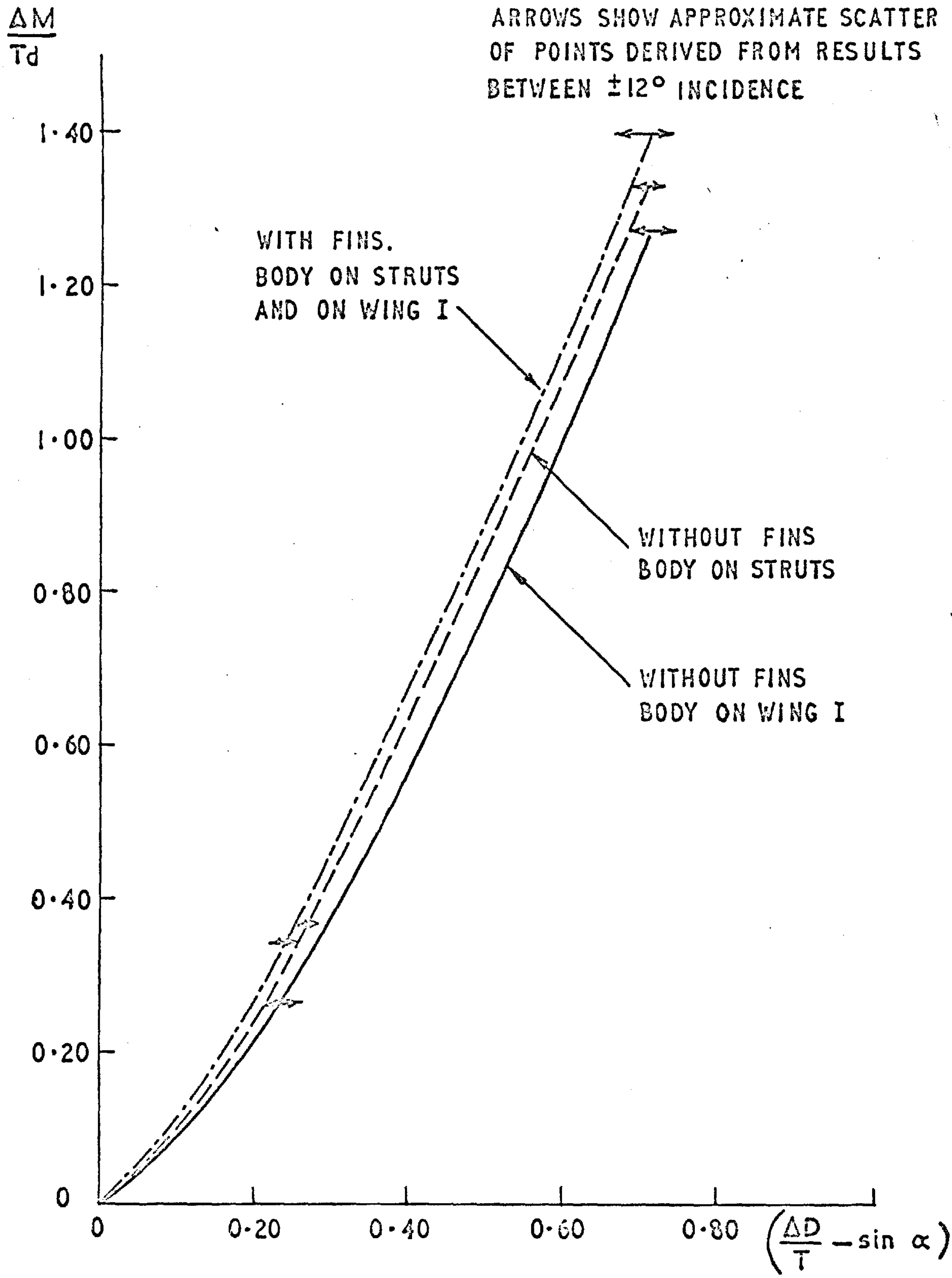

PITCHING MOMENTS DUE TO FAN OPERATION

FIGURE 7.21

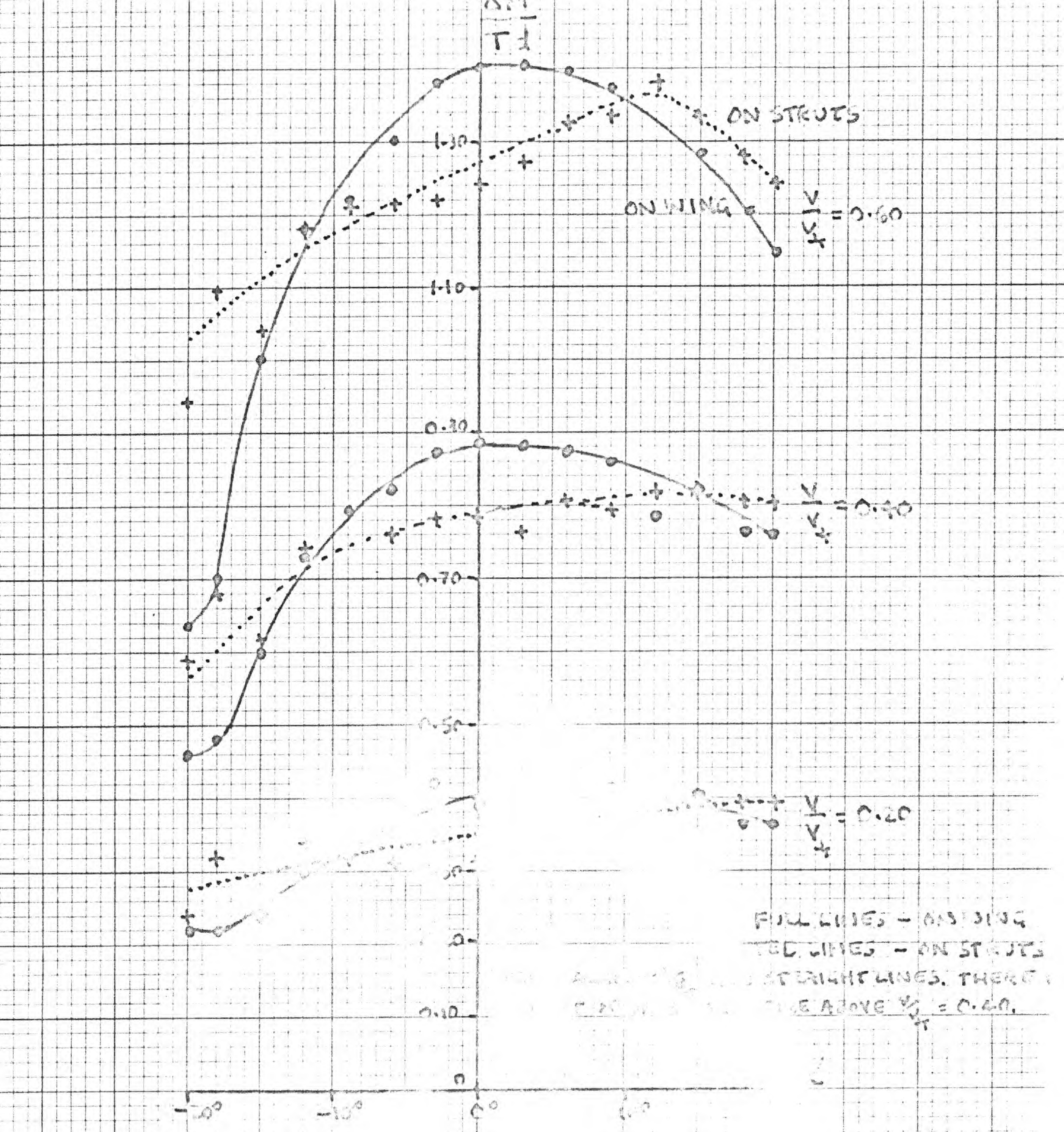
ON STRUTS
ON WING
$\frac{V}{V_t}$ = 0.60
1.30
1.10
0.90
0.70
0.50
0.10
0
$\frac{V}{V_t}$ = 0.40
$\frac{V}{V_t}$ = 0.20
-20°
-10°
0°

(SEE ... 2)

APPENDIX VII

Further plots of the results of force measurements.

(In the following diagrams equivalent values of $\frac{\Delta L}{T}$ and V/V_{J_T} have been quoted in addition to the values based on tip speed divisors. The static lift coefficients measured in the Imperial College 5' x 4' tunnel, with the working section ventilated; have been used throughout.)

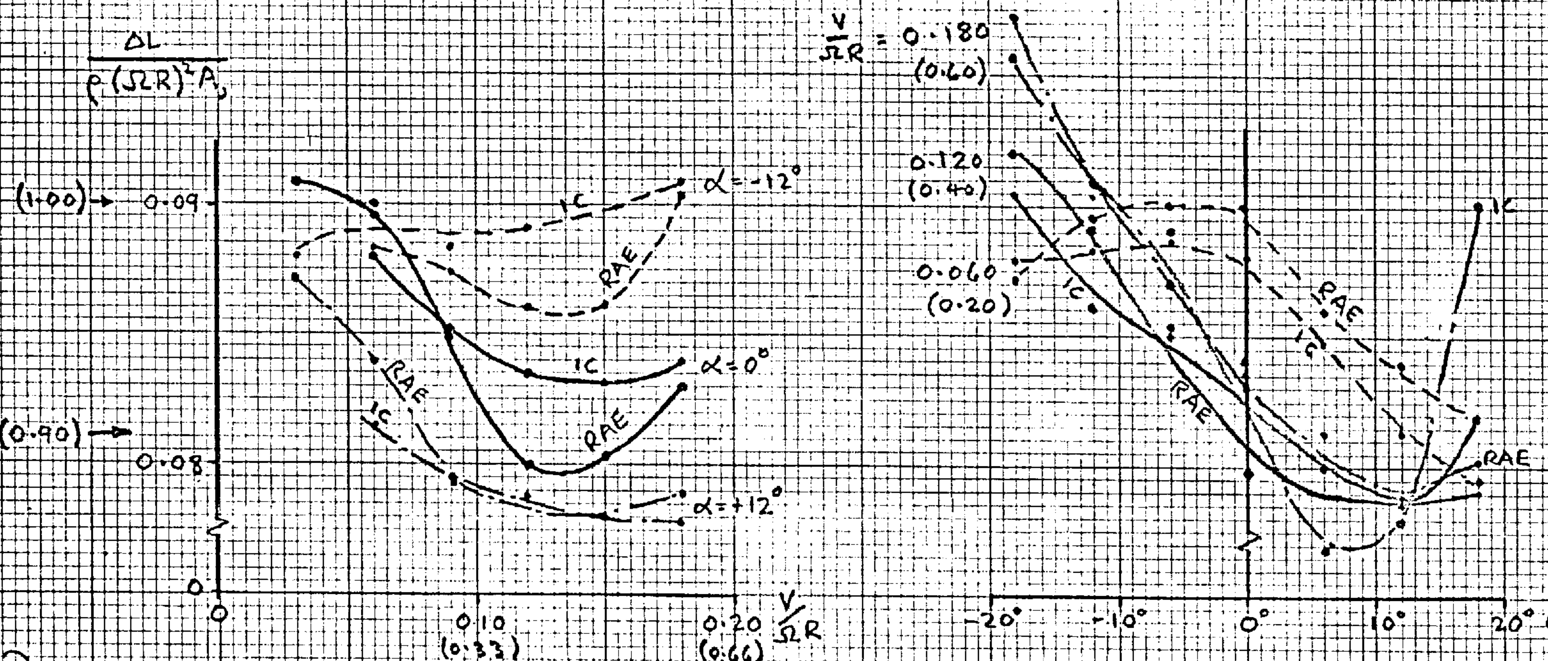

BODY ON STRUTS.

LIFT INCREMENTS IN THE I.C. 5' x 4' TUNNEL
AND IN THE R.A.E. N° 1 11½' x 8½' TUNNEL.

<u>NOTE</u> FIGURES IN BRACKETS SHOW CORRESPONDING VALUES OF $\frac{\Delta L}{T}$ AND $\frac{V}{V_T}$.

FIGURE VII A
(TAKEN FROM TABLE 7A)

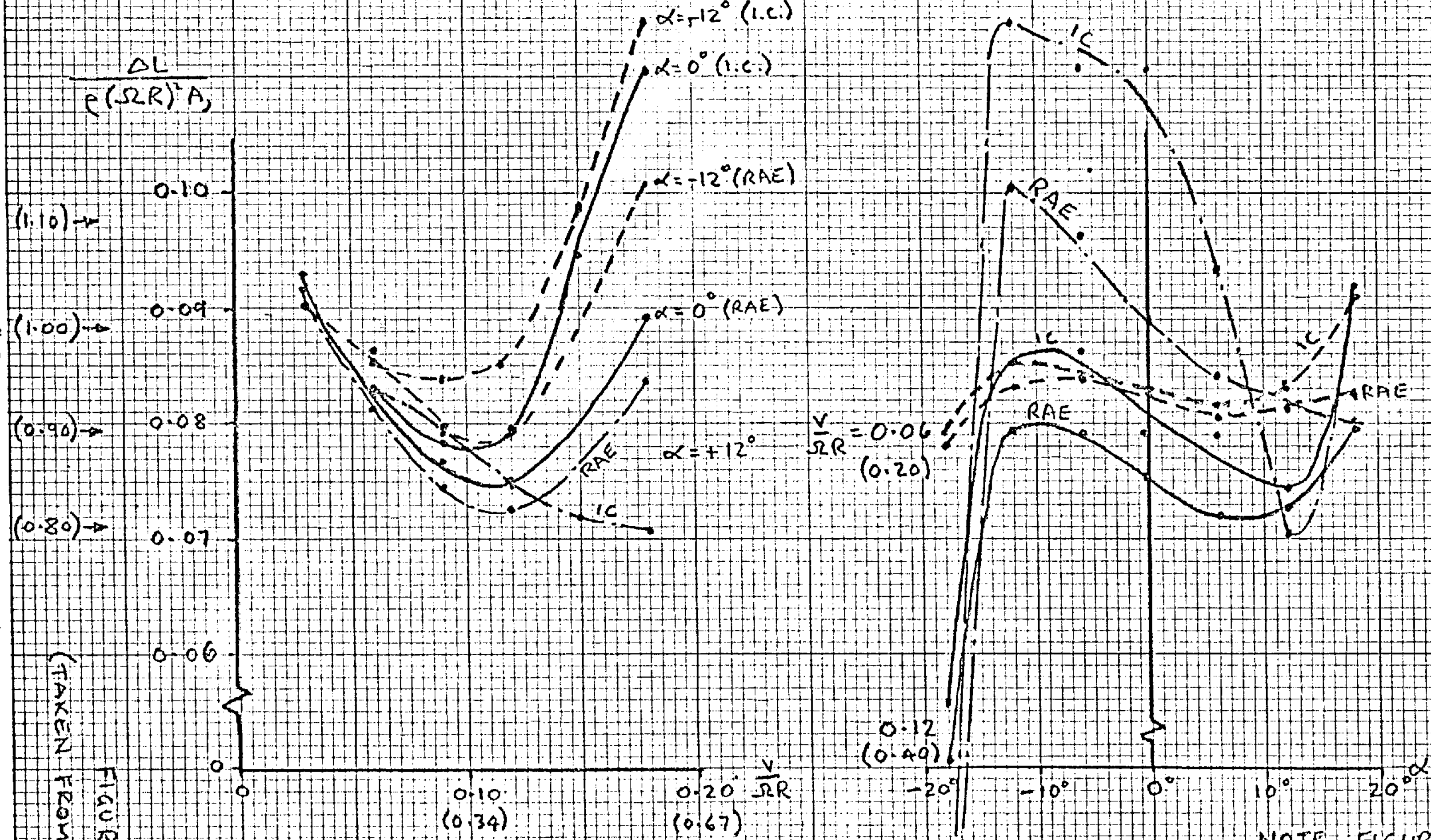

FIGURE VII B

(TAKEN FROM TABLE 7B)

BODY ON WING.

LIFT INCREMENTS IN THE I.C. 5'x4' TUNNEL AND THE R.A.E. N°1 11½'x8½' TUNNEL.

NOTE FIGURES IN BRACKETS SHOW CORRESPONDING VALUES OF $\frac{\Delta L}{T}$ AND $\frac{V}{V_{i_T}}$

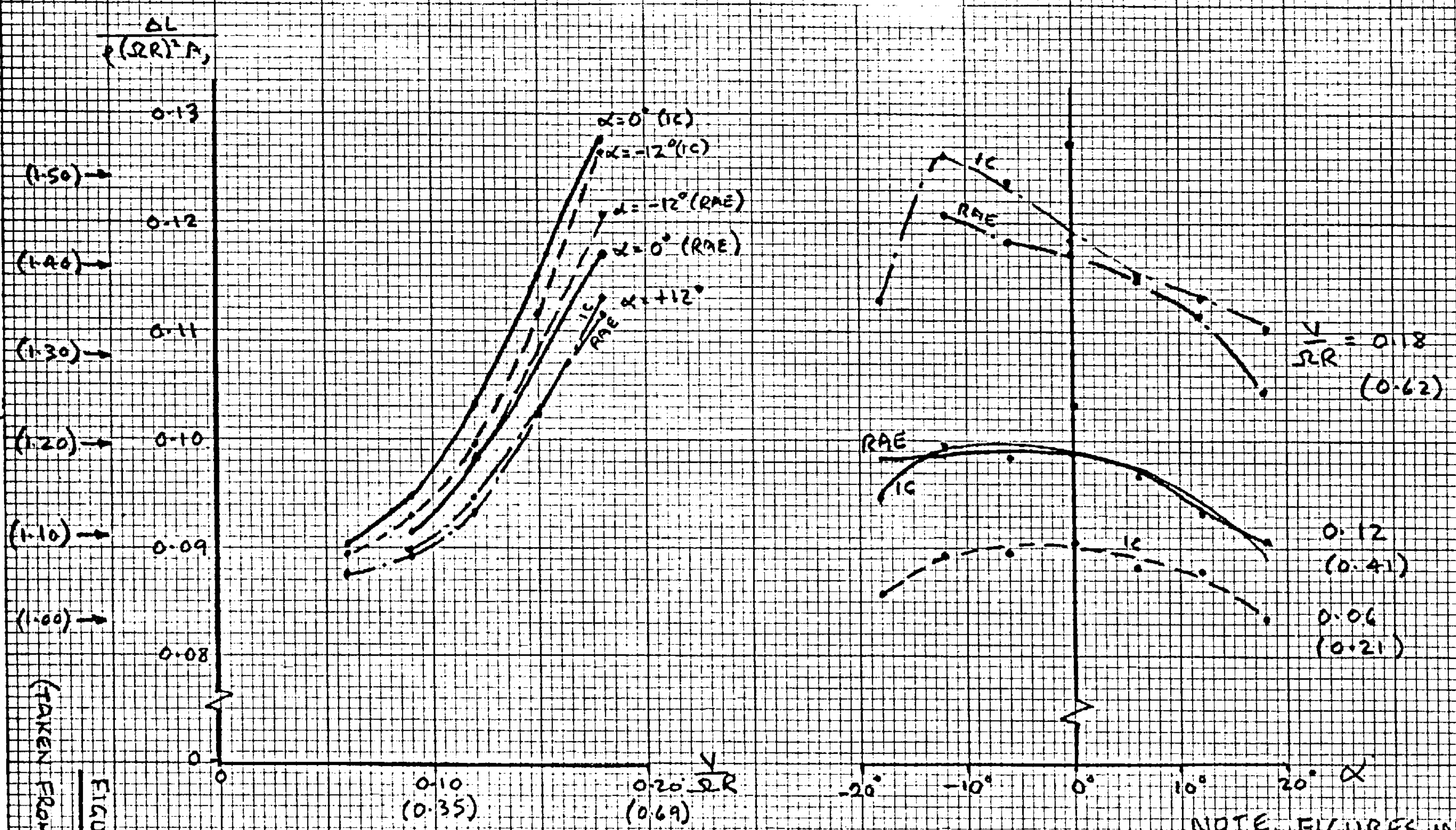

FIGURE VII C

(TAKEN FROM TABLE 7C)

BODY ON STRUTS WITH UNDERFINS.

LIFT INCREMENTS IN THE I.C. 5'×4' TUNNEL AND THE R.A.E. $11\frac{1}{2}' \times 8\frac{1}{2}'$ Nº1 TUNNEL.

NOTE. FIGURES IN BRACKETS SHOW CORRESPONDING VALUES OF $\frac{\Delta L}{T}$ AND $\frac{V}{V_1}$

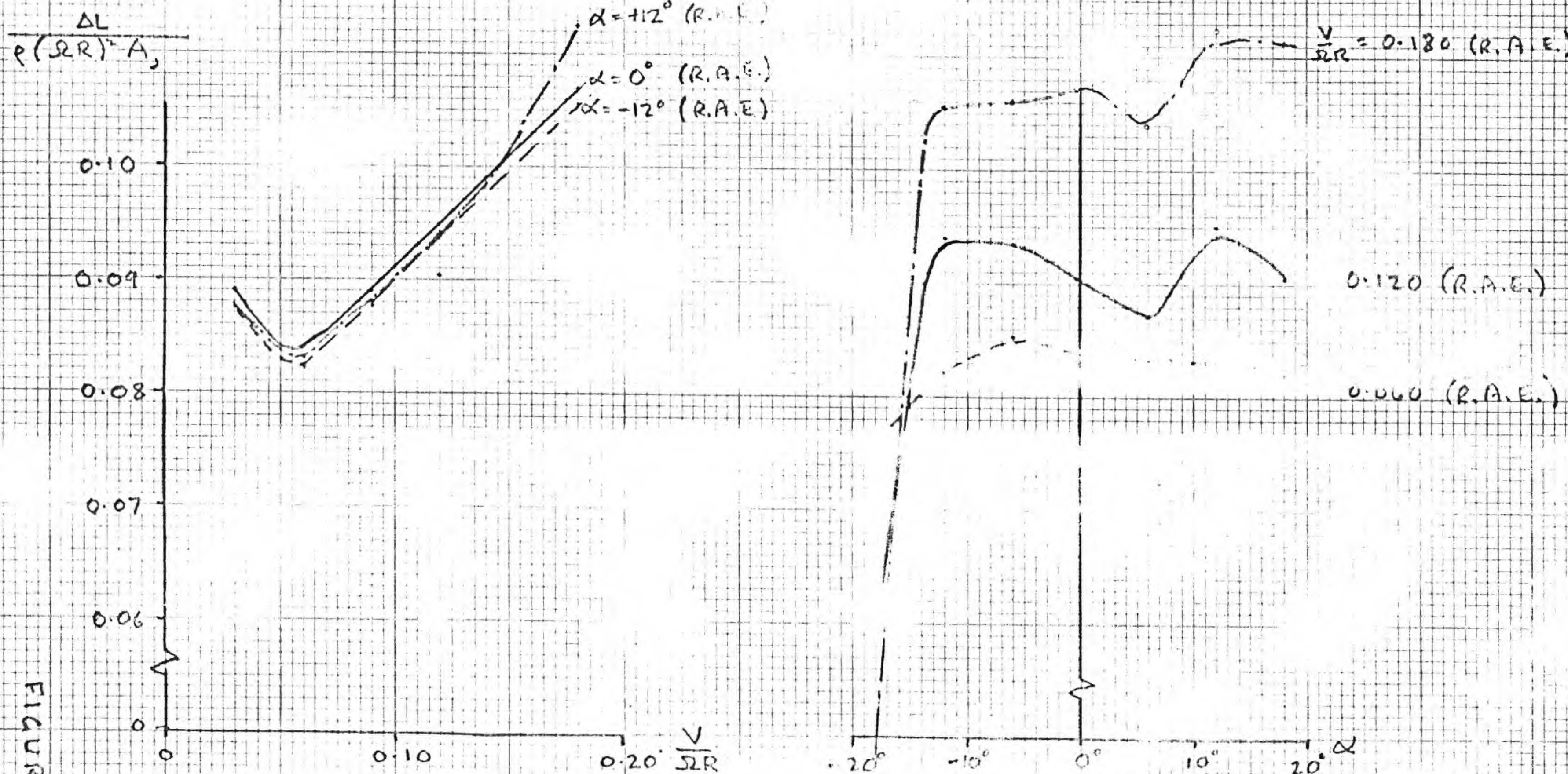

FIGURE VI

(TAKEN FROM TA[illegible]

BODY ON WING WITH UNDERFINS.

LIFT INCREMENTS IN THE R.A.E. No 4 11[illegible]

(NO TESTS PERFORMED IN THE 4'x4' TUNNEL)

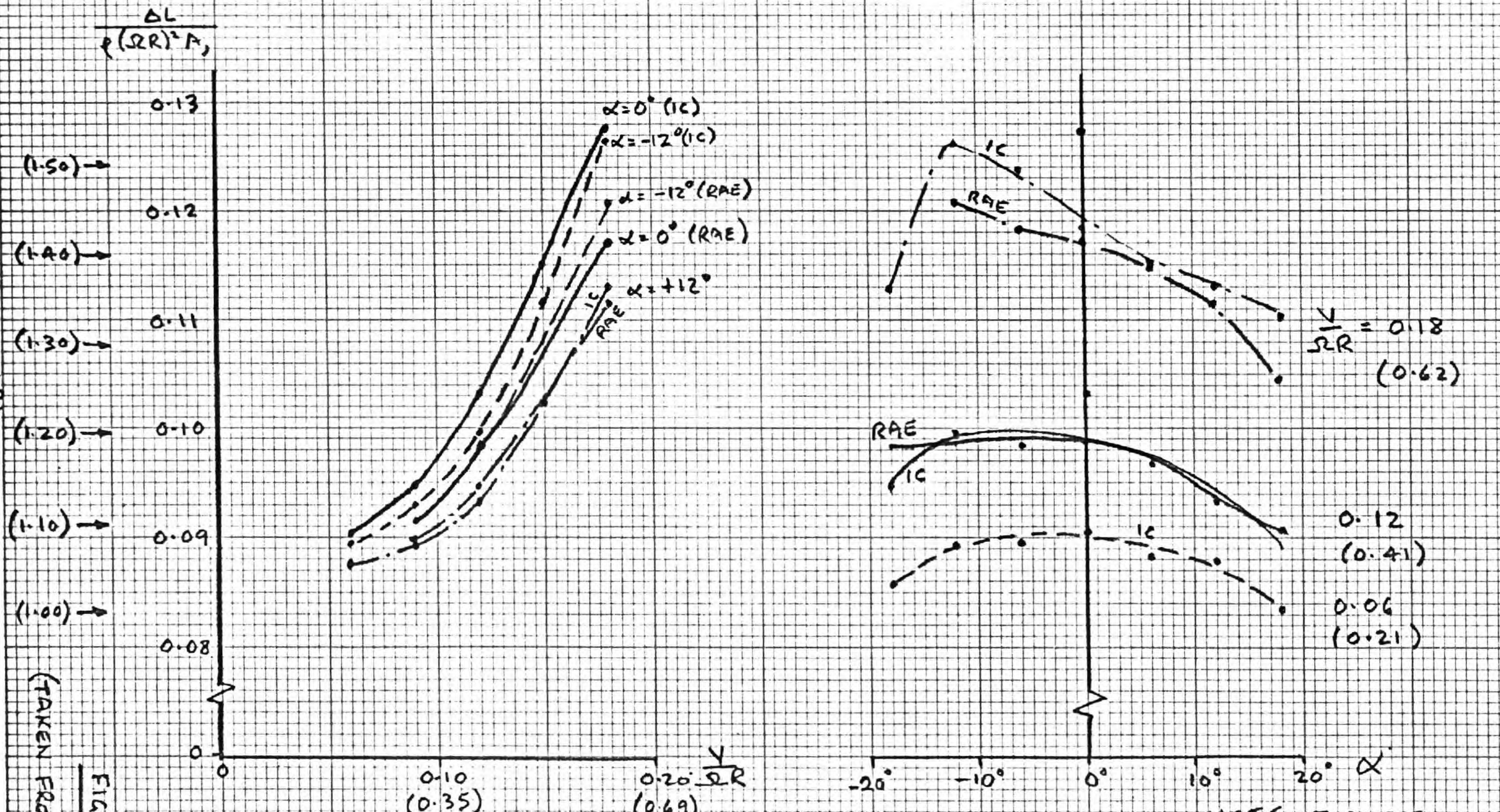

FIGURE VII C

(TAKEN FROM TABLE 7C)

BODY ON STRUTS WITH UNDERFINS.

LIFT INCREMENTS IN THE I.C. 5' × 4' TUNNEL AND THE R.A.E. $11\frac{1}{2}$' × $8\frac{1}{2}$' Nº1 TUNNEL.

NOTE. FIGURES IN BRACKETS SHOW CORRESPONDING VALUES OF $\frac{\Delta L}{T}$ AND $\frac{V}{V_t}$

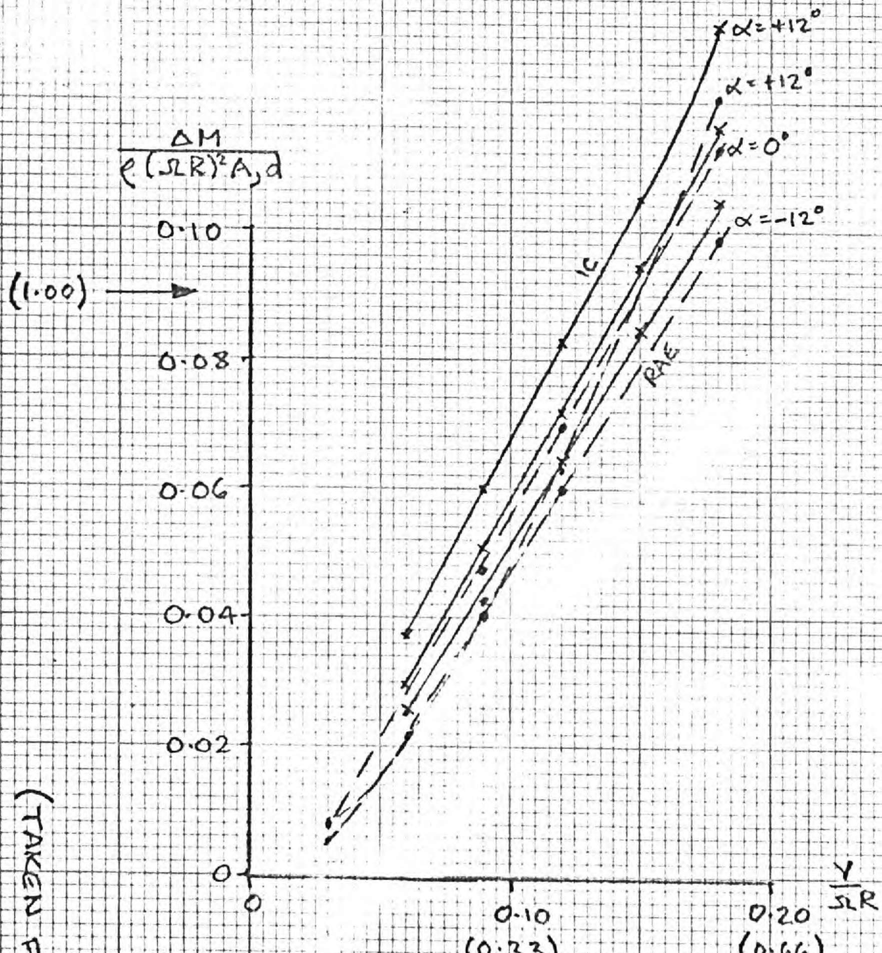

BODY ON STRUTS.

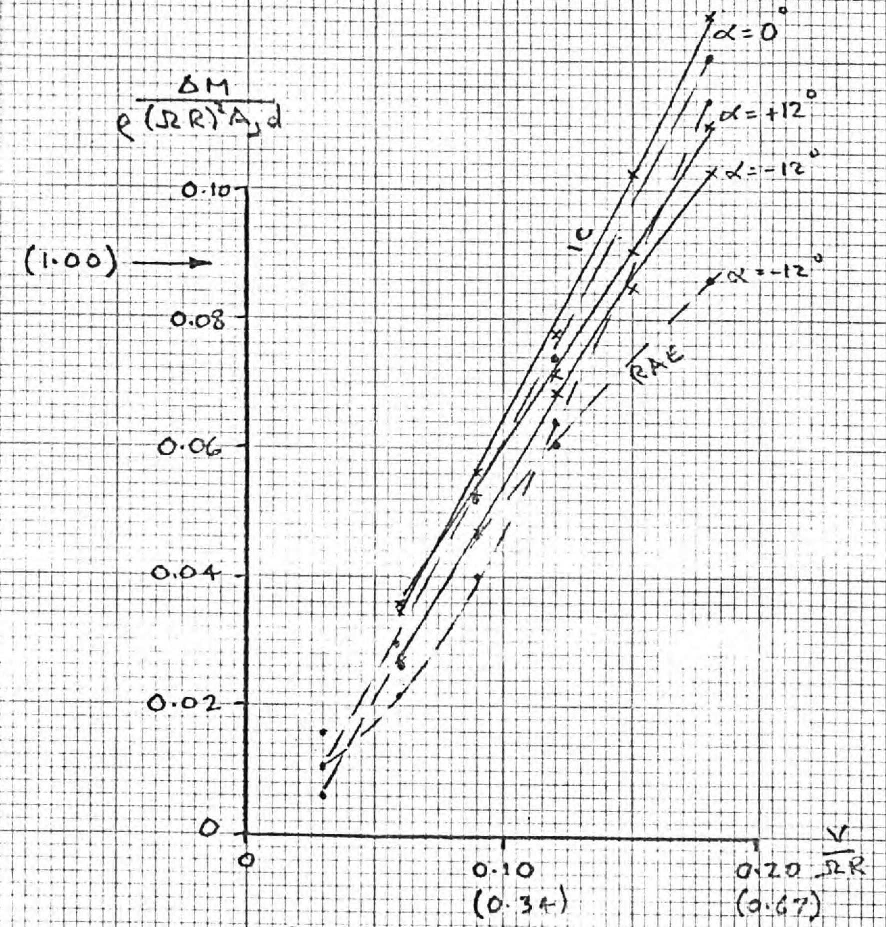

BODY ON WING.

PITCHING MOMENT INCREMENTS, NOSE UP, IN THE I.C. 5' x 4' TUNNEL AND THE R.A.E. N° 1 $11\frac{1}{2}$' x $8\frac{1}{2}$' TUNNEL.

(FIGURES IN BRACKETS SHOW CORRESPONDING VALUES OF $\frac{\Delta M}{Td}$ AND $\frac{V}{V_+}$)

FIGURE VII F

(TAKEN FROM TABLES 7A + 7B)

AER 6020

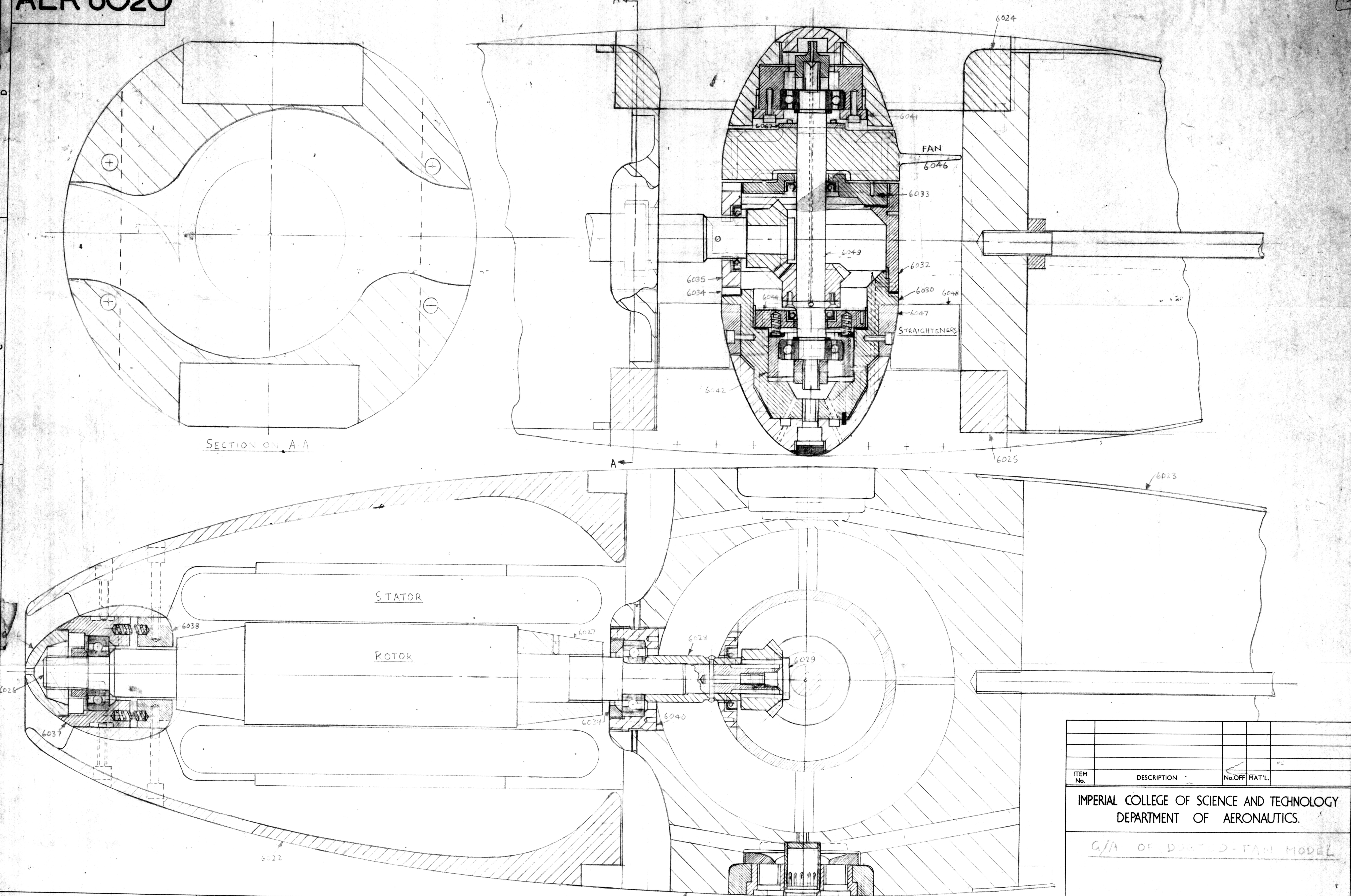

ITEM No.	DESCRIPTION	No.OFF	MAT'L.

IMPERIAL COLLEGE OF SCIENCE AND TECHNOLOGY
DEPARTMENT OF AERONAUTICS.

G/A OF DUCTED-FAN MODEL

ALL UNTOLERANCED DIMENSIONS EXPRESSED IN DECIMALS ARE TO BE WITHIN THE FOLLOWING LIMITS :-
HOLES & INTERNAL FACES, DEAD SIZE TO + ·010"
SHAFTS & EXTERNAL FACES, DEAD SIZE TO — ·010"
CENTRES OF HOLES & CENTRES TO FACES, DEAD SIZE TO + ·005". TOLERANCES NOT TO BE CUMULATIVE.

(30" × 22")

NO MEASUREMENTS TO BE TAKEN FROM THIS DRAWING, FIGURED DIMENSIONS ONLY TO BE WORKED TO.
FINISHED DIMENSIONS GIVEN IN ALL CASES.
ALLOWANCE TO BE MADE FOR MACHINING ON PARTS MARKED THUS ~~f~~ ~~f~~

A ORIGINAL ISSUE	B	C	D	E
DATE	17/8/60		24/11/60	4/10/61

AER 6020

SCALE :- DRAWN :- DATE :-